UNIVERSITY OF BIRMINGHAM

Development of Sustainable Adsorbents for Wastewater Treatment

By

James Manchisi
BSc (UNZA), MSc (UCT)

A thesis submitted to the University of Birmingham

for the degree of

DOCTOR OF PHILOSOPHY

School of Chemical Engineering

College of Engineering and Physical Sciences

University of Birmingham

United Kingdom

August 2015

ABSTRACT

The purpose of this study was to develop adsorbents from slag materials as a low cost method to purify simulated acid mine drainage of high acidity and toxic metal ions content. The study included adsorbent characterisation and adsorption experiments to understand the adsorption behaviour of a multiadsorbate system of Cd^{2+}, Co^{2+}, Cu^{2+}, Fe^{2+} and Mn^{2+} ions.

The adsorbents are amorphous, macroporous solids with low surface area and unfavourable pore size distribution. The chemical activation of blast furnace slag (BFS) by acid leaching increased pore volume, BET surface area and total pore area, and thus increased amounts of Cd^{2+}, Co^{2+} and Mn^{2+} adsorbed. The efficiency in batch studies reduced in multiadsorbates relative to single adsorbates. A 100 % adsorption of ions is achievable at alkaline pH. Also, efficiency increased with increase in phase ratio and temperature. Adsorption is only effective in dilute solutions, i.e., the highest quantities treated to acceptable discharge limits were 1014 mg/L Fe^{2+}, 334 mg/L Cu^{2+}, 206 mg/L Cd^{2+}, 56 mg/L Co^{2+} and 54 mg/L Mn^{2+}. Adsorption of metal ions by BFS was best described by pseudo second order kinetic model and double exponential diffusion model. The mechanisms involve adsorption, precipitation and ion exchange. The adsorbents exhibit high affinity for metal ions but easily attain saturation. The maximum capacities were 2.83 mg/g Cd^{2+}, 0.95 mg/g Co^{2+} and 0.51 mg/g Mn^{2+} using blast furnace slag (BFS and 16.38 mg/g Cu^{2+} and 26.97 mg/g Fe^{2+} using electric arc furnace slag (EAF). The selectivity is Fe^{2+}>Cu^{2+}> Cd^{2+}>Co^{2+}>Mn^{2+}. The fixed bed efficiencies in the first cycle were 93.6 % Cd^{2+}, 56.8 % Co^{2+}, 96.2 % Cu^{2+}, 53.0 % Fe^{2+} and 28.5 % Mn^{2+} using BFS but it was easily exhausted. The high loss of efficiency during the second cycle indicated a limited ability for the BFS to be regenerated, however, desorption of ions with H_2SO_4 (aq) was favourable.

DEDICATION

This is for you, Mom

Ms Elizabeth Musonda

And

In loving memory of my late Dad

Mr David T Manchisi

ACKNOWLEDGEMENTS

I would like to thank the following people and institutions for their contribution to the successful completion of this study: My lead supervisor, Professor Neil Rowson for his guidance, fruitful discussions, suggestions and academic mentorship throughout my studies, I am also grateful to my co-supervisor, Professor Mark Simmons and Mrs Lynn Draper for all the administrative assistance.

My special thanks go to Commonwealth Scholarship Commission (CSC) in the United Kingdom for funding this study in collaboration with University of Zambia and University of Birmingham (UK) as well as Lafarge/Tarmac Ltd UK for providing the adsorbent materials for this PhD project. I would also like to thank the School of Chemical Engineering management through Prof Neil Rowson for the financial assistance.

Thanks are due to Peter Vlahos, Joanne Hyde, Vanessa Worthington and everybody at Commonwealth Scholarship Commission (CSC) office in London for their overwhelming support.

Many thanks to the following people for their technical assistance: Dr James Bowen (Porosimetry and Pcynometry), Ms Eimear Orgill and Dr Gillian Kingston (Atomic Absorption Spectroscopy), Mrs Theresa Morris (Electron Microscopy), Dr Jackie Deans (X-Ray Diffraction/X-Ray Fluorescence), Mr John Wedderburn (BET Surface Area) and Mr David French (Experimental rig setup). Thanks to everyone in the Minerals Engineering Research Group for their company: Zubera Iqbal, Rob Summerville, Tom Skuse and Amir Jafaripour.

I am grateful to my dearest mom Ms. Elizabeth Musonda, my fiancée Sharon Nsana, my son Ethan M Manchisi, brothers and sisters for their support, love and encouragement. Thanks to my friends Steven Mudenda, Mususu Kaonda, Gofetamang Ditalelo, Gary and Abarasi Hart for making my stay in Birmingham a memorable one.

Above all, I thank the Sovereign Lord Jehovah God for all the days of my life.

TABLE OF CONTENTS

Chapter 3 Materials and Methods

Chapter 4 Characterisation of Adsorbent Materials

Chapter 5 Adsorption Equilibria

Chapter 6 Adsorption Kinetics

Chapter 7 Fixed Bed Adsorption Kinetics

Chapter 8 Conclusions and Recommendations

LIST OF FIGURES

LIST OF TABLES

LIST OF SYMBOLS AND ABBREVIATIONS

a	Elovich's desorption rate constant	g/mg
AAS	atomic absorption spectroscopy	
α	Elovich's initial adsorption rate	mg/g min
B	rate coefficient for Boyd's diffusion model	
η	adsorption efficiency	%
AMD	acid mine drainage	
BET	Brunauer-Emmett-Teller	
BFS	blast furnace slag	
C_o	influent solute concentration to the column	mg/L
C_b, C_e,	solute concentration at column breakthrough	
	& exhaustion points respectively	mg/L
C_t	solute concentration at time (t)	mg/L
C_i, C_o	initial adsorbate concentration	mg/L
C_e	residue adsorbate conc., at equilibrium	mg/L
d_p	particle size diameter	µm, mm
D_i	effective diffusion coefficient	cm^2/s
D_1, D_2	Adsorption rate constants of 1^{st} and 2^{nd} stage adsorption	
	steps of the double exponential model	mg/L
DEM	double exponential diffusion model	
E	elution efficiency	%
EBCT	empty bed contact time	min
EAF	electric arc furnace slag	
EDS	energy dispersive spectroscopy	
h_2	pseudo second order initial adsorption rate	mg/g min
K_a	adsorption rate constant	L/mg min
K_1	pseudo first order adsorption constant or first stage	
	adsorption rate constant for double exponential model	mg/g min
K_2	pseudo second order adsorption constant or double	
	exponential second stage adsorption rate constant	mg/g min

K_d	adsorption distribution coefficient	L/g
K_i	Intraparticle diffusion rate constant	mg/g $min^{1/2}$
LUB	length of unused bed of column	cm
m	mass of adsorbent	g
m_{ads}, m_{des}	mass of solute adsorbed & desorbed respectively	mg
m_b, m_e	mass of solute adsorbed at column breakthrough & exhaustion points respectively	mg
m_c	mass of adsorbent in the column	g
N_o	dynamic adsorption capacity	mg/L
PFO	pseudo first order kinetic model	
PSO	pseudo second order kinetic model	
q	adsorption capacity	mg/g
q_b, q_e	column adsorption capacity at breakthrough & exhaustion points respectively	mg/g
q_t, Q_t	adsorption capacity at time (t)	mg/g
q_e, Q_e, max	maximum adsorption capacity at equilibrium	mg/g
Q	volumetric flow rate	mL/min
R^2	regression coefficient	
SE	standard error	
SSE	sum of squared error	
SEM	scanning electron microscopy	
t_b, t_e	column breakthrough service time & column exhaustion (saturation) time	min
V_b, V_e	cumulative volume of waste solution treated at column breakthrough & exhaustion points respectively	mL
XRD	X-ray diffraction	
XRF	X-ray fluorescence	
XPS	X-ray photoelectron spectroscopy	
Z	Column bed depth	cm
Z_o	critical column bed depth	cm

CHAPTER 1

INTRODUCTION

1.1 Background

The exploitation of natural resources to meet the ever rising global demand for industrial products inevitably generates large quantities of waste materials that pose environmental and disposal challenges. By far, mining waste contributes the highest proportion of waste produced by industrial activity, of up to 20 000 Mt per year. In Europe, around 30-50 % of mine wastes are reclaimed and the rest is dumped in landfills (Chan et al., 2008; Lottermoser, 2007). Similarly, a significant proportion of slag (waste) materials generated from iron and steelmaking industry is widely reused in civil engineering applications, however, the remainder is still discarded in landfills. This prevents the use of land for more useful purposes. Furthermore, surface and groundwater becomes susceptible to contamination (El-Haggar, 2007). Several other industries such as metal electroplating, petroleum refining, etc., produce large volumes of wastewaters, residues and sludges that are environmentally hazardous (Barakat, 2011).

Due to the high cost of waste disposal and stringent environmental regulations, emphasis is placed on waste reutilisation to also preserve the finite natural resources that serve as raw materials. Therefore, finding better solutions for effective use of industrial wastes is an important problem that has not yet been fully solved. According to Lottermoser (2008), problems of waste disposal may be eliminated if innovative uses of wastes or alternatives to current disposal practices are pursued or if wastes can be used as raw materials. Such a

holistic approach of total resource utilisation, whereby all materials extracted are put to good use is a challenging concept for researchers. These issues, therefore, coupled with scarcity of resources, have driven the need to develop technologies that can treat, reuse or recycle waste materials for a sustainable development and efficient use of the scarce resources.

1.2 Industrial Solid Wastes and Effluents

There is a growing research interest to develop adsorbents from industrial solid waste materials such as iron and steelmaking slags, fly ash, agricultural wastes (sugar bagasse, lignin, sawdust, tree bark, etc.) and other low value materials like natural zeolites and clays to treat wastewater from industrial processes. This concept is a recent development which has provided very promising results and may have applications in treating a wide range of industrial effluents (Ahmaruzzaman, 2011; Bailey et al., 1999; Barakat, 2011; Dimitrova and Mehandgiev, 2000; Kurniawan et al., 2006; Motsi et al., 2009; Sud et al., 2008).

Investigations into the use of industrial solid waste materials as adsorbents for metal ions, e.g., Zn^{2+}, Pb^{2+}, Cu^{2+}, Cr^{3+}, As^{3+} etc. have been reported. Bailey et al (1999) gave an overview of adsorption capacities and efficiencies of metal ions for many solid wastes and concluded that they are effective adsorbents and could potentially replace the relatively expensive activate carbons and ion exchange resins. However, further studies are still required to understand the mechanisms of adsorption process, address limitations such as chemical/physical instability and poor porosity and to demonstrate the technology. Kurniawan et al (2006) concluded that several agricultural wastes have outstanding

adsorption capacities for metals ions, and a promising alternative to activated carbons. Ahmaruzzaman (2011) reviewed adsorption behaviour of metal ions by several solid waste materials. The author surmised that these novel adsorbents are effective in several metal ion adsorption systems but noted several limitations and gaps that might be drawbacks to industrial application.

Previous research at the University of Birmingham has shown that in several adsorption systems of interest, it is possible to use blast furnace slag, zeolites and calcium alginate as inexpensive adsorbents to treat AMD (Darkwah, 2005; Motsi et al., 2009). Therefore, this study focussed on development of adsorbents from slag materials for the wastewater purification industry.

1.2.1 Slag Materials

Iron and steelmaking plants generate large amounts of slag materials which pose disposal challenges, environmental risks and leave considerable footprints in landfills. Thus, current research efforts aim to develop processes that can recycle steel slags for applications in road construction, cement and fertiliser production, CO_2 capture and storage, flue gas desulphurisation, wastewater treatment and many others (Yi et al., 2012). It is hoped that this approach may contribute to sustainable and efficient use of resources (Das et al., 2007). At present, slags have shown quite attractive application prospects as adsorbents to purify wastewater that may contain metal ions (Dimitrova & Mehandgiev, 2000; Xue et al., 2009c; Oh et al., 2012; Park et al., 2008), phosphates (Kostura et al., 2005; Xue et al., 2009b) and dyes (Xue et al., 2009a). Several studies have reported satisfactory adsorption results from

mostly simulated wastewater of dilute, single and/or binary adsorbate systems of typically below 1000 mg/L of metal ions in the feed streams under various experimental conditions.

1.2.2 The Problem of Acid Mine Drainage

Acid Mine Drainage (AMD) incidence at active and/or old mine sites worldwide is a major environmental problem (Akcil and Koldas, 2006; Skousen et al., 2000). The uncontrolled natural oxidation of principally iron and sulphur compounds found in mineral wastes generates AMD of typically low pH, high sulphates, several metals ions, etc. that have polluted the environment worldwide (Akcil & Koldas, 2006; Skousen et al., 2000).

There are several options currently employed to address the problem of AMD and mitigate environmental destruction. In theory AMD and industrial wastewaters may be treated by chemical precipitation, ion exchange, adsorption, electrochemical techniques and membrane based filtration processes (Fenglian and Wang, 2011). However, chemical precipitation using lime is widely used to treat AMD (Akcil & Koldas, 2006; Kuyucak et al., 2001; Kuyucak, 2002; Robb and Robinson, 1995) and wastewater streams (Barakat, 2011; Fenglian & Wang, 2011; Huisman et al., 2006). However, these chemicals have proved to be relatively expensive, kinetically slow and less efficient in the long term nature and effects of AMD (Barakat, 2011; Kuyucak, 2006; Robb & Robinson, 1995). Wetlands have also been implemented on some mine sites but are yet to be studied and understood in detail (OSMRE, 2009; Skousen et al., 1998). Bailey et al (1999) believe that an alternative option is to develop economic materials that can work as functional adsorbents to treat AMD more cheaply.

1.3 Research Problem

The most widely used chemical process option to treat AMD involves the application of basic chemicals (lime, NaOH, etc.) to reduce the acidity, sulphate levels and metal ions. However, these chemicals are thought to be less efficient in the long term nature and effects of AMD. Nevertheless, in several systems of interest, it is possible to use inexpensive absorbents such as slag materials and zeolites to treat AMD. It is also believed that there is considerable potential to increase the metal ion recoveries further.

Although the adsorption behaviour of mostly single and/or binary systems of metal ions by slag materials has been reported, the interactive effects and competitive adsorption data is limited in multiadsorbate systems that reflect actual industrial effluent compositions. Also, a full adsorbent characterisation that is crucial in understanding and interpreting adsorption data has not been fully addressed. The lack of fundamental understanding of the adsorption process is seen as the reason why this opportunity has not yet been developed into a practical process. Thus, further adsorption studies in the purification of multicomponent solutions of metal ions are required to fully understand the process and rate limiting factors involved. This may form an alternative approach to address AMD, which from a practical point of view could lead to a simple, low capital and operating cost, environmentally acceptable processing option to extract metal ions and reduce the levels of other contaminants.

1.3.1 Hypothesis and Key Questions

It was hypothesised that complete adsorption of metal ions by slag materials from a multicomponent solution to attain acceptable (legal) discharge limits of metal ions is achievable under suitable experimental and solution conditions.

The key research questions were:

(1) What are the mechanisms, kinetics and efficiency of metal ion adsorption with slag materials in a multicomponent context under batch conditions, and how does competitive adsorption phenomena of metal ions affect their recovery?

(2) What are the key adsorbent properties of slag materials? Can material pretreatment steps via chemical and thermal activation improve both adsorbent characteristics and the efficiency of metal ion adsorption above the currently achievable values?

(3) What is the extent of adsorption of metal ions in a continuous flow mode under various process variables? Under what solution conditions is desorption of metal ions from adsorbent surfaces highest?

1.4 Aims and Objectives

The aim of this research was to develop functional adsorbents from slag materials for application in the purification of industrial wastewater, taking AMD as a case study. The specific objectives were:

(1) To conduct a detailed evaluation of the adsorbent characteristics of slag materials using various materials characterisation techniques and to understand how these properties may affect the adsorption process of metal ions from solution. The specific tasks were to;

i. Determine the chemical and phase composition of the adsorbent materials.

ii. Determine the adsorbent surface morphology and chemistry.

iii. Determine the pore size distribution, internal pore structure and specific surface area.

iv. Investigate the effect of thermal and chemical pretreatment of slag materials on adsorbent characteristics.

(2) To characterise the adsorption behaviour of a multicomponent adsorption system that consists of Cd^{2+}, Co^{2+}, Cu^{2+}, Fe^{2+} and Mn^{2+} ions as a function of several key adsorption variables in batch experiments using slag materials as adsorbents. The specific tasks were to:

i. Evaluate the adsorbent efficiency and kinetics of adsorption of multiple metal ions from solution by slag materials under different solution conditions.

ii. Determine the maximum adsorption capacity, affinity and selectivity of the adsorbent materials for metal ions from batch adsorption equilibrium experiments.

iii. Analyse the mechanisms of adsorption of metal ions from solution using adsorbent surface chemistry and metal ion characteristics.

iv. Apply kinetic and equilibrium isotherm models to deduce overall adsorption rates, adsorbent capacity and to estimate model parameters and infer the mechanisms of the adsorption process.

v. Investigate the effect of adsorbent pretreatment on the extent of metal ion adsorption.

(3) To conduct continuous flow adsorption experiments in fixed bed columns in order to:

i. Assess the feasibility of a scale up of the adsorption process using slag materials as adsorbents.

ii. Determine the extent of adsorption and desorption (stripping) of metal ions from adsorbent surfaces.

iii. Establish whether spent adsorbent material can be regenerated.

iv. Address the question of how to dispose adsorbent materials to meet environmental standards where dissolution of metal ions is limited to acceptable levels.

v. Demonstrate how wastewater purification process plant may be operated from a practical point of view by using BFS material as an adsorbent.

1.5 Thesis Outline

This thesis is divided into 8 chapters that constituted a study to develop adsorbents from slag materials with a view to treat AMD.

Chapter 1 highlights the challenges of solid waste management and the problem of AMD. It then provides the motivation for conducting studies to develop a use for slag materials as adsorbents to treat AMD. The chapter also outlines the research problem, hypothesis, aims and objectives.

Chapter 2 provides a review of the current understanding of the adsorption behaviour of metal ions using slag materials as adsorbents. It analyses the efficiency, kinetics and mechanisms of the adsorption process. The chapter also describes AMD chemistry, its environmental impacts and methods of treatment. It then gives insights for further investigations.

Chapter 3 describes the materials, methods and analytical techniques that were employed in this study. These include adsorbent characterisation, preparation of synthetic AMD, experimental setup and procedure under batch and continuous flow conditions as well as analytical measurements and calculations that were conducted to generate data.

Chapter 4 presents the results of adsorbent characterisation using standard analytical techniques. The physicochemical properties of BFS and EAF materials relevant to adsorption process have been evaluated and assessed. It also discusses the modification of the adsorbent structure by chemical and thermal pretreatment to generate new characteristics.

Chapter 5 analyses adsorption capacity, affinity and selectivity of the adsorbent materials for metal ions from batch adsorption equilibrium experiments in a multicomponent system of metal ions. The chapter also discusses the application of equilibrium isotherm models to

deduce adsorbent capacity, model parameters and the mechanisms of the adsorption process.

Chapter 6 analyses the adsorbent efficiency and kinetics of adsorption of multiple metal ions by slag materials as a function of several adsorption variables, and the effect of adsorbent pretreatment on the extent of metal ion adsorption. The mechanisms of adsorption of metal ions have been analysed based on adsorbent surface chemistry and metal ion characteristics. Also, kinetic models were applied to deduce overall adsorption rates, adsorbent capacity and the mechanisms of the adsorption process.

Chapter 7 analyses the extent of adsorption and desorption of metal ions under continuous flow conditions in order to assess the scale up of the adsorption process and to establish whether spent adsorbent material can be regenerated.

Chapter 8 summarises the main findings and conclusions drawn from the study and gives recommendations for further work.

CHAPTER 2
LITERATURE REVIEW

2.1 Introduction

The concept of developing adsorbents from industrial solid waste materials (slags, fly ash, agricultural wastes (sugar bagasse, lignin, sawdust, tree bark, etc.)) and other low value natural materials (natural zeolites, clays, etc.) to treat industrial process effluents has attracted a lot of research interest. This concept has been driven by the fact the era of unregulated disposal of solid wastes and/or effluents is gone, environmental laws are becoming increasingly strict, high grade natural resources are getting depleted and the global economic development agenda's emphasis of 'sustainable development' means that existing resources of the world must be used more efficiently than ever before. Thus, finding innovative uses of industrial wastes is an important problem that has not yet been fully solved. Therefore, this study focused on developing a use for slag materials as adsorbents to treat acid mine drainage that may contain high levels of toxic metal ions, acidity and other residue chemicals.

This chapter gives a review of the current understanding on the development of adsorbents from slag materials for the wastewater purification industry. It begins by giving a brief analysis of the types of slag materials and process effluents with emphasis on acid mine drainage formation, environmental impacts and treatment methods. It goes on to examine physicochemical properties of slag materials and how they may affect adsorption of metal ions in comparison to widely used adsorbents such as active carbon. The basic principles of

adsorption and ion exchange theories are reviewed briefly. The effect of major process variables on adsorption efficiency of metal ions by slag materials is considered next, followed by an analysis of what is known about mechanisms and kinetics of adsorption process. Performance of slags in fixed bed column investigations and case studies will be assessed in relation to key variables. Attention will also be given to problems and why the technology has great potential to be adapted for use on an industrial scale. Final sections will deal with understanding the mechanisms, limiting factors and process design aspects through analysis of adsorption isotherms and kinetic modeling of adsorption systems and conclude by giving insights for further studies.

2.2 Slag Materials

2.2.1 Sources and Types

Slag materials, dusts and sludges are non-metallic, high volume waste by-products of iron and steelmaking processes and pyrometallurgical extraction processes of nonferrous metals. In the US, up to 15 Mt per year of steel slags are generated, with up to 40 % of it dumped in disposal sites (Yildirim and Prezzi, 2011). Slag classification is based on the type of steel/iron production process, i.e., blast furnace (iron making), basic oxygen furnace (BOF), electric arc furnace (EAF) and ladle furnace slags. These steelmaking operations produce slags of different chemical and physical properties due to different sources and types of feed materials and differences in the final steel product requirements (Das et al., 2007; Rao, 2006; Yi et al., 2012; Yildirim & Prezzi, 2011). However, slags present different opportunities (potential secondary source of metals, conversion into useful products, etc.) and challenges

(environmental and health risks, etc.). The forms, properties and current uses of slags of interest in this study are discussed further.

Although a waste product, slags still contain many useful components. They are potential sources of iron, manganese, silica, magnesia and alumina. However, slag properties, especially its mineralogical composition dictate other specific applications. Any metals in BFS, BOF and EAF slags are recovered by magnetic separation. Some of the slag is either recycled back into the steelmaking process or sold for cement production and road construction and the rest is land filled (Rao, 2006). According to Yi (2012), research efforts in finding better utilisation of steel slags has progressed to include wide applications such as aggregates for road and hydraulic construction, wastewater treatment, iron reclamation, fluxing agent, cement and concrete production, CO_2 capture and flue gas desulphurisation, raw material for cement clinker and as fertilizer and soil improvement. This study conducted further investigations in wastewater purification using BFS as the primary adsorbent.

There are three forms of BFS, depending on the cooling rate of its molten form, i.e., slowly air-cooled BFS (mostly glassy, porous crystalline structure), controlled water cooled and air quenched pelletized BFS (less crystalline, lower porosity), controlled water and air or steam cooled expanded (foam) BFS (higher porosity) and rapidly water quenched granulated BFS (glassy, granular, amorphous structure)(Rao, 2006). It should be noted that such surface characteristics may be important requirements in metal ion adsorption systems. BFS has been utilised as part of feed materials for producing ceramic glass, concretes, silica gel bricks and as an adsorbent in wastewater treatment (Das et al., 2007).

2.2.2 Physical and Chemical Properties

Morphologically, most iron and steelmaking slags have highly variable particle sizes, sphericity, porosity, surface texture and crystallinity. Generally, these slags have a macroporous and amorphous structure but with a low specific surface area of less than 5 m^2/g, which is far below that of commercial adsorbents (Curkovic et al., 2001; Dimitrova and Mehandgiev, 1998; Feng et al., 2004; Park et al., 2008; Rao, 2006; Talling and Krivenko, 1997; Xue et al., 2009; Yildirim & Prezzi, 2011). However, the pore structure, i.e., pore size distribution, % porosity, pore volume and pore area are rarely reported. This means that more work is necessary to characterise slag materials in terms of pore structure, and to devise activation techniques that can improve specific surface area and pore size distribution if this opportunity is to be developed into a practical process. Some of these concerns are addressed in Chapter 4 of this thesis.

In terms of chemical composition, slags in general consist of principally CaO, SiO_2, Al_2O_3, FeO/Fe_2O_3, MgO and minor oxides of Mn, K, Na, and S. Talling and Krivenko (1997) reported slag compositions of 30-50 % CaO, 28-40 % SiO_2, 8-24 % Al_2O_3 and 1-18 % MgO. Basic oxygen furnace (BOF) slag has high CaO content (> 35 %) with up to 12 % free CaO and up to 38 % iron oxides (FeO/Fe_2O_3), 7-18 % SiO_2, 0.5-4 % Al_2O_3 and 0.4-14 % MgO. Electric arc furnace (EAF) slags typically have 22-60 % CaO, 10-40% FeO, 6-34 % SiO_2, 3-14 % Al_2O_3, 3-13 % MgO with some free CaO and MgO (Yildirim & Prezzi, 2011). However, the composition of ladle furnace slags is highly variable compared to BOF and EAF. Shi (2004) as cited by Yildirim and Prezzi (2011) reported 30-60 % CaO, 2-35 % SiO_2, 5-35 % Al_2O_3, 1-10 % MgO and 0.1-15 % FeO for ladle slags. According to Rao (2006), BOF, Open Hearth, EAF and Ladle slags have broad composition of high Fe (6.8-23.4 %), 39.9-52.2 % CaO, 4.6-12.8 % SiO_2, 1.3-20.5 %

MgO and 1.9-9.3 % MnO. The range of chemical composition of blast furnace slags (BFS) is given in Table 2.1.

Table 2.1: Chemical characteristics of BFS
(Rao, 2006)

Oxide (w/w %)	CaO	SiO_2	Al_2O_3	MgO	MnO	FeO/Fe_2O_3	S
Mean	44.1	36	10	12	0.44	0.5	1.4
Range	34-43	27-38	7-12	7-15	0.15-0.76	0.2-1.6	1.0-1.9

The chemical composition, structure and morphology of slags depend on the source and type of feed (raw) materials, steel production process and method of slag cooling. The oxides combine to form various silicates, aluminosilicates, aluminates and calcium ferrites mineral phases found in slags. Granulated BFS is amorphous with little crystalline phases, but non granulated BFS is mostly crystalline consisting of larnite (Ca_2SiO_4), rankinite ($Ca_3Si_2O_7$), wollastonite ($CaSiO_3$) and melilite ($Ca_2AlSiO_7/Ca_2MgSi_2O_7$) with little glassy phases. Larnite is the commonest silicate in slags (Talling and Krivenko, 1997). BOF and EAF ladle slags have complex phases of mainly $3CaO.MgO.2SiO_2$ (merwinite), $2MgO.2FeO.SiO_2$ (olivine), $2CaO.SiO_2$, $3CaO.SiO_2$, $4CaO.Al_2O_3.Fe_2O_3$, CaO, MgO and FeO (Yildirim & Prezzi, 2011). Xue et al (2009) reported a solid solution of metal oxides, dicalcium and tricalcium silicates in BOF slag. In many studies involving the adsorption of metal ions by slag materials, it has been established that Ca^{2+} ions present in the frameworks of calcium silicate phases of slag materials participates in ion exchange interactions with metal ions (Mn^{2+}, Cd^{2+}, Cu^{2+}, etc.) in solution. However, it is difficult to delineate the extent of the reaction from that of chemical precipitation as hydroxides (Dimitrova et al., 2001; Dimitrova, 1996; Dimitrova and Mehandgiev, 2000; Komarneni et al., 1988; Lopez et al., 1995). The details of the ion exchange reaction are discussed in Section 2.5.3 of this chapter.

2.2.3 Environmental Impacts

Despite several opportunities that slags from iron and steel industry offer, they also carry several environmental risks and disposal challenges. For instance, slags can contaminate land and prevent the use of land for more useful purposes. Slags also contain residue toxic metals that have the potential to be leached out and pollute ground and surface water with severe consequences on animals and plants (El-Haggar, 2007). Disposal costs for permits and landfill taxes are also high and environmental legislation is generally strict. Consequently, finding solutions to effectively reuse most of the generated slags has gained a lot of momentum.

2.3 Acid Mine Drainage

Acid Mine Drainage (AMD) from active and/or old mine sites worldwide is a major environmental problem. The chemical processes involved in AMD generation and the environmental impacts and remediation options have all been extensively reviewed (Akcil and Koldas, 2006; Banks et al., 1997; Bell et al., 2001; Gordon, 1994; Gray, 1997). Only key concepts, risk factors and challenges associated with AMD are highlighted here.

Acid Mine Drainage (AMD), also referred to as Acid Rock Drainage (ARD) is initiated naturally when iron and sulphur bearing materials oxidise to generate an acidic outflow rich in metal ions and sulphates (Akcil & Koldas, 2006). However, Jennings et al (2008) differentiates the term ARD to refer specifically to the natural outflow of acidic water from oxidation of sulphides in undisturbed environments (or rocks). This is supported by Downing

(2000) who argued that AMD is only associated with anthropogenic (or human) activities such as mining, quarrying, etc., that increase the rates of sulphur oxidation and iron hydrolysis to generate acid. However, both AMD and ARD terms appear to be used interchangeably in the literature.

2.3.1 Chemistry

The production of AMD is a consequence of the chemical breakdown of pyrite and other metal sulphides in host materials via oxidation by oxygen and water. Pyrite frequently occurs within coal deposits and metal sulphide ores in mine sites and excavations, with up to 85 % w/w in mine tailings dumps. However, the content can be as low as 0.1-5 % w/w in lignite mine overburden/wastes while sulphur contents varies between 0.5-3 % w/w (Blodau, 2006; Skousen et al., 2000; US EPA, 2000).

The chemical interactions between iron sulphides and prevailing environmental conditions lead to iron sulphide oxidation to generate polluted water, leachate, seepage or drainage laden with low pH, various metal ions such as Fe^{2+}/Fe^{3+}, Mn^{2+}, Cu^{2+}, Pb^{2+}, Cd^{2+}, sulphates, suspended solids, etc., resulting in severe environmental pollution. Frequently, iron is the most common metal ion and occurs in higher quantities. It may be present in many forms such as soluble ferrous/ferric iron, ferrous hydroxide and ferric hydroxide precipitates depending on pH and oxygen concentration. It is the iron hydroxides that give AMD a reddish/orange colour (Mohan and Chander, 2006; Skousen et al., 2000; U.S.EPA, 1994)

The uncontrolled release of acids and ferric iron can leach more metals from waste materials that may be exposed to air and moisture, especially from mining and processing

operations (U.S.EPA, 1994) such as flotation tailings, waste rock dumps/overburdens, open pit/underground mines, other large-scale excavations and disused/abandoned/worked out coal/metal mine sites (Akcil & Koldas, 2006). The chemical composition of drainage and acidity level depends on the relative content of sulphide and carbonate minerals of the host material. The presence of sulphur and iron oxidizing bacteria greatly accelerate the decomposition of these sulphide minerals (Mielke et al., 2003).

2.3.1.1 Pyrite Oxidation

The theory of acid generation is based on largely pyrite oxidation as well as ferrous iron oxidation and ferric iron hydrolysis. Pyrite is initially attacked by oxygen and water, causing it to break down and release protons (acid), ferrous iron and sulphate (Eq. 2.1). The extent of this reaction is not clear but it is kinetically slow due to low reactivity of oxygen on pyrite surfaces (Akcil & Koldas, 2006; Blodau, 2006).

$$2FeS_2(s) + 7O_2 + 2H_2O = 2Fe^{2+} + 4SO_4^{2-} + 4H^+ \quad \text{---} \quad (2.1)$$

The rate of pyrite oxidation depends on environmental conditions (pH, temperature, oxygen), presence of bacteria, ferric/ferrous iron concentration and redox potential (Akcil & Koldas, 2006; Blodau, 2006).

2.3.1.2 Ferrous Iron Oxidation

The acid from pyrite dissolution will decrease the drainage pH if not neutralised. However, ferrous iron is oxidised by oxygen and acid to ferric form (Eq. 2.2), depending on oxygen, pH and bacteria. The microbial and chemical ferrous iron oxidation kinetics have been

extensively studied in bioleaching systems. Ferrous iron may be further oxidized to release acid and precipitate as ferric hydroxide (Eq. 2.3) (Akcil & Koldas, 2006; Boon, 1996).

$$4Fe^{2+} + O_2 + 4H^+ = 4Fe^{3+} + 2H_2O \quad \text{---} \quad (2.2)$$

$$4Fe^{2+} + O_2 + 10H_2O = 4Fe(OH)_3 + 8H^+ \quad \text{---} \quad (2.3)$$

Ferric iron subsequently reacts (pH < 3.0) with pyrite to generate more acid (Eq. 2.4). This is seen as the main reaction responsible for acid generation. It is limited by the rate of microbial ferric iron production (Blodau, 2006).

$$FeS_2(s) + 14Fe^{3+}(aq) + 8H_2O(l) = 15Fe^{2+}(aq) + 2SO_4^{2-}(aq) + 16H^+(aq) \quad \text{---} \quad (2.4)$$

Pyrite oxidation by ferric iron is kinetically faster than that achieved by oxygen. Therefore, ferrous iron oxidation to ferric iron is a critical sub-process for acid production. At higher pH, ferrous iron oxidation by oxygen is rapid and the reaction may be sustained without bacterial involvement. However at pH < 3.0, ferrous oxidation by bacteria predominates and this increases the reaction rate by up to 10^6 (Blodau, 2006). It is the acid and ferric iron that leach many different residue metal sulphides, oxides, etc., in mining waste materials, e.g., dissolution of a copper minerals (Eq. 2.5 & 2.6) (Hutchins et al., 1986; Murr, 1980; Rossi, 1990). Some representative values of chemical composition of AMD from various mine sites along with environment quality standards for the World Health Organisation (WHO) and UK are given in Table 2.2. Clearly, the concentration levels of metal ions in AMD are above acceptable limits imposed by environmental standards. Treatment of AMD is therefore mandatory before disposal.

$$CuO + 2H^+ = Cu^{2+} + H_2O \quad \text{---} \quad (2.5)$$

$$CuFeS_2 + 4Fe^{3+} = Cu^{2+} + 5Fe^{2+} + 2S^o \quad \text{---} \quad (2.6)$$

These and many other reactions give AMD a chemical composition with variable concentration of metals ions and acidity which depends on the specific mine site and its mineralogical composition (see Table 2.2).

Table 2 2: Representative chemical composition of acid mine drainages
(Grontmij, 2012; Hamilton et al., 1994a; Hamilton et al., 1994b; Kuyucak, 2001; Nieto et al., 2007; ZCCM-IH, 2005)

Mine site	Chemical composition, mg/L									
	pH	SO_4^{2-}	**Fe**	**Cu**	**Al**	**Zn**	**Mn**	**Co**	**Cd**	**Ca**
Wheal Jane mine UK	2.6-3.1	-	1720–1900	14-18	170-197	1260-1700	11-25	As, 26-29	1.4-1.9	Ni, 4-5
	2.4-6.0	-	1.9-4170	0.7-48	-	43-2430	-	-	0.1-4.8	-
Kristineberg mine, Sweden	2.5-2.8	22718-27809	3250-3535	434-485	1305-1438	1600-1765	31-34.9	-	3.89-4.78	As 0.95
Chibuluma mine, Zambia	2.3	3210	U 0.16	159	As 0.08	0.62	Ni 2.23	124	0.0042	181
Rio Tinto River, Spain	2.89	1221	123	15.7	66.5	24.1	6.8	0.48	0.11	73.9
Envir. Quality std (*EQS) UK	6-9	400	1	0.012	Pb 0.02	0.05	As 0.05	-	0.005	Ni 0.04
#WHO Guidelines	-	250	0.30	2.00	Pb 0.01	3.00	As 0.01	-	0.003	Ni 0.07

*EQS = Environmental Quality Standards (std)
#WHO = World Health Organisation

2.3.1.3 Ferric Iron Hydrolysis and Sulphide Oxidation

At about pH 3.5, ferric iron will hydrolyse to produce more protons and precipitate as ferric hydroxide (Eq. 2.7) (Akcil and Koldas, 2006). As pH drops to less than 3.0, pyrite is oxidised by ferric iron to generate more acid. Thus, under pH ≤ 3, ferric iron remains in solution and is a strong oxidant for metal sulphides. The iron oxidising bacteria oxidise ferrous iron to the ferric form while the sulphur oxidising bacteria oxidise sulphur to sulphate and protons

(Schippers and Sand, 1999). A schematic representation of AMD generation is given in Figure 2.1.

$$Fe^{3+} + 3H_2O = Fe(OH)_3 + 3H^+ \quad \text{---} \quad (2.7)$$

$$S^o + 3/2O_2 + H_2O = 2H^+ + SO^{2-}_4 \quad \text{---} \quad (2.8)$$

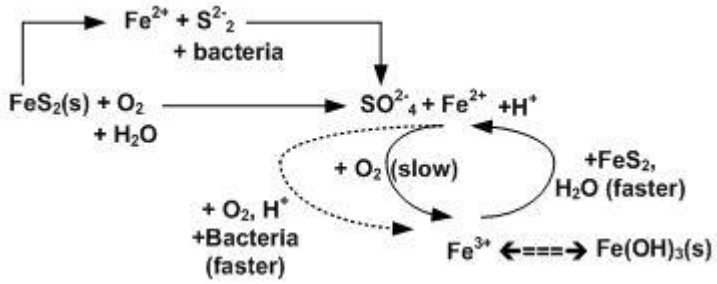

Figure 2.1: Edited pyrite oxidation cycle
(Breed and Hansford, 1999; Ferguson and Erickson, 1988)

2.3.2 Environmental Impacts

Once discharged into the natural environment, AMD is reported to have contaminated soils, polluted surface and ground waters, affected aquatic and terrestrial ecosystems, and destroyed biological resources in many countries. The destructive nature and impact of AMD on the environment is well documented (Banks et al., 1997; Bell et al., 2001; Gordon, 1994; Gray, 1997; Luis et al., 2011; Naiker et al., 2003; UK Environmental Agency, 2008; Younger, 2001). High levels of sulphates, metal ions, acidity and iron precipitates in AMD have huge negative effects on the aquatic, terrestrial ecosystems and human health. According to Bailey et al (1999), metal ions are not biodegradable and therefore accumulate in organisms causing diseases and/or disorders.

The presence of Fe^{3+}/Fe^{2+} ions in AMD form yellow/orange hydroxide precipitates (ochre mixtures) that deposit on river beds inhibiting algae, insects, fish and benthic growth and destroys their habitats. This reduces the population and diversity of fish and invertebrates. The aesthetic impact and visual damage of iron rich AMD makes the affected lands uneconomic and water becomes unsuitable for use such as source of industry water supply (UK Environmental Agency, 2008) Figure 2.2 below depicts the impacts of AMD.

(a) *(b)

Figure 2.2: Acid mine drainage (a) Disused open pit coal mine flooded with acidic AMD in Zambia with potential risk of underground water pollution (b) Flooded West Rand Basin in South Africa showing reddish-brown discharge due to AMD & iron precipitation.

*http://www.rainharvest.co.za/wp-content/uploads/2011/02/acid-mine-water.jpg

High acidity restricts the respiration and root uptake of mineral salts and water in most plants. Also, high acidity corrodes infrastructure. Al^{3+} ions are also toxic and destroy vegetation (Bell et al 2001). In humans, metal ions cause health problems, e.g., cancer (arsenic), kidney damage (cadmium, lead), liver damage (copper) and many other effects (Barakat, 2011). There are many general effects of acidity, iron precipitates, metal ions and total dissolved solids on the ecosystem. Lottermoser (2007) summarised these effects as follows: acidity (pH < 4.5) makes photosynthetic organisms lose their bicarbonate, degrades

and kills animals and plants, reduces drinking water quality, mobilizes metal ions and corrodes man-made infrastructure; Iron precipitates (100 to 1-9 x 10^3 mg/L) smothers benthic organisms, discolours and increases the turbidity of receiving water as pH increases and ferric iron precipitates, clogs up fish gills, reduces light penetrating the water column and encrusts man-made structures and finally metal ions (0.01 to 1-9 x 10^3 mg/L) and total dissolved solids (100 to 1-9 x 10^4 mg/L) degrades and kills animals and plants through bioaccumulation, reduces drinking water quality and contaminates soil and sediments.

Some of the strategies to prevent AMD formation include flooding and sealing disused underground mines, underwater storage of mine tailings and blending of acid-generating and acid-consuming mineral wastes (Johnson and Hallberg, 2005). Due to practical difficulties of preventing AMD formation at source, remediation strategies through active or passive treatment have been proposed.

2.3.3 Methods of Treatment

According to Johnson and Hallberg (2005), current remediation methods for AMD fall under abiotic and biotic processes, which are further subdivided into active and passive processes. In active systems, alkaline chemicals are continuously added to AMD to neutralise acid and precipitate metal ions while passive systems use natural or constructed wetlands with relatively low maintenance costs.

Active systems of purifying AMD involve addition of oxidants (H_2O_2, $KMnO_4$, etc.), neutralising agents ($CaCO_3$, $Ca(OH)_2$, CaO, Na_2CO_3, NH_3/NH_4OH, KOH, etc.) and coagulants/flocculants ($Al_2(SO_4)_3$, $NaAl_2O_2$, $Fe_2(SO_4)_3$, etc.) to AMD in order to raise the pH

and oxidise and precipitate metal ions as hydroxides (Johnson & Hallberg, 2005; Skousen et al., 2000). However, lime based chemical precipitation techniques are widely practiced to treat AMD (Akcil & Koldas, 2006; Kuyucak et al., 2001; Kuyucak, 2002; Robb & Robinson, 1995) and wastewater streams (Barakat, 2011; Fenglian & Wang, 2011; Huisman et al., 2006) in order to neutralise acid, and to precipitate out both sulphates and metals ions in order to meet particular effluent limits. Although the chemical process is quite effective, convenient, safe, simple and has lower capital costs, these chemicals have proved to be relatively expensive, kinetically slow and less efficient in the long term nature and effects of AMD (Barakat, 2011; Kuyucak, 2006; Robb & Robinson, 1995). It has also been argued that the resultant sludge (or flocs) is chemically complex and toxic even though earlier studies proved that sludge could be chemically stabilised to some extent by aging (Barakat, 2011; Watzlaf and Casson, 1990). This view has been supported by other researchers who stated that the long term stability and subsequent disposal of sludge is still a problem (Brown et al., 1994; Kuyucak, 2006; McDonald et al., 2006). A much more mechanised technique uses High Density Sludge (HDS) process which improves the chemical and physical properties of sludge but does not completely address the long term stability and disposal problems (Kuyucak et al., 2001; Zinck, 2005).

Passive systems of AMD control include constructed and natural wetlands (aerobic/anaerobic), anoxic limestone drains (ALD), limestone ponds (ponds filled with limestone for treatment), successive alkalinity-producing systems (SAPS) and open limestone channels (OLC) (surface channels/ditches filled with limestone). Constructed wetland consists of shallow excavations filled with gravel, soil and organic matter to support wetland plants. AMD is treated as it passes through the wetland via biogeochemical

interactions. Natural wetlands are soils/sediments saturated with water, together with supporting plants adapted to reducing conditions in their environment. ALD are abiotic systems of buried limestone cells that passively produce bicarbonate alkalinity as anoxic water passes through. SAPS combines wetlands and ALDs concepts whereby O_2 and Fe^{3+} are initially removed by organic matter followed by passage of anoxic water through ALD (Johnson & Hallberg, 2005; Skousen et al., 2000). The choice of a method to treat AMD will depend on cost, technical, economic and environmental factors.

Many natural and ecologically engineered wetlands have been studied and implemented successfully on some mine sites as a response to high costs, relative inefficiency and slow precipitation kinetics, as well as limitations and operational difficulties in handling sludge from the chemical precipitation of AMD. However, these are passive treatment techniques, which are yet to be studied and understood in detail, and have their own engineering and operational challenges (Kuyucak, 2006; OSMRE, 2009; Skousen et al., 1998). Skousen et al (1998) suggested optimisation of the design of HDS and passive treatment systems to improve efficiency. However, an alternative view is to develop economic materials that can work as adsorbents to treat AMD (Bailey et al., 1999). According to Barakat (2011) this idea has been taken further through extensive investigations to determine the potential use of a variety of natural materials and industrial solid wastes as alternative and inexpensive adsorbents to treat wastewaters and/or AMD. Sud et al (2008) stated that these materials are abundant, cheap, renewable, have high adsorptive capacity and efficiency, produce low voluminous chemical/biological sludge, easy to regenerate and potentially permits the recovery of valuable products such as metals for possible recycle or value addition, building

materials (from AMD sludge), recycle of water and use of iron oxides (as pigments) in the paint manufacturing industry (McGinness, 1999).

2.4 The Adsorption Theory & related Processes

Adsorption had its origins as an industrial process after the discovery of gas uptake by charcoal and clays. However, it was not until early studies established that tartaric acid was decolourised by charcoal by adsorbing impurities that the first application was introduced using charcoal as a decolourising adsorbent for sugar syrup in the late 18^{th} century. Subsequent research led to selective adsorption and development of several adsorbents. Today, adsorption is widely used in industrial processes to separate and purify wastewater, petroleum products, fluid mixtures, neutralise waste gases, dry various fluids, etc. (Dabrowski, 2001). The fundamental concepts of adsorption, ion exchange and precipitation on which this project is based are briefly discussed below.

Adsorption is a separation process in which components of a fluid phase are transferred to the surfaces of insoluble, solid adsorbent particles suspended either in a vessel or packed in a column. Molecules, atoms or ions in a gas or liquid diffuse to the surface of the solid where they bond with the solid surface or are held by weak intermolecular forces (Seader et al., 2011). The driving force is the reduction in interfacial surface tension between the fluid phase and adsorbent (free energy change with interfacial area) resulting from solute loading onto the adsorbent surface (Armenante, 1999a). Adsorption is attractive where adsorbates are either toxic or difficult to remove by other methods or their concentration in solution is very low such that their recovery by conventional methods is difficult (Armenante, 1999a).

Other industrial applications of adsorption include gas purification (CO_2/natural gas), gas bulk separations (H_2O/ethanol), liquid purifications (organics/water) and wastewater treatment (inorganic contaminants) (Armenante, 1999a; Seader et al., 2011). This study focussed on the treatment of industrial wastewater to remove inorganics (metal ions). Related previous studies have been reviewed in section 2.5.

Adsorption is classified into physisorption and chemisorption depending on the mechanism of adsorbate attachment to the surface of the adsorbent. In physisorption, the adsorbate is loosely held to the adsorbent surface by relatively weak van der Waals (intermolecular) forces. The process is reversible and results in multilayer adsorption. However, chemisorption involves formation of chemical bonds between adsorbent surface sites and adsorbates. It is irreversible and results into monolayer adsorption (Inglezakis and Poulopoulos, 2006b; Rouquerol et al., 2014; Ruthven, 1984). The general differences of the two processes are summarised in the Table 2.3 below.

Table 2.3: Characteristic differences between physisorption and chemisorption
(Burwell, 1976; Inglezakis & Poulopoulos, 2006b; Rouquerol et al., 2014; Seader et al., 2011)

Physisorption	Chemisorption
Involves van der Waals forces	Involves strong chemical bonds
Multilayer adsorption	Monolayer adsorption
Reversible	Irreversible
Not specific in nature	Specific in nature
Low enthalpy of adsorption (5-40 Kj/mol)	High energy of adsorption (40-400 Kj/mol)
Activation energy is not required	Activation energy is required
Favoured at low temperature and high pressure	Occurs at high temperature and high pressure

2.4.1 Characteristics of Commercial Adsorbents

The performance requirements of an adsorbent include large selectivity, large adsorption capacity, fast adsorption kinetics, easily generable, good mechanical strength and of low cost. Consequently, an adsorbent must meet the following characteristic (ideal) requirements to be suitable for commercial use (Deng, 2006; Richardson et al., 2002; Seader et al., 2011):

- Large internal pore volume
- Large internal surface area
- Controlled surface properties (functional groups)
- Controlled pore size distribution (micropore range)
- Weak adsorbate/adsorbent interaction
- Chemical, thermal and mechanical stability
- Low cost raw material

Figure 2.3 (a) and (b) and Table 2.4 below give the most common adsorbents and their characteristic properties. A highly microporous structure with a large specific surface area are especially important requirements to provide a high adsorption capacity. Pore structure of the adsorbent (pore sizes, shape and pore size distribution) also determines adsorption capacity. On the basis of porosity, adsorbents can be classified as macroporous ($d_p > 50$ nm), mesoporous ($2 \leq d_p \leq 50$ nm) and microporous ($d_p < 2$ nm) (Ruthven, 1984). Chapter 4 of this study analysed the properties of slag materials and their potential use as novel adsorbents with reference to characteristics of these commercial adsorbents discussed here.

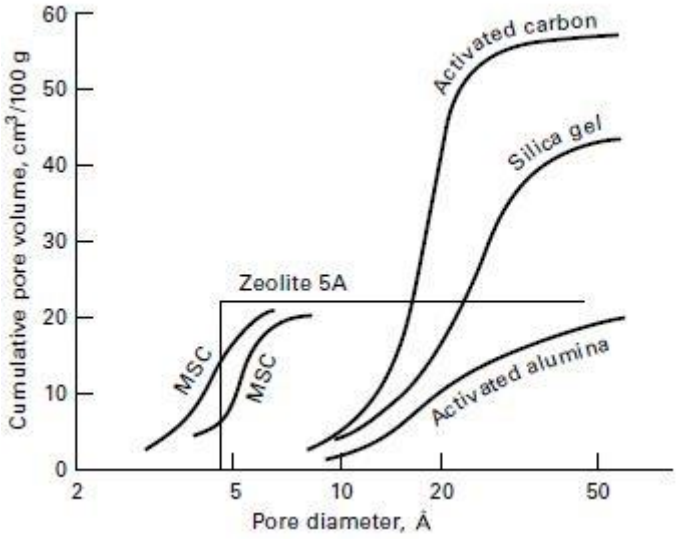

Figure 2.3: (a) Pore size distribution of commercial adsorbents
(Seader et al., 2011).

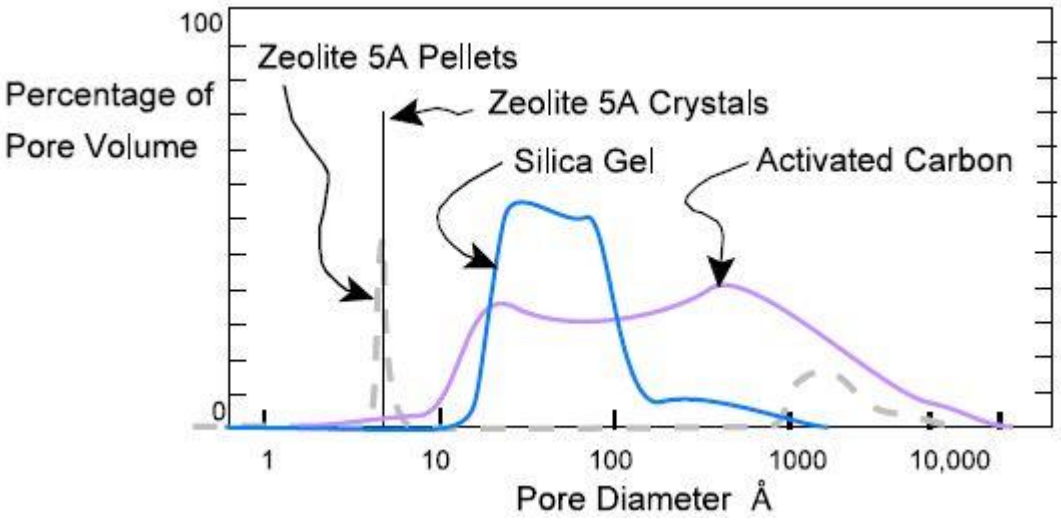

Figure 2.3 (b): Pore size distribution of commercial adsorbents
(Knael, 2012).

Table 2.4: Properties of commercial adsorbents
(Seader et al, 2011)

Adsorbent	**Nature**	**Pore diameter, d_p, Å**	**Particle porosity, ϵ_p**	**Particle density, P_p, g/cm^3**	**Surface area, S_g, m^2/g**
Activated alumina	Hydrophilic, amorphous	10-75	0.50	1.25	320
Silica gel:	Hydrophilic/ Hydrophobic, amorphous				
• Small pore		22-26	0.47	1.09	750-850
• Large pore		100-150	0.71	0.62	300-350
Activated Carbon:	Hydrophobic, amorphous				
• Small pore		10-25	0.4-0.6	0.5-0.9	400-1200
• Large pore		> 30	-	0.6-0.8	200-600
Molecular sieve carbon (MSC)	Hydrophobic	2-10	-	0.98	400
Molecular sieve zeolites	Polar-hydrophilic, crystalline	3-10	0.2-0.5	1.4	600-700
Polymeric adsorbents	-	40-25	0.40-0.55	-	80-700

A microporous silica gel (SiO_2. nH_2O) is manufactured from colloidal silicic acid and its most important application is as a dessicant. It has a highly polar surface due to the presence of hydroxyl (Si-OH) surface groups that enables it to selectively adsorb polar species, e.g., water, alcohols, etc., through hydrogen bonds over nonpolar compounds. Activated alumina ($Al_2O_3.nH_2O$), a porous solid with high specific surface area, is prepared from bauxite. The surface is more strongly polar than that of silica gel. It is commonly used as a desiccant at high temperatures, e.g., for drying warm air or gas streams (Deng, 2006; Ruthven, 1984; Seader et al., 2011)

The most frequently applied adsorbent for many uses is currently activated carbon. It is produced by thermal decomposition of carbonaceous materials and followed by activation with steam or CO_2 at 700-1100 ^oC to produce macro/microporous adsorbents with large surface area and high adsorption capacity. The properties of active carbon depend on the raw materials used and activation process conditions. The carbon surface is nonpolar (hydrophobic) and organophilic. Thus, it is widely used to adsorb organics, e.g., in water purification, decolourizing sugar solutions, etc. Carbon molecular sieves (CMS) are a specially produced adsorbents from carbonaceous material (anthracite/hard coal) under controlled manufacturing conditions to generate a narrow pore size distribution (4-9Å). This enhances selectivity in adsorption of molecules of different sizes. The major use of CMS is in separation of high-purity N_2 from air in pressure swing adsorption (PSA) process (Deng, 2006; Ruthven, 1984; Seader et al., 2011).

Zeolites are crystalline solids made of aluminosilicates that consists of SiO_4 and AlO_4 tetrahedra joined by oxygen atoms. The general formula is $M_{x/n}[(AlO_2)_x(SiO_2)_y]_zH_2O$ where x and y are integers with y/x (Si/Al) ratio ≥ 1, n is the valence of the cation M (Na^+, K^+, Ca^{2+}) and z is the number of water molecules. The different possible rearrangement of tetrahedra leads to different structures of zeolites. Different zeolites exist ranging from natural (e.g., clinoptilolite) to synthetic commercial molecular sieves (e.g., A, X, Y and mordenite). Synthesis of zeolites may be by hydrogel or clay conversion processes. Because molecular sieve zeolites are very selective, they are used in separating mixtures of molecules on the basis of their size and shape. The major applications include detergent additives (zeolite 4A), animal food additives (zeolite 4A), air separations, catalyst support and in ion exchange (Deng, 2006; Ruthven, 1984; Seader et al., 2011)

2.4.2 Methodology of Studying Adsorption Process

Immersion, circulation, chromatographic, slurry and null methods are some of the available experimental techniques for studying adsorption from solution by adsorbents under three basic types of equipment (volumetric, gravimetric and chromatographic). The choice of method depends on the system being studied and objectives. The immersion method is often chosen due to the simplicity of the experimental apparatus needed and the use of standard laboratory techniques (Everett, 1986; Knaebel, 2012; Rouquerol et al., 2014).The immersion technique was adopted in this study (Chapter 3). It is the traditional volumetric method of determining adsorption from solution. A known mass of fresh adsorbent is added to a measured volume of solution of known composition in a thermostated adsorption vessel, then sealed and equilibrated by agitation. A sample of liquid is withdrawn and analysed for a change in adsorbate concentration. Although popular, the method is tedious and relatively less accurate. Preliminary experiments are needed to determine the time required to establish equilibrium, and also outgassing of the adsorbent and/or solution, if required, may be complex (Everett, 1986; Rouquerol et al., 2014).

The circulation method avoids problems encountered with the immersion method whereby adsorption is done in the absence of air and equilibrium is achieved by circulating the solution over the adsorbent. The solution concentration is continuously monitored by passing it through a concentration measuring device (e.g., flow refractometer). One advantage is that the same sample of adsorbent can be used throughout and the adsorption vessel may be accurately thermostated. The slurry method is a type of the immersion method that avoids problems of rigorous separation of filtrate. After equilibration, the

sample is centrifuged and the slurry is weighed and analysed. In the chromatographic method, the adsorbent is packed in the column and concentration measurements are done on the inlet and outlet streams. The concentration difference is monitored by a differential refractometer. The volume of the liquid passing through the column is measured until influent and effluent concentrations are equal. The method is useful in dilute systems although it requires large volumes of solutions. The Null method is similar in operation to the circulation method (Everett, 1986). The experimental setup employed in Chapter 7 of this study is similar in scope to the chromatographic method

2.4.3 Ion Exchange

Ion exchange (IX) is a separation process in which ionic species present in a liquid phase are exchanged equivalently for ions electrostatically attached to the functional groups present in the matrix of the solid exchanger. Separation is achievable because ion exchangers exhibit high affinity for certain ions than for others. During ion exchange process, cations or anions in solution replace dissimilar and displaceable counter ions of the same charge contained in a solid ion exchanger, which also contains immobile, insoluble and permanently bound co-ions of the opposite charge. A general IX reaction involving hydrogen based ion exchanger is given in Equation (2.9). The classic example is the softening of water whereby Ca^{2+} ions replace Na^{+} ions by ion exchange as given in Equation (2.10). The process is reversible and does not alter the structure of the exchanger (Cobzaru and Inglezakis, 2015; Seader et al., 2011).

$$R\text{-}H + X^{+} \leftrightarrow R\text{-}X + H^{+} \quad \text{---} \quad (2.9)$$

$$Ca^{2+}_{(aq)} + 2NaR_{(s)} \leftrightarrow CaR_{2(s)} + 2Na^{+}_{(aq)} \quad \text{---} \quad (2.10)$$

Where R = insoluble matrix of IX resin, X = any ion in solution

IX is closely linked to adsorption because both processes involve a mass transfer step between the fluid and solid phases. However, the main distinction is that ions are involved in IX while electrically neutral species are involved in adsorption. Also, ions that are extracted from the liquid are replaced by ions from the solid matrix. There is no replacement of species in adsorption. Unlike adsorption, IX is stoichiometric in nature (Cobzaru & Inglezakis, 2015).

Ion exchangers are classified as either cation or anion exchangers. These are further subdivided into inorganic (e.g., natural ion exchangers, i.e., natural zeolites, clays and synthetic ion exchangers, i.e., synthetic zeolites) and organic ion exchangers (e.g., synthetic polymeric resins). The most widely used ion exchangers are synthetic organic polymeric resins based on styrene and acrylic monomers. However, natural ion exchangers have low exchange capacity relative to synthetic ones. The major application of IX is in water and wastewater purification, e.g., elimination of Ca^{2+}, Mg^{2+}, salts, etc., (water softening), elimination of mineral components (demineralization) and removal of metal ions from wastewater by natural zeolites (Cobzaru and Inglezakis, 2015; Inglezakis and Poulopoulos, 2006a; Seader et al., 2011)

2.4.4 Chemical Precipitation

By far, this is the most widely used process to extract metal ions from industrial wastewater. It involves the reaction of metal ions with either hydroxide, carbonate or sulphide based chemicals to form insoluble metal precipitates by suitable pH adjustment (pH 8-11). The precipitates are separated by sedimentation or filtration and the purified water can then be recycled or discharged. However, hydroxide precipitation using lime (CaO) or limestone

($CaCO_3$) is the most widely used technique to treat inorganic effluents ≥ 1000 mg/L due to its relative simplicity, low cost and easy pH control. Depending on concentration levels of metal ions, solubilities of metal hydroxides are greatly minimised at pH 8-11 as shown in Figure 2.4 which then increase their extraction from solution. The conceptual precipitation model is given in Equation 2.11 (Barakat, 2011; Fenglian and Wang, 2011; Peter et al., 1985).

$$M^{n+} + nOH^- \leftrightarrow M(OH)_n\downarrow \quad --- \quad (2.11)$$

Where M^{n+} = dissolved metal ion, OH^- = precipitant, $M(OH)_n$ = insoluble metal hydroxide.

The chemical precipitation process is convenient and safe to operate. However, it requires large quantities of chemicals to reduce metal ions to acceptable discharge standards. It also has various operational challenges and the long term environmental impact of chemical sludge is also a challenge (Barakat, 2011).

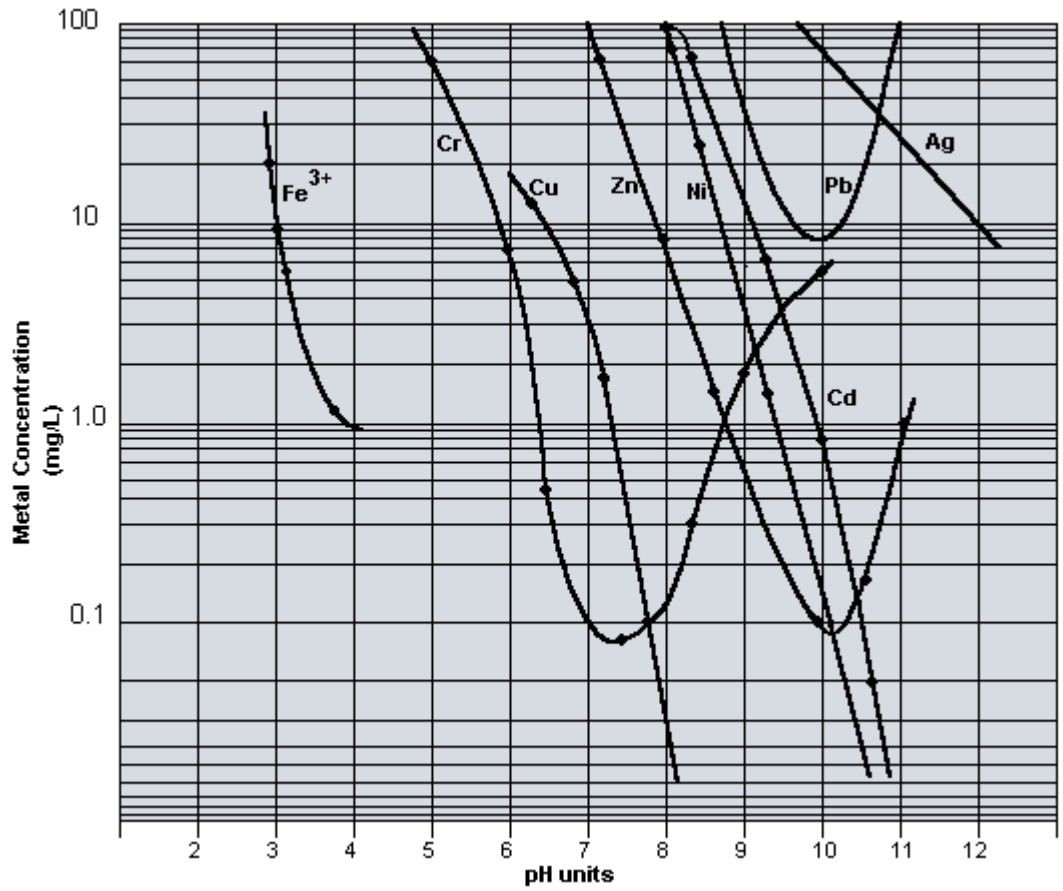

Figure 2.4: Metal hydroxide solubility diagram
(http://hoffland.net/treatment-processes-chemistry-2/hydroxide-precipitation/

2.5 Adsorption Behaviour of Metal ions using Slag Materials as Adsorbents

The adsorption behaviour of metal ions is chiefly controlled by the chemical and physical characteristics of slag materials such as surface area and internal pore structure as well as adsorption process variables. The physicochemical properties of slag materials have been examined in section 2.2. This section gives a detailed review on the current understanding of the adsorption of metal ions by slags from wastewater and identifies gaps and limitations for further study.

2.5.1 Adsorption Characteristics

This section gives a review of the adsorption behaviour of metal ions using slag materials as adsorbents, i.e., mechanisms, adsorption capacity, Kinetics and the effects of variables on the extent of adsorption (efficiency).

2.5.1.1 Effect of Adsorption Variables

pH

The efficiency (%) of adsorption of metal ions increases with an increase in pH as shown in Figure 2.5 (Dimitrova, 1996), and the mechanism of adsorption is also controlled by pH. Huang and Rhoads (1989) found Zn^{2+} ion adsorption by silicate based adsorbent materials to be only effective in alkaline pH. This view was supported by Gao et al (1995) who found that adsorption of multiple metal ions by blast furnace (BF) sludge in fixed bed columns was poor in very acidic solutions largely due to the competitive adsorption of H^+ ion (Eq. 2.12).

$$\overline{(\equiv SO)_2^-}Ca^{2+} + Me^{2+}(aq) + H^+(aq) \Leftrightarrow \overline{(\equiv SO)_2}H^+ + Me^{2+}(aq) + Ca^{2+}(aq) \quad \text{---} \quad (2.12)$$

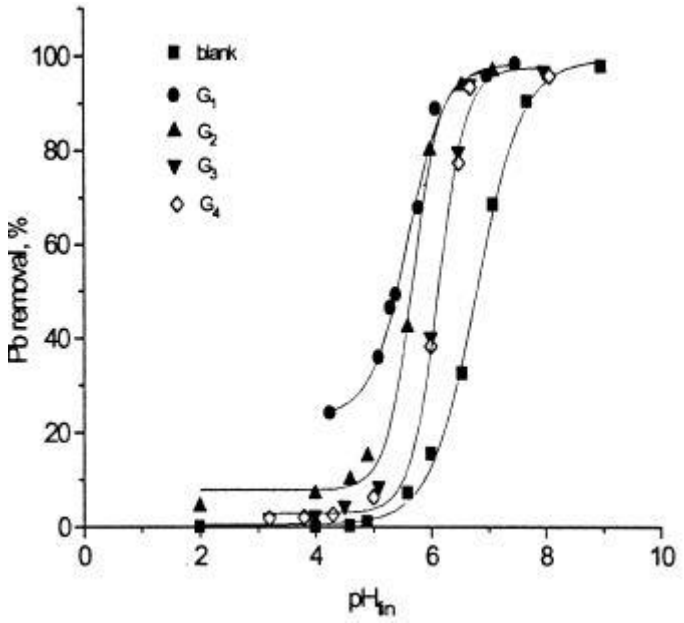

Figure 2.5:: Adsorption efficiency of Pb^{2+} ions with BFS as a function of pH and particle size (mm); G_1 (d_p < 0.25), G_2 (0.25-0.50), G_3 (0.50-0.63) and G_4 (0.63-0.80)
Dimitrova (1996)

The pH makes solid surfaces to be neutral at points of zero charge (PZC), positively charged below PZC and negatively charged above it. Thus, adsorption of positively charged ions like Me^{2+}, $MeOH^{+}$, etc. below PZC involve ion exchange with probably H^{+} from solid surfaces. However, at greater than PZC, adsorption is still possible but decreases once both solid surface and solutes are negatively charged (Ahmaruzzaman, 2011). Consequently, there is a unique pH at which different solids possess different PZC beyond which adsorption may increase or decrease depending on solid surface characteristics, speciation of metal ions, electrostatic forces and adsorption sites density (Huang and Rhoads, 1989; Rodda et al., 1993). Several studies, as discussed below, explored the effects of pH on the extent of metal ion adsorption with various solid surfaces.

Dimitrova (1996) investigated the effect of initial pH on adsorption of Cu^{2+}, Ni^{2+} and Zn^{2+} ions by blast furnace slag (BFS). Adsorption efficiency was high in alkaline pH, attributed to reduced loading of H^+ ions and creation of favourable conditions to form $MeOH^+$ and $Me(OH)_2$ that subsequently react with hydrolysed silicates to form scarcely soluble metal silicates on slag surfaces. The author established that calcium silicates in the slag hydrolysed to produce Ca^{2+}, Si^{4+} and an alkaline pH. This neutralising capacity of the slag is thought to provide favourable solution conditions for high adsorption efficiency of metal ions in alkaline pH. Later studies by Dimitrova and Mehandgiev (1998) also employed BFS to study effect of initial pH on Pb^{2+} adsorption. The authors obtained 98 % efficiency at pH > 6. The increase in pH was attributed to hydrolysis and ion exchange of glass phase (Eq. 2.13).

$$\Xi SiOCa + 2HOH = SiOH + Ca^{2+} + 2OH^- \quad --- \quad (2.13)$$

It was assumed that acid neutralisation and Pb^{2+} ion adsorption were dominant at pH < 5.5 while precipitation of Pb complexes ($PbOH^+$, $Pb_3(OH)^{2+}_4$,) occurred above pH 5.5. Dimitrova and Mehandgiev (2000) contacted single components of Cu^{2+}, Zn^{2+} and Ni^{2+} with BFS to get greater than 94 % efficiency in all cases. Partial dissolution of slag produces $2CaO.SiO_2$ (larnite), $Ca_2Al_2SiO_7$ (gehlenite) etc., which hydrolyse to give Ca^{2+}, OH^- and alkaline pH and create favourable conditions for high adsorption (Eq. 2.14 & 2.15). Dimitrova and Mehandgiev (2000) proposed that adsorption of metal ions involve ion exchange with mainly Ca^{2+} ions following slag hydrolysis. Both final pH and extent of Ca^{2+} ion dissolution depended on the presence of metal ions. The final pH decreased in the presence of metal ions and this was attributed to binding of OH^- ions with metal ions, however, Ca^{2+} ions increased in the presence of metal ions relative to blank solutions. An alkaline pH medium is therefore necessary to obtain high adsorption efficiency, rates and capacity.

$$\overline{Ca_2Al_2SiO_7} + 5H_2O = 2Ca^{2+} + 4OH^- + \overline{2SiO_2} \quad \text{---} \quad (2.14)$$

$$\overline{2CaO.SiO_2} + 2H_2O = 2Ca^{2+} + 4OH^- + H_4SiO_4 \quad \text{---} \quad (2.15)$$

Feng et al (2004) measured PZC for iron/steel slags and reported low adsorption of Cu^{2+} and Pb^{2+} ions at pH below PZC. The authors attributed low adsorption below PZC to electrostatic repulsion between metal ions and surface charges since slag surface is positively charged. However they obtained high adsorption capacities at pH 8.5 of up to 95.24 mg/g but still could not rule out the possibility of precipitation at such a pH value.

More recently, Xue et al (2009) studied adsorption of Cu^{2+}, Cd^{2+}, Pb^{2+} and Zn^{2+} ions by basic oxygen furnace slag (BOF) in both single and multicomponent systems. The authors reported an increase in adsorption efficiency with pH. The authors applied speciation diagrams and extended constant-capacitance surface complexation model to determine the mechanism of adsorption. For all ions, adsorption initially occurred on permanent charge site types at low pH through ion exchange process, followed by adsorption at variable charge sites (surface hydroxyl groups) involving complex formation at high pH. The shift in adsorption mechanism depended on the type of metal ion and pH. Selectivity was also different for different systems, i.e., Zn>Cu>Pb>Cd in single solutes and Pb>Cu>Zn>Cd in multisolutes. The differences in surface speciation reflected the fact that metal ions that readily form hydrolysis products adsorbed via complex formation on variable charge sites, i.e., Cu^{2+}, Pb^{2+} and Zn^{2+} surface species occurred as hydrolysed complexes but Cd^{2+} ion occurred and adsorbed as a divalent ion.

There is a general agreement among authors that alkaline pH favours high adsorption of metal ions and that the mechanism of adsorption process may be by ion exchange in acid solutions and by hydroxide precipitation towards alkaline pH.

Initial Concentration of Adsorbates

Dimitrova and Mehandgiev (1998) found the efficiency of metal ion adsorption to increase with increase in phase ratio at any given initial concentration, however, adsorption capacity decreased. The efficiency is also higher the lower the initial concentration and vice versa but adsorption capacity increases with an increase in initial concentration but only up to a limiting point. Dimitrova and Mehandgiev (1998) believed that adsorption of Pb^{2+} ions by BFS was not by precipitation but rather through ion exchange where Ca^{2+} ion dissolution from BFS created adsorption sites for Pb^{2+} ions. Furthermore, at high phase ratio, both Ca^{2+} ions and pH tend to maximum levels which limit adsorption sites density. Consequently, adsorption capacity of BFS was thought to be under-utilised at high phase ratios.

Xue et al (2009) found an increase in adsorbed amounts of Cu^{2+}, Pb^{2+}, Zn^{2+} and Cd^{2+} ions by basic oxygen furnace (BOF) slag with an increase in initial concentration. The selectivity sequence was Cu>Zn>Pb>Cd in single solutes but Cu>Cd>Pb>Zn in multisolutes. The adsorption of Cu^{2+} and Zn^{2+} ions via complexation on variable charge sites was highest in single solute systems, while Cd^{2+} and Pb^{2+} ion adsorption occurred via ion exchange on permanent charge sites. However, it is not certain what mechanisms dominate at either low or high solute concentration. Similarly, the efficiency of Pb^{2+} ion adsorption by steel slag increased with an increase in initial concentration beyond which efficiency was constant (Liu et al., 2010). It was explained that an increase in initial concentration increased the

concentration gradient of Pb^{2+} ions, which supports a fast transfer of Pb^{2+} ions from the bulk liquid to the BFS surfaces. However, this is contrary to the findings of many authors that have reported a high efficiency of metal ion adsorption from dilute solutions.

Adsorbent Particle Size

The efficiency of metal ion adsorption increases with a decrease in particle sizes because it is assumed that specific surface area increases. However, other diffusion rate limiting factors may be involved. Liu et al (2009) studied adsorption behaviour of Cr^{3+} ions as a function of particle size using steel slag. The authors observed an increase in adsorption efficiency with a decrease in particle size up to a certain size limit. A decrease in particle size increased surface area and this increased the opportunity for adsorption of Cr^{3+} ions on the outer surfaces of slag and possibly inside pores of particles through intraparticle diffusion. Also, diffusion resistance to mass transfer is greater for larger particles. Liu et al (2010) found similar kinetic results for Pb^{2+} ion adsorption by steel slag. Intraparticle diffusion was identified as rate controlling step, however, in the fine particle size range, resistance to intraparticle diffusion was eliminated.

Temperature

Lopez-Delgado et al (1998) obtained an increase in adsorption of several metal ions by BF sludge with increase in temperature within 20-80 ^{o}C and concluded that metal ion adsorption was an endothermic and spontaneous physical adsorption process, with surface complexation and precipitation probably involved. Dimitrova (1996) found an increase in temperature to increase both the hydrolysis of slag and adsorption capacity for Cu^{2+}, Ni^{2+} and Zn^{2+} ions by BFS. Curkovic et al (2001) explored adsorption of Pb^{2+} and Cu^{2+} ions by

electric arc furnace slag (EAF) and observed an increase in efficiency, adsorption constant (K_L) and Langmuir's adsorption capacity (Q_{max}) with temperature, with up to 30.6 mg/g Pb^{2+} and 31.8 mg/g Cu^{2+} at 40 ^{o}C. The results meant that the extent of adsorption of metal ions may require heat input to increase the efficiency of slag materials but heating requirement may be expensive.

Phase ratio

The efficiency of Cr^{3+} ion adsorption by steel slag increased with increase in phase ratio because of a possible increase in adsorption sites and/or surface area (Liu et al., 2009). Huifen et al (2011) explored adsorption of multisolute system of Cu^{2+}, Zn^{2+} Cd^{2+} and Pb^{2+} ions by steel slag as a function of phase ratio. The Zeta potential changed from negative to positive values at about 15 g/L slag. Thus, positively charged metal ions and other complexes adsorb onto slag surfaces with negative zeta potential below 15 g/L of slag dosage. Above this value, adsorption of negatively charged complexes onto slag surfaces with positive zeta potential is possible. The complexes are assumed to form through hydroxide precipitation by OH^- ions from slag hydrolysis. Thus, the mechanism of adsorption process may be by ion exchange below 15 g/L slag or hydroxide precipitation above 15 g/L of slag dose rate. Thus, mass of adsorbent has a pronounced effect on solute adsorption.

Rate of Agitation

Lui et al (2010) studied the kinetics of Pb^{2+} ion adsorption by steel slag. The efficiency of Pb^{2+} ion adsorption increased with increase in agitation rate up to a certain limit, beyond which efficiency was constant. An increase in the rate of agitation increased the diffusion coefficient of Pb^{2+} ions, thereby increasing the mass transfer flux. Thus, external diffusion

was identified as rate controlling step. At higher rates of agitation, resistance to bulk liquid diffusion was eliminated.

2.5.1.2 Adsorbent Activation

A few studies have shown that the material structure can be modified to improve adsorption. Dimitrova and Mehandgiev (2000) studied adsorption of Cu^{2+} ions with both granulated and ungranulated BFS. X-ray phase analysis depicted a crystalline structure in ungranulated BF, which gave Cu^{2+} adsorption efficiency of nearly 100 % compared to amorphous structure in granulated BFS whose copper adsorption was limited to about 35 %. Granulated BFS was then heated up to 800^{o}C transforming it into crystalline structure based on X-ray spectra. The % adsorption of Cu^{2+} increased to 100 %, that is, by nearly 3 times compared to untreated granulated BFS. However, specific surface area was low (< 1 m^2/g) with negligible change resulting from heat treatment. The authors concluded that slag crystallinity increases adsorption activity.

Dimitrova et al (2001) investigated effect of phase composition in BFS on Cu^{2+} adsorption by heating the slag in the range 400-1000 ^{o}C followed by controlled cooling. Above 600 ^{o}C, various silicates in slag had transformed to crystal form, mainly gehlenite as confirmed by SEM and X-ray analyses. Control adsorption experiments with pure but synthetic gehlenite and akermanite were also carried out. The degree of crystallisation increased with increase in activation temperature. Dimitrova et al (2001) observed an increase in adsorption capacity for Cu^{2+} ions of up to 4 times higher in crystalline BFS and concluded that crystalline slag is a more efficient adsorbent for Cu^{2+} ions than amorphous one. However, despite an increase in adsorption capacity, the surface area decreased as activation temperature

increased. Thermal treatment had no effect on finely sized slag particles yet they exhibited highest Cu^{2+} adsorption. This was attributed to the possibility of slag being already in crystal form in this size range. Adsorption data for thermally activated slag and untreated synthetic crystalline minerals were similar and this further supported the idea of improved sorption activity for metal ions in crystal phases. Adsorption of Cu^{2+} was followed by Ca^{2+} ion dissolution and increase in equilibrium pH (Dimitrova et al., 2001).

2.5.2 Proposed Mechanisms of Adsorption Process

Generally, the process of adsorption for metal ions with silicate based adsorbents occurs through ion exchange, adsorption and precipitation mechanisms (Dushina and Aleskovski, 1976; Lopez et al., 1995; Dimitrova and Mehandgiev, 1998; Feng et al., 2004; Kim et al., 2008). Silicate phases in slags undergo hydrolysis to support ion exchange and/or precipitation depending on pH and metal ion concentration.

Benjamin and Leckie (1981) studied competitive adsorption in binary systems among Cd^{2+}, Cu^{2+}, Pb^{2+} and Zn^{2+} ions on iron oxyhydroxide surface ($Fe_2O_3.H_2O$) in which the concentration of a more strongly binding metal ion was up to 100 times that of the other metal ion. Because adsorption of weakly binding metal was not significantly reduced, they concluded that competitive interactions were minimal and that the strong binding sites for one metal were not preferred binding sites for another metal, thus, suggesting that the surface of $Fe_2O_3.H_2O$ consists of several distinct groups of binding sites. Yamashita et al (1983) proposed that metal ion adsorption by converter furnace steel slag probably occurred by ion substitution with CaO and MgO phases, hydroxide precipitation at high pH, sulphide precipitation and coprecipitation by sulphur and iron oxides respectively as well as

possible adsorptive effects of $2CaO.SiO_2$ phase. Dimitrova (1996) believed the process of adsorption is facilitated by chemical interaction of dissolved slag components with metal ions and subsequent deposition of such products on slag surfaces.

Lopez et al (1995) studied Pb^{2+} adsorption with BF sludge and applied XPS/EDX techniques to calculate XPS intensity ratios to prove Pb^{2+} adsorption on sludge surface. Further, Ca Kα peak intensity decreased after Pb^{2+} adsorption to suggest Ca^{2+} substitution by Pb^{2+} ions. A control experiment with carbon showed that EDX spectra supported ion exchange only in silicate based BF sludge. It was concluded that Pb^{2+} adsorption on BF sludge surface is a physical adsorption process with partial ion exchange on the sludge surfaces. Dimitrova (1996) measured Ca^{2+} and Si^{4+} dissolution from BFS in the absence and presence of Zn^{2+} ion adsorption. They noted a constant ratio for $CaO:SiO_2$ in the system without Zn^{2+} and concluded that $2CaO.SiO_2$ undergoes partial hydrolysis. However, Ca^{2+} ion concentration was many times higher than that of Si^{4+} ions when Zn^{2+} ions were introduced, which suggested non equivalent ion exchange between Ca^{2+} and Zn^{2+} ions. The lack of equivalence during ion exchange process was attributed to interactions of metal ions with colloidal silicic acid and variations in soluble silicon.

Further studies by Dimitrova and Mehandgiev (2000) explored mechanisms of individual ion adsorption of Cu^{2+}, Zn^{2+} and Ni^{2+} ions by BFS by measuring dissolved Ca^{2+}, Si^{4+} and pH from slag hydrolysis. The authors noted low Ca^{2+} ions in blank solutions but observed high amounts of Ca^{2+} ions in the presence of metal ions. They proposed non-equivalent ion exchange between metal ions and Ca^{2+} ions partly because of incomplete slag hydrolysis. It

is likely that other alkali ions participate in the ion exchange process. They did not rule out possibility of precipitation on $Al(OH)_3$ and H_4SiO_4 components of slag hydrolysis.

A similar study by Dimitrova et al (2001) also reported non-equivalent ion exchange between Cu^{2+} and Ca^{2+} ions. Electron Paramagnetic Resonance (EPR) spectroscopy revealed oxidation state of Cu(II) for adsorbed copper ions. However, X-ray photoelectron (XPS) spectroscopy could not identify any chemical species to provide other definitive copper compounds. This was evident from EPR and XPS spectra of predominantly Cu^{2+} ions. Copper silicates are believed to form but could not be distinguished in solid phases. The non-equivalence nature of ion exchange is attributed to either competitive adsorption effect of H^+ ions, formation of $Ca(OH)_2$ or possibility of blockage of active sorption sites by soluble Ca^{2+} and/or Mg^{2+}. Dimitrova et al (2001) explained that high adsorption of Cu^{2+} ions in crystalline slag was due to the creation of active adsorption sites through isomorphous substitution (type Al^{3+} -> Si^{4+}) induced during crystallisation. Adsorption occurred inside the crystal lattice and spaces relative to amorphous slag where adsorption is limited to the surface. Adsorption of Cu^{2+} ions occurred on (Al, SiO^-) sites whose negative charge is initially balanced by divalent alkali ions. In acidic pH, ΞSOH sites (S = Si/Al) may also support Cu^{2+} ion adsorption as shown in Equations 2.16 and 2.17 below.

$$\overline{(Al,SiO)_2^-}Ca^{2+} + 2H^+(aq) \Leftrightarrow 2\overline{(Al,SiO)^-}H^+ + Ca^{2+}(aq) \quad \text{---} \quad (2.16)$$

(Blank solutions)

$$\overline{(Al,SiO)_2^-}Ca^{2+} + Me^{2+}(aq) \Leftrightarrow \overline{(Al,SiO_2)^-}Me^{2+} + Ca^{2+}(aq) \quad \text{---} \quad (2.17a)$$

or $$\overline{(\equiv SO)_2^-}Ca^{2+} + Me^{2+}(aq) \Leftrightarrow \overline{(\equiv SO)_2}Me^{2+} + Ca^{2+}(aq) \quad \text{---} \quad (2.17b)$$

Where overbar = solid phase, $\equiv SO^-$ = deprotonated surface site, S = Al/Si; Me^{2+} = metal ion (Cu^{2+}, Zn^{2+}, Ni^{2+} etc.)

Feng et al. (2004) varied mass of steel slag addition and measured pH and Ca^{2+} ions released and observed that both had increased with increase in mass of slag. This reaction was thought to indicate ion exchange between H^+ and Ca^{2+} ions. Consequently, metal ions tend to be suppressed in preference to H^+ adsorption. Iron slag had higher ion exchange ability because of higher Ca^{2+} ions released relative to steel slag. This conclusion is in agreement with higher adsorption of metal ions obtained for iron slag which also had higher surface area and highly porous structure. SEM images revealed loose floc deposits on slag surfaces suspected to be copper hydroxide and silicate complexes. Feng et al (2004) concluded that iron slag possess higher ion-exchange, adsorption and acid-neutralising abilities relative to steel slag and that metal removal occurred by both precipitation and ion-exchange, but the relative contributions is not clear. Kim et al. (2008) used Langmuir adsorption capacity values to calculate that about 88 % of Cu^{2+} ions were removed as $Cu(OH)_2$ precipitates at pH ≥ 3.0 and only 12% by adsorption. The authors concluded that the principle mechanism of copper extraction was by hydroxide precipitation supported through slag hydrolysis and not adsorption on the surfaces of slags without direct empirical evidence. This is also contrary to views held by Dimitrova (1996; 1998; 2000) and other studies.

More recently Xue et al (2009) studied a multisolute adsorption system of Cu^{2+}, Cd^{2+}, Pb^{2+} and Zn^{2+} ions by Basic Oxygen Furnace (BOF) slag at same initial concentration. Solute adsorption decreased relative to their respective single system which was attributed to competitive adsorption. The Cu^{2+} ions possibly suppressed uptake of Cd^{2+} and Zn^{2+} ions on

variable adsorption sites by complex formation while Cd^{2+} ions decreased adsorption of Cu^{2+} and Pb^{2+} on ion exchange sites. It is assumed that an increase in amounts of a more strongly bonded Cu^{2+} ions reduced the number of available sites. Liu et al (2009) conducted a multisolute adsorption study involving Cr^{3+}, Cu^{2+}, Pb^{2+} and Zn^{2+} ions at the same concentration and found the level of adsorption of these metal ions to be different and selective (Cr^{3+}>Zn^{2+}> Cu^{2+}>Pb^{2+}) although adsorption was carried out at the same initial concentration. Similar to the results of Xue et al (2009), Liu et al (2009) also observed a decrease in adsorption capacity of steel slag in multisolutes compared to single solutes. It was not clear why loading of these metal ions was selective and lower in multisolute system. In many instances, supporting evidence for the proposed mechanisms of metal adsorption with slags is not clear.

2.5.3 Modeling of Adsorption Systems of Metal ions

2.5.3.1 Adsorption Isotherms

An adsorption isotherm governs the retention of an adsorbate from an aqueous phase to a solid phase at constant pH and temperature. These mathematical correlations depict graphical expression of solid phase concentrations against the residual concentration. The isotherms are important in design and industrial application of adsorption systems. Foo and Hameed (2010) reviewed many isotherms such as Brunauer–Emmett–Teller (BET), Redlich–Peterson, Dubinin–Radushkevich, etc. but the Langmuir and Freundlich adsorption Isotherms, given in Equations 2.18 and 2.19, are commonly used to determine the adsorption capacity of different adsorbents (Foo and Hameed, 2010).

Langmuir: $$q_e = \frac{Q_o b C_e}{1 + b C_e}$$ --- (2.18)

Freundlich: $$q_e = K_F C_e^{1/n}$$ --- (2.19)

Where q_e (mg/g) = amount of solute adsorbed at equilibrium, Q_o = maximum amount of solute adsorbed, C_e = residual liquid phase concentration at equilibrium (mg/l), b = Langmuir adsorption coefficient; K, n = empirical Freundlich constants

Linear fits of either Langmuir or Freundlich or both isotherms appear to offer satisfactory interpretation of the mechanism of adsorption process and evaluation of slag capacity of single solutes. On the basis of regression coefficients (R^2), Langmuir isotherm was better fitted to adsorption data than Freundlich isotherm for Pb^{2+} ion adsorption (Lopez et al., 1995) as well as Cu^{2+}, Pb^{2+}, Zn^{2+}, Cd^{2+}, Cr^{3+} adsorption (Lopez-Delgado et al., 1998) by BF sludge. In other articles Freundlich isotherm gave a better description of Cu^{2+}, Ni^{2+} and Zn^{2+} adsorption by BFS (Dimitrova, 1996). Further, Dimitrova and Mehandgiev (1998) found Pb^{2+} ion adsorption by BFS to fit Freundlich adsorption isotherm well, while Curkovic et al (2001) established that Langmuir isotherm was a better model to describe Pb^{2+} and Cu^{2+} adsorption on EAF slag than that of Freundlich. Other applications of Langmuir Isotherm are Pb^{2+} and Cu^{2+} ion adsorption with iron and steel slags (Feng et al., 2004), better fits of Langmuir than Freundlich isotherms have been reported for Cu^{2+} ion adsorption by slags (Kim et al., 2008) and Pb^{2+} ion adsorption by steel slag (Liu et al., 2010). However, complex interaction of metal ions with slag surfaces and hydrolysis products make it difficult to interpret and predict multicomponent adsorption data.

Multisolute adsorption may be complicated by the effects of interaction and competition between solutes and adsorbent (McKay, 1991). The use of multicomponent adsorption models such as non-modified and modified Langmuir, extended Langmuir and Freundlich etc. have been published but Ahmaruzzaman (2011) argued that one cannot obtain a meaningful physical interpretation of the mechanism of the adsorption process with such. Xue et al (2009) applied extended constant-capacitance surface complexation model to describe adsorption of Cu^{2+}, Cd^{2+}, Pb^{2+} and Zn^{2+} ions by BOF. This model proposes an ion exchange process at low pH on permanent charge sites, and formation of metal complexes on variable charge sites (surface hydroxyl groups) at high pH. The model provided good fits of adsorption data for all metal ions in both single and multisolute systems. However, lack of good fits in multisolutes particularly for Cu^{2+} and Pb^{2+} ions was attributed to complicated surface chemistry of these metal ions that probably involved surface co-precipitation and/or formation of multi-solute adsorbates. The authors proposed direct methods such as extended X-ray absorption fine structure spectroscopy (EXAFS) to determine the mechanism of adsorption in multisolute systems.

2.5.3.2 Kinetic models

The rate of solute adsorption is controlled by three classical steps, i.e., external diffusion across liquid film that surrounds adsorbent particles, pore diffusion in the internal pore sites of the adsorbent and adsorption step which may involve physisorption, chemisorption, ion exchange, precipitation, complexation (Qiu et al., 2009). The overall rate of kinetic process is then determined by the rate of the slowest step (Dabrawski, 2001). The use of pseudo first order, pseudo second order and Elovich's rate equations based on chemical adsorption as well as intra particle diffusion and Boyd's film diffusion models appear frequently in

literature to analyse the kinetics of adsorption. A summary of commonly used kinetic models is given in Table 2.5 below.

Table 2.5: Some of the commonly used kinetic models

Rate Equation	Differential	Non Linear	Linear transformations	Linearized plots
Lagergren's pseudo first order	$\frac{dq_t}{dt} = k_1(q_e - q_t)$	$q_t = q_e(1 - e^{-kt})$	$\log(Q_e - Q_t) = \log(Q_e) - \frac{k_1}{2.303}t$	log $(Q_e\text{-}Q_t)$ vs. t
Ho's pseudo second order	$\frac{dQ_t}{dt} = k_2(Q_e - Q_t)^2$	$q_t = \frac{q_e^2 kt}{1 + q_e kt}$	$\frac{t}{Q_t} = \frac{1}{kQ_e^2} + \frac{1}{Q_e}t$	t/Q_t vs. t
Elovich	$\frac{dQ_t}{dt} = a\, e^{-\alpha Q_t}$	-	$Q_t = \alpha\ln(a\alpha) + \alpha\ln(t)$	Q_t vs. ln(t)
Weber-Morris Intraparticle diffusion	$Q_t = k_i\sqrt{t}$	-	-	Q_t vs. $t^{1/2}$
Boyd's diffusion	-	-	$\ln\left(1 - \frac{q_t}{q_e}\right) = -R^1 t$	$\ln\left(1 - \frac{q_t}{q_e}\right) vs\, t$

Where (Q_t, Q_e) = amount of metal ions adsorbed per unit weight of adsorbent (mg/g) at any time t (min) and at equilibrium respectively, k_1 is first order adsorption constant (mg/g min), $h = kQ^2_e$ = second order initial adsorption rate (mg/g min); a = desorption constant (g/mg), α = initial adsorption rate (mg/g min), k_i = intraparticle diffusion rate constant (mg/g $min^{-1/2}$), k_2 is second order adsorption constant (mg/g min)

Several researchers have applied chemical and diffusion models to analyse the kinetics of different adsorption systems. Liu et al (2009) observed an initially high rate of Cr^{3+} ion adsorption by steel slag, and attributed it to the availability of large surface area at the start of the adsorption process. However, as adsorption progressed, adsorption sites probably

become exhausted and the rate of adsorption become controlled by the rate at which Cr^{3+} ions diffused from exterior to the interior sites of slag particles. Curkovic et al (2001), Dimitrova (1996) and others (Huifen et al., 2011; Motsi et al., 2009; Xue et al., 2009) have reported a kinetically fast initial adsorption step followed by slower second phase during adsorption of various metal ions with slags and zeolites. Dimitrova (1996) attributed limited mass transfer kinetics of Cu^{2+}, Ni^{2+} and Zn^{2+} ions to low rates of internal solute diffusion inside BFS structure. Slower kinetics were also evident in solutions of high solute concentrations. The authors suggested that possible formation of sparingly soluble silicate complexes and precipitates on slag surfaces decreased solute diffusion rates by limiting solute access to the internal slag structure.

Feng et al (2004) studied the kinetics of Cu^{2+} and Pb^{2+} ion adsorption. Pb^{2+} ions adsorbed faster and higher than Cu^{2+} ions in both slags. Iron slag had higher loading capacity than steel slag possibly due to higher CaO content, % porosity and specific surface area. The data was fitted to pseudo second order kinetic model where the rate constant increased with pH for slag with high CaO, suggesting that adsorption rate was probably controlled by CaO content. Liu et al (2010) reported that the pseudo second order kinetic equation gave a better linear fit of data for Pb^{2+} ion adsorption by steel slag than pseudo first order equation.

2.5.4 Continuous Flow Adsorption Kinetics and Case Studies

Gao et al (1995) investigated adsorption and desorption of metal ions in continuous flow fixed bed columns packed with iron slag and compared its efficiency to polymeric chelating

ion exchangers. The authors hypothesised the gypsum phase to be filler material, iron oxides as the adsorbent whilst akermanite hydrolysed slowly to give OH^- ions and maintain an alkaline pH (Eq. 2.20).

$$\overline{Ca_2MgSi_2O_7}(solid) + 3H_2O = 2Ca^{2+} + Mg^{2+} + 6OH^- + \overline{2SiO_2}(solid) \text{ ---} \quad (2.20)$$

A multiadsorbate feed stream of 250 mg/L Na^+; 2 mg/L Cd^{2+}, Ni^{2+}, Pb^{2+}; and 0.1 mg/L Cu^{2+} were nearly completely adsorbed, with the sequence of adsorption reported as $Pb^{2+} > Cu^{2+} >> Ni^{2+} > Cd^{2+}$. The slag had a high affinity for metal ions despite the likely competitive effect of high Na^+ ion concentration. Cd^{2+} ion adsorption by the slag compared well with that of commercial chelating ion exchangers. Complete Zn adsorption was also achieved at relatively high concentration. However, adsorption of 3 mg/L Zn^{2+} ions in the presence of respective 100 mg/L Na^+ and 50 mg/L Ca^{2+} ions decreased Zn ion adsorption, with stronger competitive effects from divalent Ca^{2+} than monovalent Na^+ ions. Benjamin and Leckie (1981) obtained similar results using iron oxyhydroxides as adsorbent.

Gao et al (1995) believed electrostatic and acid-base interactions in slags were responsible for metal ion adsorption. Hydrolysis of akermanite eliminates H^+ adsorptive competition thus improving metal ion adsorption. The stoichiometry of metal ion adsorption involves both an akermanite phase and adsorption sites on iron oxides (Eq. 2.21). Column interruption tests suggested akermanite hydrolysis and intra particle diffusion to be rate limiting.

$$\overline{Ca_2MgSi_2O_7} + \overline{2(\equiv SO^-)Na^+} + 6H^+(aq) + Me^{2+}(aq) + 3H_2O = 2Ca^{2+}(aq) + Mg^{2+}(aq) + 2Na^+(aq) + 6H_2O + \overline{2SiO_2} + \overline{(\equiv SO^-)_2 Me^{2+}} \quad \text{... (2.21)}$$

The adsorption mechanism was considered more prevalent over precipitation based on low metal ion concentrations (below solubility limit) at all pH values. The slag also had high neutralizing capacity of about 1-2 m_{eq} H^+/g.

Slag regeneration involving ethylenediamine and ammonia were effective in metal ion desorption and slag regeneration, and did not attack slag components (e.g. akermanite) relative to other organic and mineral acids. Akermanite is sparingly soluble and desorbs metals through ion exchange and complexation processes (Eq. 2.22) (Gao et al., 1995).

$$\overline{\left(\equiv SO^-\right)_2 Me^{2+}} + 2Na^+(aq) + nNH_3(aq) = 2\overline{\left(\equiv SO^-\right)Na^+} + \left[Me\left(NH_3\right)_n\right]^{2+}(aq) \quad \text{--- (2.22)}$$

The disposal of slags whose surfaces are loaded with metal ions is a challenge. In a paper by Lopez et al (1995), Pb loaded BF sludge leaches easily to release back potentially toxic and hazardous Pb^{2+} ions. Thus, to recover and recycle metals ion present in BF sludge, Lopez et al (1995) suggested Pb recovery with NaOH. Other options use pyrometallurgical steps to recover Fe and Pb and to make use of potential energy in coke present in BF sludge, although another slag is produced.

Feng et al (2004) conducted batch experiments to determine the effect of phase ratio on adsorption efficiency with actual AMD containing multiple metal ions at pH 2. At 30 g/L dosage, iron slag performed better than steel slag to give final Cu^{2+}, Pb^{2+} and Cr^{3+} adsorption to below 0.05 mg/L, with near neutral pH at equilibrium. However, adsorption of Fe^{2+}, Mn^{2+}, Al^{3+}, Si^{2+} and precious metal ions were unsatisfactory. Although slags were effective in binary systems, they were ineffective in the real adsorption system of several ions. This

clearly suggests that studies must focus a lot more on multicomponent systems in order to fully understand the adsorption process involving slag materials and various interactions and variables at play. This approach has been adopted in this thesis.

Direct acid mine drainage (AMD) treatment using steel slag was studied by placing slags directly in a stream of AMD as lime replacement with mixed results (Ziemkiewicz and Skousen, 1998). Constructed steel slag leach beds (SLB) have also been studied to treat acid mine drainage (AMD). High alkalinity that was leached from steel slag surfaces was contacted with AMD to give promising acid neutralisation and metal ion precipitation results. However, there were problems of a decrease in alkalinity production and flow rates and formation of thick precipitate layers within effluent pipes and slag (Goetz and Riefler, 2014).

Real AMD was effectively treated by a combination of oxidation with H_2O_2, precipitation by lime and H_2S followed by filtration of precipitates magnetically to give acceptable discharge limits of metal ions. Finally, AMD, free of heavy metal ions, was subjected to ion exchange process to extract alkali ions (Ca^{2+}, Mg^{2+}, K^{+}, Na^{+}) and anions (SO^{2}_{-4}, Cl^{-}, Br^{-}, F^{-}) (Feng et al., 2000). However, the cost implication of such a practical process with multiple stages may need to be addressed fully. Electrolytic recovery of copper and iron from AMD has been demonstrated (Bunce et al., 2001; Gorgievski et al., 2009). It has been argued that the low cost of electricity is an advantage in electrochemical remediation relative to cost of chemicals in precipitation processes. The determination of the feasibility of electrodeposition in complex mixtures of metal ions is required.

2.6 Summary of Literature Review

Several studies indicate that most of the methods currently in use to treat AMD and other process effluents involve application of chemicals to reduce the acidity and sulphate levels and precipitate metal ions. However, these chemicals are less efficient and may be uneconomic in treating effluents with metal ion concentration below 1000 mg/L. The purification of AMD by adsorption process using solid wastes (slags, fly ash, etc.) and low value natural materials (zeolites, etc.) has provided promising results as an alternative to chemical precipitation. However, several knowledge gaps must be addressed in order for this opportunity to be developed into a practical process. For instance, further studies in multicomponent systems of metal ions that reflect actual industrial effluent composition are required in both batch and continuous flow reactors to fully understand the adsorption process. There is also a limited use of adsorbent characterisation results to interpret observed metal ion adsorption behaviour. There is need to identify and improve key adsorptive properties like surface area, micro/mesoporosity and surface functional groups. The proposed mechanisms of metal ion adsorption with slag materials appear to be inconsistent in similar adsorption systems. There is lack of detailed studies on desorption and recovery of metal ions and methods of adsorbent improvement and/or regeneration and subsequent disposal challenges of exhausted/spent adsorbents and eluates.

Consequently, this study was proposed to understand multicomponent adsorption behaviour of metal ions using slag materials as adsorbents under various experimental and solution conditions. The next chapter describes the materials, methods and analytical procedures that were employed in this study.

CHAPTER 3
MATERIALS AND METHODS

3.1 Introduction

This chapter describes the materials, methods and analytical techniques that were employed to study the development of sustainable, novel adsorbents from slag materials for application in the purification of waste solutions. Some of the experimental methods of determining solid phase extraction by adsorption from solid/liquid systems include immersion, circulation, chromatographic and slurry methods (Everett, 1986; Rouquerol et al., 2014). This study employed the immersion method of adsorption from solutions to characterise the adsorptive capacity, mechanisms, equilibria, kinetics and efficiency of slag materials by investigating the effect of key adsorption variables and slag activation techniques. Immersion method is simple and widely used with acceptable accuracy but the technique may be tedious. It involves adding a known mass of fresh adsorbent to a measured volume of solution of known concentration in a suitable thermostated adsorption vessel, which is sealed and equilibrated by agitation. A sample is withdrawn and analysed to obtain change in concentration.

The chapter also discusses the preparation of synthetic waste solutions to simulate chemical compositions of common metal ions and acidity levels typical in actual acid mine drainage (AMD) systems. Furthermore, the chapter gives the main experimental framework subdivided into detailed characterisation of slag materials (Section 3.2.2), batch adsorption experiments using both stirred tank reactor (STR) and bottle-rolling techniques (Section

3.3.2), and continuous flow adsorption experiments in a fixed bed adsorption column (Section 3.3.3) to investigate the adsorptive performance of slags in single and multicomponent adsorptive systems.

3.2 Materials, Sampling and Characterisation

This section describes the types of iron and steelmaking slag materials that were used as adsorbents, characterization techniques and procedures that were employed to measure and assess various physical and chemical properties of slags relevant to the adsorption process.

3.2.1 Sample Collection and preparation

This study employed granulated blast furnace slag (BFS) as the primary adsorbent material to study the development of sustainable adsorbents from slag materials to treat synthetic acid mine drainage (AMD) wastewater but the study also conducted less extensive investigations involving electric arc furnace slag (EAF). Samples of these slag materials were supplied by Lafarge/Tarmac Ltd UK.

3.2.2 Characterisation of Adsorbent Materials

The relevant adsorptive properties of blast and electric arc furnace slags were examined by using standard materials characterization techniques. The properties that were analysed include particle size distribution, pore size distribution, surface morphology, chemical and mineral phase composition, specific surface area and density.

3.2.2.1 Particle Size Distribution

The particle size distribution (PSD) of as-received slag materials was carried out by dry sieve analysis using a series of seven (7) sieves, i.e., 4.00 mm; 2.80 mm; 1.70 mm; 1.00 mm; 0.50 mm; 0.36 and 0.18 mm. A representative slag sample of about 300 g was prepared from bulk dried slags by means of a riffle splitter, and transferred to the nest of sieves which were then mechanically vibrated on a vibratory sieve shaker for 20 minutes. This time was sufficient to achieve complete particle classification. The weights of each size fraction retained on each sieve were measured and recorded. A plot of cumulative % undersize against sieve aperture was carried out to determine particle mean, median and mode diameters and various other key diameters. Sieve analysis was also conducted on slag samples to generate various size fractions as specified in Sections 3.3.3.4.1 and 3.3.2.5.1 in order to study the effect of particle size on adsorption efficiency. A Malvern Mastersizer was employed to establish PSD for the material below 45 μm size. The mastersizer instrument is a laser diffraction particle size analyser that was based on wet dispersion systems (Malvern Instruments Ltd, 2015).

3.2.2.2 Pore Size Distribution

An AutoPore IV 9500 V1.09 Micromeritics Mercury Porosimeter UK was employed to determine pore size distribution of various samples of slags. Samples of about 0.500-1.000 g were added to glass penetrometers. Each penetrometer was sealed using a sealing plate, sealing ring and Apiezon H hydrocarbon grease. Hg intrusion into samples was measured using an AutoPore IV mercury porosimeter at pressures in the range 3 kPa - 207 MPa. The data were analysed using the Washburn equation (Eq. 3.1) in order to determine the pore size distribution, assuming cylindrical pore geometry.

$$D = -\frac{4\gamma}{P}\cos(\theta) \qquad \text{---} \quad (3.1)$$

Where *D* = pore diameter, *P* = applied pressure, γ = surface tension of Hg at 18 °C (assumed to be 0.485 N/m), and θ = contact angle between the Hg and the solid (assumed to be 130 ^{o})

3.2.2.3 Surface Morphology

A Philips XL-30 Environmental Scanning Electron Microscope (ESEM)-FEG fitted with an Oxford Inca 300 Energy Dispersive Spectroscopy (EDS) software was used to determine the morphology and chemical composition of slag surfaces. Slag samples were treated with a thin coating of carbon/gold in a vacuum chamber to increase their conductivity. A thin coating results in better scans but still preserves the identity of the material. Samples were then fixed on a brass disc/stage by sticky carbon tape. Both carbon/gold coating and sticky carbon tape help to suppress accumulation of surface charge on samples during analysis. Samples were placed into a microscope vacuum chamber stage and analysed at various magnifications.

3.2.2.4 Specific Surface area

The surface area and pore size distribution of slags were measured using the BET method by performing nitrogen adsorption and desorption on slag samples at a temperature of 77K using Micromeritics Instrument ASAP® 2010 to obtain an adsorption isotherm. About 3-6 g of slags were initially degassed at elevated temperature of about 200 ^{o}C to remove moisture and other contaminants. The integrated ASAP 2010V5 03 software facilitates the collection and analysis of data by BET Equation (3.2) which relates N_2 adsorbed at a given partial pressure to the volume adsorbed at monolayer coverage. The formation of surface

monolayer of gas molecules on slags is used to estimate specific surface area, while capillary condensation of N_2 gas enables determination of pore sizes, pore volume and pore size distribution. N_2 is used because it is cost-effective, inert, and available in high purity and its molecular size is well established.

$$\frac{P}{V(P_o - P)} = \frac{1}{V_m C} + \frac{(C-1)P}{V_m C P_o} \qquad \text{----} \qquad (3.2)$$

Where P = partial pressure of N_2, P_o = saturation pressure at the experimental temperature, V = volume adsorbed at P, V_m = volume adsorbed at monolayer at N_2 coverage, C = constant.

The BET surface area (S_{BET}) is then calculated by equation 3.3.

$$S_{BET} = \frac{V_m N_a a_m}{m_v} \qquad \text{----} \qquad (3.3)$$

where N_a = Avogadro's number (6.022 x 10^{23} mol^{-1}), a_m = cross-sectional area occupied by each adsorbate molecule at 77K (0.162 nm^2) and m_v = gram-molecule volume (22.414 mL)

3.2.2.5 Chemical Composition

A quantitative analysis of the chemical composition of slags was conducted by using a Bruker S8 Tiger Wavelength Dispersive X-Ray Spectrometer (XRF). The analysis was conducted on pressed pellets formed from a mixture of slag samples and XRF binding wax. The slag samples were ground into fine powder and mixed with XRF binding wax in the ratio of approximately 0.500 g slag sample to 0.100 g of wax. The mixture was again ground to a homogenous powder and subsequently pressed into a 8 mm pressed pellet at 2-3 tonnes pressure. This resulted into a pressed pellet with a flat surface that gives more accurate

results than loose powder. The pellet is placed into the sample holder assembly and loaded into the XRF machine. Using QuantExpress software, a full analysis of elements or oxides was conducted for 20 minutes to obtain best detection and analysis. Helium is used to displace air between the sample and detector for better X-ray transmission. The XRF data is then evaluated to determine both qualitative and quantitative elemental/oxide composition of slag samples.

3.2.2.6 Phase Composition

The chemical phases present in slags were examined by Siemens D5005 powder X-Ray diffractometer (XRD). The slag samples were ground into fine powder and placed into a sample holder. The top surface of the sample was smoothed with a microscope slide to produce a flat surface and then loaded into the sample holder of the XRD machine, with care not to disturb the surface. The phases were identified with CuKα radiation on these powdered samples. The angles explored were 5^{o} to 80^{o} in 2θ at a fixed scanning rate for 10-60 minutes. The Eva XRD software was used for data analysis. This was carried out by matching elements with peaks of the XRD pattern by searching XRD database for chemical compounds or phases which could be present based on elements detected from results of XRF analysis.

3.2.2.7 Density

The true densities of slags were measured by AccuPyc II 1340 V1.05 Micromeritics Helium Pycnometer UK employing 20 measurements per sample. The sample chamber was allowed to equilibrate at 134 kPa for each measurement cycle.

3.2.2.8 Surface Chemistry

Fresh slag samples and those with surfaces adsorbed with metal ions from multicomponent adsorption systems as a function of solution pH were sent to Kratos Analytical Ltd (Manchester, UK) for X-ray photoelectron spectroscopy (XPS) analysis to quantitatively measure the elemental composition, empirical formula, chemical/oxidation states, bonding energies and electronic state of the elements on slag surfaces. This is useful in order to deduce the mechanisms of adsorption process for metal ions, which is presented in Section 6.3.5 of Chapter 6 in this thesis.

3.3 Methods, Experimental Setup & Procedure

This section describes the specifications, type and setup of adsorption equipment used. It also describes the experimental procedure for both batch and continuous adsorption methods that were chosen to evaluate the adsorption potential of slag materials. Further, the sampling procedure, analytical measurements and calculations to monitor the progress of adsorption of metal ions are discussed.

3.3.1 Preparation of Stock and Waste Solutions

All adsorption experiments were based on treating synthetic waste solutions of single and multicomponent systems of different metal ions, concentration and acidity in a metal-sulphate system that simulated average chemical compositions of actual acid mine drainage systems and related waste solutions. Stock solutions of between 1000-5000 mg/L metal (Me^{2+}) ion concentrations for Cd^{2+}, Co^{2+}, Cu^{2+}, Fe^{2+} and Mn^{2+} ions were prepared separately from their respective analytical grade (AR) chemicals of $3CdSO_4.8H_2O$, $CoSO_4.7H_2O$,

$CuSO_4.5H_2O$, $FeSO_4.7H_2O$ and $MnSO_4.4H_2O$ procured from Fisher Scientific UK. At the desired concentration level of Me^{2+} ions, these stock solutions were prepared by measuring and dissolving a calculated mass of the solid chemicals to make 1 litre solutions with distilled water. A sample calculation for the mass of solid iron (II) sulphate salt required to achieve a stock concentration of 2000 mg/L Fe^{2+} ions is given in Equation (3.4) below. Molecular mass of $FeSO_4.7H_2O$ = 278.02 g/mol and molecular mass of Fe = 55.85 g/mol, therefore;

$$55.85\frac{g}{mol}\ Fe^{2+}ions \quad \rightarrow \quad 278.02\frac{g}{mol}FeSO_4.7H_2O$$

$$2000\frac{g}{mol}Fe^{2+}ions \quad \rightarrow \ ??$$

--- (3.4a)

Therefore, mass of $FeSO.4H_2O$ required to produce 2000 mg/L Fe^{2+} ions of stock solution is;

$$\frac{2000\frac{mg}{L}\times 278.02\frac{g}{mol}}{55.85\frac{g}{mol}} = 9956\frac{mg}{L} = 9.956\frac{g}{L}FeSO_4.7H_2O$$

--- (3.4b)

Subsequent waste solutions composed of single metal ions to be treated were prepared by diluting stock solutions with distilled water using the dilution Equation 3.5 below to obtain the desired metal ion concentration. Similarly, multicomponent solutions of metal ions were also prepared by diluting stock solutions of individual metal ions followed by mixing the resulting volume fractions to obtain the desired metal ion concentration levels in the desired final working volumes of waste solutions to be treated, usually 0.5-1.0 litres. The chemical compositions of either single or multicomponent adsorptive systems to be purified simulated average compositions of actual acid mine drainage. These metal ions were

selected to represent some of those ions prevalent in reported incidences of acid mine drainages at Wheal Jane Mine UK and the Zambian Copperbelt. The desired acidity (solution pH) was adjusted manually using 1 M NaOH or H_2SO_4 solutions. An example of necessary calculations to determine the required volume from a stock solution of 2000 mg/L Fe^{2+} ions that must be diluted to obtain 400 mg/L Fe^{2+} ions in 1 litre as the final working volume of waste solution to be treated in an adsorption vessel is given in Equations 3.5 and 3.6 below.

$$M_1 \times V_1 = M_2 \times V_2 \qquad \text{---} \qquad (3.5)$$

Where M_1 = Initial (known) Me^{2+} ion concentration (mg/L) of stock solution, V_1 = Required volume (mL) from stock solution, M_2 = Desired (final) Me^{2+} ion concentration of waste solution, V_2 = Total (final) working volume (mL) of waste solution.

Given M_1 = 2000 mg/L Fe^{2+}, V_1 = ??? (Required unknown volume from stock solution), V_2 = 1000 mL (1L), M_2 = 400 mg/L Fe^{2+};

$$V_1 = \frac{400\,\frac{mg}{L} \times 1000\,mL}{2000\,\frac{mg}{L}} = 200\,mL$$

$$\text{---} \qquad (3.6)$$

Thus, 200 mL should be measured from a stock solution of 2000 mg/L Fe^{2+} ions and diluted with distilled water to obtain 1000 mL as the final working volume of the waste solution to be treated containing 400 mg/L Fe^{2+} ions.

3.3.2 Batch Adsorption Equilibria and Kinetics

This study employed the immersion method to characterise adsorption systems of Cd^{2+}, Co^{2+}, Cu^{2+}, Fe^{2+} and Mn^{2+} ions from waste solutions using blast and electric arc furnace slags as adsorbents. Batch adsorption experiments using both stirred tank reactors and bottle rolling techniques were conducted to investigate the effects of various adsorption variables and slag activation techniques on adsorbent capacity, efficiency, adsorption rates and mechanisms in order to establish adsorption equilibria and kinetics for the slag-metal adsorptive systems.

3.3.2.1 Stirred Tank Reactor & Bottle Adsorption Vessels

The stirred tank reactor (STR) and a schematic bottle roller setup that were used to conduct batch adsorption experiments are shown in Figures 3.1 and 3.2 respectively. The STR is free standing, baffled, double walled (jacketed) glass reactor vessel made of borosilicate glass with 2.2 litres total working volume. It has a control unit that provides stirrer speed control with digital readout/display unit for pH, temperature and other variables. It is fitted with overhead variable speed stirrer with a four pitched blade, axial flow turbine impeller fitted at the end of the shaft to provide proper mixing and ensure effective particle suspension. The stirrer assembly is a top mounted agitator shaft driven by a detachable electric motor with variable speed control. The air tight stainless steel top plate is provided with ports for stirrer shaft, pH probes and sampling frit. The pH readout and control was via an in-house manufactured pH control unit with Broadley-James pH probe. The pH was controlled by additions of acid or alkali solutions via an in-house manufactured peristaltic triple header

pump unit. The STR is thermostated by circulating heated water from an external Grant GD120 constant temperature water bath through the reactor jacket.

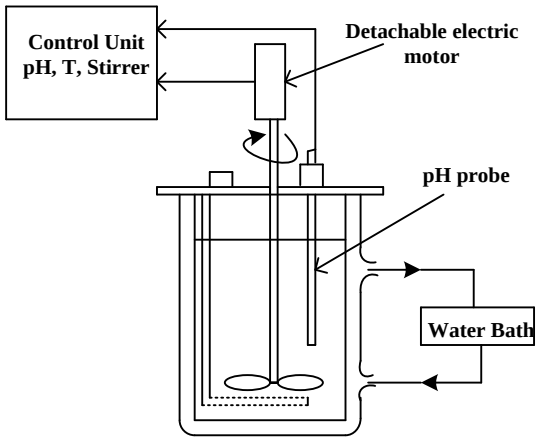

Figure 3.1: Stirred Tank Reactor (STR) adsorption Vessel

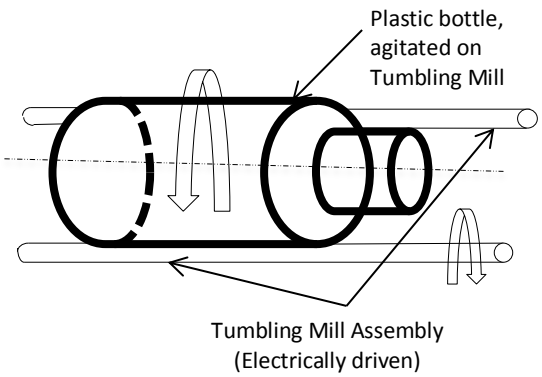

Figure 3.2: Bottle-Roller adsorption vessel agitated by a Tumbling Mill

3.3.2.2 Experimental & Sampling Procedure

Batch adsorption experiments were conducted initially in ½ Litre capacity plastic bottles with tight screwed caps agitated on a tumbling mill at 110 rpm and later in 2 Litre capacity stirred tank reactors (STR) with automated pH and temperature controls; to study the effects of solid/liquid phase ratios (mass of adsorbent), particle sizes of adsorbent, temperature, initial pH of waste solution, initial concentration of metal ions and the rate of agitation on adsorbent capacity and efficiency, adsorption rates and selectivity of metal ions, and adsorption mechanisms in single and multicomponent adsorption systems of metal ions using slags as adsorbents. The effects of slag activation by chemical leaching with concentrated HCl solution and thermal pretreatment on adsorptive performance of slags were also studied.

The desired volume of waste solution to be treated with the desired (known) initial concentration levels of metal ions were prepared from stock solutions according to section 3.3.1 and added to the adsorption vessel. This was followed by adjusting the temperature and pH of waste solution to the required initial value. Apart from automated online pH monitoring on control unit with a combination probe attached to the STR, pH measurements were also done by using a bench Model HI 2211 pH Meter with a combination probe filled with 3.0 M KCl electrolyte solution. Then, a desired mass of adsorbent of known particle size distribution was subsequently added into the adsorption vessel, which was then sealed and the mixture equilibrated by agitation for a predetermined time. Because the adsorbent was heterogeneous in nature, duplicate adsorption experiments were initially carried out, each with a fresh random sample of adsorbent prepared by a riffle splitter to obtain sufficiently reliable adsorption results at the same solid/liquid ratio and to assess the variance in atomic absorption spectroscopy (AAS) measurements for metal ions. No pretreatment, e.g., heating, washing or outgassing of the adsorbent or solution were carried out except where these were variables. It was also assumed that the dissolution of adsorbent and/or its effect, if any, was negligible.

Preliminary experiments were conducted to determine the time required to establish equilibrium under various experimental and solution conditions. Thus, it was necessary to ensure that equilibrium was achieved where possible. The adopted standard solution conditions were 22 ^{o}C (room temperature), pH 3.50, solid/liquid ratio of 30 g/L slag (3 % w/v) and 0.18-0.36 mm particle sizes of slag except where these were variables. The solid/liquid phase ratio was chosen such that a measurable change in adsorbate concentration was achieved to obtain accurate adsorption data. The progress of adsorption

of metal ions was monitored by analysing the changes in concentrations of metal ions and solution pH as a function of mixing time.

During the course of adsorption and after equilibrium, slurry samples of about 20 mL containing loaded adsorbent were periodically taken from the adsorption vessel by syringe and tube assembly via sampling ports. The method of sampling was carefully performed to ensure that a representative slurry sample of adsorbent/solution mixture was obtained. The loaded adsorbent with metal ions was then separated from its bulk solution by filtration through 0.20/0.45 μm acrodisc filter syringes at the same adsorption temperature where possible. The sampling time intervals and residence time for adsorption of metal ions was predetermined and fixed. The filtrate was preserved with 0.15% w/w HCl or H_2SO_4 solutions and stored at 4 ^oC which was later diluted accordingly and subjected to chemical analysis for change in concentration of metal ions by Perkin Elmer AAnalyst 300 Flame Atomic Absorption Spectrophotometer. The filtered solid slag residues loaded with metal ions from selected adsorption experiments were air dried at ambient conditions for 48 hours and their surfaces examined by SEM and EDS techniques.

3.3.2.3 Chemical Analyses and Adsorption Calculations

The determination of the concentration of metal ions of interest in solution was performed by Perkin Elmer AAnalyst 300 Flame Atomic Absorption Spectrophotometer. This analytical method was considered sensitive and accurate. By applying the dilution principle (Equation (3.5)), the required standards for preparing the calibration curves that are necessary in the analysis of metal ion concentrations in solutions by AAS technique were prepared from specially prepared AAS reference standard solutions of 1000 mg/L of metal ions procured

from Fisher Scientific UK. The concentration range of standards for metal ion analyses was 0.25-5.00 mg/L which gave a satisfactory linear relationship between absorbance and concentration of standards at the chosen wavelengths with a high sensitivity for all ions. Solutions which had a high concentration of metal ions to be measured were diluted accordingly to this range.

Computations of adsorption capacity (q_t, mg/g), efficiency (η, %), distribution coefficient (K_d, L/g) and other response variables (parameters) were based on changes in metal ion concentrations (C, mg/L) determined by AAS measurements as given in Equations (3.4) to (3.7) below. From duplicate adsorption experiments conducted, the reproducibility of AAS results was assessed and mean values were used. The % error (variance) in AAS analyses of metal ion concentration was approximately ±1.00-8.00%. This error increased with increase in metal ion concentration.

The adsorption capacity was established by carrying out a basic mass balance of adsorbate across the adsorption vessel to obtain Equation (3.7) as shown below.

$$V(C_o - C_t) = m(q_t - q_t); \quad q_t = 0 \quad at \quad t = 0; \qquad Also \quad q_e = \frac{V(C_o - C_t)}{m}$$

$$\therefore \quad q_t = \frac{V(C_o - C_t)}{m} \qquad \text{--- (3.7)} \qquad \text{--- (3.8)}$$

$$\eta = \frac{(C_o - C_t)}{C_o} \times 100\ \% \qquad k_d = \frac{q_e}{C_e}$$

--- (3.9) --- (3.10)

Where q_o (mg/g) = Initial amount of adsorbate per unit mass of adsorbent at time t (min) = 0; q_t (mg/g) = Amount of adsorbate per unit mass of adsorbent at time t = t; q_e (mg/g) = Amount of adsorbate per unit mass of adsorbent at equilibrium; C_o (mg/L) = initial adsorbate concentration in solution at time t = 0; C_t (mg/L) = adsorbate concentration in solution at time t (min) = t; C_e (mg/L) = adsorbate concentration in solution at equilibrium; m (g) = mass of adsorbent; V (L) = volume of solution; k_d (L/g) = distribution coefficient.

3.3.2.4 Single Component Adsorption Systems

Batch adsorption experiments were conducted to characterise single component adsorption systems of Cd^{2+}, Co^{2+}, Cu^{2+}, Fe^{2+} and Mn^{2+} ions from acidic waste solutions using blast furnace slag as adsorbent. The experiments were conducted in bottles agitated on a tumbling mill to investigate the effects of particle size of adsorbent and initial pH of waste solutions on adsorbent capacity, efficiency, adsorption rates, selectivity and adsorption mechanisms of slags in order to establish adsorption equilibria and kinetics. A fixed volume of 0.50 litres of waste solution with a theoretical initial metal ion concentration of 100 mg/L was added to the adsorption vessel and pH adjusted to the desired values at room temperature. The desired particle size fraction of adsorbent at a fixed solid/liquid phase ratio of 30 g/L slag was then added and the mixture equilibrated by agitation. Aliquots of 20 mL slurry samples were periodically taken and filtered. Change in metal ion concentrations were measured in the filtrate by AAS from which efficiency (η, %), adsorption capacity (q, mg/g), distribution coefficients (k_d, L/g) and other parameters were calculated by Equations (3.7) to (3.10) above. A detailed experimental procedure is described in Sections (3.3.2.1) to (3.3.2.3).

3.3.2.4.1 Effect of Particle Size of Adsorbent

Batch bottle-rolling adsorption experiments using 0.5 L bottles agitated at 110 rpm were conducted in single component adsorption systems of Cd^{2+}, Co^{2+}, Cu^{2+}, Fe^{2+} and Mn^{2+} ions from acidic waste solutions at initial pH 3.50 using blast furnace slag as adsorbent with four different size fractions, i.e., $d_p < 45$ µm, $180 < d_p < 36$ µm, $360 < d_p < 500$ µm and $500 < d_p < 100$ µm to investigate the effect of particle size on adsorption kinetics. A pH of 3.50 is an approximate mean value of the range reported in incidences of acid mine drainages. The experiments were conducted at a solid/liquid phase ratio of 30 g/L slag (3 % w/v) which is a slag dosage of 3 g per 100 ml of waste solutions with initial theoretical concentration of each adsorbate at 100 mg/L, 22 ^{o}C for 5 hours.

3.3.2.4.2 Effect of Initial pH of Waste Solutions

Similar to the experimental procedure of Section 3.3.2.4.1, batch adsorption experiments were conducted in single component adsorption systems of Cd^{2+}, Co^{2+}, Cu^{2+}, Fe^{2+} and Mn^{2+} ions with theoretical initial concentration of 100 mg/L for each metal ion from acidic waste solutions using blast furnace slag as adsorbent to investigate the effect of solution pH on adsorption kinetics. The different pH levels employed were 1.50, 3.50, and 5.50 in 0.5 L bottles agitated at 110 rpm, 22 ^{o}C, 30 g/L solid/liquid phase ratio and a size fraction of +500-1000 µm for 5 hours.

3.3.2.5 Multicomponent Adsorption Systems

Batch adsorption experiments were conducted to characterise multicomponent adsorption systems of Cd^{2+}, Co^{2+}, Cu^{2+}, Fe^{2+} and Mn^{2+} ions from acidic waste solutions using both blast and electric furnace slags as adsorbents. The experiments were conducted both in bottles

agitated on a tumbling mill and in stirred tank reactors (STR) to investigate the effects of solid/liquid phase ratios, particle sizes, temperature, initial pH, initial concentration of metal ions and rate of agitation on adsorbent capacity, efficiency, adsorption rates, selectivity and adsorption mechanisms of slags in order to establish adsorption equilibria and kinetics. A fixed volume of 0.5 or 1.0 L of waste solution with a desired initial metal ion concentration was added to the adsorption vessel and pH and temperature adjusted to the desired values. The desired solid/liquid phase ratio (mass) and particle size fraction of adsorbent was then added and the mixture equilibrated by agitation. Aliquots of 20 mL slurry samples were periodically taken and filtered. Change in metal ion concentrations were measured in the filtrate by AAS from which efficiency (η, %), adsorption capacity (q, mg/g) and distribution coefficients (k_d, L/g) and other parameters were calculated by Equations (3.7) to (3.10) above. A detailed experimental procedure is described in Sections (3.3.2.1) to (3.3.2.3).

3.3.2.5.1 Effect of Adsorbent Particle Size

Batch adsorption experiments were conducted in multicomponent adsorption systems of Cd^{2+}, Co^{2+}, Cu^{2+}, Fe^{2+} and Mn^{2+} ions from acidic waste solutions at initial pH 3.50 using blast furnace slag as adsorbent to investigate the effect of particle size on adsorption kinetics. The different size fractions employed were; d_p < 45 µm, +180-360 µm, +360-500 µm and +500-1000 µm in 0.5 L bottles agitated at 110 rpm, 30 g/L solid/liquid phase ratio, with theoretical initial concentration of each metal ion at 100 mg/L as well as +45-53 µm, +90-106 µm, +180-212 µm, +355-425 µm, +710-1000 µm and +1400-1700 µm in 1-Litre STR agitated at 600 rpm, 22 ^{o}C, 50 g/L solid/liquid phase ratio, with theoretical initial metal ion concentration of 40 mg/L Cd^{2+}; 30 mg/LCo^{2+}; 60 mg/L Cu^{2+}; 100 mg/LFe^{2+}; 20 mg/L Mn^{2+} at each size fraction up to 8 hours.

3.3.2.5.2 Effect of Initial Concentration of Metal Ions

The effect of initial concentration of metal ions on adsorption equilibrium isotherms and kinetics was investigated in batch adsorption experiments in multicomponent adsorption systems of Cd^{2+}, Co^{2+}, Cu^{2+}, Fe^{2+} and Mn^{2+} ions from acidic waste solutions at initial pH 3.50 using both blast and electric furnace slags as adsorbents. Two sets of adsorption experiments were conducted with blast furnace slag under the following conditions; (1) at several values of same initial concentration for each metal ion in the range 20-1000 mg/L using 0.5 L bottles agitated at 110 rpm, 50 g/L solid/liquid phase ratio and a particle size fraction of dp < 45 μm, and (2) at several values of different initial concentration for each metal ion in the ranges 20-200 mg/L Cd^{2+}, 15-150 mg/L Co^{2+}, 30-1000 mg/L Cu^{2+}, 50-1600 mg/L Fe^{2+} and 20-100 mg/L Mn^{2+} using 0.5 L bottles agitated at 110 rpm, 30 g/L solid/liquid phase ratio and a particle size fraction of d_p < 45 μm. However a single set of adsorption experiments was carried out with electric furnace slag at several values of different initial concentration for each metal ion in the ranges 20-200 mg/L Cd^{2+}, 15-150 mg/L Co^{2+}, 30-1000 mg/L Cu^{2+}, 50-1600 mg/L Fe^{2+} and 20-100 mg/L Mn^{2+} using 0.5 L bottles agitated at 110 rpm, 22 ^{o}C, 30 g/L solid/liquid phase ratio and a size fraction of dp < 45 μm for 8 hours.

3.3.2.5.3 Effect of initial pH of Waste Solutions

Batch adsorption experiments were conducted in multicomponent adsorption systems with initial metal ion concentration of 40 mg/L Cd^{2+}, 30 mg/LCo^{2+}, 120 mg/L Cu^{2+}, 200 mg/LFe^{2+} and 20 mg/L Mn^{2+} from acidic waste solutions using blast furnace slag as an adsorbent to investigate the effect of solution pH on adsorption kinetics. The different pH levels

employed were 1.50, 3.50, 5.50 and 7.50 in 1-L STR agitated at 600 rpm, 22 ^{o}C, 30 g/L solid/liquid phase ratio and a size fraction of +90-106 μm for 6 hours.

3.3.2.5.4 Effect of Temperature

Batch adsorption experiments were conducted in multicomponent adsorption systems with initial metal ion concentration of 100 mg/L Cd^{2+}, 60 mg/L Co^{2+}, 500 mg/L Cu^{2+}, 800 mg/L Fe^{2+} and 40 mg/L Mn^{2+} from acidic waste solutions at initial pH 3.50 using blast furnace slag as an adsorbent to investigate the effect of temperature on adsorption kinetics. The different values of temperature employed were 30, 45, 60 and 75 ^{o}C in 1-L STR agitated at 600 rpm, 50 g/L solid/liquid phase ratio and a size fraction of d_p < 45 μm for 8 hours.

3.3.2.5.5 Effect of Solid/Liquid Phase Ratio

Batch adsorption experiments were conducted in multicomponent adsorption systems with initial concentration of each metal ion at 100 mg/L for Cd^{2+}, Co^{2+}, Cu^{2+}, Fe^{2+} and Mn^{2+} ions from acidic waste solutions at initial pH 3.50 using blast furnace slag as adsorbent to investigate the effect of solid/liquid phase ratios on adsorption equilibria and kinetics. The different solid/liquid phase ratios employed were 2 g/L, 10 g/L, 30 g/L, 50 g/L and 100 g/L in 0.5 L bottles agitated at 110 rpm, 22 ^{o}C and a size fraction of d_p < 45 μm for 5 hours.

3.3.2.5.6 Effect of the Rate of Agitation

Batch adsorption experiments were conducted in multicomponent adsorption systems with initial metal ion concentration of 100 mg/L Cd^{2+}, 60 mg/L Co^{2+}, 500 mg/L Cu^{2+}, 800 mg/L Fe^{2+} and 40 mg/L Mn^{2+} from acidic waste solutions at initial pH 3.50 using blast furnace slag as adsorbent to investigate the effect of agitation rate on adsorption kinetics. The different

values of agitation rates employed were 400, 600 and 1000 rpm in 1-L STR at 50 g/L solid/liquid phase ratio, 22 ^{o}C and a size fraction of d_p < 45 µm for 8 hours.

3.3.2.6 Effect of Pretreatment of adsorbent

Pretreatment of representative samples of blast furnace slag was conducted by leaching and heating processes to investigate their effect on adsorptive properties of slag and kinetics of metal ion adsorption.

3.3.2.6.1 Effect of Leaching

The effect of slag activation by a two-stage leaching with HCl on its adsorptive properties and adsorptive performance was investigated. Leaching of granulated blast furnace slag was conducted in a 2 L capacity stirred tank reactor (STR) in a fume cupboard, based on a previous study (McCauley, 2001). It was necessary to ensure sufficient agitation of slurry to obtain good mixing and keep solids off bottom. During the first stage leaching, a 200 g sample of slag with a particle size of +180-360 µm was charged into the reactor with 2 Litres of distilled water to make a 10% w/v pulp density or 100 g/L solid/liquid phase ratio. The final slurry pH was manually maintained at about 3-4 by slow addition of concentrated (37%) HCl drops as a leachant from a burette for 3 hours. The volume of HCl used was noted in order to calculate acid consumption of slag under these conditions. After leaching for 3 hours, the slurry was filtered by decantation. The filtrate was discarded but the solid leach residues were subjected to a second stage leaching for a further 2 hours under similar conditions except that final pH was set to 2.0-2.5. The volume of acid consumed was noted and the slurry was filtered as before.

A sample of leach residue material from second stage leaching was then analysed for changes in adsorptive properties by XRD, XRF, N_2 adsorption for BET surface area and SEM/EDS. The rest of the material was employed as adsorbent at 30 g/L solid/liquid phase ratio in a batch adsorption experiment at 22 ^{o}C for 5 hours using 0.5 L bottles agitated at 110 rpm in order to evaluate its adsorptive performance. This was carried out in an acidic waste solution at initial pH 3.50 of a multicomponent system for Cd^{2+}, Co^{2+}, Cu^{2+}, Fe^{2+} and Mn^{2+} ions with initial concentration of 100 mg/L for each metal ion.

3.3.2.6.2 Effect of Heating

The effect of heating granulated blast furnace slag on its adsorptive properties and adsorptive performance was investigated based on previous studies (Dimitrova et al., 2001;Mihailova et al., 2013). The slag was heated in a Carbolite muffle furnace whose chamber is heated electrically by coiled wire elements. Three slag samples of about 65 g each with a particle size range of +180-360 µm were charged into the furnace one sample at a time and heated at 400, 600 and 800 ^{o}C respectively for 3 hours each. The samples were allowed to cool slowly in the furnace atmosphere and later stored in sealed plastic sample bags.

Representative samples of slag materials that were heated at 400, 600 and 800 ^{o}C were then analysed for changes in adsorptive properties by XRD, XRF, N_2 adsorption for BET surface area and SEM/EDS. A reference sample that was not heated was also analysed and acted as a control. The rest of three slag samples heated at 400, 600 and 800 ^{o}C were employed as adsorbents in three respective batch adsorption experiments using 1-L STR agitated at 600 rpm in order to evaluate the adsorptive performance of slag heated at

various temperature values as stated above. This was done in an acidic waste solution at initial pH 3.50 with a 30 g/L solid/liquid phase ratio at 22 ^{o}C for 6 hours in a multicomponent system with initial metal ion concentration of 40 mg/L Cd^{2+}, 30 mg/L Co^{2+}, 250 mg/L Cu^{2+}, 400 mg/L Fe^{2+} and 20 mg/L Mn^{2+} ions. A control adsorption experiment was conducted with slag sample that was not heated.

3.3.3 Continuous Flow Adsorption Kinetics

Continuous flow adsorption experiments were conducted in fixed bed adsorption columns to assess the adsorptive performance of slags for practical applications. Adsorption data from continuous flow experiments is useful in the design and scale up of adsorption systems. The experiments were conducted in multicomponent adsorptive systems of Cd^{2+}, Co^{2+}, Cu^{2+}, Fe^{2+} and Mn^{2+} ions from acidic waste solutions using blast furnace slag (BFS) material as adsorbent. The effects of bed heights and flow rates on cycle time and breakthrough curves were investigated in order to establish adsorption equilibria and kinetics.

3.3.3.1 Preparation of Waste Solutions

About 15-30 L of waste solution to be treated with the desired initial concentration levels of metal ions were prepared from stock solutions according to the procedure described in Section 3.3.1 and added to the feeder tank of the fixed bed adsorption column.

3.3.3.2 Fixed Bed Adsorption Column & Experimental Procedure

The experimental setup that was used to conduct continuous flow adsorption experiments is shown in Figure 3.3 below. It is essentially a fixed bed column made of Plexiglas tube which has an inside diameter of 4.4 cm and a height of 110 cm with 1 m working bed height and a height/diameter (H/D) ratio of about 25. It is fitted with wire mesh at the inlet (base) and outlet points to retain adsorbent particles. The column is also provided with control valves, connecting pipelines, solution storage tanks and Watson (Marlow) peristaltic pump with a variable control for volumetric flow rates.

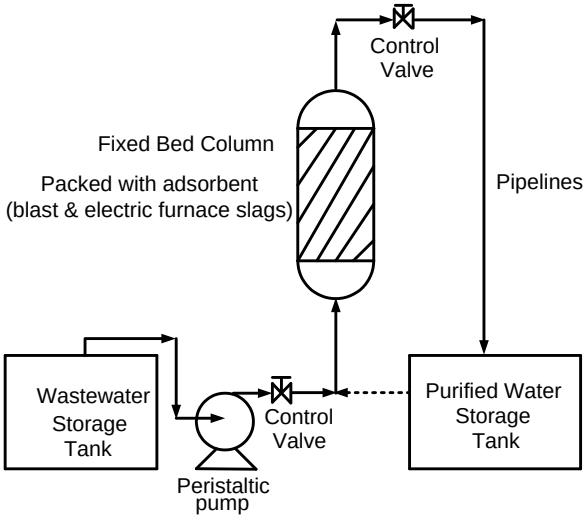

Figure 3.3: Fixed Bed Column Setup

A quantity (~850±10 g) of untreated adsorbent with +500-1400 µm particle size range was packed into the column until the desired height of the bed was obtained. Then, waste solutions at initial pH 3.50 with the known initial concentration of metal ions were pumped at the desired volumetric flow rate into the column bed in an upward flow motion by a Watson peristaltic pump to eliminate solution channelling and ensure effective adsorbent/solution contact. Furthermore, the liquid phase is fed in an upward flow mode to provide better flow quality and ensure complete wetting of BFS adsorbent material

(Cobzaru & Inglezakis, 2015). Samples of about 20 mL were periodically taken from the discharge point of the column and filtered. The filtrate was preserved, diluted and analysed by AAS as outlined in Section 3.3.2.3 from which various parameters were calculated.

3.3.3.3 Multicomponent Adsorption Systems

Continuous flow adsorption experiments were conducted in multicomponent adsorptive systems of Cd^{2+}, Co^{2+}, Cu^{2+}, Fe^{2+} and Mn^{2+} ions from acidic waste solutions using blast furnace slag as adsorbent. The effects of bed height and flow rate on cycle time and breakthrough curves were investigated. A detailed experimental procedure is described in Sections 3.3.3.2.

3.3.3.3.1 Effect of Volumetric flow Rate

The experiments were conducted in multicomponent adsorption systems with initial metal ion concentration of 40 mg/L Cd^{2+}, 30 mg/L Co^{2+}, 250 mg/L Cu^{2+}, 400 mg/L Fe^{2+} and 20 mg/L Mn^{2+} from acidic waste solutions at initial pH 3.50 that were pumped at various flow rates through a fixed bed column of blast furnace slag as adsorbent to investigate the effect of volumetric flow rate on cycle time and breakthrough capacity. Three different values of volumetric flow rates employed were 20, 40 and 60 mL/min through a bed height of 52.5 cm packed with BFS of +500-1400 µm particle size range at room temperature for 6-13 hours.

3.3.3.3.2 Effect of Bed Height

The experiments were conducted in multicomponent adsorption systems with initial metal ion concentration of 40 mg/L Cd^{2+}, 30 mg/L Co^{2+}, 250 mg/L Cu^{2+}, 400 mg/L Fe^{2+} and 20 mg/L Mn^{2+} from acidic waste solutions at initial pH 3.50 that were pumped at a fixed volumetric

flow rate of 20 ml/min through various bed heights using blast furnace slag as adsorbent to investigate the effect of bed height on cycle time and breakthrough capacity. Three different values of bed heights employed were 27, 52 and 82 cm packed with slag of +500-1400 µm particle size range at room temperature for 13-28 hours.

3.3.3.3.3 Adsorption and Desorption Cycles

Two (2) cycles of multicomponent adsorption and one (1) desorption cycle with a wash cycle in between were carried out under the following conditions; The first adsorption cycle was conducted in multicomponent adsorption systems with initial metal ion concentration of 40 mg/L Cd^{2+}, 30 mg/L Co^{2+}, 250 mg/L Cu^{2+}, 400 mg/L Fe^{2+} and 20 mg/L Mn^{2+} from acidic waste solutions at initial pH 3.50 that were pumped at a fixed volumetric flow rate of 20 ml/min through a bed height of 52 cm using blast furnace slag as adsorbent to investigate the effect of regeneration ability of slags on cycle time and breakthrough capacity. A column bed height employed was 52.5 cm packed with slag of +500-1400 µm particle size range at room temperature for 13 hours. Samples were periodically taken from the discharge point of the column, filtered and analysed by AAS.

The first adsorption cycle was immediately followed by desorption cycle whereby metal ions were stripped from loaded slag surfaces of slags. Dilute sulphuric acid solution at about pH 2.50 (0.40 % w/w H_2SO_4) at room temperature was used as a regenerating or stripping reagent. Higher concentration of stripping solution could not be used due to the detected emission of toxic H_2S gas that resulted from a possible reaction of acid with sulphur in the slag. The stripping solution was pumped at 20 mL/min for 6 hours through the 52 cm

column bed height. The flow of the stripping reagent was in the same direction as the loading solution, i.e., up flow or co-flow regeneration mode.

After the first stripping or desorption cycle, the column was subjected to an intermediate wash cycle using distilled water, and further subjected to second adsorption cycle under the same experimental and solution conditions as the first cycle. However, the second strip cycle could not be done due to operational challenges whereby the bed compacted and practically prevented the solution from flowing through it.

CHAPTER 4
CHARACTERISATION OF ADSORBENT MATERIALS

4.1 Introduction

The development of functional adsorbents from inexpensive (or waste) materials such as iron and steel slags and natural zeolites is of great interest to the waste water purification industry. The work described here aims to develop functional adsorbents from blast furnace and other related slag materials. According to Deng (2006), the ideal characteristic requirements of an adsorbent material include large internal pore volume and surface area, controlled pore size distribution, chemical and mechanical stability, weak adsorbate/adsorbent interactions, controlled surface properties and must be of low-cost to have potential for commercial adoption by industry. A quantitative analysis of the physicochemical properties of adsorbent materials is therefore critical in understanding the design and control of adsorption systems. Thus, it is also crucial to understand how the characteristic material properties, such as specific surface, pore size distribution, surface chemistry, etc., affect such phenomena as mass transfer kinetics, mechanisms, efficiency and rates of the adsorption process. Extensive studies have been conducted to understand the potential use of iron and steelmaking slags as adsorbents. A brief review of key adsorptive properties reported in literature for these novel adsorbent materials, with emphasis on those based on iron and steelmaking waste slags is presented in this section.

The chemical composition of slag materials from iron and steelmaking processes is well known. Using X-Ray Fluorescence (XRF) and X-Ray Diffraction (XRD) techniques, slags have

been shown to consist of predominantly CaO, SiO_2, Al_2O_3, FeO and MgO with several minor oxides of Mn, K, Na, S, and others (Dimitrova, 1996; Dimitrova & Mehandgiev, 1998; Lopez et al., 1995; Xue et al., 2013). These oxides combine to constitute a framework of complex mineral phases of aluminium, calcium and iron silicates. These materials exhibit various proportions of both crystalline and amorphous structures. It is believed there is potential to modify the crystal structure of slags by various techniques such as thermal pretreatment to improve adsorption capacity (Dimitrova et al., 2001; Dimitrova & Mehandgiev, 2000; Mihailova et al., 2013). However, differences in chemical composition exist due to different production processes and different sources of raw materials.

The specific role of each chemical phase component of slags in relation to adsorption is not fully understood and therefore subject to further study. An early publication by Yamashita et al (1983) made several assumptions that metal ion adsorption on converter furnace steel slag surfaces occurs by ion substitution caused by CaO and MgO, hydroxide precipitation at high pH, sulphide precipitation and coprecipitation by sulphur and iron oxides respectively as well as possible adsorptive effects of $2CaO.SiO_2$ phase. Dimitrova (1996) believed the process of adsorption is facilitated by chemical interaction of dissolved slag components with metal ions and subsequent deposition of such products on slag surfaces. Also, Dimitrova and Mehandgiev (2001) observed higher adsorption capacity in crystalline blast furnace slag than in amorphous one.

A high specific surface area is required in any adsorbent to create a high adsorption capacity. Typical values of specific surface area for various types of slags, as determined by BET method using N_2 gas adsorption, range between 0.1-5.0 m^2/g (Curkovic et al., 2001;

Dimitrova, 1996; Xue et al., 2009) with Type (III) isotherms that predict unrestricted multilayer adsorption as shown in Figure 4.0 (Sing, 1982; Rouquerol et al., 2014). This partly explains why reported adsorptive performance of slags is relatively low. A few material pretreatment steps have been proposed to alter the structure and increase the surface area and therefore improve the adsorption capacity. Pore size distribution is another key property of porous solids that is often analysed by both N_2 gas adsorption and mercury porosimetry. The performance of adsorbents is largely dependent on internal pore structure with large pore volume and surface area (Deng, 2006). Thus, pore structure of adsorbents is of great interest in adsorption. Lopez et al (1995) and Xue et al (2013) used mercury porosimetry to analyse the porosity of blast furnace sludge and basic oxygen furnace slags respectively, and found the materials to be macroporous and mesoporous respectively. Liu et al (2011), Curkovic et al (2001) and others deduced mean pore sizes of steel slags and electric furnace slags respectively using the BET method. However, detailed studies to understand and control pore size distribution in several slag materials that were employed as adsorbents are limited.

The density for most iron and steel making slag materials lies between 2-3 g/cm^3 and is as high as 27 g/cm^3 for sludge (Dimitrova, 1996; Lopez et al., 1995). However, not much use has been shown of density data in relation to adsorption performance. Lopez et al (1995) analysed the surface elements of sludge materials by XPS/EDAX techniques before and after adsorption process in order to deduce the underlying mechanisms of adsorption. Such knowledge of surface chemistry of adsorbent materials is necessary to fully interpret adsorption data. Xue et al (2013) examined surface morphology of BOF slags by SEM that revealed various sizes and shapes of particles with porous surfaces.

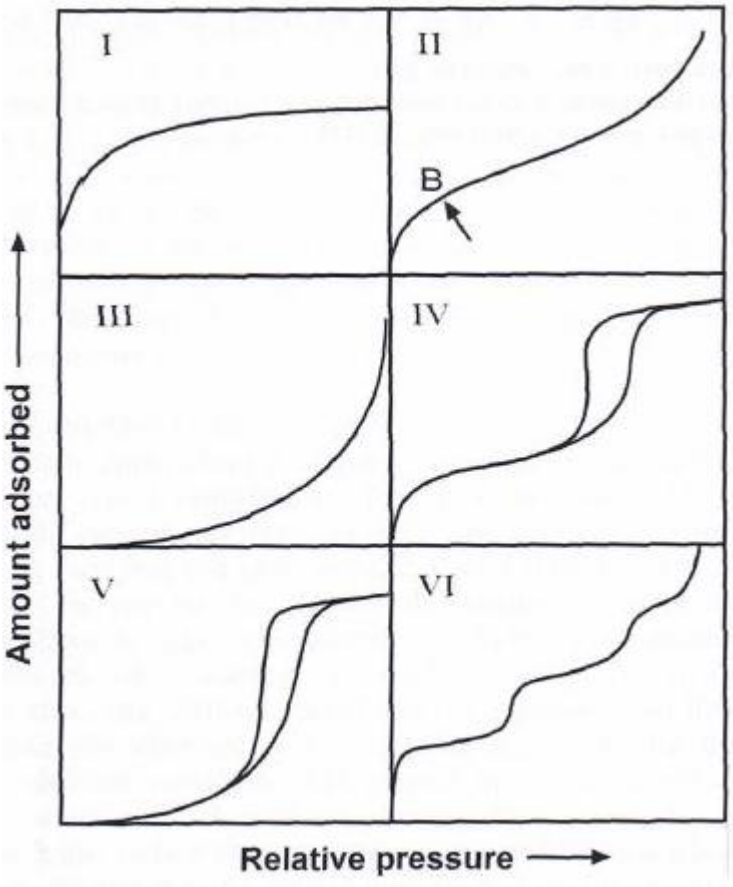

Type (I): Obtained with macroporous adsorbents; Adsorption limited to few layers; Indicative of small external surface area

Type (II): Obtained with non-porous or macroporous adsorbents; unrestricted mono/multilayer adsorption; Point B indicative of the completion of monolayer adsorption & onset of multilayer adsorption

Type (III): Obtained with non-porous or macroporous adsorbents; Shape indicative of weak adsorbent/adsorbate interaction; unrestricted multilayer adsorption

Type (IV): Obtained with mesoporous adsorbents; exhibits hysteresis due to capillary condensation; mono/multilayer adsorption with limited uptake

Type (V): Similar to Type (III); Obtained with micro/mesoporous adsorbents; Shape indicative of weak adsorbent/adsorbate interaction; exhibits hysteresis due to capillary condensation; Multilayer adsorption

Type (VI): Stepwise multilayer adsorption; Obtained with uniform, non-porous adsorbent surfaces

Figure 4.0: Classification of adsorption isotherms
(Sing, 1982; Rouquerol et al., 2014)

Despite intense research interests to develop inexpensive adsorbents from industrial solid wastes, several key properties such as pore size distribution and surface chemistry have not been fully addressed. Further, correlations between reported adsorption properties (e.g., oxide composition) and observed adsorption performance have not been exploited in detail. However, these waste materials have huge potential in environmental remediation and may offer economic benefits. Thus, a detailed evaluation of adsorptive properties of slag

materials and how these properties may affect adsorption process will be subject to investigation in this chapter.

4.2 Materials and Methods

A detailed experimental procedure for characterisation of slag materials is presented in Section 3.2 of Chapter 3 in this thesis. However, a brief summary of the methods is given in this section. The relevant adsorptive properties of blast and electric furnace slags, supplied by Lafarge/Tarmac Ltd UK, were examined by using standard materials characterization techniques. The properties that were analysed include particle size distribution, pore size distribution, surface morphology, chemical and mineral phase composition, specific surface area and density.

The particle size distribution was carried out by both sieve analysis and Malvern mastersizer. An AutoPore IV 9500 V1.09 Micromeritics Mercury Porosimeter was employed to determine pore size distribution. A Philips XL-30 Environmental Scanning Electron Microscopy (ESEM)-FEG fitted with an Oxford Inca 300 Energy Dispersive Spectroscopy (EDS) system was applied to determine structure, surface morphology and chemical composition. The mineral phases and chemical composition were conducted by Siemens D5005 powder X-Ray diffractometer (XRD) and Bruker S8 Tiger Wavelength Dispersive X-Ray Spectrometer (XRF) respectively. The surface area and pore size distribution of slags were measured using the BET method by N_2 adsorption using Micromeritics Instrument ASAP® 2010. True densities were measured by AccuPyc II 1340 V1.05 Micromeritics Helium gas Pycnometer. Slag samples were also sent to

Kratos Analytical Ltd for X-ray photoelectron spectroscopy (XPS) analysis to determine the surface chemistry.

Pretreatment of slag materials was conducted by leaching and heating processes to investigate their effect on adsorptive properties. Both leach residue and heated BFS products were analysed for changes in adsorptive properties by XRD, XRF, N_2 adsorption for BET surface area and SEM/EDS.

4.3 Results and Discussion

This section presents a detailed discussion of results from analytical experiments that were carried out to characterise blast and electric furnace slags. Various physical and chemical properties of slags relevant to the adsorption process were measured and assessed.

4.3.1 Physical and Chemical Adsorptive Properties

The physicochemical properties data that were analysed and reported include particle and pore size distribution, surface morphology, chemical and mineralogical phase composition and density under different physical states of slags, with particular emphasis on pore size distribution, surface chemistry, elemental composition and specific surface area. By the use of different modification techniques, the crystal structures of slags were modified to achieve a range of new characteristics. These properties are presented and discussed in detail in the sections that follow.

4.3.1.1 Particle Size Distribution

The size of particles dictates the magnitude of many parameters such as surface area, diffusion coefficients and mass transfer kinetics. Therefore, particle characterisation is an important procedure in design and control of many industrial processes. In adsorption processes, the particle size of adsorbents may determine available surface area of adsorbents and affects adsorption equilibria and kinetics. Furthermore, the pressure drop and cycle time in a fixed bed adsorption process are partly controlled by the particle size distribution of adsorbents (Holdich, 2002).

The particle size distribution results from a sieve analysis of 'as received' blast furnace slag (BFS) is given in Figure 4.1 below. About 90 % of the material is greater than 0.200 mm (200 µm), with mean particle diameter of 0.700 mm. Various size fractions were employed to study their effect on adsorption equilibria and kinetics. The size distribution data obtained from Malvern mastersizer for BFS powder (d_p < 45 µm) showed a mean size of 20 µm.

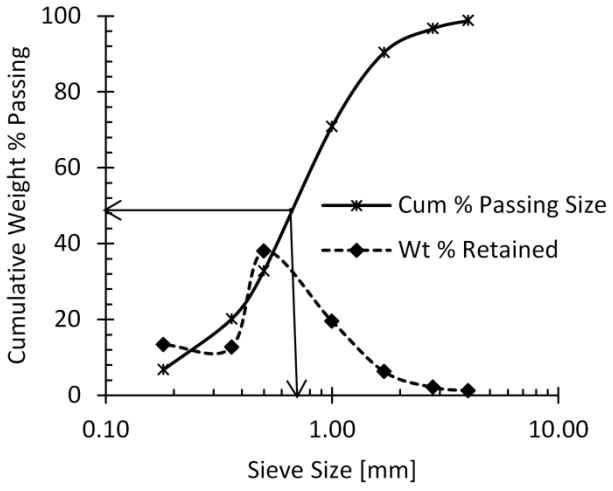

Figure 4.1: Particle size distribution for BFS adsorbent material (as received)

4.3.1.2 Pore Size Distribution

Amongst the available techniques to analyse porosity in materials, gas adsorption and mercury porosimetry, and to some extent SEM/TEM are often used. In this study, both gas adsorption and mercury porosimetry were employed to determine pore size distribution and other parameters for several samples of adsorbent materials. Focusing on mercury porosimetry in this section, the technique is used extensively to determine pore size distribution, pore volume, specific surface area and other pore structure factors of porous materials. This technique has the ability to analyse a relatively wide range of pore sizes of roughly between 0.0035 μm and 500 μm. The volume of mercury that penetrates pores is measured as a function of applied pressure to obtain unique P-V relationships that are utilised to determine internal pore characteristics (Giesche, 2006; Webb, 1993; Webb, 2001; Webb, 2010).

The relative performance of different adsorbents in several applications such as purification and separation processes is largely dependent on internal pore structure with large pore volume and surface area (Deng, 2006). Thus, an understanding of the characteristics of the pore structure of adsorbents is of fundamental interest in adsorption processes. While the porosity of active carbons and many other adsorbents has been studied extensively, it is less well established in slag materials whose pore characteristics could be quite different due to their heterogeneous nature of the structure. The aim of this mercury porosimetry study was to determine the pore size, pore volume, pore surface area and their distribution characteristics of adsorbent slag materials. The study also investigated the effects of heat and chemical pretreatments of the materials on their internal pore structures. A detailed

knowledge of pore structure of adsorbents is necessary to obtain an improved interpretation and understanding of experimental data in adsorption systems.

The internal pore characterisation results from mercury porosimetry measurements for adsorbent slag materials are presented and discussed below. Figures 4.2(A) and (B) show mercury intrusion-extrusion graphs obtained for BFS and EAF materials respectively. The graphs indicate a typical hysteresis loop as observed in many studies for porous solids due to mercury entrapment or changes in mercury contact angle (Webb, 2001; Webb, 2010). The intruded and extruded cumulated volume of mercury is also shown as a function of pore size diameter. Figure 4.2(A) illustrates the pore filling mechanism of how the BFS sample took up mercury during the intrusion cycle and how much mercury was subsequently trapped during the extrusion cycle when pressure was reduced. Mercury was forced into smaller and smaller pore sizes as pressure was increased. The initial volume of mercury intruded from the lowest pressure to roughly 20 psia filled the inter-particle void space. The subsequent peak reflected the filling process of pores within the individual particles. The observed steep rise followed by flattening of the intrusion graph indicates that the majority of porosity or pore volume occurs in the pore size range between about 50 nm and 3000 nm. The shape of extrusion graph in relation to intrusion provides more data about pore geometry (Webb, 1993). Figure 4.2(B) shows the intrusion/extrusion graph for EAF, whose shape and pore size distribution are similar to those of BFS depicted in Figure 4.3(A).

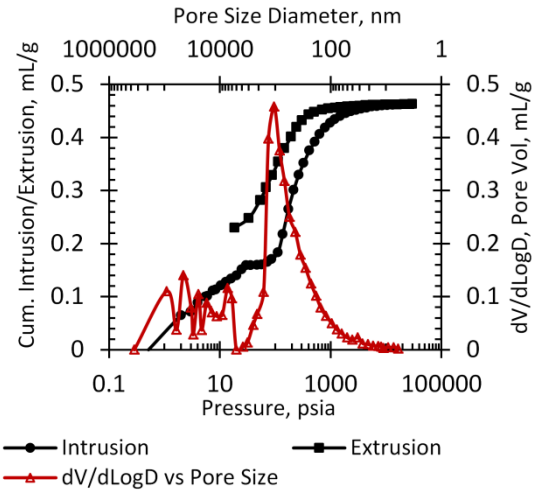

(A)

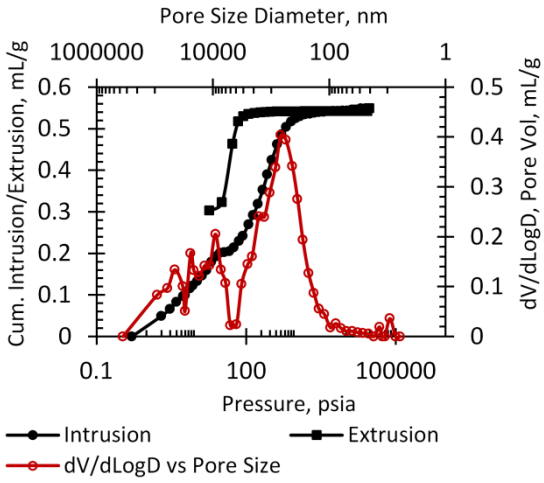

(B)

Figure 4.2: Intrusion-Extrusion vs pressure graphs with Pore volume vs Pore size distribution for (A) BFS and (B) EAF Powders

The distribution of pores is shown in Figure 4.2 above from which it can be deduced that majority of pore sizes are greater than 50 nm, it can therefore be inferred the slag materials are macroporous (Deng, 2006). Further, the intrusion-extrusion curves shows a typical hysteresis loop as observed in many samples during mercury porosimetry measurements, caused by several factors such as mercury entrapment or changes in mercury contact angle. The other characteristic porosimetry parameters of interest in adsorption are given in Table 4.1 below. It can be observed that both BFS and EAF materials in powdered form have comparable porosity (55-60 %) to commercial inorganic adsorbents, that are often microporous, such as zeolites, silica gels and activated alumina (Deng, 2006). However, the adsorbent materials used in this study have inferior pore structure and pore size distribution, much dense and low internal pore surface area which might limit their effectiveness for application in adsorption of relatively high metal ion solute concentrations. The macroporosity nature and relatively large pore sizes limits internal pore surface area and consequently adsorption capacity.

Table 4.1: Porosimetry data for adsorbent materials used in this study

	Adsorbent Materials						
Parameter	**BFS**	**BFS leached**	**EAF**	**BFS, Not heated**	**BFS, heated at 400 °C**	**BFS, heated at 600 °C**	**BFS, heated at 800 °C**
Particle diameter (dp), µm or mm	dp<45 µm	0.18-0.36 mm	dp<45 µm	0.18-0.36 mm	0.18-0.36 Mm	0.18-0.36 mm	0.18-0.36 mm
BET surface area, m^2/g	2.461	5.075	2.991	1.460	1.302	0.827	0.119
True density, g/cm^3	2.892	2.720	4.157	2.809	2.809	2.822	2.783
Total Intrusion Volume, mL/g	0.463	0.500	0.548	0.559	0.552	0.612	0.561
Total Pore Area, m^2/g	4.316	7.936	4.624	3.009	2.416	2.339	2.235
Median Pore Diameter (Vol), nm	1230	69622	1550	80794	101862	116310	105069
Median Pore Diameter (Area), nm	102.1	11.2	93.6	11.5	13.6	11.6	9.1
Average Pore Diameter (4V/A), nm	428.9	251.9	474.3	743.4	913.0	1046.4	1004.3
Bulk Density at 0.52 psia, g/mL	1.177	1.179	1.279	1.082	1.063	1.029	1.082
Apparent (Skeletal) Density, g/mL	2.584	2.871	4.283	2.741	2.570	2.778	2.754
Porosity, %	54.46	58.92	70.13	60.52	58.63	62.96	60.71

The effect of BFS activation by two-stage leaching with HCl on its adsorptive properties was investigated based on a similar study by McCauley (2001), who leached BFS materials by controlling temperature, rate of addition of acid, type and its concentration and solids concentration of BFS in the slurry. The authors reportedly obtained a porous material with high surface area which has potential for application as an adsorbent or for catalyst support. In this study, the effect of pretreatment of BFS by leaching on the internal pore characteristics and distribution is shown in Figure 4.3 (A) and (B). The leaching conditions were fixed and not optimised, partly due to the challenges of handling traces of H_2S gas emissions evident by its characteristic smell. It was hypothesised that a controlled leaching

process of BFS granules (0.18 < dp < 0.36 mm) with HCl would produce a more porous structure with higher surface area and better pore size distribution, by selective dissolution of certain elements from the structure.

Figure 4.3(A) shows a major peak for differential pore volume with pore size diameter that corresponds to interparticle void space for BFS material without major change in pore sizes after leaching. However, pores with a much smaller diameter size range are noticeable in the leached BFS as shown in Figure 4.3(B). Both differential pore volume and total pore area increased more than three (3) and two (2) times respectively after leaching. As will be shown later, even BET surface area increased more than three times. There was negligible effect on % porosity. See Table 4.1 for a comparison between leached BFS and not-heated BFS materials. Chapter 6 of this thesis explored the effect of leaching the adsorbent materials on adsorption kinetics.

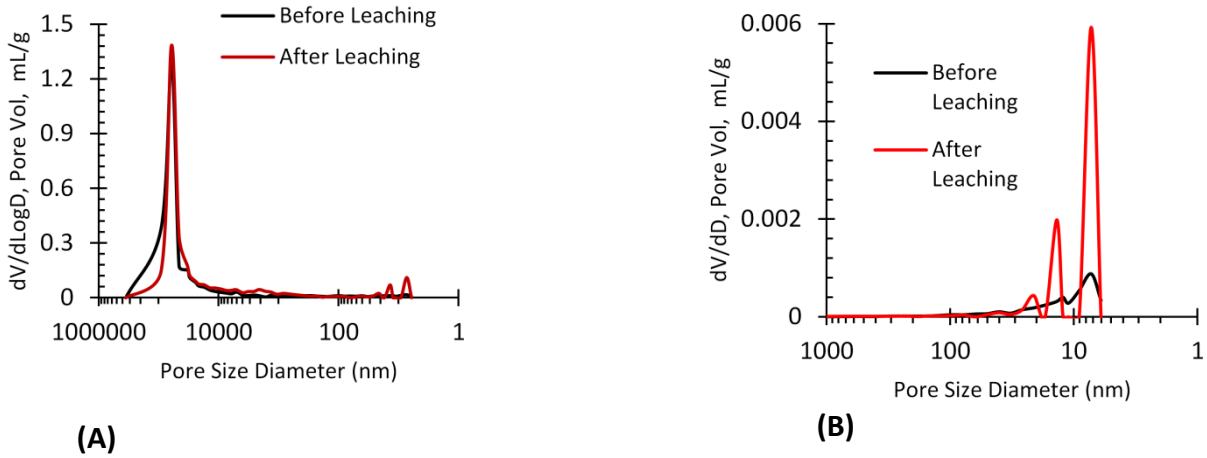

Figure 4.3: (A) Effect of leaching BFS on pore size distribution; (B) Effect of leaching BFS on pore size distribution depicting smaller pore size range

The effect of preheating BFS granules on its pore size characteristics was also investigated in this study. Dimitrova and Mehandjiev (2001) investigated the effect of preheating within 400-800 ^{o}C for several sets of different size fractions of BFS granules on crystallographic changes, surface chemistry and adsorptive activity towards single adsorbate Cu^{2+} ions. As the starting material was predominantly amorphous, preheating facilitated the formation of crystalline phases in larger size fractions, with little crystallographic change in the finer sizes. These finer size fractions still possessed relatively highest surface area values and exhibited highest Cu^{2+} ion adsorption as a function of increasing preheating temperature. Consequently, the presence of crystalline phases was thought to be responsible for the observed increase in adsorption capacity of BFS as preheating temperature was increased. However, surface area decreased across all size fractions. Changes in pore size characteristics were not reported. In a similar study by Mihailova et al (2013), BFS was preheated in a narrow temperature range (860-960 ^{o}C) and the researchers observed formation of crystalline phases. However, surface area increased with increase in preheating temperature while adsorption capacity towards Pb^{2+} ions decreased. This is contrary to the findings of Dimitrova and Mehandjiev (2001).

Figures 4.4(A) and (B) below show the effect of preheating BFS at various temperatures (400-800 ^{o}C) on pore size distribution plotted with pore volume. Again, the major peak in Figure 4.4(A) corresponds to interparticle void space with evidence of intraparticle porosity towards smaller pore sizes. Preheating had negligible effect on differential pore volume and pore size. Similarly, there is no apparent correlation between pore volume, pore size and preheating temperature within 400-600 ^{o}C in the smaller pore size diameter range as shown in Figure 4.4(B). However, a relatively high pore volume around 6-10 nm pore sizes for BFS

heated at 800 ^{o}C is noticeable. There was significant decrease in BET surface area and total pore area as preheating temperature was increased. Dimitrova and Mehandjiev (2001) obtained similar BET surface area results. As shown in Table 4.1 above, there was negligible effect on % porosity, density and total intrusion volume. In Chapter 6, the effect of preheating the adsorbent materials on adsorption kinetics is explored.

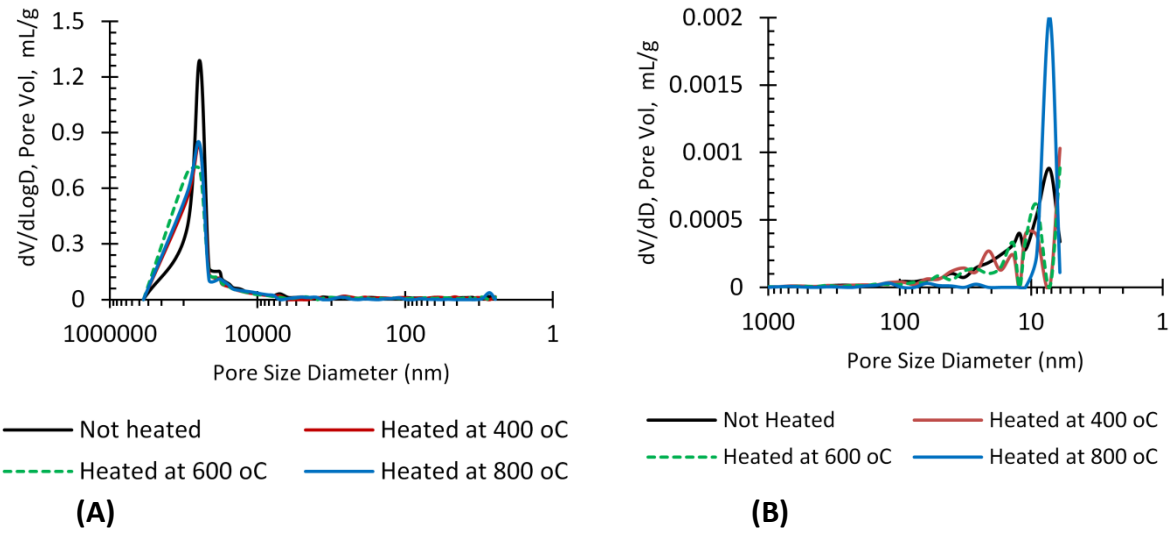

Figure 4.4: (A) Effect of preheating BFS on pore size distribution; (B) Effect of heating BFS on pore size distribution depicting smaller pore size range

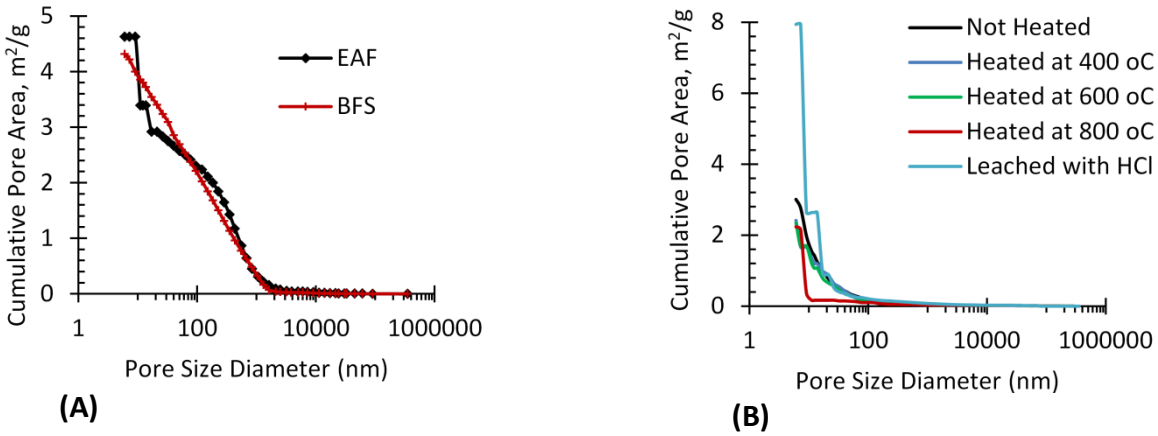

Figure 4.5: Variation of cumulative pore area with pore size for (A) BFS and EAF untreated powders and (B) preheated and leached BFS granules

In Figure 4.5(A), the pore area for EAF powder is slightly higher than that for BFS powder. Interestingly, Figure 4.5(B) depicts the fact that leaching of BFS granules increases the pore area whilst preheating decreases it.

4.3.1.3 Surface Morphology

The surface appearance, roughness, shapes and sizes of pores for the adsorbent materials were examined by SEM, which gives several magnitudes of magnifications. It extends the capabilities of light microscopy to give better focus and images. The preparation of samples is fast and easy. SEM technique is extremely popular across all research fields.

Figures 4.6(A) and (B) show SEM micrographs of BFS granules showing a highly rough, macroporous surface with pores of various sizes and irregular shapes. These characteristics are attractive for the material to be exploited as adsorbents. Similar observations were reported by Dimitrova and Mehandjiev (2001), Mihailova et al (2013) and others (Lopez-Delgado et al., 1998; Xue et al., 2013) with a keen interest to develop inexpensive adsorbents from slag materials.

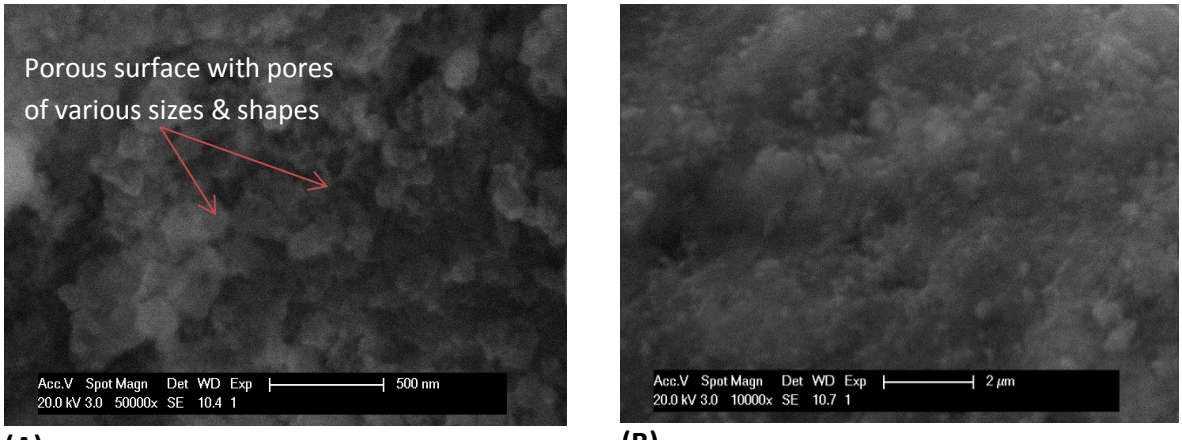

(A) **(B)**

Figure 4.6: SEM micrographs for (A) BFS granules (50000x), and (B) BFS powder (10000x)

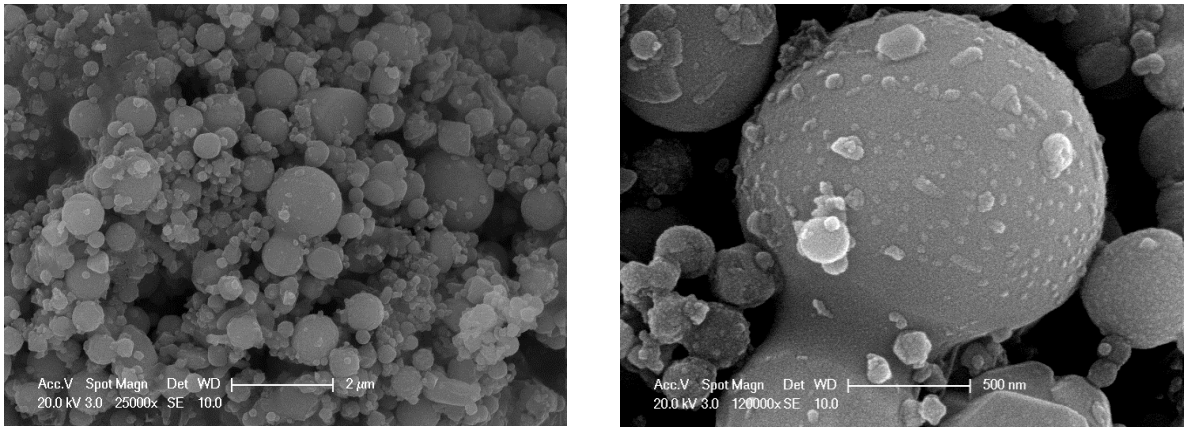

(A) **(B)**

Figure 4.7: SEM micrographs for EAF Powders at magnifications of (A) 25000x, and (B) 120000x

Unlike BFS surface morphology, EAF has mostly rounded shapes of particles of various sizes as shown in Figure 4.7(A) above. A highly magnified image shown in Figure 4.7(B) hardly reveals any surface porosity. Results of mercury porosimetry showed that the internal structure of EAF is mainly macroporous.

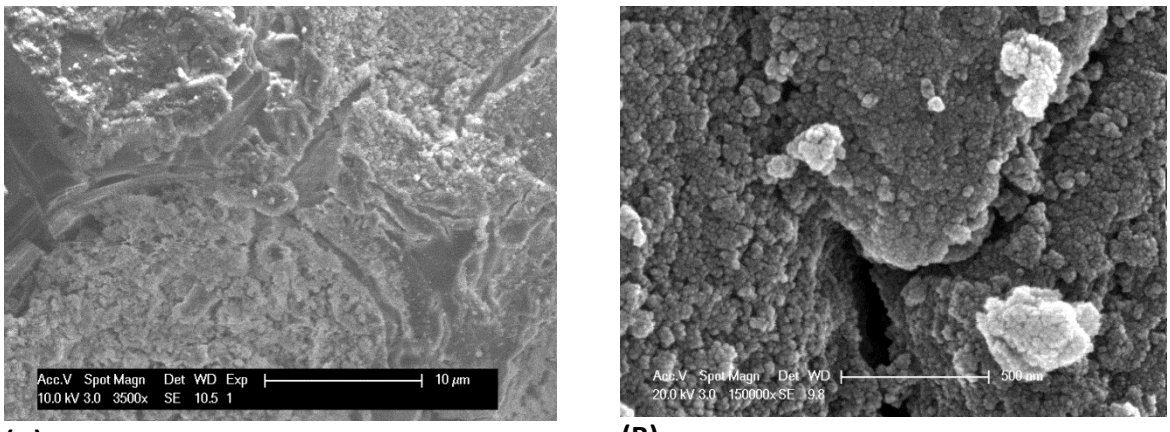

(A) **(B)**

Figure 4.8: SEM micrographs for leached BFS granules at magnifications of (A) 3500x, and (B) 150000x

Acid Leaching has the effect of making BFS surface extremely rough as shown in Figures 4.8(A) and (B) above. Both BET surface area and total pore area of leached BFS were shown

to increase. This is expected to have a positive effect on the extent and rate of adsorption of metal ions. The SEM images of preheated BFS as a function of temperature are given in Figure 4.9, which shows shiny (glassy) appearance in some patches with a relatively less porous surface and distorted grain boundaries. The changes in surface area, chemical composition and pore size distribution have been discussed in the next sections.

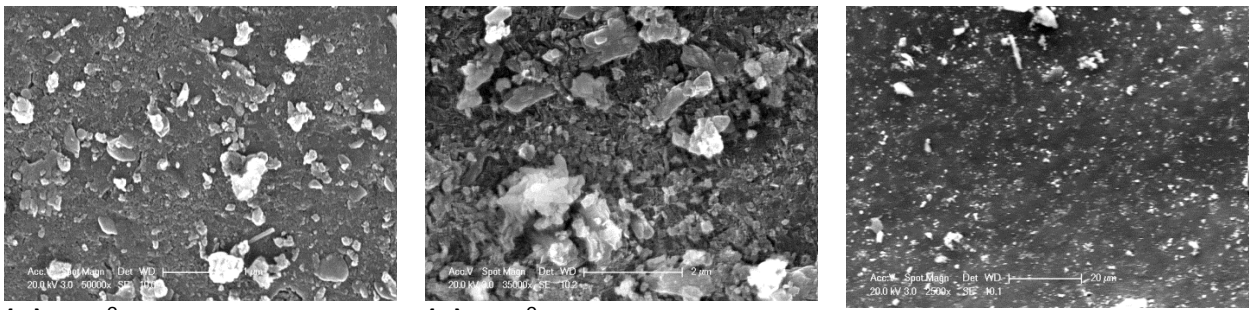

(A) 400 ^{o}C **(B)** 600 ^{o}C **(C)** 800 ^{o}C

Figure 4.9: SEM micrographs for preheated BFS granules at magnifications of (A) 50000x, (B) 350000x and (C) 2500x

The chemical composition for the surfaces of BFS and EAF adsorbent materials were analysed by EDS technique fitted to SEM. The SEM images together with their respective elemental composition are shown in Figures 4.10 and 4.11 below. Both samples of BFS powders and granules contain same surface elements in slightly different quantities. EAF surface contains additional elements to those of BFS surfaces. Many authors believe the process of adsorption of metal ions from solution occurs through ion exchange with mainly Ca^{2+} ions on the adsorbent surface and to some extent Si^{4+} ions (Dimitrova et al., 2001; Dimitrova, 1996; Dimitrova & Mehandgiev, 1998; Lopez et al., 1995). The roles of many other surface elements as seen in this study have not been elucidated. Motsi (2009) suggested that Ca^{2+}, Mg^{2+}, K^{+} and Na^{+} found on natural zeolite surfaces are potentially

exchangeable cations. The details of the proposed ion-exchange mechanisms are discussed further in Chapter 2 of this thesis.

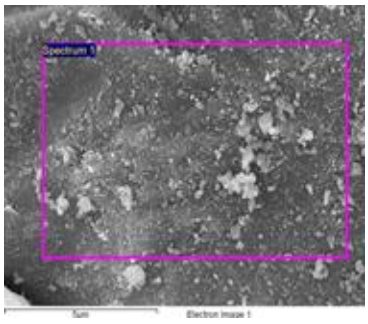

BFS Powder

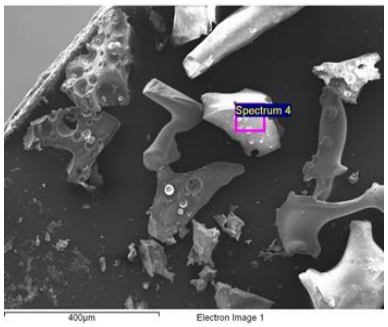

BFS Granules

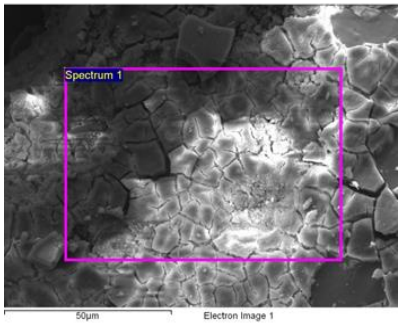

Leached BFS Granules

Adsorbent type	Wt. % elemental surface Analysis										
	*C	O	Mg	Al	Si	K	Ca	Ti	Mn	Fe	Na
BFS Powder	5.91	39.96	3.13	4.49	13.10	0.37	31.19	0.53	0.75	-	0.16
BFS Granules	9.62	52.50	3.84	4.44	10.35	0.34	17.92	0.37	0.22		0.22
Leached BFS Granules	12.05	56.87	0.88	7.11	18.55	-	3.69	0.84	-	-	-

Figure 4.10: SEM/EDS Elemental Analysis for BFS Surfaces

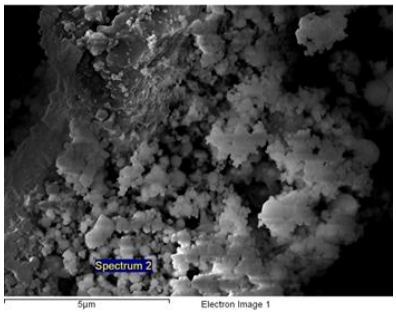

EAF Powder

Adsorbent type	Wt. % elemental surface Analysis											
	C	O	Mg	Cl	Si	K	Ca	Cr	Mn	Fe	Zn	Cu
EAF Powder	15.4	29.6	1.78	1.11	0.66	0.41	5.75	0.28	3.1	24.9	16.4	0.47

Figure 4.11: SEM/EDS Elemental Analysis for EAF Surface

4.3.1.4 BET Surface area

A key analytical step during characterisation of adsorbent materials is the determination of surface area. Brunauer-Emmett-Teller (BET) and Barrett-Joyner-Halenda (BJH) methods based on nitrogen (N_2) gas adsorption theory are widely used to determine surface area and pore size distribution respectively. N_2 gas adsorption is a standard method for micropore and mesopore size analysis (d_p < 50 nm) that employs Kelvin equation to analyse measured data in order to interpret the pore characteristics of the material. As discussed in Section 3.2.2.4, the BET method uses the BET equation (3.2) to estimate the surface area of porous solid materials. However, the BJH method is a procedure for calculating pore size distribution of pore volumes or surface area as a function of pore size diameter using the Kelvin equation (4.1), given below, also from experimental isotherms of N_2 adsorption/desorption data (Rouquerol et al., 2014).

$$r_K = \frac{-2\gamma V_m}{RTln\left(\frac{P}{P_o}\right)} \quad \text{---} \quad 4.1(a)$$

For N_2 as adsorbate, Equation 4.1(a) simplifies to;

$$r_K(\text{Å}) = \frac{4.15}{log\left(\frac{P}{P_o}\right)} \quad \text{---} \quad 4.1(b)$$

Where;

γ = Surface tension of N_2 at its boiling point (8.85 m/Nm at 77 K); V_m = Molar volume of liquid N_2 (34.71 cm^3/mol); R = Gas constant (8.31434 J mol^{-1} K^{-1}); T = Boiling point of N_2 (77 K); P/P_o = Relative pressure of N_2; r_K = Kelvin radius of the pore

Adsorption isotherms for gas/solid systems are classified into six (6) types (Fig. 4.0) (Rouquerol et al., 2014). The isotherms for BFS and EAF powders used in this study are given in Figures 4.12(A) and (B) respectively. They are convex to the relative pressure axis over the entire range and thus do not exhibit a knee, and show minimal hysteresis. Therefore, they fall under a Type (III) classification. Although such true isotherms are rare, Rouquerol et al (2014) stated that such shapes indicate weak adsorbent/adsorbate interactions on macroporous adsorbents.

Table 4.2 below shows BET surface area, pore volume and BJH pore size distribution analysis. Although porosity (54.5-58.9 %) for BFS and EAF powders is comparatively satisfactory, BET surface area is very low (2.46-2.99 m^2/g) relative to similar inorganic adsorbents in use (Zeolites, silica gels, activated alumina, etc.) which have values in excess of 300 m^2/g for practical applications (Deng, 2006; Thomas and Crittenden, 1998). Dimitrova and Mehandgiev (1998), Curkovic et al (2001) and other studies also found low values of surface area of less than 3 m^2/g for various adsorbent slag materials. However, a high surface area is a key requirement in any adsorbent to create a high adsorption capacity.

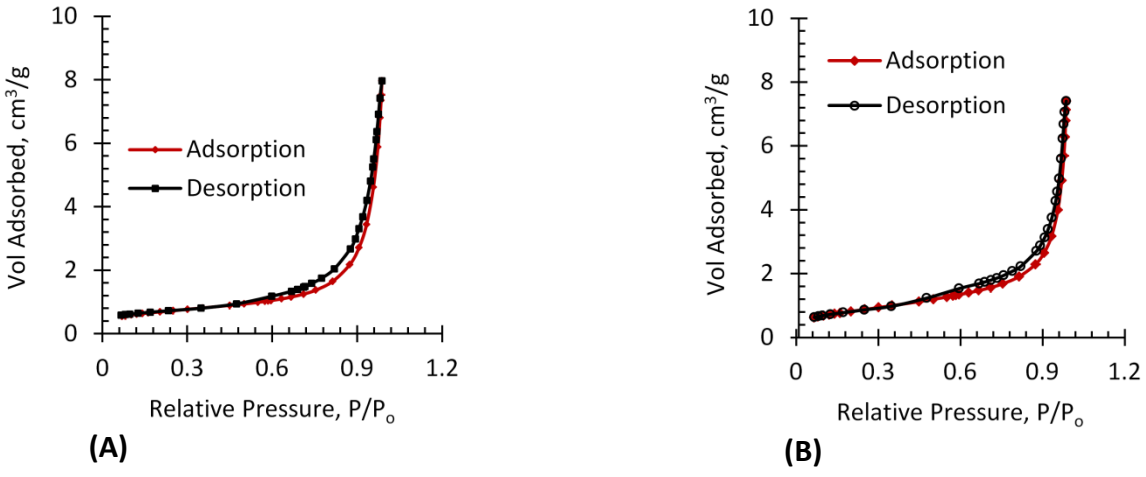

Figure 4.12: N_2 gas adsorption Isotherms for (A) BFS, and (B) EAF powders

The average pore size distribution is plotted against both pore volume and pore area in Figure 4.13. The graphs depict a nearly bimodal mesopore sizes of roughly 20-50 Å and 50-1000 Å for both BFS and EAF powders. The pore volume for BFS is higher than that of EAF. Pore area for EAF is higher between 20-50 Å but lower between 50-1000 Å relative to BFS. However total pore area, as determined by porosimetry, for EAF is slightly higher than that of BFS (Table 4.1).

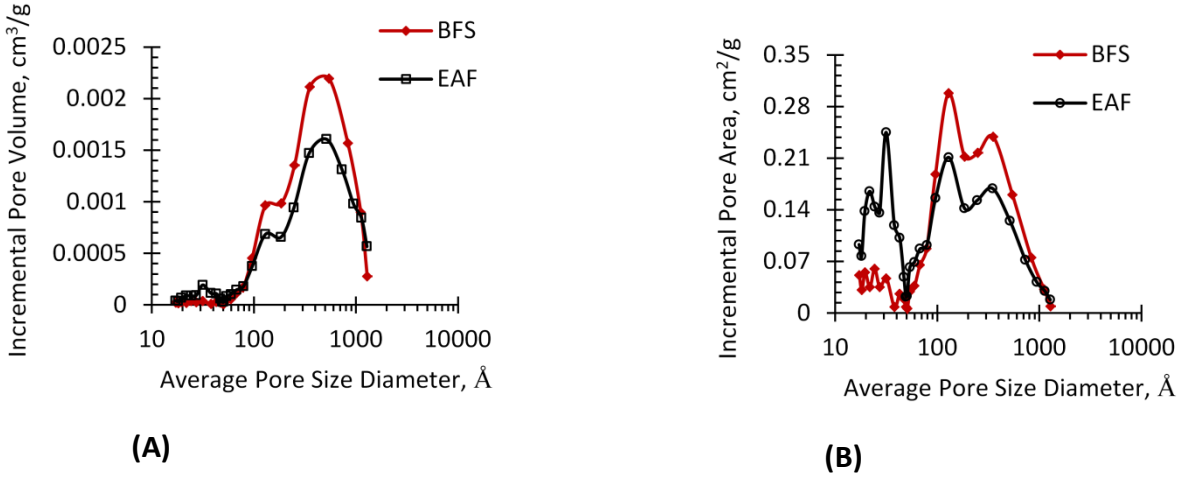

Figure 4.13: Pore size distribution for BFS and EAF powders from N_2 gas adsorption data (A) vs incremental pore volume and (B) vs incremental pore area

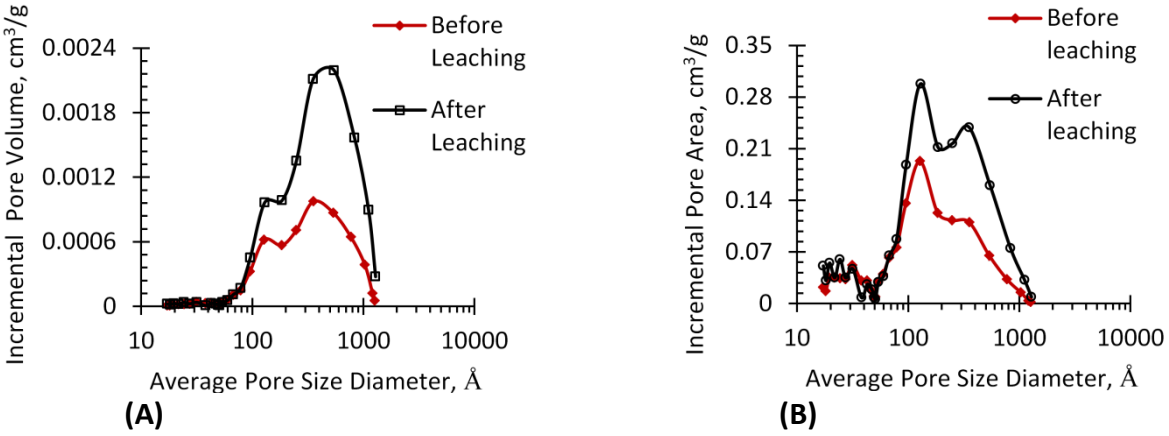

Figure 4.14: Effect of leaching BFS granules on pore size distribution from N_2 gas adsorption data (A) vs incremental pore volume and (B) vs incremental pore area

Figure 4.14 presents the effect of leaching BFS granules on pore size distribution. Both incremental pore volume and pore area are nearly doubled after leaching. Also, BET surface area increased by over three (3) times. Therefore, pretreatment of BFS by a leaching process has the potential to improve the adsorptive properties.

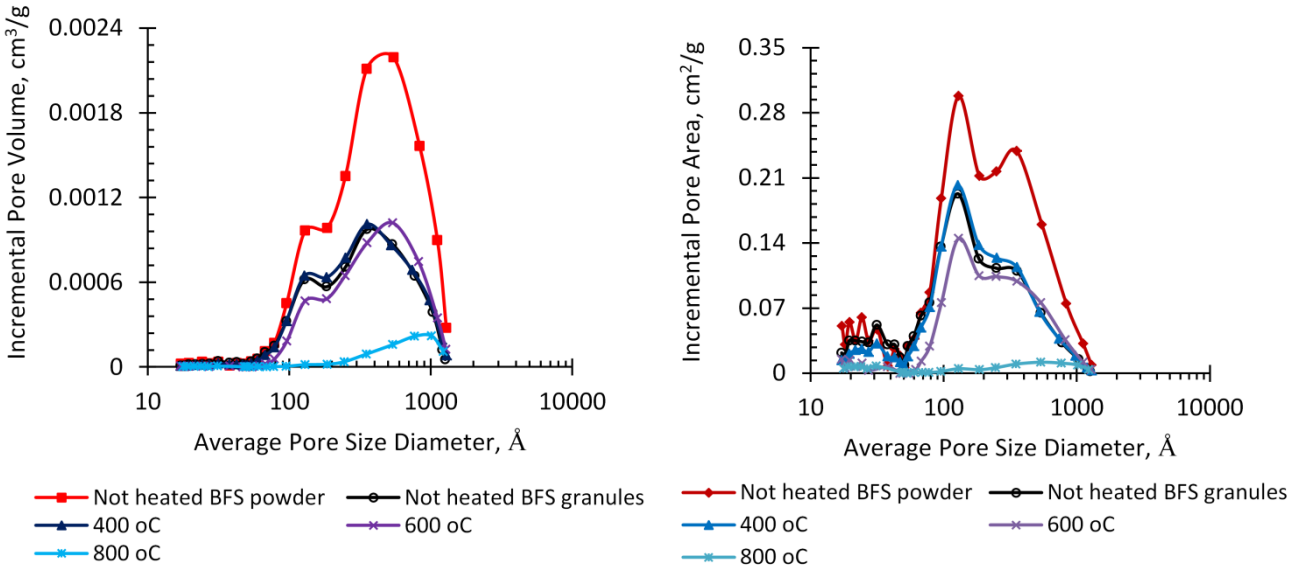

Figure 4.15: Comparison of the effects of pretreatment of BFS granules by a heating process on pore size distribution from N_2 gas adsorption data (A) vs incremental pore volume and (B) vs incremental pore area

A comparative summary of the effect of pretreatment of BFS granules on pore size distribution is presented in Figure 4.15 above. BFS powder has superior characteristics relative to granules. For this study, it is evident that leaching the coarse size fraction of BFS (granules) improves pore volume, pore area and surface area while preheating destroys the internal structure of BFS material. The structural changes may be due to possible sintering of the material as temperature was increased (Dimitrova and Mehandgiev, 2001) to form

glassy-like surfaces with collapsed pores leading to a decrease in adsorbent properties. From Table 4.2, BET surface area decreased with increase in preheating temperature. At the highest temperature of 800 ^{o}C, surface area is over ten (10) times lower than the untreated material. As shown previously, leaching improves BET surface area by over three (3) times.

It must be note that the BET analyses in Table 4.2 were based on single representative adsorbent samples. For a comparison of pore sizes in the adsorbent relative to the sizes of metal ions, see Table 5.4 in Chapter 5.

Table 4.2: N_2 adsorption data for BET surface area, pore volume and BJH pore size analysis

	Characteristics of Adsorbent Materials						
Parameter	**BFS granules (Control)**	**BFS Powder**	**BFS Leached**	**BFS, heated at 400 °C**	**BFS, heated at 600 °C**	**BFS, heated at 800 °C**	**EAF powder (As received)**
Particle diameter (dp), µm or mm	0.18-0.36 mm	d_p<45 µm	0.18-0.36 mm	0.18-0.36 mm	0.18-0.36 mm	0.18-0.36 mm	d_p<45 µm
Surface area;							
Single point Surface area, m^2/g	1.408 at P/P_o 0.2017	2.381 at P/P_o 0.2039	4.864 at P/P_o 0.1991	1.252 at P/P_o 0.1999	0.791 at P/P_o 0.2019	0.109 at P/P_o 0.2000	2.846 at P/P_o 0.1995
BET surface area, m^2/g	1.4601 ± 0.0025	2.4609 ± 0.0126	5.0753 ± 0.0116	1.3019 ± 0.0018	0.8273 ± 0.0015	0.1191 ± 0.0004	2.9912 ± 0.0050
Micro Pore Area, m^2/g	0.1044	0.2621	0.2802	0.0785	0.0122	-	-
External Surface Area, m^2/g	1.3558	2.1988	4.7951	1.2235	0.8152	0.1413	3.0280
BJH Adsorption Cumulative Surface area of pores between 17 and 3000 Å *Dia., m^2/g	1.3274	2.0295	4.9402	1.2285	0.7674	0.1071	2.7383
BJH Desorption Cumulative Surface area of pores between 17 and 3000 Å Dia., m^2/g	2.3670	2.3732	6.0064	2.2034	1.1891	0.1023	3.0132
Pore Volume							
Single Point Adsorption Total Pore Volume of Pores, cm^3/g	0.0061 cm^3/g of pores < 1441.71 Å dia at P/P_o 0.9865	0.0123 cm^3/g of pores < 1558.94 Å dia at P/P_o 0.9875	0.0092 cm^3/g of pores < 1483.02 Å dia at P/P_o 0.987	0.0063 cm^3/g of pores < 1448.34 Å dia at P/P_o 0.9866	0.0052 cm^3/g of pores < 1389.69 Å dia at P/P_o 0.9860	0.00097 cm^3/g of pores < 1348.21 Å dia at P/P_o 0.9856	0.0115 cm^3/g of pores < 1427.89 Å dia at P/P_o 0.986
Micropore Volume, cm^3/g	0.000033	0.000098	0.000066	0.000022	-	-	-
BJH Adsorption Cumulative Pore Volume of pores between 17 and 3000 Å dia, cm^3/g	0.005864	0.011422	0.008833	0.006132	0.005018	0.000902	0.010890
BJH Desorption Cumulative Pore Volume of pores between 17 and 3000 Å dia,cm^3/g	0.006124	0.012205	0.009320	0.006342	0.005165	0.000953	0.011480
Pore Size							
Adsorption Average Pore Diameter (4V/A by BET), Å	167	200	72	194	249	327	153
BJH Adsorption Average Pore Dia., (4V/A), Å	177	225	72	200	262	337	159
BJH Desorption Average Pore Dia., (4V/A), Å	103	205	62	115	174	373	152

*Dia = diameter

4.3.1.5 Phase Composition

The XRD pattern for BFS and EAF adsorbent materials are shown in Figures 4.16 and 4.17 respectively. BFS is mainly amorphous with minor crystalline phases of calcite ($CaCO_3$). EAF consists of predominantly magnetite (Fe_3O_4) with minor calcium iron oxides and magnesium iron oxides. Both amorphous and crystalline phases have been shown to support solute adsorption from solutions, with crystalline phases reported to be superior (Dimitrova et al., 2001). However, the contributions of all these phases to adsorption mechanisms are not clear. Also, there were no observed crystallographic changes due to the effects of pretreatments by leaching and preheating processes. Evidence from XRD patterns (not shown) of pretreated materials indicated that they remained predominantly amorphous.

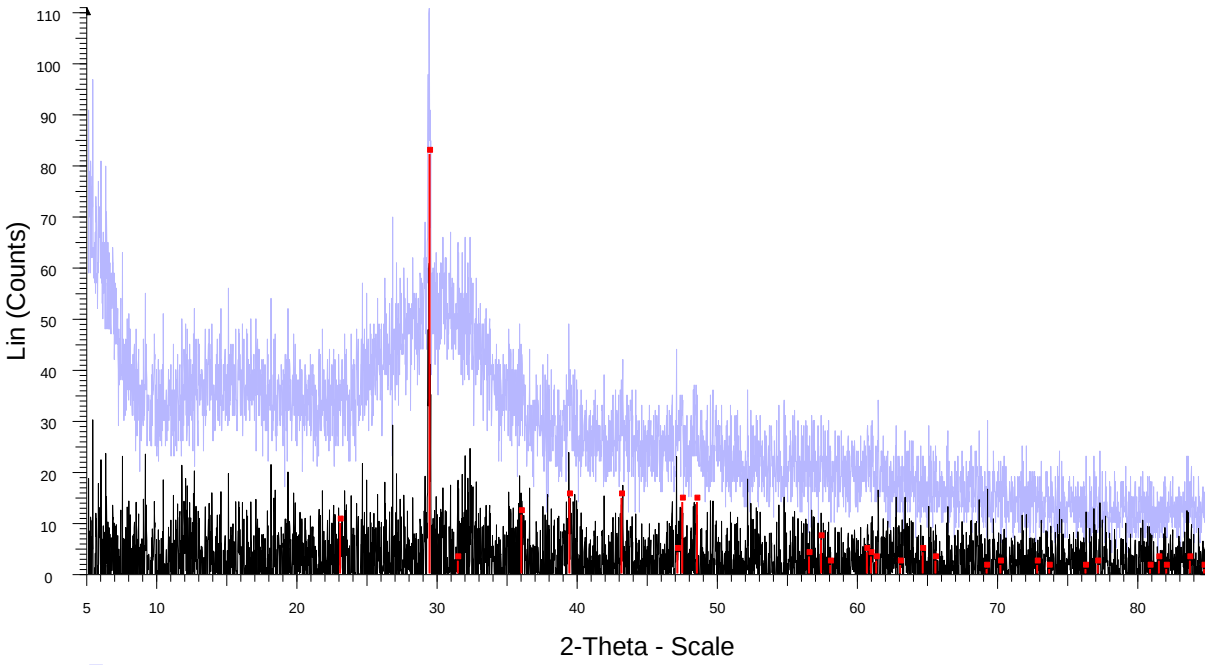

Figure 4.16: XRD pattern for BFS showing $CaCO_3$ peaks

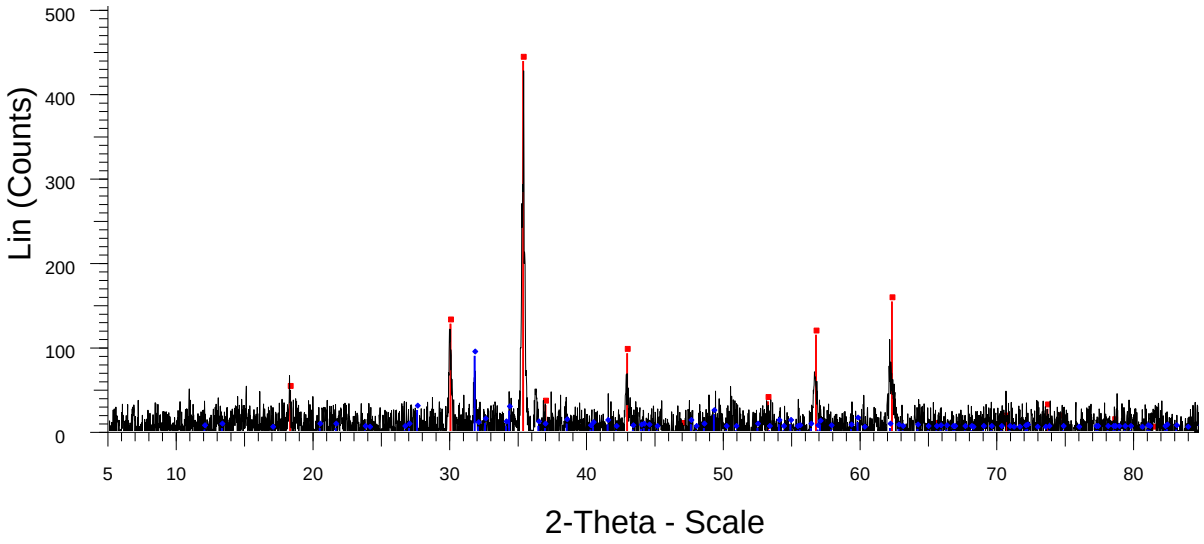

Figure 4.17: XRD pattern for EAF showing magnetite (Fe_3O_4) peaks being predominant with minor Calcium iron oxides and magnesium iron oxides.

4.3.1.6 Chemical Composition

Table 4.3 below gives the chemical composition (as oxides) of leached, preheated and as-received BFS and EAF adsorbent materials. On the basis of XRF results, over 90% of BFS (powders/granules) consists mainly of CaO, SiO_2, Al_2O_3 and MgO with other minor oxides making up the remainder. EAF powder, however, has Fe_2O_3, ZnO, as main oxides and significant amounts of CaO, SiO_2, MgO, Na_2O, trace Al_2O_3 and several other oxides. The high lime (CaO) content of BFS means that the material has a potentially high neutralizing capacity for acidic effluents with ability to precipitate metal ions (Bodurtha and Brassard, 2000; Yan et al., 2000).

There was no definitive correlation between preheating temperature and changes in the chemical composition of the major oxides (CaO, SiO_2, Al_2O_3 & MgO) whilst the concentration of the rest of the (minor) oxides remained relatively constant. Interesting results were obtained from leaching the BFS granules by HCl. The first stage leaching (leached x1, in

Table 4.3) partially extracted Ca^{2+} ions (28 %) to give relative increments in quantities of some oxides (SiO_2, Al_2O_3, etc.,). Further leaching at the second stage (leached x2) resulted in 83 % Ca^{2+} ion extraction, increasing SiO_2 content to 80 % and TiO_2 to 8.7 %. The quantities of all other oxides were reduced. HCl consumption under the employed experimental and solution conditions was quite high due to several chemical leaching reactions taking place. The production of SiO_2-rich material is desirable since it can potentially provide a specific surface area of up to 400 m^2/g at 80 % SiO_2 content (McCauley, 2001).

Table 4.3: Chemical composition (% w/w) of Adsorbent Materials

Adsorbent Material	**Oxide composition, % w/w**										
	CaO	**SiO_2**	**Al_2O_3**	**MgO**	**K_2O**	**MnO**	**Fe_2O_3**	**TiO_2**	**Na_2O**	**SO_3**	
EAF Powder	7.3	2.5	0.7; (Cr_2O_3, 0.8)	2.8	0.8	3.4	44.5	ZnO 19.6	2.7	2.3	PbO 1.0
BFS Powder	44.1	30.7	10.6	5.8	0.6	0.7	0.4	0.7	0.3	2.0	-
BFS, Granules (Control)	34.6	22.9	8.0	5.5	0.6	0.4	0.3	0.9	0.6	2.1	-
BFS Leached Granules (x1)	30.5	29.6	11.1	4.1	0.4	0.5	0.2	0.9	0.5	1.6	-
BFS Leached Granules (x2)	7.2	80.0	5.6	0.3	0.2	0.2	0.6	8.7	-	P_2O_5 0.2	ZrO_2 1.9
Preheated BFS Granules at 400 ^oC	32.4	19.4	6.1	4.2	0.6	0.4	0.3	0.8	0.6	2.2	-
Preheated BFS Granules at 600 ^oC	36.2	25.5	9.1	6.0	0.6	0.4	0.3	0.8	0.5	2.0	BaO 0.1
Preheated BFS Granules at 800 ^oC	35.1	24.0	8.7	5.9	0.6	0.4	0.3	0.8	0.6	2.1	-

4.3.1.7 Density

Values of true densities of BFS and EAF materials are given in Table 4.1. The density of BFS is around 2.8 g/cm^3 which is lower than that of EAF at 4.2 g/cm^3. Specific surface area depends on density, more dense and porous materials tend to have large surface areas depending on pore sizes. Pretreatment of the BFS granules had no effect on the density of the material.

4.3.1.8 Surface Chemistry

The oxidation states, possible types of bonding and surface elements/compounds for BFS and EAF fresh samples as well as adsorbed BFS surfaces with multiple metal ions of Cd^{2+}, Co^{2+}, Cu^{2+}, Fe^{2+} and Mn^{2+} ions (as a function of pH (1.5-7.5)) were analysed by XPS, which was carried out using a Kratos AXIS Ultra. The area of acquisition was 700 x 300 µm and the X-ray power was 300 W. A pass energy of 160 eV was used to obtain survey spectra and a pass energy of 40 eV was used to obtain high resolution spectra of the samples. Effective charge neutralisation was achieved using Kratos' patented coaxial charge neutralisation system. The spectra were calibrated to C1s for C-C/H at 285.0 eV.

There was no evidence of Cd^{2+}, Co^{2+}, Cu^{2+}, Fe^{2+} or Mn^{2+} ions on the adsorbent surfaces possibly due to their low concentration falling below the instrument detection limit. It is sometimes possible to detect low concentration elements with XPS if each scan is ran for a very long time at low resolution (high pass energy gives greater sensitivity), to increase the number of counts detected. However, Kratos Analytical Ltd (Manchester) is unable to do such a scan in their laboratory. The possible chemical functionality of fresh BFS and EAF materials for the high resolution spectra are given in Figures 4.18 and 4.19 respectively. The XPS results for the surface elements are consistent with data from XRF and SEM/EDS

analyses. More work is necessary to identify surface compounds in order to assist with interpretation of the adsorption mechanisms.

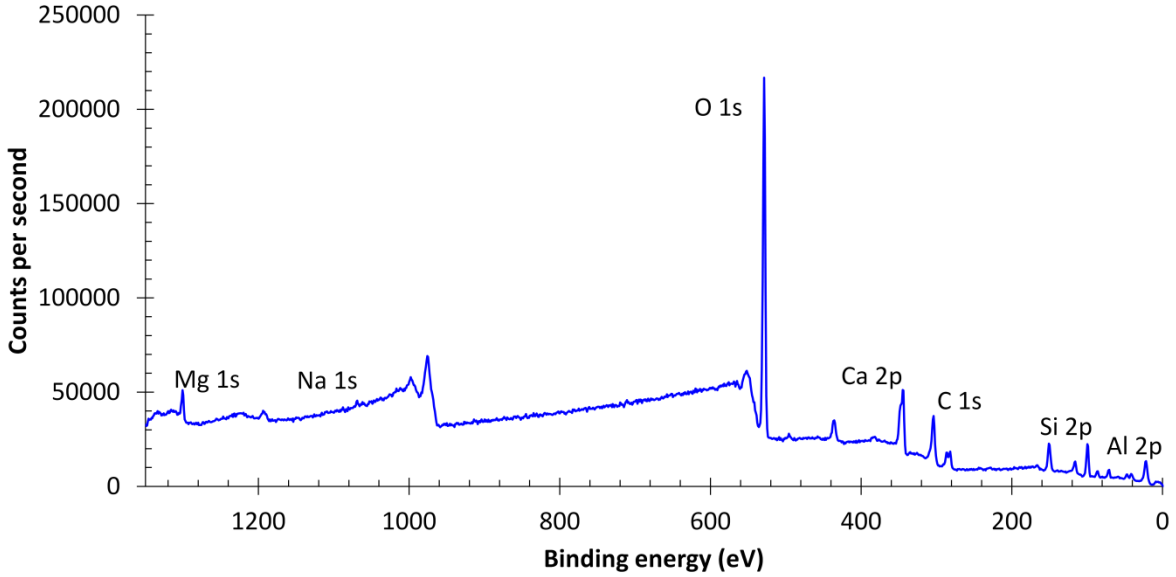

Figure 4.19: XPS spectra for fresh BFS granules

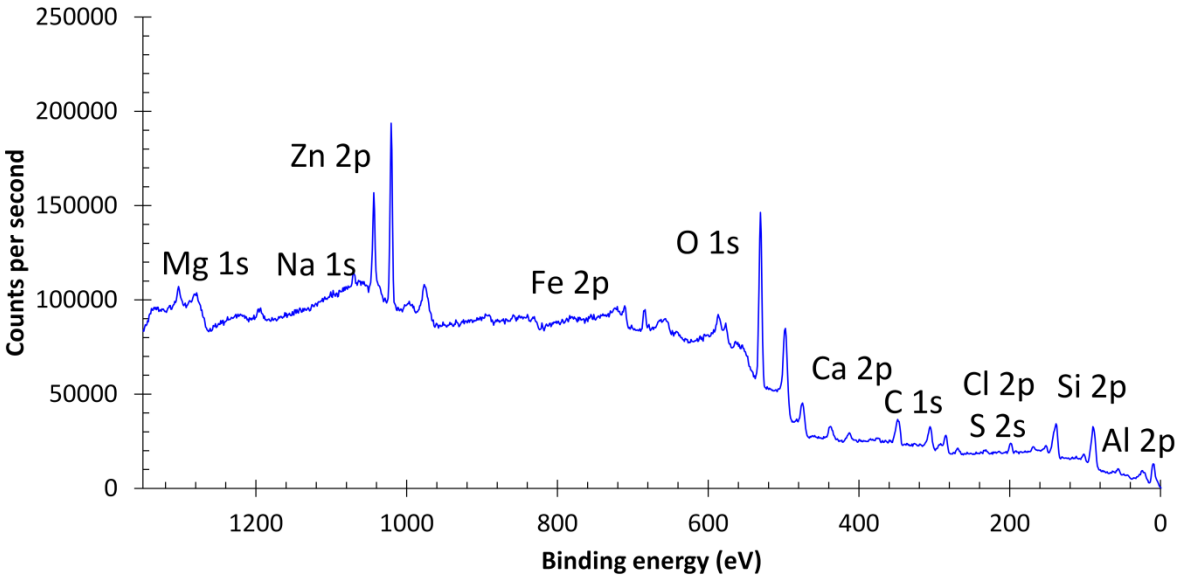

Figure 4.19: XPS spectra for fresh EAF powder

4.4 Conclusions

The physicochemical properties of BFS and EAF materials relevant to adsorption process have been evaluated and assessed in this study. Evidence has been provided in support of improving these properties. Slag materials possess attractive characteristics for them to be exploited as adsorbents.

Both BFS and EAF adsorbent materials are mainly amorphous with minor crystalline phases of calcite ($CaCO_3$) and magnetite (Fe_2O_3) respectively. Their chemical (oxide) composition is typical of that reported in literature. Several elements/ions exist on adsorbent surfaces which are believed to be involved in ion exchange mechanisms of adsorption process.

It can be deduced that the majority of pore sizes are greater than 50 nm, implying that the materials are macroporous. Therefore, the macroporosity nature of the materials and relatively large pore sizes limit internal pore surface area and consequently adsorption capacity. Although % porosity for these novel adsorbent materials is comparatively satisfactory, BET surface area is extremely low relative to similar inorganic adsorbents currently in use. Further, they have inferior pore structure and pore size distribution, and are much denser with low internal pore surface area which might limit their effectiveness for wide applications such as in adsorption systems of relatively high metal solute concentration.

The results of this study further provide supporting evidence that a leaching process for BFS greatly improves pore volume, total pore area and BET surface area. Pretreatment of BFS by leaching also produced a desirable SiO_2-rich material which could potentially provide a specific surface area of up to 400 m^2/g at 80 % SiO_2 content. This is expected to have a positive effect on the extent and rate of adsorption of metal ions. Pretreatment by heating destroys the internal structure of the material. In fact, BET surface area and total pore area decreased with increase in preheating temperature.

EAF possesses slightly better adsorptive characteristics than BFS. However, BFS powder showed superior characteristics to its granulated form. Thus, an optimal particle size reduction may be necessary to improve the adsorptive properties. However, it is imperative to employ as coarse BFS particles as possible for the concept to be economically attractive and viable since size reduction has cost implications such as high energy input requirement.

It is therefore recommended that further studies to optimise leaching of BFS be conducted to improve key properties. Also, more studies on these novel adsorbents are needed to understand their surface chemistry. Material characterisation is useful to obtain an improved interpretation and understanding of experimental data in adsorption systems. Nevertheless, despite limitations, deeper understanding of the material characteristics to develop adsorbents for application in treating waste solutions of low metal concentrations may be justified where most purification methods are either inefficient and/or uneconomic.

CHAPTER 5
ADSORPTION EQUILIBRIA

5.1 Introduction

The analysis of adsorption systems requires information on adsorbate/adsorbent equilibrium, in addition to adsorption kinetics that is discussed in Chapter 6 of this thesis, to fully understand the system. This chapter therefore describes multicomponent adsorption equilibria of Cd^{2+}, Co^{2+}, Cu^{2+}, Fe^{2+} and Mn^{2+} ions with slag materials as adsorbents. Significant attention has focussed on adsorption of metal ions by several novel adsorbents from single component systems of metal ions. However, one of the challenges in describing adsorption behaviour of metal ions from waste solutions is that many industries discharge effluents that contain multiple metal ions. Hence, any design of an adsorption system must be based on actual experimental data from multicomponent effluents. This necessitated adsorption study based on multicomponent systems of metal ions to generate equilibria data that is important in environmental applications and/or industrial separations (Dabrowski, 2001).

Adsorption equilibrium is a thermodynamic state that is established when the liquid phase containing the adsorbate has been contacted with the solid phase (adsorbent) for sufficient time normally at constant temperature and pH. At this point, the rate at which the adsorbate in the bulk solution adsorbs onto the adsorbent surface is equal to the rate at which it desorbs, and thus, its equilibrium concentration remains constant. When the solid phase concentration is plotted against the residue liquid phase concentration, the

equilibrium adsorption isotherm is obtained, which is a correlation of the distribution of the adsorbate between the adsorbent and solution. In the design of adsorption systems, the most appropriate mathematical relationship for the equilibrium curve, termed adsorption isotherm must be established. Several isotherm models have been formulated to describe equilibrium relationship between adsorbate and adsorbent in systems of one or more adsorbates from which adsorption mechanisms, surface characteristics and degree of affinity of the adsorbent can be evaluated. The concept of adsorption equilibrium is also a valuable tool to measure and compare capacity and selectivity of different adsorbents (Dabrowski, 2001; Deng, 2006; Foo & Hameed, 2010; Knaebel, 2012; Richardson et al., 2002).

Adsorbent capacity is often evaluated by Langmuir and Freundlich isotherms with most of the studies conducted in single solute systems. The Langmuir isotherm assumes monolayer adsorption without solute interaction while the Freundlich model provides for multilayer adsorption. High Langmuir adsorption capacities of 64.17 mg/g Pb^{2+} ions, 16.07 mg/g Cu^{2+}, 9.55 mg/g Cr^{3+}, 6.74 mg/g Cd^{2+} and 4.36 mg/g Cd^{2+} (20 ^{o}C, 50 g/L phase ratio) for blast furnace (BF) sludge have been reported by Lopez et al (1995) and Lopez-Delgado et al (1998), which increased with temperature, with up to 79.87 mg/g Pb^{2+} loading at 80 ^{o}C. The selectivity was Pb^{2+}>Cu^{2+}>Cr^{3+}>Cd^{2+}>Zn^{2+} and this relationship was attributed to possible differences in either electronegativity or hydrated ionic radii as well surface complex formation and precipitation (Allred, 1961; Farley et al., 1985; Nightingale, 1959). The mechanism of adsorption involved physisorption and ion exchange processes. The authors recommended further studies based on both synthetic and actual wastewater solutions containing multiple metal ions. Similarly, Curkovic et al (2001) found relatively high

Langmuir adsorption capacities of 33.78 mg/g Pb^{2+} and 32.68 mg/g Cu^{2+} ions (20 ^{o}C, 10 g/L phase ratio) with electric arc furnace (EAF) slag material, which increased slightly with temperature.

Dimitrova (1996) and Dimitrova and Mehandgiev (1998) fitted a Freundlich isotherm to analyse equilibrium data for adsorption of for Cu^{2+}, Ni^{2+}, Zn^{2+} and Pb^{2+} ions by blast furnace slag (BFS) with high regression coefficients. High Langmuir adsorption capacities of up to 300.1 mg/g Cu^{2+} using steel slag (20 ^{o}C, 100 g/L phase ratio, pH 5.0) were reported by Kim et al (2008), which increased with increase in pH. The principle mechanism was hydroxide precipitation which increased with increase in pH and adsorption contribution increased with decrease in pH. Other values of Langmuir capacities from studies involving single adsorption systems of metal ions by slag materials include 88.50 mg/g Cu^{2+} and 95.24 mg/g Pb^{2+} ions with steel slags (2 g/L phase ratio, pH 5.5, 18 ^{o}C) (Feng et al., 2004). Other studies have reported satisfactory fits of Langmuir and/or Freundlich models to adsorption equilibrium data of metal ions by steel slags (Gupta, 1998; Liu et al., 2009). The capacity of slag materials demonstrates the potential application to treat industrial effluents such as acid mine drainage and metal electroplating waste solutions.

Liu et al (2009) found adsorption capacities of metal ions in a multiple adsorption system to be lower than values in their respective single solute system. Selectivity was reported as $Cr^{3+}>Zn^{2+}>Cu^{2+}>Pb^{2+}$. Xue et al (2009) studied adsorption of several metal ions by basic oxygen furnace (BOF) slag and applied extended constant-capacitance surface complexation model to describe adsorption of Cu^{2+}, Cd^{2+}, Pb^{2+} and Zn^{2+} ions. This model requires knowledge of proton stoichiometry of surface reactions, speciation of metal ions and

concentration of surface sites. It proposes an ion exchange process at low pH and complexation at high pH. The model provided satisfactory fits of adsorption data in most single and multisolute systems, with selectivity that differed for single solutes relative to multiple systems. However, studies involving adsorption of multiple metal ions by slag materials and the application of competitive isotherms are limited. Thus, the objective of this chapter was to determine the adsorption capacity, affinity and selectivity of blast furnace slag (BFS) and electric arc furnace slag (EAF) materials in the adsorption system of multiple metal ions of Cd^{2+}, Co^{2+}, Cu^{2+}, Fe^{2+} and Mn^{2+} ions, and to apply the extended Langmuir isotherms to deduce adsorbent capacity and underlying mechanisms of adsorption of metal ions.

5.2 Materials and Methods

Reference is made to Chapter 3 of the thesis for a detailed description of materials, experimental setup and procedure. Only a brief summary of the experimental procedure is presented here. Synthetic waste solutions containing variable acidity and concentrations of Cd^{2+}, Co^{2+}, Cu^{2+}, Fe^{2+} and Mn^{2+} ions were prepared from stock solutions according to the procedure described in Chapter 3 to generate multicomponent solutions of metal ions that simulated average compositions of acid mine wastewater solutions.

Batch adsorption experiments were carried out in agitated bottles to study the effects of solid/liquid phase ratio and initial metal ion concentration on adsorption equilibria. Two sets of adsorption experiments were conducted with BFS material (d_p < 45 μm) firstly at the same initial concentration for each metal ion in the range 20-1000 mg/L at 50 g/L BFS and secondly at different initial concentration for each metal ion in the ranges 20-200 mg/L Cd^{2+},

15-150 mg/L Co^{2+}, 30-1000 mg/L Cu^{2+}, 50-1600 mg/L Fe^{2+} and 20-100 mg/L Mn^{2+} at 30 g/L BFS. To compare the effect of phase ratio, the total ion concentration at each increment was kept at the same value for both phase ratios as an indirect measure of ionic strength. However, only one set of experiments was carried out with EAF material (d_p < 45 μm) at different initial concentration for each metal ion in the same ranges as for BFS, i.e., 20-200 mg/L Cd^{2+}, 15-150 mg/L Co^{2+}, 30-1000 mg/L Cu^{2+}, 50-1600 mg/L Fe^{2+} and 20-100 mg/L Mn^{2+} at 22 ^{o}C, 30 g/L phase ratio for 8 hours.

0.5 L of waste solution at pH 3.50 containing the desired initial metal ion concentration was fed to the adsorption vessel and the required adsorbent mass of either BFS or EAF was then added and the mixture agitated. Aliquots of about 10 mL slurry samples were taken at equilibrium and filtered. Changes in equilibrium metal ion concentrations were measured in the filtrate by Perkin Elmer AAnalyst 300 Flame Atomic Absorption Spectrometer from which adsorption capacities, selectivity and affinity were calculated. The error as a standard deviation in AAS analyses of metal ion concentration was in the range of up to ± 5 %.

5.3 Results and Discussion

The effectiveness of slag materials as adsorbents for multiple metal ions was analysed by determination of the adsorption equilibrium curves by plotting adsorption capacity (q_e, mg/g) vs. residue adsorbate concentration (C_e, mg/L), from which maximum adsorption capacity and distribution coefficient (q_e, L/mg) were calculated by Equations (3.8) and (3.10) respectively. For adsorption/ion exchange based separations, equilibrium isotherms depend

on temperature, pH, initial solute concentration and ion exchanger or adsorbent characteristics (Inglezakis et al., 2002)

$$q_e = \frac{V(C_o - C_t)}{m} \qquad \text{---} \quad (3.8)$$

$$k_d = \frac{q_e}{C_e} \qquad \text{---} \quad (3.10)$$

In the analysis of multicomponent equilibria of metal ions, the objective of equilibrium experiments carried out at same initial concentration of metal ions was to evaluate the adsorbent capacity, selectivity and competitive loading of the ion mixture by assuming that the concentration gradient is the same and thus the driving force for the adsorption reaction. The aim of the equilibrium experiments carried out at different initial concentration was to also assess competition for adsorption sites, i.e., whether all ions compete for the same adsorption sites or different ions adsorb to different adsorption sites based on level of adsorption efficiency and capacity. Here, the assumption was that ions kept at lower concentration could adsorb preferentially relative to others if all adsorption sites were available to all ions and vice versa. As reported in the literature, the adsorption level of single solutes is high in dilute solutions.

5.3.1 Effect of Initial Concentration and phase ratio

The adsorption isotherms of metal ions as a function of phase ratio for BFS material are given by equilibrium curves in Figure 5.1 and results are summarised in Table 5.1. The high isotherm slopes indicate that metal ions have a high affinity for BFS and that BFS material attains saturation at relatively low concentration. The isotherms obtained are characteristic

of adsorbent/solute interactions in dilute solutions, similar to Type (I) for pure gases (Seader et al., 2011). The isotherms further fall under 'L' (Langmuir) and 'H' (high affinity) classifications. The 'L' isotherms are indicative of progressive saturation of the adsorbent and 'H' isotherms are a subset of 'L' isotherms whereby the initial slope is very high. Here, the solute exhibits a very high affinity for the adsorbent such that the initial slope cannot be distinguished from infinity (Giles et al., 1974; Limousin et al., 2007). Although isothermal data were collected over a wide metal ion concentration, the isotherms presented here are for low solute concentration range that models the approach to maximum adsorption capacity of the adsorbent. Adsorption capacity decreased at high concentration.

The most important adsorbent characteristic is the adsorption capacity. It depends on initial condition of adsorbent, temperature, pH, liquid phase concentration among others. From a practical point of view, adsorption capacity determines some design requirements of an adsorption system such as the quantity of adsorbent required and volume/size of adsorption vessel which are important to the capital costs (Knaebel, 2012). The results in Figure 5.1 further show that higher phase ratio did not influence the shape of the isotherms but increased the maximum adsorption capacity of BFS at equilibrium for metal ions. Probably total surface area and/or adsorption sites increased with increase in adsorbent mass. This observation may be useful when treating relatively concentrated waste solutions.

At both phase ratios studied, adsorption capacity increased with increase in concentration to the maximum levels for Cd^{2+}, Co^{2+} and Mn^{2+} ions, which correspond to adsorbent saturation. It is thought that high concentration of adsorbate in solution provides a high concentration gradient that acts as a driving force for adsorption and/or ion exchange

reactions (Du et al., 2005). However, adsorption capacities for Cu^{2+} and Fe^{2+} ions increased continuously with increase in concentration with no observable adsorption saturation under the employed experimental conditions. That is, the isotherms for Cu^{2+} and Fe^{2+} ions do not show a graphically horizontal portion characteristic of adsorbent saturation, which means that saturation point for these ions was not attained. As discussed in Chapter 6, besides adsorption other additional extraction mechanisms such as chemical precipitation are significant for these ions. The distribution coefficients for Cu^{2+} and Fe^{2+} ions are larger than those of Cd^{2+}, Co^{2+} and Mn^{2+} ions reflecting high affinity and preferential adsorptive separation for Cu^{2+} and Fe^{2+} ions. Similar results trend were reported for adsorption of multiple metal ions by basic oxygen furnace (BOF) slag in a nitrate system (Xue et al., 2009) and single metal ions by zeolites in a sulphate system (Motsi et al., 2009). However, additional precipitation mechanism is likely to be significant in a sulphate system in this study relative to a nitrate system where metal ions may remain solubilised over a wide pH range.

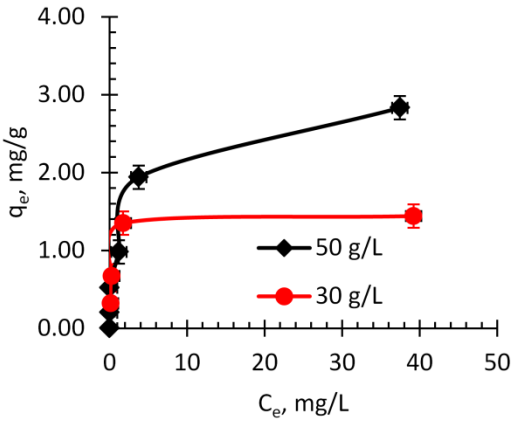

(a) Cd^{2+}

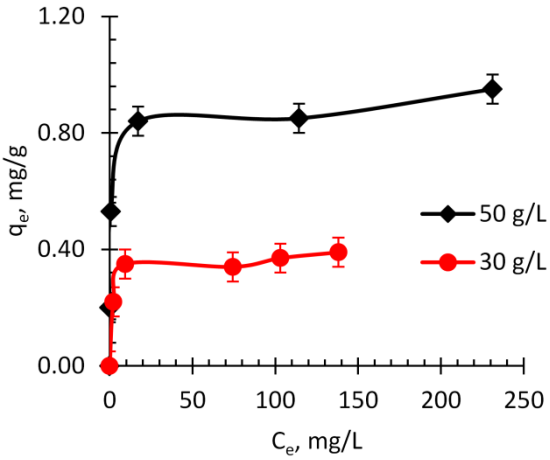

(b) Co^{2+}

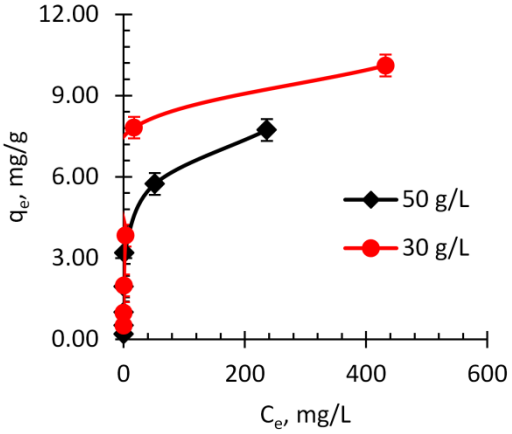

(c) Cu^{2+}

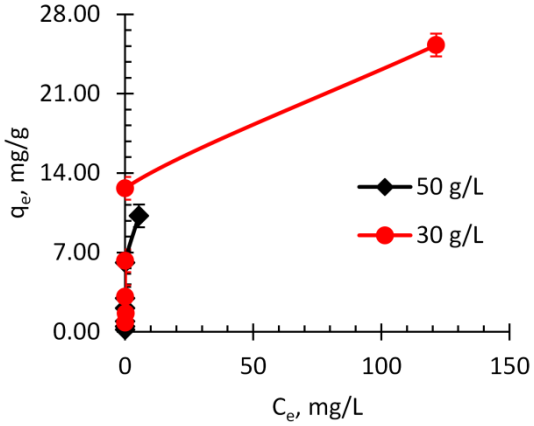

(d) Fe^{2+}

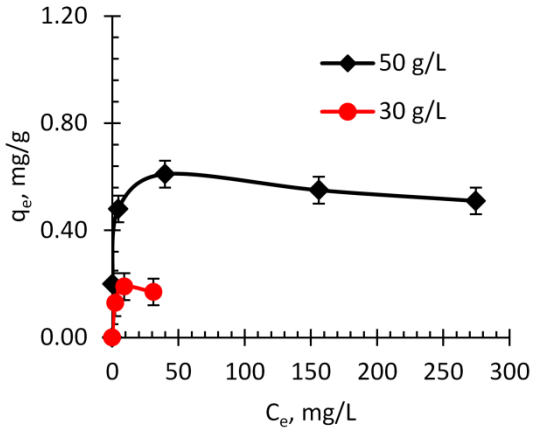

(e) Mn^{2+}

Figure 5.1: Equilibrium isotherms for multiple loading of metal ions by BFS material as a function of phase ratio; pH 3.50, 22 °C.

In Table 5.1 below, the experimentally derived maximum adsorption capacities for Cd^{2+}, Co^{2+} and Mn^{2+} ions were obtained at the higher phase ratio as 2.83 mg/g Cd^{2+}, 0.95 mg/g Co^{2+} and 0.51 mg/g Mn^{2+}. However, capacities for Cu^{2+} and Fe^{2+} were obtained at the lower phase ratio as 10.11 mg/g Cu^{2+} and 25.28 mg/g Fe^{2+}. These are merely highest values (not maximum) since BFS saturation was not attained for these ions. This means that BFS material has a relatively high capacity for Cu^{2+} and Fe^{2+} ions probably due to additional extraction processes, i.e., hydroxide precipitation discussed in detail in Chapter 6. On the

basis of equilibrium isotherms and adsorption capacity values, the selectivity series is Fe^{2+} > Cu^{2+} > Cd^{2+} > Co^{2+} > Mn^{2+} at both phase ratios of 50 g/L BFS (where ions were at same initial concentration) and 30 g/L BFS (where ions were at different initial concentration) but at same total ion concentration or ionic strength in both cases.

Adsorption of metal ions is selective whether ions are at the same initial concentration or not. Competition for adsorption sites among ions is therefore possible. However, it cannot be deduced whether adsorption sites of BFS material are specific or general in character. In solutions with different initial solute concentration, ions at low concentrations could have been suppressed by those at high concentrations. In this case, a competitive adsorption effect among metal ions is also possible whereby ions at high concentration take up most of the available adsorption sites. Competitive adsorption of metal ions by slag materials has been reported by other researchers (Liu et al., 2009; Xue et al., 2009). An analysis of the kinetic and chemical precipitation effects of metal ions on the level of adsorption is presented in Chapter 6.

Table 5.1: Experimental maximum adsorption capacity of powdered BFS (d_p < 45 µm) as a function of phase ratio; pH 3.50, room temperature (~22 ^oC).

Metal ion	**Cd^{2+}**		**Co^{2+}**		**Cu^{2+}**		**Fe^{2+}**		**Mn^{2+}**	
Phase ratio (g/L)	30	50	30	50	30	50	30	50	30	50
q_e, max, (mg/g)	1.44	2.83	0.39	0.95	10.11	7.73	25.28	10.23	0.17	0.51
C_e, (mg/L)	39.21	37.44	138.12	231.16	432.15	236.30	121.40	5.40	31.08	274.57
K_d (L/g)	0.037	0.076	0.003	0.004	0.023	0.033	0.208	1.894	0.006	0.002

The equilibrium pH decreases with increase in total initial ion concentration (Fig. 5.2). This observation might be explained by possible competition for adsorption between metal ions and H^+ ions (Gao et al., 1995; Huang and Rhoads, 1989) as given by Equation (5.1). More metal ions could have been selectively adsorbed than H^+ ions as the total initial concentration of metal ions was increased, leaving H^+ ions in solution that subsequently decreased the pH.

$$\overline{(\equiv SO)_2^-}Ca^{2+} + Me^{2+}(aq) + H^+(aq) \Leftrightarrow \overline{(\equiv SO)_2}H^+ + Me^{2+}(aq) + Ca^{2+}(aq) \qquad \text{---} \qquad (5.1)$$

Also, OH^- ions generated by slag hydrolysis (Dimitrova & Mehandgiev, 1998) were possibly consumed at higher metal ion concentration to form metal hydroxide precipitates since the minimum pH to initiate precipitation might have been attained based on equilibrium pH, however, required pH range for complete hydroxide precipitation was not achieved. Reference is given to Section 6.3.5 of Chapter 6 for a detailed discussion of the adsorption mechanisms.

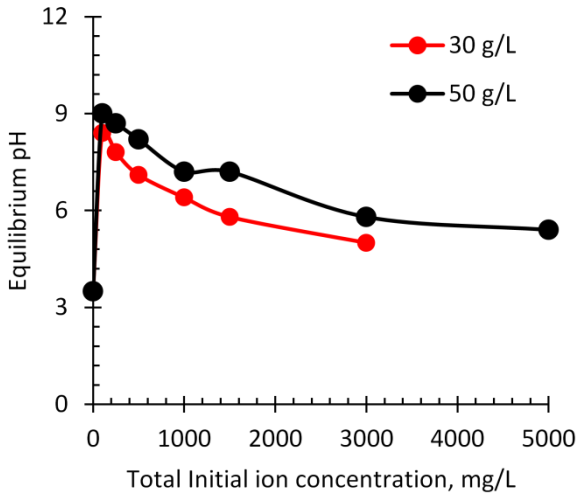

Figure 5.2: Variation of pH with total ion concentration as a function of BFS phase ratio; initial pH 3.50, 22 °C.

An analysis of the mechanisms of the solid phase extraction of metal ions from waste solutions is given in Chapter 6. The process of adsorption of metal ions by silicate based adsorbents is generally believed to involve non-equivalent cation exchange between metal ions in the solution to be purified and Ca^{2+} ions present in the adsorbent matrix. However, it is likely that other related alkali ions present in the adsorbent matrix participate in the ion exchange process. In this study, the concentration of Ca^{2+} ions at equilibrium was found to increase with decrease in initial pH during single solute adsorption of Cu^{2+} ions, with no observable relationship between level of Cu^{2+} ion adsorption and solubilised Ca^{2+} ions. More studies are necessary in order to establish the cation exchange of the adsorbent materials.

The equilibrium isotherms for the extraction of metal ions from wastewater solution by EAF material are shown in Figure 5.3, with maximum adsorption capacities given Table 5.2 and compared with values for BFS material at the same phase ratio of 30 g/L and pH 3.50. The isotherm slopes and shapes for EAF are similar to those of BFS depicting type 'H' classification with high affinity for metal ions. Similarly, adsorption of metal ions by EAF is selective and follows the same selectivity series as BFS. However, BFS has higher capacities for Cd^{2+}, Co^{2+} and Mn^{2+} ions than EAF whose capacities for Cu^{2+} and Fe^{2+} ions are higher than that of BFS. Despite the fact that BFS material had higher capacity for Cd^{2+}, Co^{2+} and Mn^{2+} ions, its BET surface area, pore volume and % porosity were lower than those of EAF material although the pore size distribution of both adsorbents is similar (Chapter 4). The high capacities of EAF for Cu^{2+} and Fe^{2+} ions may also be explained in terms of equilibrium pH given in Figure 5.4. Equilibria pH values for EAF are higher than those of BFS despite it having higher lime content (44 %) than EAF (7 %). This suggests hydroxide precipitation of

Cu^{2+} and Fe^{2+} ions could have contributed significantly to overall extraction in adsorption systems that employed EAF to give higher ion loading than BFS.

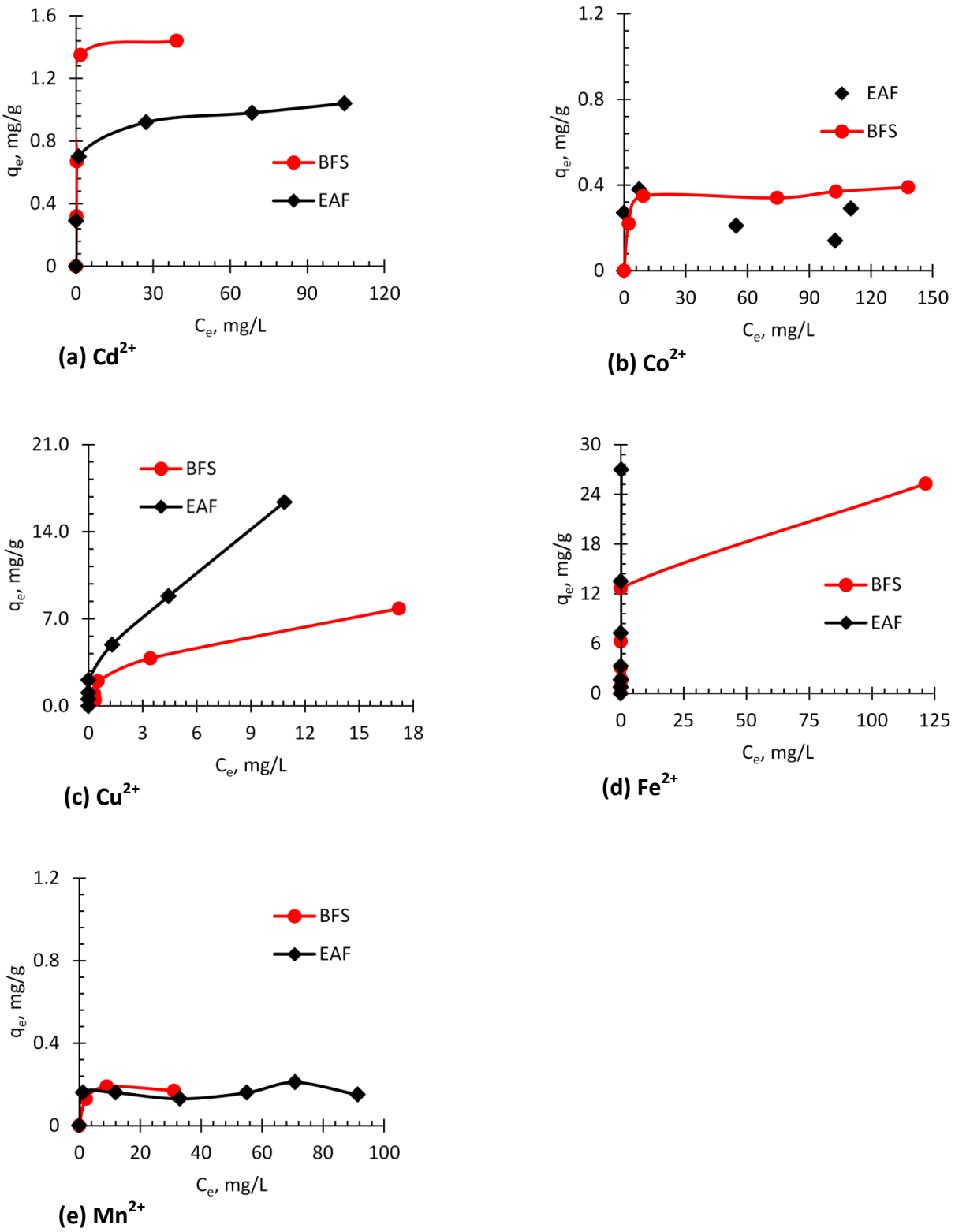

Figure 5.3: Comparison of equilibrium isotherms for multiple loading of metal ions by BFS and EAF materials at 30 g/L phase ratio, pH 3.50, 22 ^{o}C.

Table 5.2: Comparison of experimental maximum adsorption capacities of powdered BFS and EAF at 30 g/L phase ratio

Metal ion	**Cd^{2+}**		**Co^{2+}**		**Cu^{2+}**		**Fe^{2+}**		**Mn^{2+}**	
Phase ratio (g/L)	BFS	EAF	BFS	EAF	BFS	EAF	BFS	EAF	BFS	EAF
q_e, max, (mg/g)	1.44	1.04	0.39	0.29	10.11	16.38	25.28	26.97	0.17	0.13
C_e, (mg/L)	39.21	104.4	138.12	110.24	432.15	10.86	121.40	0.18	31.08	33.00

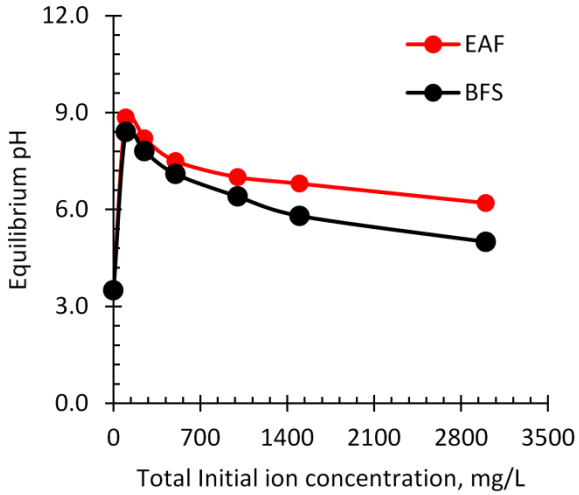

Figure 5.4: Variation of equilibrium pH with total ion concentration as a function of adsorbent type; initial pH 3.50, 22 ^{o}C, 30 g/L phase ratio

5.3.2 Comparative analysis of adsorbent capacity and selectivity

In Table 5.3 below, values of adsorbent capacities and selectivity series of BFS and EAF materials for metal ions were compared with literature data for zeolites, active carbon and related materials.

Table 5.3: Literature data of the maximum adsorption capacities and selectivity series for batch adsorption of various metal ions by slag materials, active carbon and zeolites

Metal ions	Experimental conditions	Adsorbent type	Maximum adsorption capacity, mg/g	Selectivity series	Author(s)
Cd^{2+}, Co^{2+}, Cu^{2+}, Fe^{2+}, Mn^{2+},	pH 3.50, d_p<45 µm, 22 ^{o}C, phase ratio 30 g/L (multiple ions system)	Blast furnace slag (BFS), s/area 2.46 m^2/g	1.44 mg/g Cd^{2+} 0.39 mg/g Co^{2+} 10.11 mg/g Cu^{2+} 25.28 mg/g Fe^{2+} 0.17 mg/g Mn^{2+}	Fe^{2+}>Cu^{2+}> Cd^{2+}>Fe^{2+}>Mn^{2+}	This study
		Electric arc furnace (EAF) slag, s/area 2.99 m^2/g	1.04 mg/g Cd^{2+} 0.29 mg/g Co^{2+} 16.38 mg/g Cu^{2+} 26.97 mg/g Fe^{2+} 0.13 mg/g Mn^{2+}	Fe^{2+}>Cu^{2+}> Cd^{2+}>Fe^{2+}>Mn^{2+}	
Fe^{2+}, Mn^{2+}, Zn^{2+}, Ca^{2+},	pH 3.50, 25 ^{o}C, phase ratio 6 g/L, d_p<44 µm	Carbon B4 (in single solutes)	0.51 mg/g Mn^{2+} 25.6 mg/g Fe^{2+}	---	(Mohan and Chander, 2001)
		Carbon B4 (Effect of Mn^{2+}, Zn^{2+}, & Ca^{2+} on Fe^{2+})	9.7 mg/g Fe^{2+} (decreased value in a multiple ion system)	---	
Fe^{3+}, Zn^{2+}, Cu^{2+}, Mn^{2+},	pH 5.70, 22 ^{o}C, phase ratio 30 g/L, 1<d_p<3 mm, (Single ions)	Natural Zeolite, s/area = 15.88 m^2/g	6.09 mg/g Cu^{2+} 6.61 mg/g Fe^{3+} 8.85 mg/g Zn^{2+} 2.60 mg/g Mn^{2+}	Fe^{3+}>Zn^{2+}> Cu^{2+}>Mn^{2+}	(Motsi, 2010)
Zn^{2+}, Cu^{2+}, Pb^{2+}, Cd^{2+},	pH 6.0, phase ratio 13.6 mg/L, d_p<0.6 mm, Room T.,	Basic oxygen Furnace (BOF) slag, s/area = 1.15 m^2/g	---	Cu^{2+}>Zn^{2+}>Pb^{2+} >Cd^{2+} (single ions)	(Xue et al., 2009)
				Cu^{2+}>Cd^{2+}>Pb^{2+} >Zn^{2+} (Multiple ions)	
Pb^{2+}, Cu^{2+},	pH 4.5, phase ratio 10g/L, 20^{o}C, 0.05<d_p<0.63 mm,	EAF, s/area 0.142 m^2/g	32.68 mg/g Cu^{2+}, 33.78 mg/g Pb^{2+},	Pb^{2+}>Cu^{2+} (single ions)	(Curkovic et al., 2001)
Pb^{2+}, Cu^{2+}, Cr^{3+}, Cd^{2+}, Zn^{2+},	20^{o}C, phase ratio 50 g/L, d_p< 40 µm,	Blast Furnace (BF) sludge; (single ions), s/area = 27.43 m^2/g	64.17 mg/g Pb^{2+}, 16.07 mg/g Cu^{2+}, 9.55 mg/g Cr^{3+}, 6.74 mg/g Cd^{2+}, 4.26 mg/g Zn^{2+},	Pb^{2+}>>Cu^{2+}> Cr^{3+}>Cd^{2+}>Zn^{2+}	(Lopez-Delgado et al., 1998)
Co^{2+}, Cr^{3+}, Cu^{2+}, Ni^{2+}, Zn^{2+},	pH 3.0, phase ratio 5 g/L, 25^{o}C, 1<d_p<3 µm,	Zeolite 4A (multiple ion system), s/area = 71.41 m^2/g	11.52 mg/g Co^{2+}, 45.29 mg/g Cr^{3+}, 53.45 mg/g Cu^{2+}, 7.90 mg/g Ni^{2+}, 31.58 mg/g Zn^{2+},	Cu^{2+}>Cr^{3+}>Zn^{2+}> Co^{2+}>Ni^{2+}	(Hui et al., 2005)
Pb^{2+}, Hg^{2+}, Cu^{2+},	pH 6.0, phase ratio 2 g/L, 30^{o}C, 63<dp<177 µm,	Activated Carbon (AC), s/area = 479 m^2/g	92. 72 mg/g Pb^{2+}, 78.84 mg/g Hg^{2+}, 73.60 mg/g Cu^{2+}, (Single ions)	Pb^{2+}>Hg^{2+}>Cu^{2+}	(Anirudhan and Sreekumari, 2011)

The adsorbent capacities and selectivities presented in Table 5.3 above indicate the relative performance of different silicate based adsorbent materials as well as commercial zeolite 4A and active carbon (AC). In general, the high adsorbent capacities for AC and zeolite 4A can be attributed to their high specific surface area relative to slag materials. Also, capacities and selectivity sequence of metal ions tend to be different in single or multiple ion adsorption systems under similar conditions. Apart from differences in experimental conditions employed (pH, phase ratio, etc.) and adsorbent characteristics as well as possible involvement of several surface functional groups and participation of several extraction mechanisms (ion exchange, adsorption and precipitation), other crucial factors that possibly affect capacity and selectivity may be differences in adsorbent pore sizes relative to metal ionic radii, ion solubility, electronegativity, size and enthalpy of hydrated ionic radii (Erdem et al., 2004; Hui et al., 2005; Inglezakis et al., 2002; Motsi, 2010).

The selectivity sequence in this study was established as Fe^{2+}>Cu^{2+}>Cd^{2+}>Co^{2+}>Mn^{2+}. This series is not consistent with ionic radii size, hydrated ionic radii size, electronegativity and hydration enthalpy as shown in Table 5.4 below. Because of the favourable pH for the possible oxidation of Fe^{2+} to Fe^{3+}, it was assumed that most of Fe^{2+} converted to Fe^{3+} and precipitated at pH ≥ 3.50 (Skousen et al., 2000). Consequently, the selectivity sequence may be consistent with solubility products of metal hydroxides, whereby Fe^{3+} is the least soluble while Mn^{2+} is the most soluble. This observation confirms hydroxide precipitation to be a significant mechanism of extraction of ions from wastewater, mainly for Fe^{2+} and Cu^{2+} ions.

Table 5.4: Metal ion characteristics
(Ahrens, 1951; Allred, 1961; Averill and Eldredge, 2011; Nightingale, 1959; Smith, 1977)

Metal ion	Ionic radii (Å)	Hydrated ionic radii (Å)	Electro-negativity (eV)	Hydration enthalpy kJ/mol	Solubility product of metal hydroxide (K_{sp})	Oxidation state(s)
Fe^{2+}	0.74	4.30	1.83	-1946	4.87×10^{-17}	+2, +3
Fe^{3+}	0.64	4.57	1.83	-4430	2.79×10^{-39}	+2, +3
Cu^{2+}	0.72	4.19	1.90	-2100	4.80×10^{-20}	+1, +2
Cd^{2+}	0.97	4.26	1.69	-1809	7.20×10^{-15}	+2
Co^{2+}	0.72	4.23	1.88	-1996	5.92×10^{-15}	+2, +3
Mn^{2+}	0.80	4.38	1.55	-1841	2.00×10^{-13}	+2, +3, +4, +7

5.3.3 Adsorption Isotherms and Modeling

Many types of adsorption isotherms have been proposed to model adsorption data (Ahmaruzzaman, 2011; Foo & Hameed, 2010). The simple, widely used Langmuir and Freundlich isotherms for the description of single adsorbate systems were applied in this study to analyse multicomponent adsorption data of metal ions from dilute solutions. This is on the assumption that interactive effects among multiple metal ions in the dilute range studied are low and negligible. The isotherms were fitted to the experimental data by nonlinear least squares fitting approach using Microsoft Excel (2010) solver in order to determine the mechanisms of adsorption and adsorption capacity of slag materials. The goodness of fits were assessed by a comparison of regression coefficients (R^2) and sum of squared errors (SSE).

The Langmuir and Freundlich equations are reproduced below from Chapter 3 (Eq. 2.18 & 2.19) (Foo & Hameed, 2010). Adsorption capacity (q_e) was calculated using Equation (3.8) give in Chapter 3. As already discussed under the introductory section, several researchers

have applied these two models to describe single component adsorption of metal ions by slag materials (Curkovic et al., 2001; Dimitrova, 1996; Dimitrova & Mehandgiev, 1998; Feng et al., 2004; Kim et al., 2008; Liu et al., 2010; Lopez et al., 1995; Lopez-Delgado et al., 1998).

Langmuir: $$q_e = \frac{q_m b C_e}{1 + b C_e}$$ --- (2.18)

Freundlich: $$q_e = K_F C_e^{1/n_F}$$ --- (2.19)

Where q_e (mg/g) = amount of solute adsorbed per unit mass of adsorbent at equilibrium, q_m (mg/g) = maximum amount of solute adsorbed per unit mass of adsorbent, C_e (mg/L) = residual solute concentration in the liquid phase at equilibrium, b (L/mg) = Langmuir adsorption coefficient (measure of adsorption affinity); K_F & n = empirical Freundlich constants (K_F = an indicator of adsorption capacity, n_F = measure of adsorption intensity).

It is assumed that Langmuir isotherm is limited to monolayer adsorption and that adsorbates do not interact on the adsorbent surface. Also, solutes are assumed to adsorb at fixed (homogenous) surface sites with same energy of adsorption. However, the Freundlich isotherm, applicable to mostly heterogeneous surfaces, assumes that energy of adsorption is not the same and that multilayer adsorption is possible (Richardson et al., 2002).

The results of fitting Langmuir and Freundlich models to adsorption data of metal ions are shown in Figures 5.5 and 5.6 and Table 5.5 below. The shapes and trends of the experimentally obtained adsorption equilibrium curves have been elucidated in Section 5.3.1 above. From Table 5.5 and on the basis of relatively high regression coefficients (R^2) and low sum of squared errors (SSE), Langmuir isotherm gave better fits of experimental

data for Cd^{2+}, Co^{2+}, Cu^{2+} and Mn^{2+} ions than Freundlich isotherm when BFS adsorbent was used. The predicted maximum adsorption capacities (q_m) correlate closely with the experimentally derived values (q_e, max). Experimental data for Fe^{2+} ions was insufficient to be modelled, i.e., the equilibrium concentration values (C_e) were below detection limit. These results give an indication of the possibility of the applicability of the Langmuir theory of adsorption. Darkwah (2005) found the competitive adsorptive effects (with BFS) in the systems of Cu^{2+}, Zn^{2+} and Mn^{2+} on Fe^{2+} ion adsorption; Zn^{2+} and Mn^{2+} on Cu^{2+} ion adsorption and Zn^{2+} on Mn^{2+} ion adsorption to vary significantly from negligible to significant. Fe^{2+} ion had the greatest negative effect on the extent of Mn^{2+} ion adsorption. Thus, due to the suspected competitive adsorption among metal ions, it is suggested that extended adsorption equilibrium experiments be conducted to generate enough equilibrium data in order to apply multicomponent adsorption isotherms such as non-modified, modified and extended Langmuir isotherms that take into account interactive effects of adsorbates (Ahmaruzzaman, 2011).

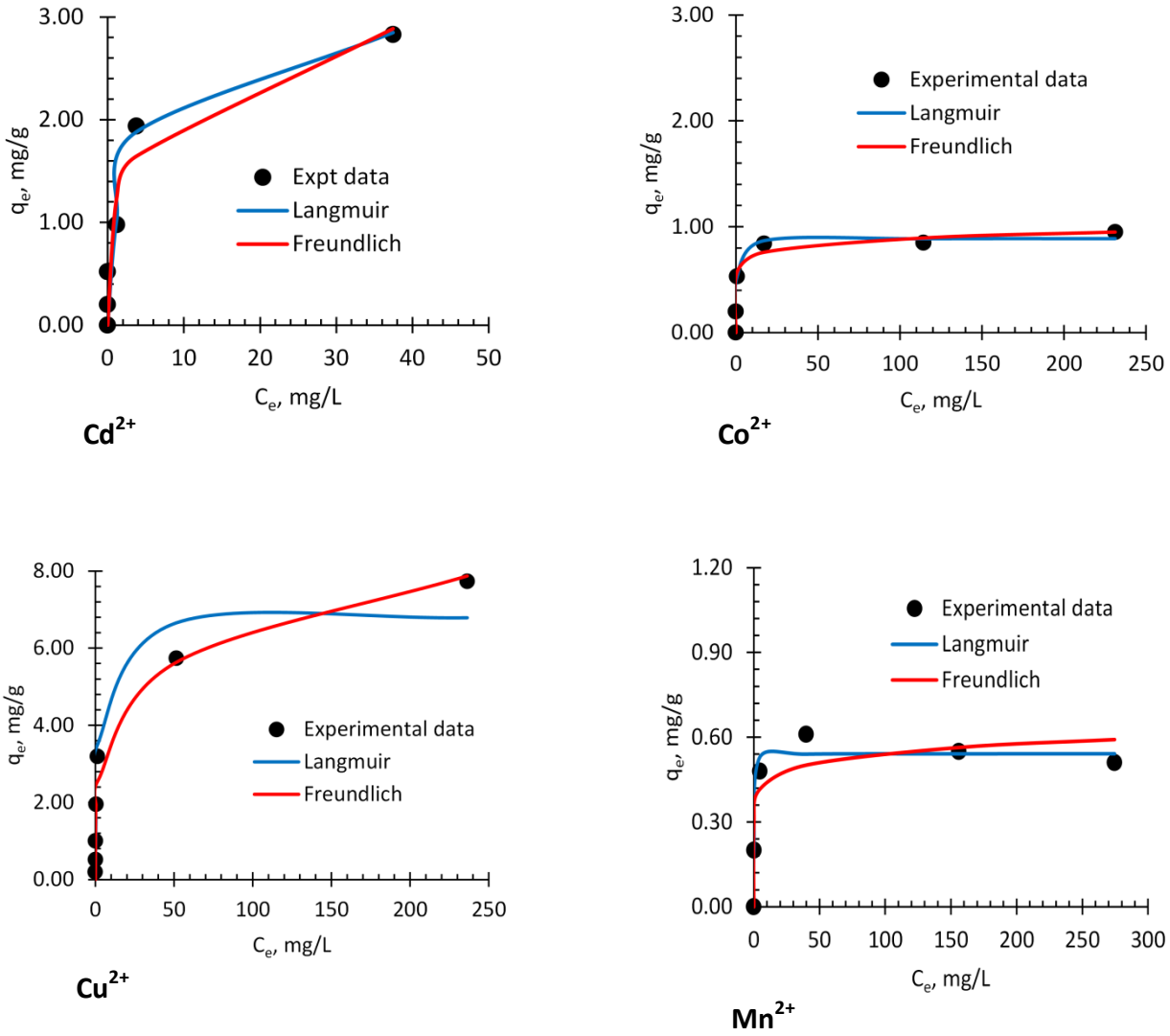

Figure 5.5: Nonlinear Langmuir and Freundlich model fits to multicomponent adsorption data of metal ions with powdered BFS at 30 g/L, pH 3.50, 20 ^{o}C.

In Figure 5.6 below, the Freundlich isotherm was a more satisfactory adsorption theory to describe Cd^{2+} and Cu^{2+} ion adsorption than the Langmuir theory when EAF adsorbent was used. The mechanism of adsorption may be chemisorption with multilayer adsorption. However, data for Co^{2+} and Mn^{2+} ions fitted poorly to both isotherms while Fe^{2+} data were insufficient. As discussed above, more multicomponent adsorption data of these metal ions is needed and that multicomponent models are tested. The next Chapter (6) gives a detailed analysis of the adsorption kinetics of the same adsorption system of metal ions.

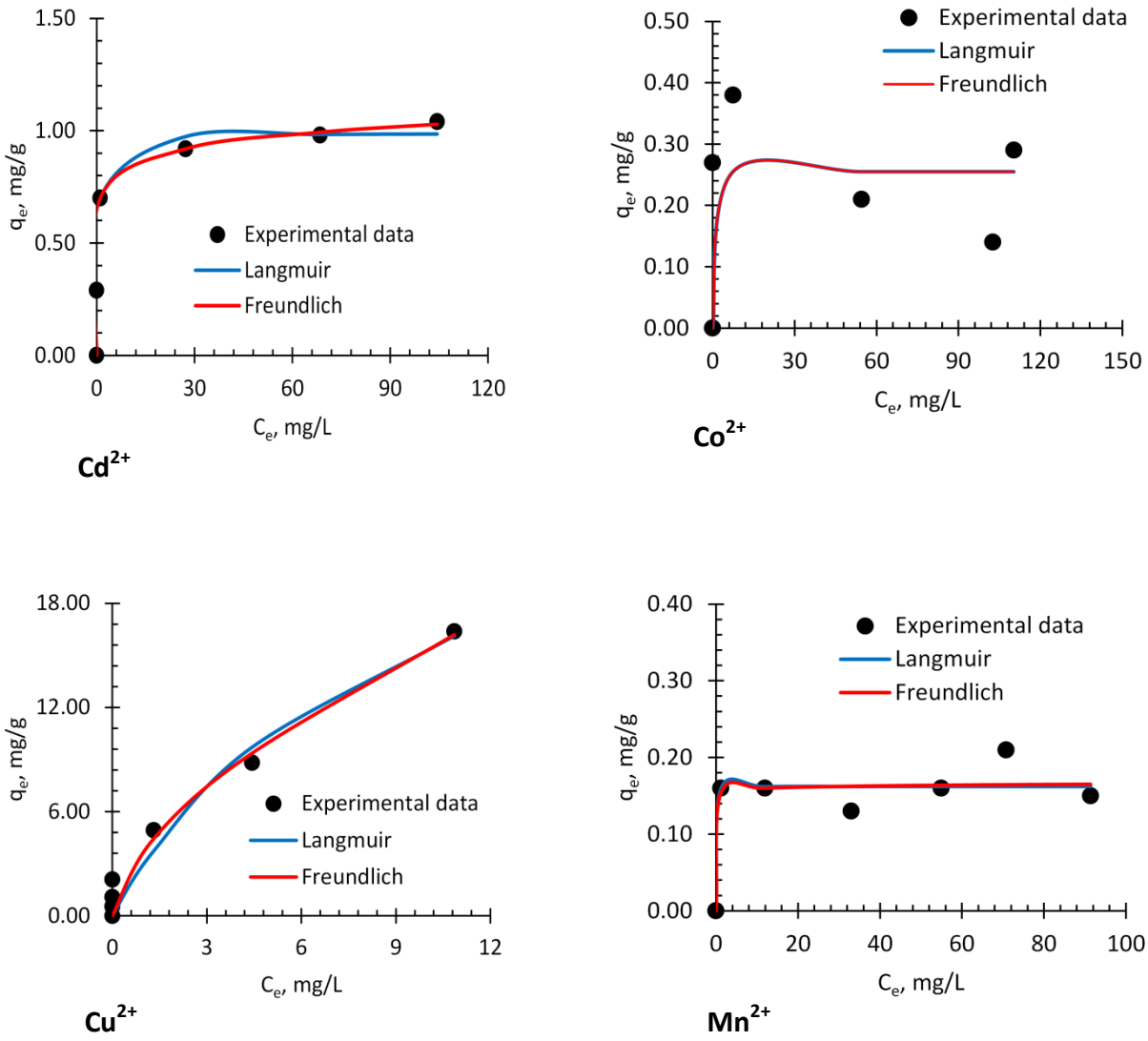

Figure 5.6: Nonlinear Langmuir and Freundlich model fits to multicomponent adsorption data of metal ions with powdered EAF at 30 g/L, pH 3.50, 20 °C.

Table 5.5: Experimental and estimated model parameter values in multicomponent systems of metal ions using BFS & EAF Adsorbents

(a) BFS Adsorbent

Metal Ion	Variable	Experimental values		Langmuir				Freundlich			
	Phase ratio, (g/L)	q_e, max, (mg/g)	C_e, (mg/L)	q_m, (mg/g)	$b_{L,}$ (L/mg)	SSE	R^2	$K_{F,}$ (L/mg)	$n_{F,}$	SSE	R^2
Cd^{2+}	30	1.44	39.21	1.56	2.80	0.019	0.977	0.864	6.270	0.270	0.713
	50	2.83	37.44	3.02	0.44	0.317	0.997	1.189	4.086	0.469	0.880
Co^{2+}	30	0.39	138.12	0.38	0.68	0.002	0.950	0.237	10.158	0.005	0.747
	50	0.95	231.16	0.89	2.43	0.046	0.979	0.594	11.616	0.050	0.917
Cu^{2+}	30	10.11	432.15	10.13	0.21	1.375	0.958	2.727	4.403	11.517	0.862
	50	7.73	236.30	6.83	0.76	2.759	0.959	2.372	4.556	1.142	0.980
Mn^{2+}	30	0.17	31.08	0.19	1.17	0.005	0.829	0.134	11.177	0.001	0.508
	50	0.51	274.57	0.54	9.45	0.008	0.988	0.365	11.640	0.030	0.807

(a) EAF adsorbent

Metal Ion	Variable	Experimental values		Langmuir				Freundlich			
	Phase ratio, (g/L)	q_e, max, (mg/g)	C_e, (mg/L)	q_m, (mg/g)	$b_{L,}$ (L/mg)	SSE	R^2	$K_{F,}$ (L/mg)	$n_{F,}$	SSE	R^2
Cd^{2+}	30	1.04	104.40	0.99	2.337	0.090	0.951	0.697	11.953	0.084	0.997
Cu^{2+}	30	16.38	10.86	29.64	0.109	8.812	0.966	3.763	1.634	6.381	0.989

5.4 Conclusions

This study has addressed the adsorption capacity, selectivity and affinity of slag materials for metal ions in multicomponent adsorption systems as opposed to single components that have been studied extensively. The slag materials can effectively extract multiple metal ions by adsorption process from dilute aqueous solutions.

The BFS and EAF adsorbent materials have a very high adsorption affinity for metal ions, and exhibit Type (I) isotherms and the sub-type 'L' (Langmuir) and 'H' (high affinity) isotherms but easily attain saturation within the low metal ion concentration range. The experimentally determined values of the maximum adsorption capacities were 2.83 mg/g Cd^{2+}, 0.95 mg/g Co^{2+} and 0.51 mg/g Mn^{2+} using BFS material and 16.38 mg/g Cu^{2+} and 26.97 mg/g Fe^{2+} using EAF material. Values of adsorption capacity for Cu^{2+} and Fe^{2+} ions compares well with literature data of other slags, sludges and zeolites than those of Cd^{2+}, Co^{2+} and Mn^{2+} ions that are relatively low. The reduction in adsorption capacities for metal ions in multicomponent systems in comparison to reported capacities in single adsorbate systems may be attributed to limited adsorptive properties of slag materials. This highlights the need for any design of adsorption system to be based on actual experimental data from multicomponent system. Also, the effectiveness of slag materials is much lower than that of commercial zeolites and active carbon probably due to the large difference in specific surface area. However, slag materials may be economically attractive adsorbents in dilute systems of metal ions.

BFS has higher capacity for Cd^{2+}, Co^{2+} and Mn^{2+} ions than EAF whose capacity for Cu^{2+} and Fe^{2+} ions is higher than that of BFS. The adsorption capacity increased with increase in phase ratio for metal ions except Cu^{2+} and Fe^{2+} ions. Furthermore, the adsorption capacities and distribution coefficients for Cu^{2+} and Fe^{2+} ions are larger than those of Cd^{2+}, Co^{2+} and Mn^{2+} ions which reflect high affinity and preferential adsorption for Cu^{2+} and Fe^{2+} ions. This is attributed to additional extraction by chemical precipitation for these ions.

Based on distribution coefficients and adsorption capacities the selectivity sequence is proposed as Fe^{2+}>Cu^{2+}> Cd^{2+}>Co^{2+}>Mn^{2+} for both BFS and EAF materials. That is, adsorption of metal ions is selective whether ions are at the same initial concentration or not. Therefore, it was concluded that competition for adsorption sites among ions may be possible. However, the selectivity sequence was not consistent with ionic radii size, hydrated ionic radii size, electronegativity and hydration enthalpy but consistent with solubility products of metal hydroxides. This observation supports hydroxide precipitation to be a significant mechanism of extraction of metal ions from wastewater mainly for Fe^{2+} and Cu^{2+} ions.

The mechanism of adsorption of metal ions is probably by chemisorption as indicated by Langmuir and Freundlich models. Langmuir isotherm gave better fits of adsorption data for Cd^{2+}, Co^{2+}, Cu^{2+} and Mn^{2+} ions than Freundlich isotherm when BFS adsorbent was used. However, Freundlich isotherm was a more satisfactory adsorption theory to describe Cd^{2+} and Cu^{2+} ion adsorption than the Langmuir theory when EAF adsorbent was used. This is probably because EAF supports multilayer adsorption with the possibility for adsorbate interaction.

It is therefore recommended that further adsorption equilibrium studies in multicomponent systems are conducted to determine the effect of pH, adsorbent particle size, etc., on adsorption capacity. It is also suggested that extended adsorption equilibrium experiments should be conducted to generate enough equilibrium data in order to apply multicomponent adsorption isotherms such as non-modified, modified and extended Langmuir and Freundlich isotherms as well as any other relevant competitive isotherms that take into account interactive effects of adsorbates.

CHAPTER 6
ADSORPTION KINETICS AND MODELING

6.1 Introduction

This chapter describes experimental results for the kinetics and efficiency of adsorption of metal ion adsorbates in solid/liquid systems, and the use of widely accepted kinetic models based on both chemical and diffusion adsorption mechanisms to assess the adsorptive performance of slag materials as adsorbents for practical applications. A study of the time dependence of solute adsorption, or adsorption kinetics, helps to estimate the rates of solute adsorption, residence time, adsorption mechanisms, efficiency of adsorbents, size of adsorption vessels and other mass transfer kinetic factors that are useful in design, scale up, control and operation of adsorptive systems (El-Khaiary et al., 2010; Knaebel, 2012). Furthermore, kinetics data is exploited in adsorptive separations on the basis of differences in diffusion rates of adsorbates into the adsorbent, and also affects the quantity of adsorbent requirement (Knaebel, 2012). This section gives a brief literature review of current understanding on the efficiency, mechanisms and kinetics of adsorption of metal ions by adsorbent slag materials. The objectives of this chapter are also stated.

Several researchers have studied adsorption kinetics of metal ions from solutions using the immersion method by measuring amounts of adsorbed ions as a function of time. Liu et al (2009) observed an initially high rate of Cr^{3+} ion adsorption by steel slag. The overall rate of adsorption became controlled by the intraparticle diffusion. Liu et al (2009) observed that efficiency of Cr^{3+} ion adsorption by steel slag increased with increase in solid/liquid phase

ratio because of a possible increase in active adsorption sites and/or surface area. Other researchers also reported a kinetically fast initial adsorption step followed by slower phase during adsorption of various metal ions with slags and zeolites (Curkovic et al., 2001; Dimitrova, 1996; Huifen et al., 2011; Motsi et al., 2009; Xue et al., 2009). Liu et al (2010) reported that pseudo second order (PSO) kinetic equation gave better linear fit of experimental data for Pb^{2+} ion adsorption by steel slag than pseudo first order (PFO) equation.

The early work of Huang and Rhoads (1989) established that Zn^{2+} ion adsorption by synthetic zeolites and oxides of γ-Al_2O_3 and SiO_2 is most effective in alkaline pH systems. They concluded that the ion exchange mechanism was dominant at low pH with precipitation more pronounced at alkaline pH. Similarly, Motsi (2009) assumed ion exchange to have occurred during adsorption of Mn^{2+}, Zn^{2+}, Fe^{3+} and Cu^{2+} ions using natural zeolite. These are the views of many other researchers who have investigated the adsorption efficiency of metal ions by several slag materials. Gao et al (1995) found adsorption of multiple metal ions by blast furnace (BF) sludge to be low in acidic solutions attributed to the competitive effect of H^{+} ion adsorption. Similarly, Dimitrova (1996) obtained a high adsorption efficiency of Cu^{2+}, Ni^{2+} and Zn^{2+} ions by blast furnace slag (BFS) in alkaline pH. These observations have been confirmed by Dimitrova and Mehandjiev (1998, 2000), Kim et al (2008), Xue et al (2009) and Huifen et al (2011) who investigated metal ion adsorption using various slag materials. They proposed ion exchange reactions with Ca^{2+} ions at low (acidic) pH values allied to some precipitation reactions towards alkaline pH. Thus, efficiency and rate of metal ion adsorption increase with increase in pH, and pH also controls the mechanisms of adsorption process.

Liu et al (2010) reported an increase in adsorption efficiency of Pb^{2+} ions by steel slag with increase in initial Pb^{2+} ion concentration. However, this is contrary to the views of many authors that believe that efficiency is higher the lower the initial concentration of adsorbates. Lui et al (2010) found the efficiency of Pb^{2+} ion adsorption will increase with increase in agitation rate. An increase in the rate of agitation increased the diffusion coefficient of Pb^{2+} ions, thereby increasing the mass transfer flux. Thus, external diffusion was identified as rate limiting step. At higher rates of agitation, resistance to bulk liquid diffusion was eliminated. Huifen et al (2011) reported adsorption efficiency to increase with increase in mass of slag dose rate. The mechanism of adsorption process was by ion exchange or hydroxide precipitation.

Lopez et al (1995) and Lopez-Delgado et al (1998) explored adsorption of Pb^{2+}, Cu^{2+}, Cr^{3+}, Zn^{2+} and Cd^{2+} ions by BF sludge in single adsorbates. The adsorption efficiency decreased with increase in initial metal ion concentration, but efficiency increased with increase in mass of BF sludge. A complete adsorption was noted in low adsorbate concentrations even at the lowest amount of BF sludge dosage. Also, efficiency and capacity increased with increase in temperature and mass of BF sludge. At high metal ion concentration, adsorption was poor even after an extended residence time. The authors suggested further studies in multiadsorbate and actual wastewater systems to fully understand adsorption behaviour. Feng et al (2004) found iron/steel slags to be ineffective in purifying actual multicomponent system of acid mine drainage consisting of several metal ions.

Dimitrova (1996) employed blast furnace slag (BFS) to achieve a complete adsorption of Cu^{2+} and Zn^{2+} ions and up to 72% Ni^{2+} adsorption from dilute solutions. However, adsorption was limited to 60% Cu^{2+}, 46% Zn^{2+} and 32% Ni^{2+} in relatively high solutes concentration. This suggests that adsorption efficiency is high in dilute systems relative to concentrated solutions. Furthermore, high adsorption efficiency correlates with high adsorption capacity, which increased with initial concentration. Dimitrova (1996) and Curkovic (2001) both established that temperature increases both the hydrolysis of slag and adsorption capacity for metal ions with BFS. They concluded that the process of adsorption was endothermic. Xue et al (2009) also observed an increase in adsorption capacity of metal ions with BOF as initial concentration was increased.

Many authors believe the mechanisms of adsorption process of metal ions by adsorbent slag materials occurs through ion exchange and precipitation but these mechanisms are not well understood, and their relative contribution is not clear (Dushina and Aleskovski, 1976). In many instances, comprehensive studies on the proposed mechanisms in multiple metal ion adsorption systems with iron/steelmaking slags are limited, inconsistent and not yet clearly understood. Although adsorption of one or two metal ions by slags has been reported, data in multiadsorbate systems is limited; however, this reflects actual industrial effluent compositions. The lack of fundamental understanding of adsorption process is seen as the reason why this technology has not yet been developed into a practical process applied at industrial scale. Thus, further studies in multicomponent systems of metal ions are required to fully understand the adsorption process and rate limiting factors involved. This was the primary objective of this study.

This study investigated the adsorption behaviour of a multicomponent system of Cd^{2+}, Co^{2+}, Cu^{2+}, Fe^{2+} and Mn^{2+} ions as a function of several key adsorption variables. These ions are representative of those found in acid mine drainage incidences of the Zambian Copperbelt mining region. The effects of BFS pretreatments on adsorption kinetics were also studied. Initial adsorption experiments were conducted in single component systems to validate the reported kinetics of adsorption for metal ions. The experimental data were then analysed by chemical and diffusion based kinetic models. The objectives of this chapter were; (1) to evaluate the adsorbent efficiency and rates of adsorption of metal ions from waste solutions as a function of several key adsorption variables and, (2) to deduce the overall adsorption rates, adsorbent capacity, and to estimate model parameters and infer the mechanisms of adsorption process and limiting steps based on various kinetic models. Pseudo first order (PFO), pseudo second order (PSO) and Elovich's rate equations (all based on chemical adsorption), as well as Webber-Morris intraparticle diffusion, double exponential and Boyd's film diffusion models were identified and applied to analyse adsorption kinetics. These models are preferable and widely applied in simulations and research context due to their relative simplicity and accuracy. Granulated BFS and EAF slags were used as adsorbents in single and multicomponent systems of Cd^{2+}, Co^{2+}, Cu^{2+}, Fe^{2+} and Mn^{2+} ions. The question of how to dispose slag materials adsorbed with metal ions to meet environmental standards such that dissolution of metal ions is limited to acceptable levels is discussed in Chapter 7, where potential stripping of metal ions from slag surfaces after adsorption stage was investigated.

6.2 Materials and Methods

A brief summary of the experimental procedure is presented below. However, a detailed description of materials, experimental setup and procedure is given in Chapter 3 under section 3.3. Standard stock solutions of 1000-5000 mg/L Cu^{2+}, Mn^{2+}, Fe^{2+}, Cd^{2+} and Co^{2+} ions were prepared separately for individual ions from their respective analytical grade chemicals, i.e., $CuSO_4.5H_2O$, $MnSO_4.4H_2O$, $FeSO_4.7H_2O$, $3CdSO_4.8H_2O$ and $CoSO_4.7H_2O$ procured from Fisher Scientific UK. Subsequent solutions of different metal ion concentrations were prepared by appropriate dilutions of stock solutions and mixing (Chapter 3, Equations 3.4 to 3.6) to produce single or multicomponent solutions that simulated average compositions of acid mine wastewater solutions. The pH was adjusted to the required value using 1.0 mol/L of either NaOH or H_2SO_4 solutions.

Batch adsorption experiments were conducted either in agitated bottles or in thermostated STR (Chapter 3, Figures 3.1 & 3.2) to study the effects of solid/liquid phase ratio, particle size, temperature, initial metal ion concentration, initial pH, adsorbent mass, and rate of agitation on adsorption equilibria and kinetics. Unless stated otherwise, all adsorption experiments were carried out at pH 3.50, phase ratio of 30 g/L and at room temperature (~ 22 ^{o}C). The required volume of waste solution containing the desired initial metal ion concentration was added to the adsorption vessel, followed by pH adjustment to the required value with a bench HI 2211 pH meter. The required adsorbent mass of slags with desired particle size distribution was then added and the mixture agitated for a predetermined time. Aliquots of about 20 mL slurry samples were periodically taken and filtered. Changes in equilibrium metal ion concentrations with time were measured in the

filtrate by Perkin Elmer AAnalyst 300 Flame Atomic Absorption Spectrometer from which efficiency (η), adsorption capacities (q) and other parameters were calculated by equations (3.7) to (3.10) reproduced below. The error as a standard deviation in AAS analyses of metal ion concentration was in the range of ± 6 %. The loaded surfaces of slag material with metal ions were analysed by SEM and EDS techniques.

$$q_t = \frac{V \times (C_o - C_t)}{m} \quad \text{--- (3.7)} \qquad q_e = \frac{V \times (C_o - C_t)}{m} \quad \text{--- (3.8)}$$

$$\eta = \frac{(C_o - C_t)}{C_o} \times 100\ \% \quad \text{--- (3.9)} \qquad k_d = \frac{q_e}{C_e} \quad \text{--- (3.10)}$$

q_t (mg/g) = amount of adsorbate per unit mass of adsorbent at time t = t; q_e (mg/g) = amount of adsorbate per unit mass of adsorbent at equilibrium; C_o (mg/L) = initial adsorbate concentration in solution at time t = 0; C_t (mg/L) = adsorbate concentration in solution at time t (min) = t; C_e (mg/L) = adsorbate concentration in solution at equilibrium; m (g) = mass of adsorbent; V (L) = volume of solution; k_d (L/g) = distribution coefficient.

6.3 Results and Discussion

The experimental results for adsorption kinetics of metal ions by BFS and EAF adsorbent materials are presented and discussed in detail in this section. Using an immersion adsorption method in both agitated bottles and stirred tank reactor (STR), rates of solute adsorption, adsorbent efficiency and adsorption mechanisms of metal ions in single and multicomponent adsorption systems have been evaluated in order to generate new information and enhance our understanding of the effects of a range of key adsorption

variables. Further, the effect of pretreatment of adsorbent materials on metal ion adsorption has been investigated. Using relevant kinetic models, adsorption data was modelled to deduce overall adsorption rates, adsorbent capacity, and to estimate model parameters and infer the mechanisms of adsorption process and rate limiting steps.

6.3.1 Single Component Adsorption Systems

Adsorption characteristics for single component systems of several single metal ion adsorbates have been studied extensively. In this study, batch adsorption experiments in agitated bottles were conducted to obtain experimental data that would validate and subsequently improve the efficiency and kinetics of metal ion adsorption using BFS as an adsorbent under different experimental conditions. Therefore, the effects of particle size of BFS and initial pH of wastewater solutions on adsorption mechanisms, efficiency and kinetics in single component adsorption systems of Cd^{2+}, Co^{2+}, Cu^{2+}, Fe^{2+} and Mn^{2+} ions are discussed in the sections that follow.

6.3.1.1 Effect of Initial pH

The pH values of waste solutions employed were 1.50, 3.50 and 5.50 in agitated bottles to investigate its effect on adsorption kinetics by BFS with metal ions at about 100 mg/L each. Solution pH controls metal ion speciation and their oxidation states, surface charge density of adsorbents, electrostatic forces and several other variables. These factors consequently affect the extent of adsorption and mechanism of adsorption of metal ions. At an unique pH, different solids possess different points of zero charge (PZC) above which adsorption may increase or decrease (Huang and Rhoads, 1988; Ortiz et al., 2001; Feng et al., 2004).

In Figure 6.1(A), an increase in pH increased adsorption efficiency (%) for all metal ions, and the variations of efficiency with time for each ion at different pH values are shown in Figures 6.1 (B) to (F) which show an initially fast loading kinetic profile followed by a slower phase towards equilibrium. In Table 6.1, adsorption capacity, distribution coefficient and equilibrium pH are shown to increase with increase in initial pH. The results supports the fact that metal ion adsorption by slag materials is only effective in alkaline solution (Huang and Rhoads, 1988). Adsorption was low for Cu^{2+} and Cd^{2+} ions and negligible for Mn^{2+}, Co^{2+} and Fe^{2+} ions at pH 1.50 possibly due to the competitive effect of H^{+} adsorption (Gao et al., 1995) and electrostatic repulsion between metal ions and charged surfaces (Feng et al., 2004). Metal ion adsorption increased with a gradual increase in equilibrium pH supported by slag hydrolysis (Dimitrova and Mehandgiev, 2000).

BFS hydrolyses to support ion exchange during metal ion adsorption. Depending on pH and metal ion concentration, hydroxide or silicate precipitation may also be involved (Dimitrova, 2001; Dimitrova and Mehandgiev, 2000). From SEM micrographs and EDX surface analysis of slag and observed pH, ion exchange type of adsorption may be dominant for Mn^{2+}, Co^{2+} and Cd^{2+} removal due to the presence of exchangeable surface ions such as Ca^{2+}, K^{+} and Na^{+}. This was also confirmed by dissolution of about 600 mg/L Ca^{2+} at pH 1.5, reducing to 55 mg/L Ca^{2+} at pH 3.5 and 5.5 in solutions of 100 mg/L Cu^{2+} with 50 g/L powdered BFS. The pH necessary for complete precipitation as hydroxides for Cd^{2+} (pH 9.4-9.7), Co^{2+} (pH > 8.0) and Mn^{2+} (pH 9.8-10.2) are higher than observed experimental pH values for these ions (Zhuang, 2009). As for adsorption of Fe^{2+} and Cu^{2+} ions, probably a combination of ion exchange, adsorption and precipitation may be the major mechanisms of adsorption process as

proposed in several studies (Dimitrova, 1996; Dimitrova and Mehandgiev, 1998, 2000; Feng et al., 2004; Kim et al., 2008). Hydroxide precipitation for Cu^{2+} and Fe^{2+} is likely to be significant since these ions precipitate at pH 7.5-8.0 and 4.5-5.0 respectively whereby Fe^{2+} is first oxidized to Fe^{3+} by dissolved oxygen. An ion exchange and precipitation reactions on protonated or unprotonated negative slag surface site (Al, SiO^-) are given in Equations 6.1 to 6.3 below (Dimitrova, 2001; Dimitrova and Mehandgiev, 2000; Gao et al., 1995). A more detailed analysis of mechanisms of adsorption is given in Section 6.3.5 of this Chapter.

$$\overline{(\equiv SO)_2^-Ca^{2+}} + Me^{2+}(aq) \Leftrightarrow \overline{(\equiv SO)_2Me^{2+}} + Ca^{2+}(aq) \quad \text{---} \quad (6.1)$$

Where overbar = solid phase, $\equiv SO^-$ is a deprotonated surface site, S = Al, or Si; Me^{2+} = any metal ion. In strongly acidic solutions, competitive adsorption is represented by Equation 6.2. Slag (or CaO) hydrolysis produces OH^- ions which may result in metal hydroxide precipitation as given by the precipitation model reaction in Equation (6.3).

$$\overline{(\equiv SO)_2^-Ca^{2+}} + Me^{2+}(aq) + H^+(aq) \Leftrightarrow \overline{(\equiv SO)_2H^+} + Me^{2+}(aq) + Ca^{2+}(aq) \quad \text{---} \quad (6.2)$$

$$Me^{2+} + OH^- = Me(OH)_2 \quad \text{---} \quad (6.3)$$

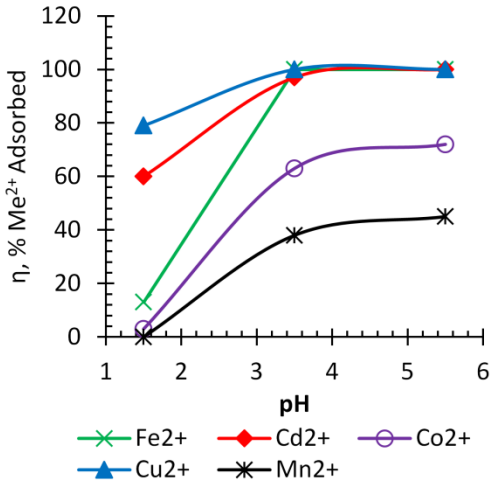

(A) All Me^{2+} ions

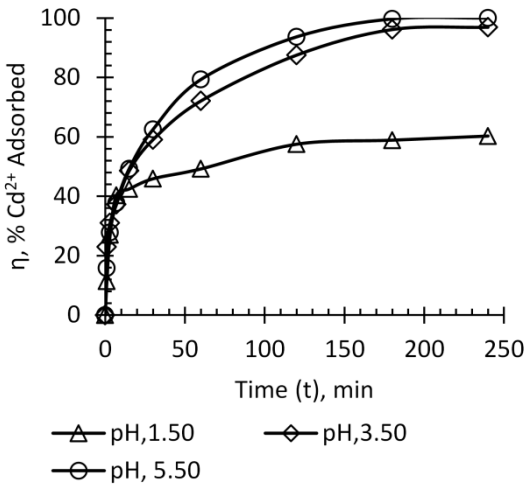

(B) Cd^{2+} ions

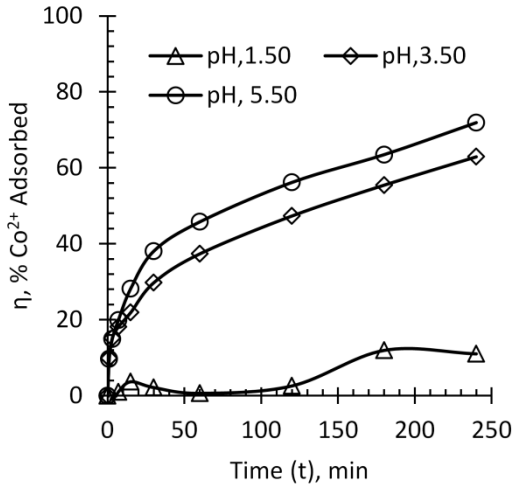

(C) Co^{2+} ions

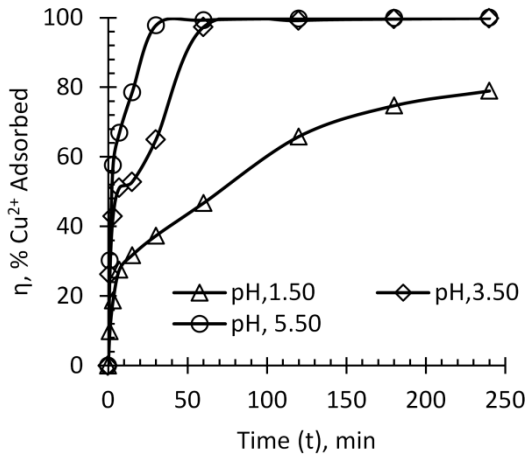

(D) Cu^{2+} ions

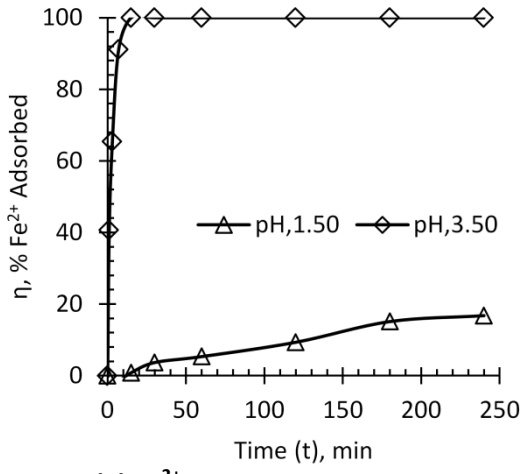

(E) Fe^{2+} ions

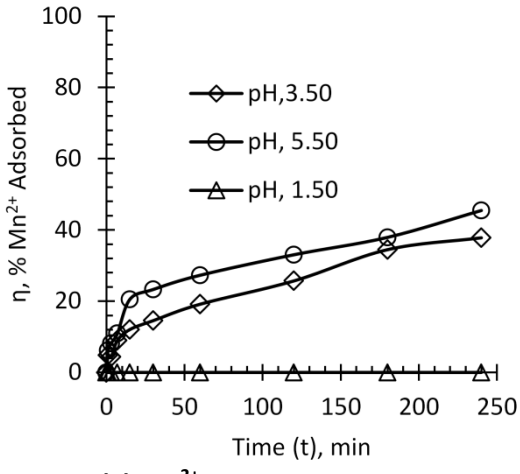

(F) Mn^{2+} ions

Figure 6.1: Effect of pH on adsorption efficiency of metal ions in single component systems, 30 g/L BFS granules, 95±6 mg/L Me^{2+} ions, (A) η vs initial pH; (B) to (F) η vs time

Table 6.1: Summary of kinetic parameters as a function of pH in single component system with BFS granules (+0.50-1.00 mm) in agitated bottles

Me^{2+} Ions	Effect of Initial pH	Theoretical Initial Conc, C_i, (mg/L)	Actual Initial Conc, C_i, (mg/L)	Equilibrium Conc, C_e (mg/L)	Max adsorbed η, (%)	Q_e max, mg/g	Equil pH	Distrib. Coeff. , K_d, (L/g)
Cd^{2+}	1.5	100	93.55	37.18	60	0.902	5.8	0.0243
	3.5	100	101.90	3.18	97	1.580	8.5	0.4969
	5.5	100	98.50	BDL	100	1.576	9.1	-
Co^{2+}	1.5	100	95.00	93.0	~3	0.033	6.0	0.0004
	3.5	100	100.0	37.10	63	1.006	8.0	0.0271
	5.5	100	98.15	27.58	72	1.129	8.2	0.0409
Cu^{2+}	1.5	100	115.70	24.36	79	1.461	5.6	0.0560
	3.5	100	116.06	0.25	100	1.853	7.7	7.4120
	5.5	100	111.88	BDL	100	1.790	8.2	-
Fe^{2+}	1.5	100	106.90	88.98	17	0.287	5.8	0.0032
	3.5	100	101.54	BDL	100	1.625	7.9	-
	5.5*	100	-	-	-	-	-	-
Mn^{2+}	1.5#	100	91.88	95.28	0	0	5.9	-
	3.5	100	87.95	54.70	38	0.532	8.5	0.0097
	5.5	100	92.15	50.25	45	0.670	8.5	0.0133

*pH 5.5: Fe^{2+} oxidised & precipitated before adsorption experiment
#pH 1.5: Mn^{2+} dissolution from adsorbent matrix increased quantities in solution
BDL = Below detection limit

6.3.1.2 Effect of Particle Size Distribution of Adsorbent

The effect of four different size fractions of BFS on adsorption kinetics were investigated, i.e., dp < 45 µm, 0.18 < dp < 0.36 mm, 0.36 < dp < 0.50 mm and 0.50 < dp < 1.00 mm. Figure 6.2(A) shows that adsorption efficiency (%) of Co^{2+} and Mn^{2+} ions increased with decrease in nominal (mean) particle size of adsorbent across the three (different) size fractions studied as expected. However, a complete (100%) adsorption was obtained for Cu^{2+}, Cd^{2+} and Fe^{2+} ions across all particle sizes. It is possible that surface area and the number of adsorption sites increase to give a higher opportunity for solute adsorption. The highest metal ion uptake of up to 100% Fe^{2+}, 100% Cu^{2+}, 100% Cd^{2+}, 87% Co^{2+} and 57% Mn^{2+} were obtained

with finest size fraction (0.18<dp<0.36 mm) from comparable initial concentration values of 97±6 mg/L Me^{2+} solutions**.** Figures 6.2(B) to (F) show the kinetic adsorption profiles as a function of time for metal ions investigated. As observed previously, adsorption process was rapid initially but gradually decreased with time for all ions. The trends indicate differences in the adsorption characteristics of the five metal ions involved. Dimitrova and Mehandgiev (1998) and other researchers reported similar results from similar adsorption systems of metal ions using slags as adsorbents.

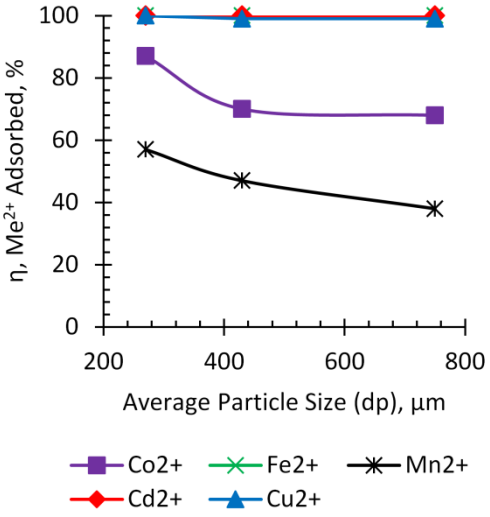

(A) Me^{2+} ions

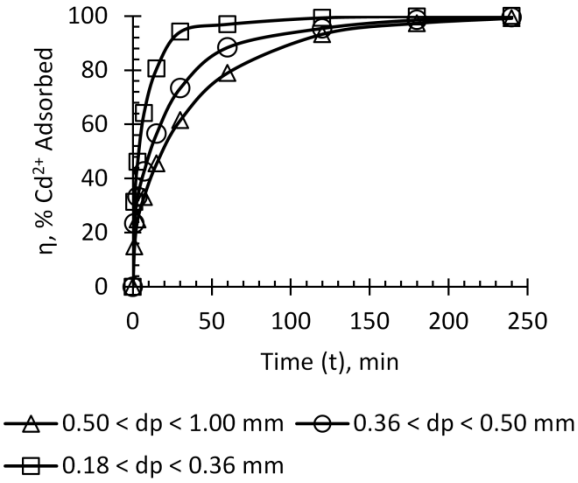

(B) Cd^{2+} ions

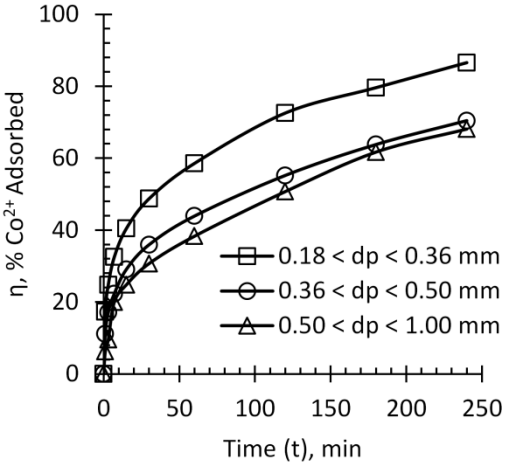

(C) Co^{2+} ions

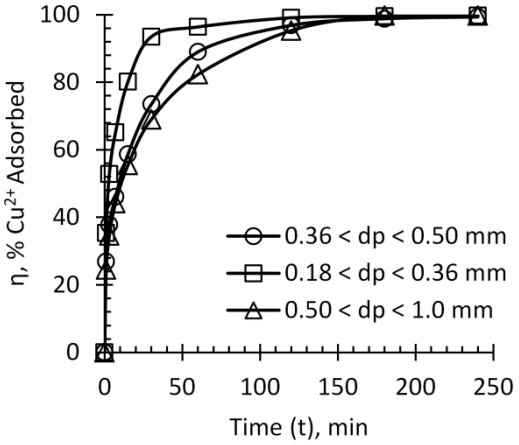

(D) Cu^{2+} ions

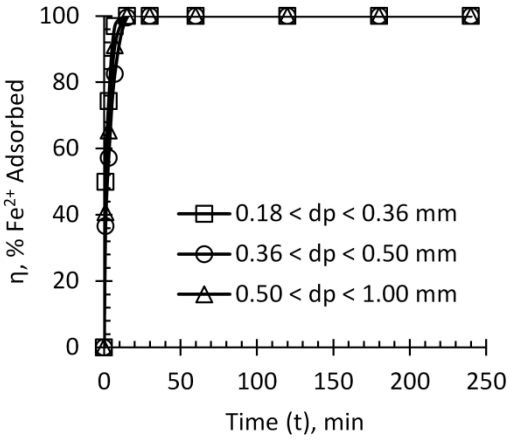

(E) Fe^{2+} ions

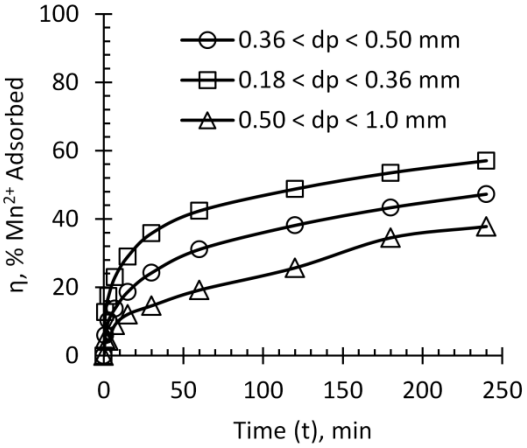

(F) Mn^{2+} ions

Figure 6.2: Effect of particle size on adsorption efficiency of metal ions in single component systems with BFS granules, 95±6 mg/L Me^{2+} ions, (A): η vs average particle size; (B) to (F): η vs time

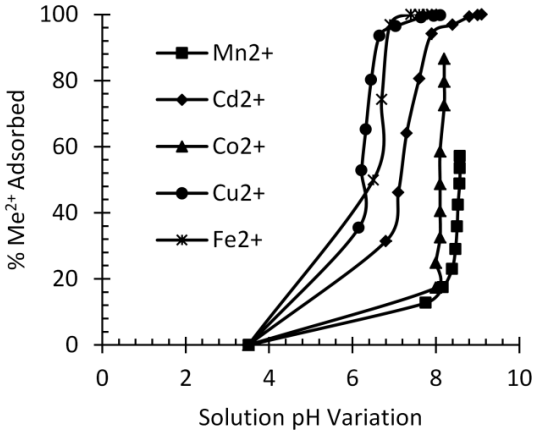

Figure 6.3: Variation of efficiency with pH in single components with BFS granules, 97±6 mg/L Me^{2+}

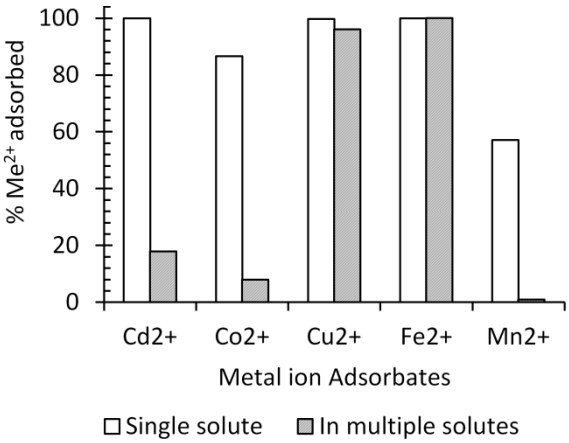

Figure 6.4: Comparison of adsorption efficiency between single- & multi-components with BFS granules, 97±6 mg/L Me^{2+}

From Figure 6.3, variation of system/solution pH is different for all metals at the same experimental conditions. This might be helpful in assessing selective metal ion adsorption based on initial pH in a multiadsorbate system. The increase in solution pH from an initial value of 3.50 as shown in Figure 6.3, is caused by the dissolution of the high free lime (44 %

CaO) content in BFS material, that gives it a potentially high neutralizing capacity for acidic effluents with ability to precipitate metal ions (Bodurtha and Brassard, 2000; Yan et al., 2000). Based on the theoretical solubility of metal hydroxides as function of pH and metal concentration, the observed metal ion concentrations against equilibrium pH suggests metal removal involve metal hydroxide precipitation for Cu^{2+} and Fe^{2+} except probably Cd^{2+} , Mn^{2+} and Co^{2+} for which precipitation may be negligible. However, Gao et al (1995) has reported that adsorption process is kinetically much faster than chemical precipitation of metal hydroxide. Thus, efficiency of adsorption appears to be implicitly controlled by equilibrium pH and not necessarily initial pH as reported in the literature.

A sample of BFS granules was ground to obtain a powdered (finely sized) fraction (d_p<45 μm), which was used as an adsorbent in single adsorption systems of metal ions. At 100 mg/L solute concentration, adsorption was nearly instantaneous and complete (100%) in all single solutes using a powdered BFS fraction (results not shown) with final pH values > 7.5. However, the efficiency reduced to 87% for Co^{2+} and 57% for Mn^{2+} but remained at 100% for Fe^{2+}, Cu^{2+} and Cd^{2+} when a coarse fraction of BFS granules (0.18-0.36 mm) was employed. This is the finest size fraction among the three (3) BFS granules studied in the coarser size ranges, which gave the highest adsorption efficiency. Mass transfer resistance may be high for larger particles. A detailed analysis of mass transfer kinetics is discussed in Section 6.3.4. Efficiency of adsorption was high and selective towards Fe^{2+} and Cu^{2+} but moderate towards Cd^{2+} and low for Co^{2+} and Mn^{2+} ions.

Comparatively, % adsorption drastically reduced in multiadsorbates relative to single adsorbates, i.e., 100 to 18% Cd^{2+}, 87 to 7.6% Co^{2+}, 100 to 96% Cu^{2+}, 57% to negligible value

for Mn^{2+} but Fe^{2+} was unaffected at 100% with a 0.18-0.36 mm size fraction as shown in Figure 6.4 above. Xue et al (2009) obtained similar results for Cu^{2+}, Cd^{2+}, Pb^{2+} and Zn^{2+} adsorption with basic oxygen furnace (BOF) slag. It is not certain whether all adsorbates compete for the same free adsorption sites or there is preferential solute adsorption. Table 6.2 generally shows an increase in adsorption capacity, distribution coefficient and equilibrium pH with decrease in particle size diameter. The adsorption preference was deduced to be $Fe^{2+}>Cu^{2+}>>>Cd^{2+}>>Co^{2+}>Mn^{2+}$ in this system.

It is evident therefore that adsorption of metal ions from single component systems using BFS has been demonstrated. The adsorption efficiency of metal ions was greatly improved by decreasing slag particle sizes. A high pH promotes adsorption possibly by precipitation and/or ion exchange processes (Section 6.3.5). Mn^{2+} and Co^{2+} ions are resistant to adsorption relative to other ions. However, the presence of competing adsorbates reduced adsorption of other metal ions in multiadsorbates. Thus, the rate and extent of adsorption depend on the type of metal ion involved and interactive effects among these ions. In this research, therefore, it was imperative to understand conditions under which a complete adsorption of metal ions could be achieved in a multicomponent context, discussed in the next sections. Furthermore, this study explored techniques to improve adsorption efficiency above the currently achievable values in multicomponent systems of different metal ions, concentration and acidity in a metal-sulphate system that simulate chemical compositions of actual acid mine drainage systems and related waste solutions.

Table 6.2: Summary of kinetic parameters as a function of particle size in single component system with BFS granules in agitated bottles

Me^{2+} Ions	Effect of Particle size (mm)	Theoretical Initial Conc, C_i, (mg/L)	Actual Initial Conc, C_i, (mg/L)	Equilibrium Conc, C_e (mg/L)	Max adsorbed η, (%)	Q_e max, mg/g	Equil pH	Distrib. Coeff. , K_d, (L/g)
Cd^{2+}	0.18-0.36	100	83.83	0.04	100	1.341	9.1	33.53
	0.36-0.50	100	87.85	0.38	100	1.400	8.9	3.68
	0.50-1.00	100	98.43	0.83	99	1.600	8.9	1.93
Co^{2+}	0.18-0.36	100	92.70	12.45	87	1.284	8.2	0.103
	0.36-0.50	100	97.60	28.85	70	1.100	8.2	0.038
	0.50-1.00	100	96.13	30.63	68	1.048	8.2	0.034
Cu^{2+}	0.18-0.36	100	94.68	0.29	100	1.510	8.1	5.21
	0.36-0.50	100	99.4	0.65	99.3	1.580	7.7	2.43
	0.50-1.00	100	116.06	0.25	99.8	1.853	7.7	7.41
Fe^{2+}	0.18-0.36	100	92.85	BDL	100	1.486	7.9	-
	0.36-0.50	100	98.45	BDL	100	1.575	7.9	-
	0.50-1.00	100	101.54	BDL	100	1.625	7.9	-
Mn^{2+}	0.18-0.36	100	100.60	43.20	57	0.918	8.6	0.021
	0.36-0.50	100	102.10	53.85	47	0.772	8.6	0.014
	0.50-1.00	100	87.95	54.70	38	0.532	8.5	0.010

6.3.2 Multicomponent Adsorption Systems

This section consists of adsorption results that were obtained from experiments conducted in multicomponent systems of Cd^{2+}, Co^{2+}, Cu^{2+}, Fe^{2+} and Mn^{2+} ions with BFS and EAF as adsorbents using immersion adsorption technique in both agitated bottles and STR. The competitive and interactive effects, the quantity of adsorbent requirement and its capacity and efficiency have been evaluated as a function of solid/liquid phase ratios, particle sizes, temperature, initial pH, initial concentration of metal ions and rate of agitation.

6.3.2.1 Initial pH

The different initial pH values studied were 1.50, 3.50, 5.50 and 7.50 in a STR at 30 g/L solid/liquid phase ratio with initial metal ion concentrations of 40 mg/L Cd^{2+}, 30 mg/L Co^{2+}, 120 mg/L Cu^{2+}, 200 mg/L Fe^{2+} and 20 mg/L Mn^{2+} ions using BFS as an adsorbent. The choice of concentration values fell within reported range in acid mine drainages. The theoretical aspects of influence of pH on adsorption process are discussed in Section 6.3.1.1.

The effect of pH on adsorption efficiency in multicomponent solutions is similar to that for single solutes. Efficiency generally increases with increase in initial pH as shown in Figure 6.5(A) below. However, the extent of adsorption varies from one metal ion to another at each pH level studied. Key indicators for adsorption performance are given in Table 6.3.

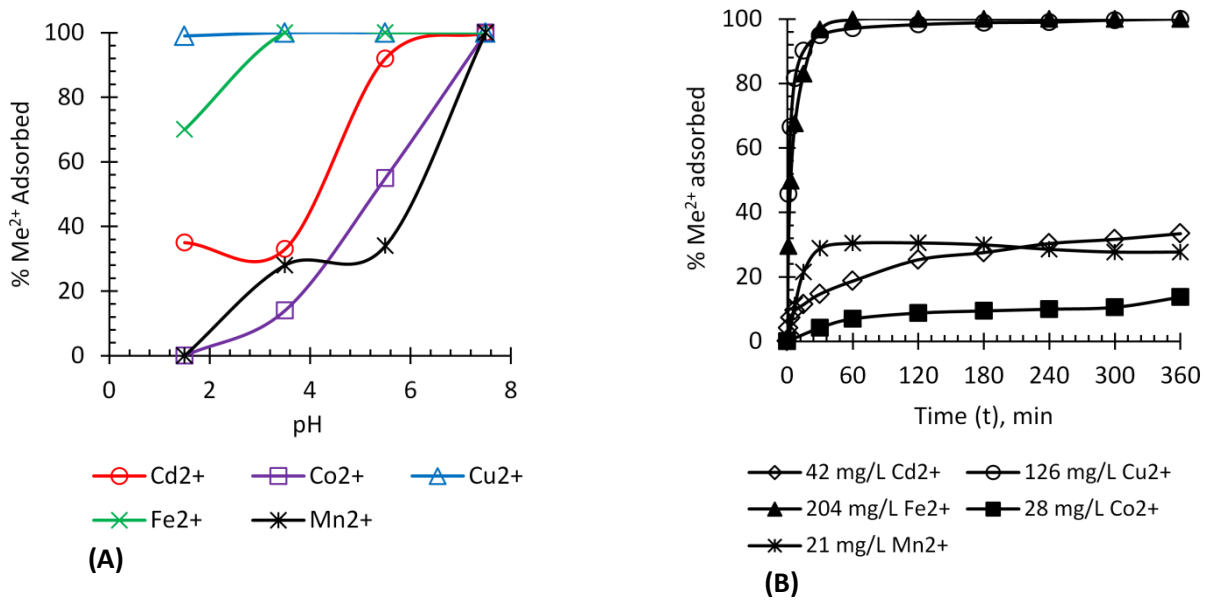

Figure 6.5: Effect of pH on adsorption efficiency of metal ions in multicomponent systems with BFS granules in STR, (A) η vs initial pH, (B) η vs time at pH 3.50

Table 6.3: Summary of kinetic parameters as a function of pH in multicomponent system with BFS granules in STR

Effect of Initial pH	Me^{2+} Ions	Theoretical Initial Conc, C_i, (mg/L)	Actual Initial Conc, C_i, (mg/L)	Equilibrium Conc, C_e (mg/L)	Max adsorbed η, (%)	Q_e max, mg/g	Equil pH	Distrib. Coeff. , K_d, (L/g)
pH 1.50	Cd^{2+}	40	41.68	27.02	35	0.50	5.2	0.019
	Co^{2+}	30	30.82	31.69	0	0	5.2	0
	Cu^{2+}	120	134.79	1.59	99	4.40	5.2	2.767
	Fe^{2+}	200	220.44	66.14	70	5.1	5.2	0.077
	*Mn^{2+}	20	21.59	-	0	0	5.2	0
pH 3.50	Cd^{2+}	40	41.97	27.94	33	0.50	6.2	0.018
	Co^{2+}	30	27.75	23.94	14	0.1	6.2	0.004
	Cu^{2+}	120	126.43	BDL	100	4.20	6.2	-
	Fe^{2+}	200	204.18	BDL	100	6.7	6.2	-
	Mn^{2+}	20	20.93	15.13	28	0.2	6.2	0.0132
pH 5.50	Cd^{2+}	40	40.14	3.28	92	1.20	7.2	0.366
	Co^{2+}	30	24.13	10.90	55	0.4	7.2	0.037
	Cu^{2+}	120	46.71	BDL	100	1.50	7.2	-
	Fe^{2+}	200	96.82	BDL	100	3.2	7.2	-
	Mn^{2+}	20	19.32	12.68	34	0.2	7.2	0.0158
pH 7.50	Cd^{2+}	40	12.84	BDL	100	0.40	8.5	-
	Co^{2+}	30	4.74	BDL	100	0.1	8.5	-
	Cu^{2+}	120	BDL	BDL	-	-	8.5	-
	Fe^{2+}	200	BDL	BDL	-	-	8.5	-
	Mn^{2+}	20	15.00	BDL	100	0.5	8.5	-

* Significant dissolution of Mn from BFS into solution, increasing solution concentration of Mn^{2+} ions.

In very acidic solutions to be purified, i.e., at pH 1.50, Cu^{2+} adsorption was completed (100%) while that of Fe^{2+} was very high. Co^{2+} adsorption is practically zero and Cd^{2+} loading was significant. However, adsorption of Mn^{2+} posed a different challenge since at pH 1.50 there is a unique limitation in its adsorption. Rather than adsorb Mn^{2+} ions from solution, BFS material was found to be leached and released Mn^{2+} ions into solution as determined by AAS analyses. At higher pH value of 3.5, adsorption of Cd^{2+}, Co^{2+} and Mn^{2+} ion improved but remained low. Again, adsorption was 100 % for Cu^{2+} and Fe^{2+} ions. These trends are shown

in Figure 6.5(B). Interestingly, an instantaneous 100 % adsorption of Cu^{2+} and Fe^{2+} was obtained at pH 5.5. However, over 50 % of these ions precipitated out before adsorption experiment was conducted. This is reflected in actual initial concentration of ions when compared to theoretical values in Table 6.3 above. Finally, at pH 7.5, a total (100%) precipitation of Cu^{2+} and Fe^{2+} ions was observed before adsorption experiment was conducted. Also, a very high precipitation of Cd^{2+} and Co^{2+} was noticeable and up to 25 % Mn^{2+} ions precipitation with remainder subjected to some kind of adsorption process. On the basis of η (%), q (mg/g) and K_d (L/g) values given in Table 6.3, adsorption preference and affinity is proposed as $Fe^{2+}>Cu^{2+}>Cd^{2+}>Co^{2+}>Mn^{2+}$. A direct comparison with published studies is not very meaningful because most studies have been conducted in metal-nitrate systems where most metal ions remain soluble without any significant precipitation over a wider pH range relative to metal-sulphate systems for this study in which precipitation of metal hydroxide occurs at much lower and narrow pH range. The sulphate system is a more representative anion carrier of metal ions in acid mine drainage compositions around mine sites.

6.3.2.2 Initial Concentration of Metal Ions

The adsorbent capacity, efficiency, competitive and interactive effects of metal ions in multicomponent equilibria were investigated as a function of initial concentration using powdered BFS and EAF adsorbents. It was hypothesised that the use of powdered adsorbents (d_p < 45 μm) in agitated adsorption vessels (STR) could provide optimum conditions to obtain maximum adsorption efficiencies for metal ions. This was conducted by either keeping the initial concentration of each solute in the mixture at the same value or independently varying each solute concentration in the mixture. The assumption was that

adsorption surface is sufficient and that adsorption sites may not be specific in character, that is, each solute was free to adsorb to any surface site.

6.3.2.2.1 All metal ions at same values of initial concentration

Adsorption experiments were conducted to assess the extent of adsorption, competitive adsorptive effects, selectivity and relative adsorption affinities in a system comprising Cd^{2+}, Co^{2+}, Cu^{2+}, Fe^{2+} and Mn^{2+} ions, with all ions fixed at the same initial values of concentration as it (concentration) was increased. Within the 20–1000 mg/L range investigated, adsorption efficiency decreased with increase in initial concentration as illustrated in Figures 6.6(A) to (F) below, except for values of Fe^{2+} ions that remained constant at 100 % as shown in Figure 6.7(A). Further, adsorption (loading) profiles were different for different metal ions, particularly those of Cd^{2+}, Co^{2+} and Mn^{2+} ions where at relatively high concentration, adsorption was very poor. At 20 mg/L of each ion, a complete (100%), non-selective adsorption was achieved for all ions. Within 20-100 mg/L, multiple adsorption of Cd^{2+}, Cu^{2+} and Fe^{2+} ions was instantaneous and completed within a minute. Adsorption of Co^{2+} and Mn^{2+} ions was fast and showed a very high initial adsorption phase, reaching different levels (%) of adsorption towards equilibrium. At 200-300 mg/L, only Cu^{2+} and Fe^{2+} ions showed instantaneous adsorption and reached completion within minutes. Again, adsorption of Cd^{2+} ions depicted a very high initial adsorption phase followed by a gradual loading to near completion towards equilibrium. Adsorption of Mn^{2+} and Co^{2+} ions was poor. Finally, within 600-1000 mg/L range, adsorption of Cu^{2+} and Fe^{2+} ions was no longer instantaneous but rather very high initial adsorption periods were obtained for both ions, with Fe^{2+} ions reaching complete adsorption at equilibrium and Cu^{2+} ions showing high but limited adsorption level. Adsorption of Cd^{2+}, Co^{2+} and Mn^{2+} ion was either poor and/or negligible.

Within the entire range of concentration levels of metal ions studied, the adsorption process was observed to occur within a pH range ≥ 5.0 in which adsorption process is reportedly highly favourable. However, Co^{2+} and Mn^{2+} ions in particular, did not adsorb to completion in some cases despite achieving neutral to alkaline solution environments in this study. As discussed later, the adsorption limitation may be due to 1) limited available surface area/adsorption sites of adsorbent, 2) poor adsorbate/adsorbent interactions (affinity, selectivity), 3) depressive ionic effects of fast and highly adsorbing adsorbates as their concentration is increased and 4) precipitation effects of metal ions on slag surfaces. This is on the assumption that if metal ions are at the same solution concentration then diffusion gradients may be similar. However, different metal ions have different diffusivities as will be shown in later sections.

High adsorption efficiency in dilute single solute systems has been noted relative to a multisolute system (Manchisi et al., 2013). The exact interactive effects among solutes on the extent of adsorption are difficult to ascertain. Darkwah (2005) reported Mn^{2+} and Cu^{2+} ions to be depressed in the presence of Fe^{2+} ions in their respective binary adsorption systems. However, initial pH of solutions had stronger effect on the extent of adsorption in several binary adsorption systems. One possible explanation for these observations is probably a limitation in the materials' key adsorptive properties such as low surface area, low internal pore area and poor pore size distribution towards larger pore sizes (macroporosity), all of which limit adsorption capacity and may lead to competitive effects for few adsorption sites among adsorbates. These adsorbent properties, discussed in detail in Chapter 4, were evaluated and found to be relatively very low when compared to other

adsorbents currently in use. This confirms the low adsorptive performance that has been observed as concentration of adsorbates is increased. Furthermore, the depressive effects of quick adsorbing Cu^{2+} and Fe^{2+} ions on Cd^{2+}, Co^{2+} and Mn^{2+} is possible. Rather than adsorption sites being available to all ions, these may be specific in character with preferential adsorption for Cu^{2+} and Fe^{2+} ions. However, whether all adsorbates compete for same free adsorption sites or there is preferential adsorption is not certain. An analysis of ionic properties such as differences in electronegativities and values of hydrated ion sizes did not explain the observed adsorption sequence. Precipitation, dealt with later in Section 6.3.5, is probably a major mechanism of adsorption for Cu^{2+} and Fe^{2+} ions.

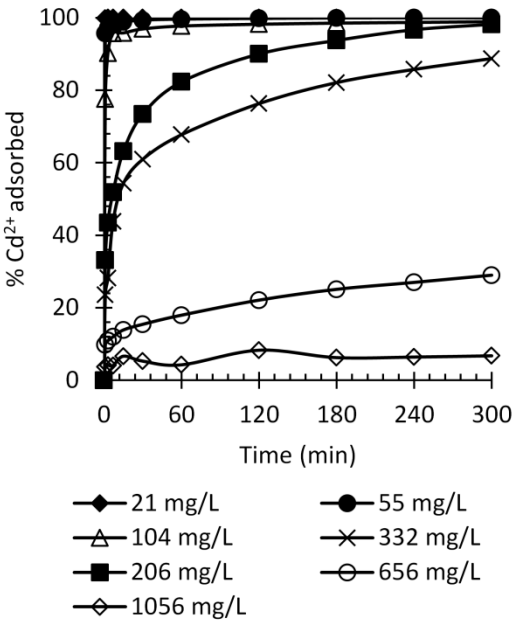

(A) Cd^{2+}

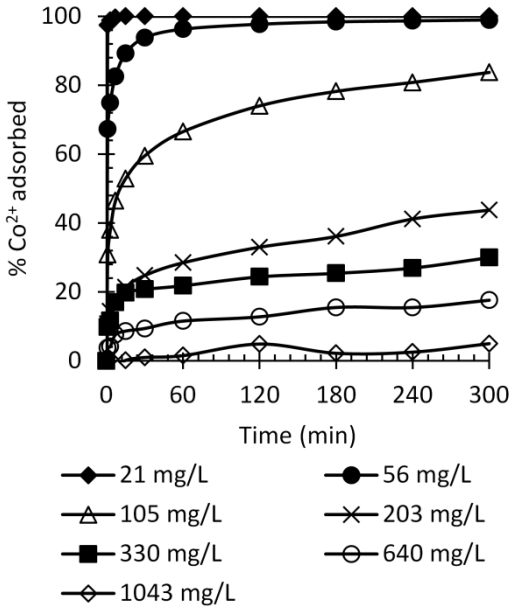

(B) Co^{2+}

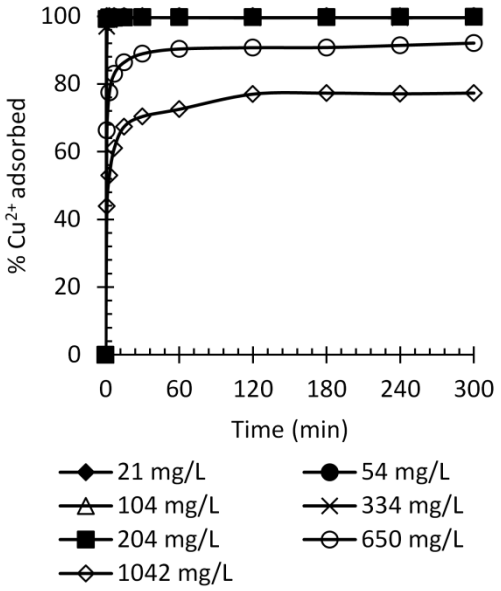

(C) Cu^{2+}

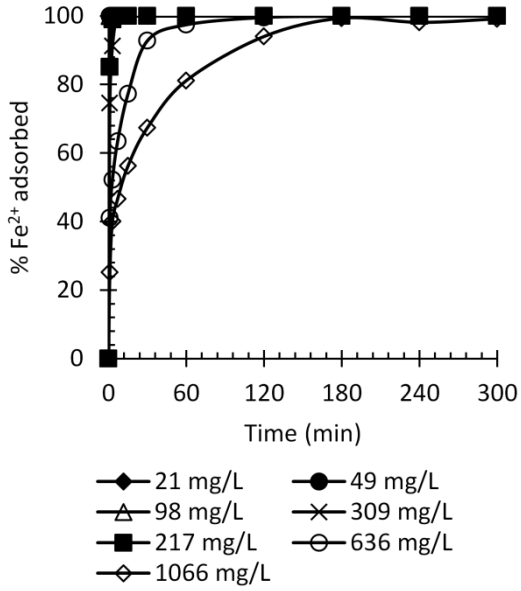

(D) Fe^{2+}

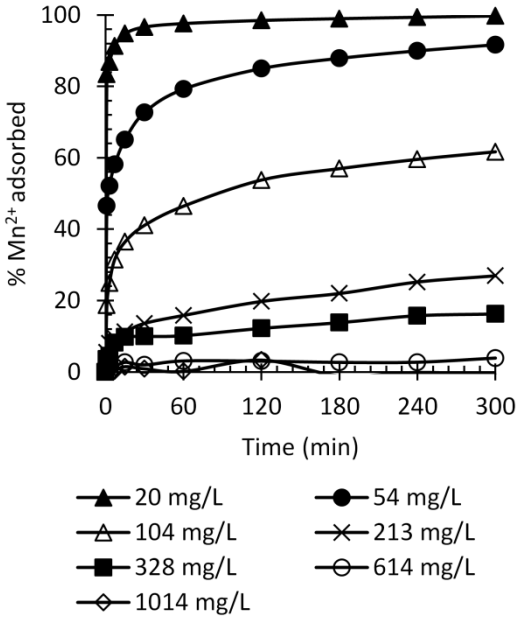

(E) Mn^{2+}

Figure 6.6: Effect of Initial Concentration on adsorption efficiency of individual metal ions in multicomponent systems, 50 g/L BFS powder, (A) to (F) η vs time

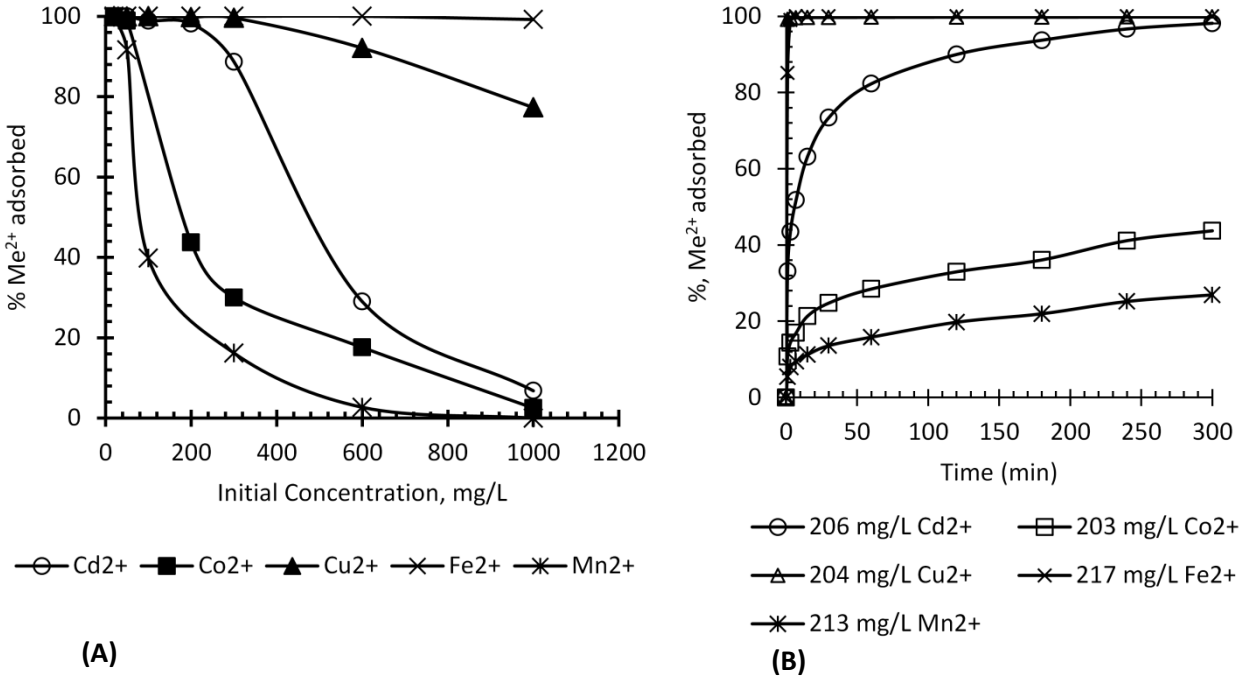

Figure 6.7: Comparison of the effect of Initial Concentration on adsorption efficiency of metal ions in multicomponent systems, 50 g/L BFS powder, (A) η vs initial conc.; (B) η vs time at 200 mg/L me^{2+}

Loading isotherms for individual metal ions at about 200 mg/L each are shown in Figure 6.7 (B) which reveal interesting kinetic aspects of adsorption. The application of kinetic effects could separate Cu^{2+} and Fe^{2+} ions from solution fairly quickly. At equilibrium, Cd^{2+} ions might be extracted with limited amounts of Co^{2+} and Mn^{2+} ions. Similar trends of kinetic profiles and adsorption preferences (not shown) at other different levels of initial adsorbate concentration were observed. The extent of adsorption varies for the different metal ions at the same level of initial concentration. The possible reasons for these observations may be due to differences ionic characteristics discussed in Chapter 5. Initial rates of adsorption are high perhaps due to high mass transfer rates, high concentration gradients and high adsorption sites. This in turn drives diffusion flux across the film boundary layer around adsorbent particles into slag pores. The theory of Intraparticle diffusion by Weber and Morris (1963) predicted both film and intraparticle diffusion steps to limit adsorption at

higher concentration. On the basis of the pseudo second order kinetics model, overall adsorption appeared to be controlled by chemisorption step (Manchisi et al., 2013).

The variation of adsorption capacity, Q_e, with concentration is shown in Figure 6.8(A) which increased with increase in initial adsorbate concentration for Cd^{2+}, Co^{2+} and Mn^{2+} ions up to a certain maximum beyond which it decreased. However, Q_e values for Cu^{2+} and Fe^{2+} ions showed a continuous increase with concentration under same conditions. A summary of maximum adsorption capacity values (Q_{max}), distribution coefficients (K_d) and other adsorptive parameters are given in Tables 6.4 and 6.5. The values of Q_{max}, K_d and separation factors of Cu^{2+} and Fe^{2+} ions are much greater than those of Cd^{2+}, Co^{2+} and Mn^{2+} ions, reflecting high affinity and preferential (selective) adsorption towards Cu^{2+} and Fe^{2+} ions. Adsorption equilibria of this system are covered in detail in Chapter 5. Therefore, adsorptive separation of Cu^{2+} and Fe^{2+} ions from the rest may be possible but multiple adsorption of all metal ions to meet the permissible regulatory discharge limits (EPPCA, 1990), one of the primary objectives of this study, is difficult at relatively higher concentration. However, an optimum particle size and mass of BFS in relation to initial concentration of metal ions is expected to work effectively in dilute solutions. The effects of particle size and mass of adsorbents are investigated in the sections that follow.

Table 6.4: Some adsorption parameters at same initial concentration of metal ions (20-1000 mg/L), 50 g/L BFS powder

	Cd^{2+}	**Co^{2+}**	**Cu^{2+}**	**Fe^{2+}**	**Mn^{2+}**
Experimental maximum adsorption capacity, Q_{max} (mg/g)	2.83	0.95	7.73	10.23	0.51
Initial conc., at Q_{max}, mg/L	332	640	1041	1066	104
Highest Distribution Coefficient K_d , (Q_e/C_e) at $C_e \leq 5$ mg/L	0.52	0.89	2.31	210	0.11
Initial Conc., at $C_e \leq 5$ mg/L	≤ 205.6	≤ 56	≤ 334	≤ 636	≤ 54

Table 6.5: Summary of kinetic parameters as a function of initial concentration in multicomponent system, 50 g/L BFS powder, agitated bottles, metal ions at same values of initial concentration.

Initial conc	Metal Ion	Theoretical Conc, (mg/L)	Actual Conc, (mg/L)	Max Adsorbed, η (%)	Equil. Conc, C_e (mg/L)	Q_e max mg/g	Equil pH	Distrib. Coeff., K_d (L/g)
20 mg/L	Cd^{2+}	20	21.02	100	BDL	0.202	9.0	-
	Co^{2+}	20	21.15	100	BDL	0.203	9.0	-
	Cu^{2+}	20	21.04	100	BDL	0.202	9.0	-
	Fe^{2+}	20	20.96	100	BDL	0.201	9.0	-
	Mn^{2+}	20	20.48	100	0.06	0.196	9.0	3.267
50 mg/L	Cd^{2+}	50	54.50	100	BDL	0.523	8.7	-
	Co^{2+}	50	55.95	99	0.60	0.531	8.7	0.885
	Cu^{2+}	50	53.87	100	0.07	0.516	8.7	7.371
	Fe^{2+}	50	48.88	100	BDL	0.469	8.7	-
	Mn^{2+}	50	54.23	92	4.53	0.477	8.7	0.105
100 mg/L	Cd^{2+}	100	103.63	99	1.19	0.983	8.2	0.826
	Co^{2+}	100	105.07	84	17.14	0.844	8.2	0.049
	Cu^{2+}	100	104.14	100	0.03	0.999	8.2	33.30
	Fe^{2+}	100	97.92	100	BDL	0.940	8.2	-
	Mn^{2+}	100	103.87	62	39.81	0.615	8.2	0.015
200 mg/L	Cd^{2+}	200	205.60	98	3.76	1.938	7.2	0.515
	Co^{2+}	200	203.14	44	114.30	0.852	7.2	0.007
	Cu^{2+}	200	203.68	100	0.39	1.952	7.2	5.005
	Fe^{2+}	200	217.05	100	BDL	2.084	7.2	-
	Mn^{2+}	200	213.41	27	155.95	0.552	7.2	0.004
300 mg/L	Cd^{2+}	300	332.03	89	37.44	2.828	7.2	0.076
	Co^{2+}	300	330.01	30	231.16	0.949	7.2	0.004
	Cu^{2+}	300	333.60	100	1.38	3.189	7.2	2.311
	Fe^{2+}	300	309.216	100	BDL	2.968	7.2	-
	Mn^{2+}	300	327.75	16	274.57	0.511	7.2	0.002
600 mg/L	Cd^{2+}	600	655.96	29	465.79	1.826	5.8	0.004
	Co^{2+}	600	639.78	18	527.22	1.081	5.8	0.002
	Cu^{2+}	600	649.55	92	51.45	5.742	5.8	0.112
	Fe^{2+}	600	636.15	100	0.029	6.107	5.8	210
	Mn^{2+}	600	613.95	4	590.02	0.230	5.8	0.0004
1000 mg/L	Cd^{2+}	1000	1056.11	7	984.81	0.684	5.4	0.001
	Co^{2+}	1000	1043.33	5	991.36	0.499	5.4	0.001
	Cu^{2+}	1000	1041.76	77	236.30	7.732	5.4	0.033
	Fe^{2+}	1000	1065.69	100	5.397	10.179	5.4	1.886
	Mn^{2+}	1000	1014.09	0	1021.93	-	5.4	-

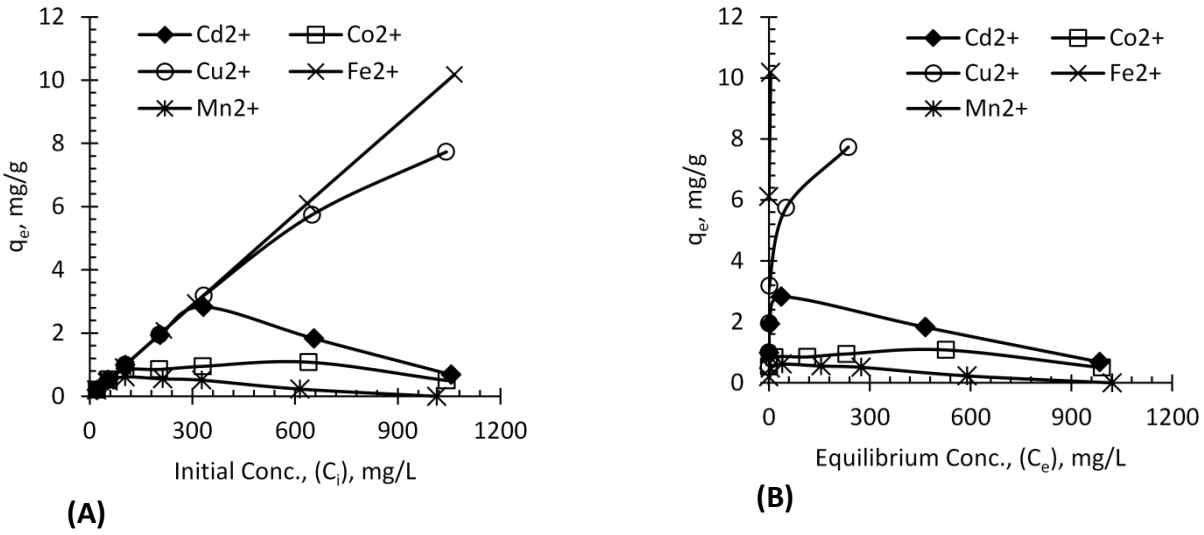

Figure 6.8: Variation of adsorption capacity with (A) initial concentration, (B) equilibrium concentration, 50 g/L BFS powder, 20-1000 mg/L Me^{2+};

6.3.2.2.2 All metal ions at different values of initial concentration

Multisolute adsorption was also assessed by independent variation of individual solute concentration within the mixtures (20-200 mg/L Cd^{2+}, 15-150 mg/L Co^{2+}, 30-1000 mg/L Cu^{2+}, 50-1600 mg/L Fe^{2+} and 10-100 mg/L Mn^{2+}) such that the more strongly adsorbing metal ion concentration was 2-15 times that of the weakly binding metal ion. The hypothesis was that if adsorption efficiency is relatively high for metal solutes that are at low concentration levels, but which also have low affinity to adsorb then competitive effects of adsorption is low, assuming that each solute was free to adsorb to any surface sites and that there is sufficient adsorptive surface area, sites density and negligible precipitation side reactions. Efficiency is generally expected to be higher the lower the initial adsorbate concentration.

The loading isotherms and kinetic profiles for metal ions as a function of initial concentration are shown in Figures 6.9(A) to (F). The solutes were not at the same

concentration levels as it was varied independently for each metal ion in the mixtures. Adsorption kinetics, efficiency and capacity profiles are similar to those observed for metal ions fixed at the same level of initial concentration (Fig. 6.7(A)). Table 6.6 gives a summary of adsorption performance indicated by three key response variables, i.e., η (%), Q_e (mg/g) and K_d (L/g). Adsorption of Cd^{2+}, Co^{2+} and Mn^{2+} ions is poor and/or negligible when the initial concentration of any of these ions is 5-15 times lower than the concentration of Cu^{2+} and Fe^{2+} ions. Here, adsorption of metal ions at low concentration in the mixture appears to be suppressed by the quickly and strongly adsorbing metal ions (Cu^{2+}, Fe^{2+}) which are at higher concentration in the six (6) different solution mixtures investigated. This observation partly supports the hypothesis of competitive adsorptive effects among metal ions, with those at high concentration taking up most of the available adsorption surfaces sites.

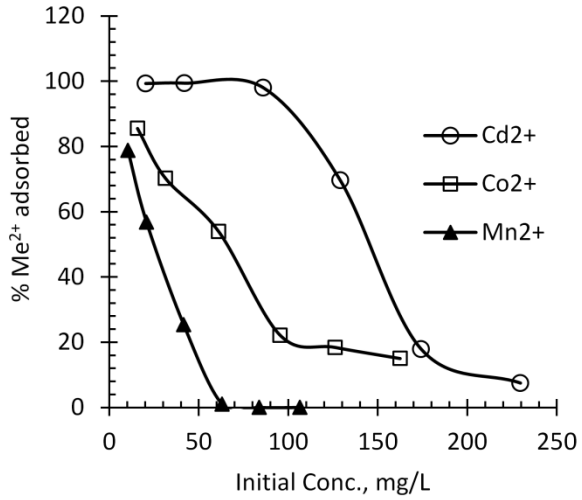

(A)

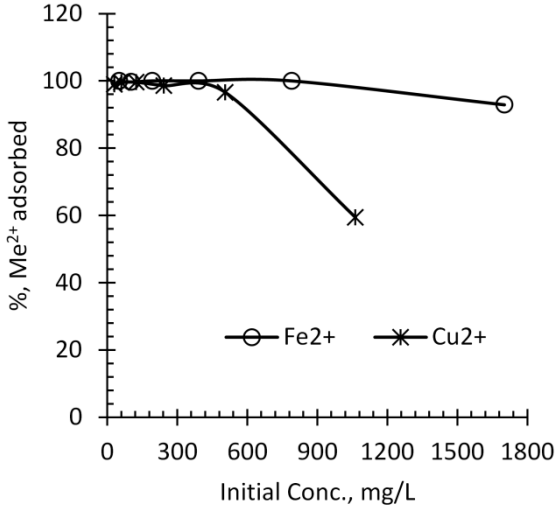

(B)

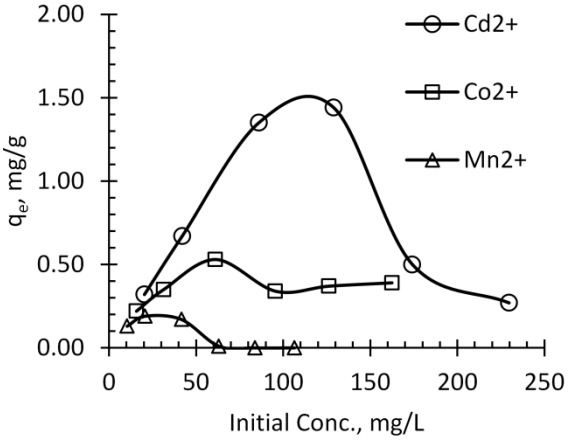

(C)

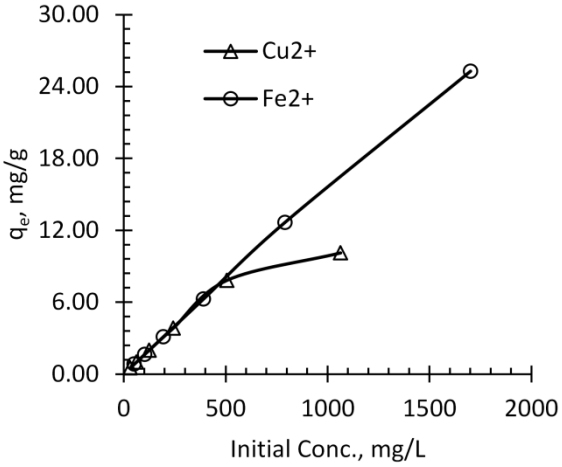

(D)

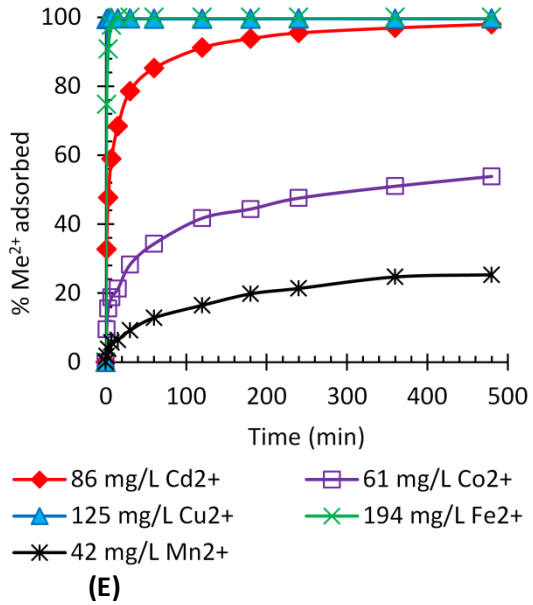

(E)

Figure 6.9: Effect of Initial conc. on adsorption efficiency of metal ions in multicomponent systems with BFS powder, (A) & (B) η vs initial conc., (C) & (D) Q_e vs initial conc., (F) η vs time at specified conc.

Table 6.6: Summary of kinetic parameters as a function of initial concentration in multicomponent system with BFS powder, agitated bottles, and solute concentration varied independently of each other

Metal Ion	Theoretical Conc, (mg/L)	Actual Conc, (mg/L)	Max Adsorbed (%)	Equil. Conc, (mg/L)	Q_e max mg/g	Distrib. Coeff., K_d (L/g)	Equil pH (Measured)
Cd^{2+}	20	20.34	99.3	0.02	0.32	16.0	8.4
Co^{2+}	15	15.76	85.5	2.29	0.22	0.096	
Cu^{2+}	30	31.74	98.9	0.36	0.50	1.39	
Fe^{2+}	50	51.07	100	BDL	0.82	∞	
Mn^{2+}	10	10.4	78.8	2.21	0.13	0.059	
Cd^{2+}	40	42.01	99.4	0.27	0.67	2.48	7.8
Co^{2+}	30	31.43	70.2	9.36	0.35	0.037	
Cu^{2+}	60	61.55	99.5	0.31	0.98	3.16	
Fe^{2+}	100	102.78	99.7	0.3	1.64	5.47	
Mn^{2+}	20	20.81	56.8	8.98	0.19	0.021	
Cd^{2+}	80	86.03	98	1.75	1.35	0.77	7.1
Co^{2+}	60	61.12	53.9	28.2	0.53	0.019	
Cu^{2+}	120	124.8	99.6	0.51	1.99	3.90	
Fe^{2+}	200	194.18	100	BDL	3.11	∞	
Mn^{2+}	40	41.63	25.3	31.08	0.17	0.005	
Cd^{2+}	120	129.05	69.6	39.21	1.44	0.037	6.4
Co^{2+}	90	95.5	22.1	74.38	0.34	0.005	
Cu^{2+}	240	242.9	98.6	3.42	3.83	1.12	
Fe^{2+}	400	391.71	100	BDL	6.27	∞	
Mn^{2+}	60	63.07	1	62.45	0.01	0.0002	
Cd^{2+}	160	174.19	17.9	143.08	0.50	0.003	5.8
Co^{2+}	120	126.28	18.4	103.05	0.37	0.004	
Cu^{2+}	500	505.81	96.6	17.21	7.82	0.45	
Fe^{2+}	800	790.94	100	BDL	12.66	∞	
Mn^{2+}	80	83.8	0	83.8	0	0	
Cd^{2+}	200	229.68	7.5	212.56	0.27	0.001	5.0
Co^{2+}	150	162.45	15	138.12	0.39	0.003	
Cu^{2+}	1000	1064.02	59.4	432.15	10.11	0.023	
Fe^{2+}	1600	1701.65	92.9	121.38	25.28	0.208	
Mn^{2+}	100	106.5	0	106.5	0	0	

6.3.2.2.3 Adsorption Characteristics of Metal ions by EAF Adsorbent

The adsorbent efficiency of EAF relative to BFS was analysed in multicomponent adsorption systems by independent variation of individual solute concentration within the mixtures (20-200 mg/L Cd^{2+}, 15-150 mg/L Co^{2+}, 30-1000 mg/L Cu^{2+}, 50-1600 mg/L Fe^{2+} and 10-100 mg/L Mn^{2+}). The adsorption profiles for efficiency (η) and capacity (Q) as a function of initial concentration (C_i) and time (t) are plotted in Figures 6.10(A) to (E). The trends are similar to those observed for adsorption of metal ions by BFS at similar solution conditions. However, Cu^{2+} and Fe^{2+} adsorption was instantaneous and completed (100 %) in the entire concentration range investigated (30-1000 mg/L Cu^{2+}, 50-1600 mg/L Fe^{2+}). This observation appeared to be pH controlled and is discussed further under adsorption mechanisms in Section 6.3.5. The trend as a function of time at specific concentration is shown in Figure 6.10(E) below. The % adsorption of Cd^{2+}, Co^{2+} and Mn^{2+} ions was low relative to Cu^{2+} and Fe^{2+} ions with gradual increase in concentration, for which adsorption preference is proposed as $Fe^{2+}>Cu^{2+}>Cd^{2+}>Co^{2+}>Mn^{2+}$. Table 6.7 gives a summary of adsorption performance indicated by η (%), Q_e (mg/g) and K_d (L/g).along with final pH (discussed in detail in Chapter 5). The % adsorption of Cd^{2+}, Co^{2+} and Mn^{2+} ions was again poor when the concentration of any of these ions is 5-15 times lower than that of Cu^{2+} and Fe^{2+} ions. This may be attributed to several factors that may include depressive effect of ions at higher concentration and competition for adsorption sites.

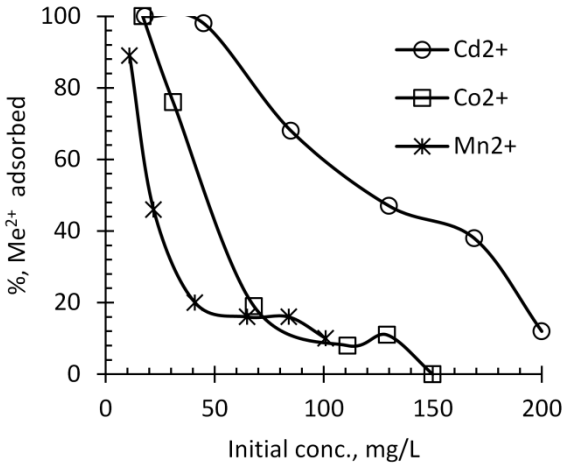

(A)

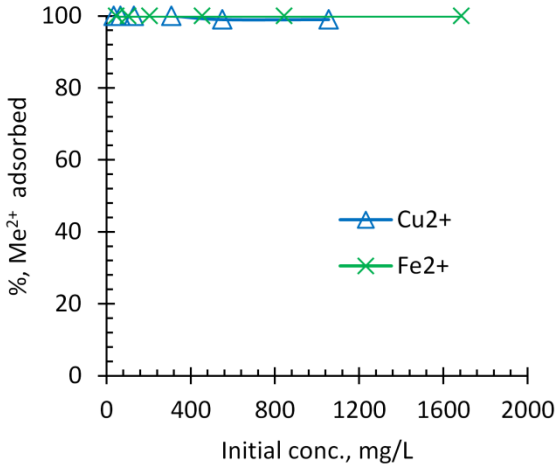

(B)

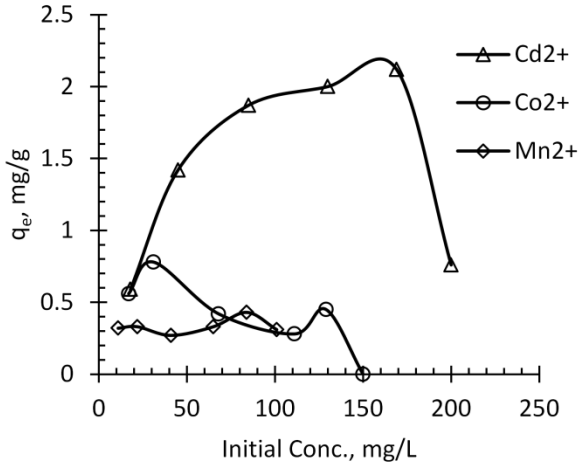

(C)

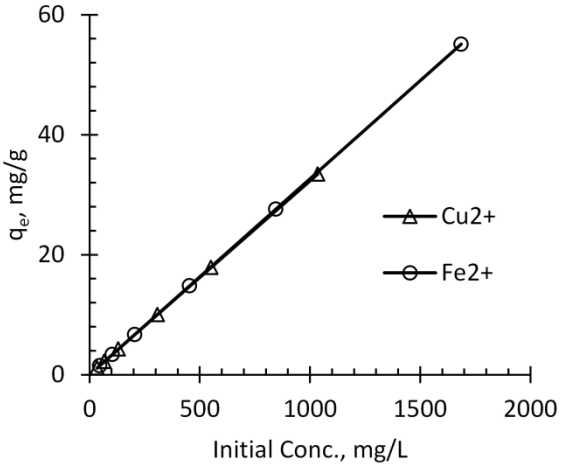

(D)

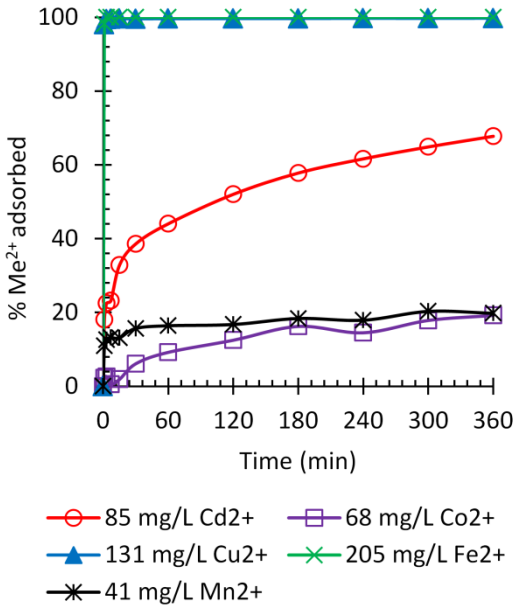

(E)

Figure 6.10: Effect of conc. on efficiency of Me^{2+} ions in multicomponents with EAF powder, (A) & (B) η vs conc.; (C) & (D) q_e vs conc., (E) η vs time at specified conc.

Table 6.7: Summary of kinetic parameters as a function of initial concentration in multicomponent system with EAF powder, agitated bottles, and solute concentration varied independently in the mixtures

Metal Ion	Theoretical Conc, (mg/L)	Actual Conc, (mg/L)	Max Adsorbed (%)	Equil. Conc, (mg/L)	Q_e max mg/g	Distrib. Coeff., K_d (L/g)	Equil pH (Measured)
Cd^{2+}	20	18	100	*BDL	0.59	∞	8.9
Co^{2+}	15	17	100	BDL	0.56	∞	
Cu^{2+}	30	34	100	BDL	1.10	∞	
Fe^{2+}	50	46	100	BDL	1.50	∞	
Mn^{2+}	10	11	89	1.19	0.32	0.269	
Cd^{2+}	40	45	98	1.02	1.42	1.39	8.2
Co^{2+}	30	31	76	7.40	0.78	0.105	
Cu^{2+}	60	67	100	BDL	2.18	∞	
Fe^{2+}	100	103	100	BDL	3.35	∞	
Mn^{2+}	20	22	46	11.88	0.33	0.028	
Cd^{2+}	80	85	68	27.29	1.87	0.069	7.5
Co^{2+}	60	68	19	54.5	0.42	0.008	
Cu^{2+}	120	131	100	0.32	4.26	13.31	
Fe^{2+}	200	205	100	BDL	6.70	∞	
Mn^{2+}	40	41	20	33	0.27	0.008	
Cd^{2+}	120	130	47	69	2.00	0.029	7.0
Co^{2+}	90	111	8	103	0.28	0.003	
Cu^{2+}	240	308	100	1.31	10.01	7.64	
Fe^{2+}	400	454	100	BDL	14.82	∞	
Mn^{2+}	60	65	16	55	0.33	0.006	
Cd^{2+}	160	169	38	104	2.12	0.020	6.7
Co^{2+}	120	129	11	115	0.45	0.004	
Cu^{2+}	500	551	99	4.44	17.86	4.02	
Fe^{2+}	800	845	100	BDL	27.59	∞	
Mn^{2+}	80	84	16	71	0.43	0.006	
Cd^{2+}	200	200	12	177	0.76	0.004	6.2
Co^{2+}	150	150	0	-	-	-	
Cu^{2+}	1000	1035	99	11	33.44	3.04	
Fe^{2+}	1600	1686	100	0.18	55.1	306.11	
Mn^{2+}	100	101	10	91	0.31	0.003	

*BDL = Below Detection Limit

A comparison of adsorbent efficiencies between BFS and EAF is shown in Figures 6.11(A) and (B). Cu^{2+} and Fe^{2+} ions depicted instantaneous adsorption to completion (100 %) in the entire concentration range using EAF (results are not shown). However, progress of adsorption towards equilibrium by BFS was slower, limited and/or poor at higher concentration. The loading profile for Cd^{2+} and Co^{2+} ions by BFS was kinetically faster and higher than that obtained by EAF at moderate to low concentration. EAF, however, appears to perform better than BFS at higher concentration although efficiency was still unsatisfactory for both adsorbents. Faster adsorption kinetics for Mn^{2+} ions by BFS were observed relative to that of EAF at lower concentration, but EAF appear to have higher capacity for Mn^{2+} ions than BFS especially at high concentration for which adsorption efficiencies associated with BFS were poor. Furthermore, higher equilibria pH values were observed for adsorption systems that employed EAF than those of BFS. This is despite the fact that BFS has higher lime (CaO) content at 44 % than EAF at 7 % CaO. This suggests that most of lime contained in EAF is not chemically bound and therefore free to easily hydrolyse to produce a solution of higher alkaline pH at equilibrium.

These experimental adsorption results and observations suggest that the extent of adsorption of various metal ions is dependent on the type of adsorbate metal ions, initial concentration and specific metal ion/adsorbate interactions involved. A multiple adsorption of metal ions is generally feasible at low concentration under these conditions, after which adsorption efficiencies quickly falls off to low values at moderate to higher concentration. The marginally higher surface and internal pore area of EAF provides higher adsorption surface/sites for metal ions as established in Chapter 4, giving it higher adsorption capacity and efficiency than that of BFS at moderate to higher concentration. BFS has a higher

adsorption affinity and faster initial adsorption kinetics than EAF, towards certain ions especially Cd^{2+} and Co^{2+} ions. A quantitative analysis of mass transfer kinetics is given in Section 6.3.4.

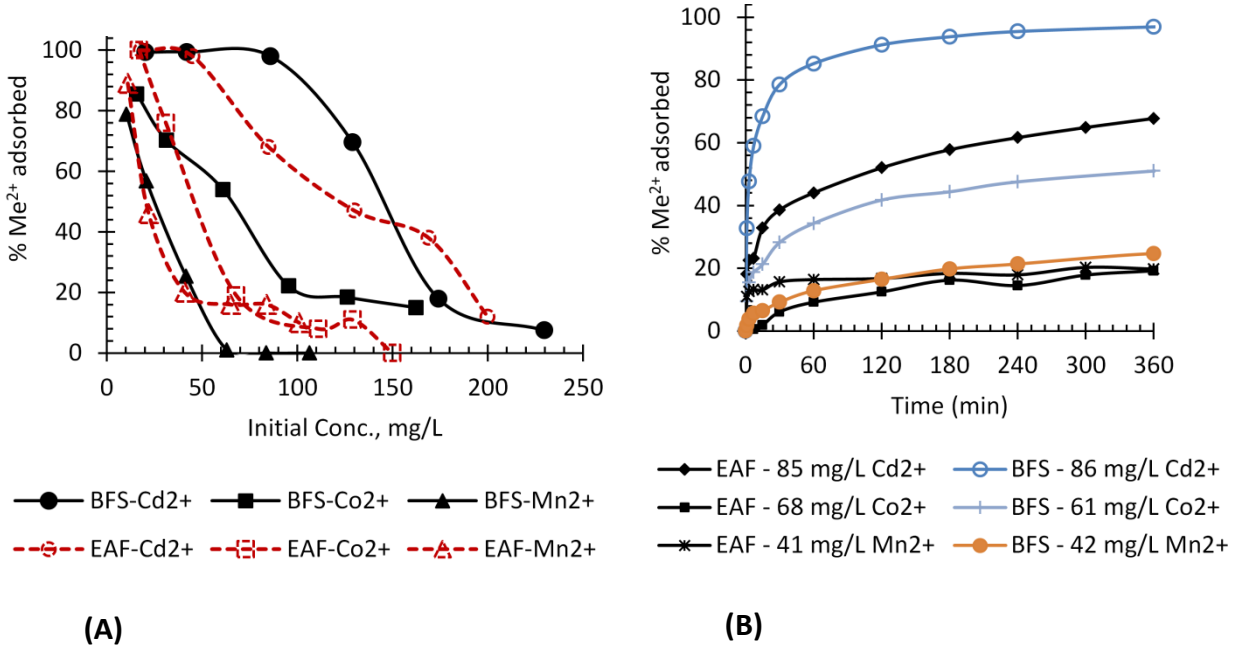

(A) **(B)**

Figure 6.11: Comparison of adsorbent efficiencies between BFS and EAF vs initial conc. for metal ions in multicomponent systems with adsorbent powders, (A) η vs initial conc., (B) η vs time at specified conc.

6.2.2.3 Particle Size Distribution of Adsorbent

The effect of two size fractions of BFS on adsorption kinetics, i.e., powdered BFS (dp < 45 µm) and its granulated form (0.18 < d_p < 0.36 mm), was studied in a multiple metal ion system at same initial concentration of 100 mg/L for each ion. Four other size fractions of BFS granules (+45-53, +90-106, +180-212, +355-425 µm) were also tested in a multiple metal ion system at different initial concentrations of 40 mg/L Cd^{2+}; 30 mg/L Co^{2+}; 60 mg/L Cu^{2+}; 100 mg/L Fe^{2+} and 20 mg/L Mn^{2+} ions.

The use of powdered BFS (d_p < 45 µm) resulted in high adsorption efficiency relative to granulated BFS. The reduction in the amount adsorbed were 99 to 18 % Cd^{2+}, 84 to 8 % Co^{2+}, 100 to 96 % Cu^{2+}, 62 % to negligible value for Mn^{2+} but Fe^{2+} was unaffected at 100 %. Therefore, of the two size fractions, better adsorption results were obtained with powdered adsorbent, which demonstrates the sensitivity of adsorption to particle size of adsorbent. The results also emphasize the preferential (selective) adsorption and high affinity towards certain ions (Cu^{2+}, Fe^{2+}) despite the fact that initial concentration of all metal ions were fixed at the same initial values.

The amount of metal ions adsorbed increased with a decrease in particle size diameter of BFS as shown in Figure 6.12, probably due to an increase in surface area and adsorption sites as particle size decreases, giving a higher opportunity for metal ion adsorption. Also, mass transfer resistance may be high for larger particles. These mass transfer kinetic factors are analysed quantitatively in Section 6.3.4. Again, efficiency of adsorption was high and selective towards Fe^{2+} and Cu^{2+} ions, moderate towards Cd^{2+} and low for Co^{2+} and Mn^{2+} ions across all size fractions. As stated previously, it is not clear if all ions compete for same adsorption sites or there is preferential adsorption of specific metal ions. Several factors may be evident such as differences in metal ion characteristics, high affinity of BFS for specific ions and probably a limitation in specific surface area (shown in Chapter 4). Therefore, the best adsorption results were obtained with the finer size fraction of adsorbent. However, the particle size distribution has important applications in adsorption columns operation. Manchisi et al (2013) analysed the kinetics of adsorption from single and multisolute systems using the widely used kinetic models (Intraparticle diffusion, pseudo kinetic models, etc.) and suggested that adsorption process was controlled by both diffusion

and chemisorption steps as particle diameters of adsorbent were increased. Initial adsorption rates and rate constants based on pseudo second order model increased with decrease in particle size diameter. Adsorption capacity was more sensitive to variations in initial solute concentration than to particle size diameter. Table 6.8 gives a summary of the experimental and solution conditions and adsorption performance represented by η (%), Q_e (mg/g) and K_d (L/g) response variables.

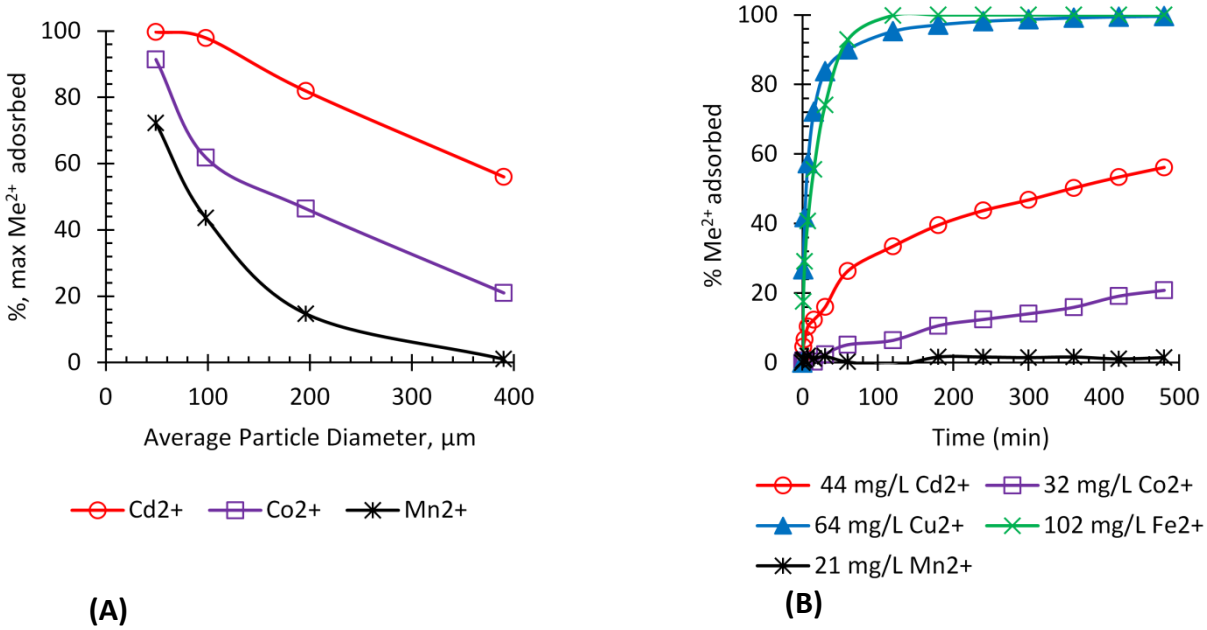

Figure 6.12: Effect of particle size on adsorption efficiency of metal ions in multicomponent systems, with BFS powder, (A): η vs particle size, (B) η vs time at +355-425 µm size fraction

Table 6.8: Summary of kinetic parameters as a function of particle size of adsorbent in multicomponent system with BFS granules in agitated bottles

(a) Metal ions at the same initial concentration (BFS powder vs granules)								
Particle diameter (d_p)	**Metal Ion**	**Theoretical Conc, (mg/L)**	**Actual Conc, (mg/L)**	**Max Adsorbed (%)**	**Equil. Conc, (mg/L)**	**Q_e max mg/g**	**Equil pH**	**Distrib. Coeff., K_d (L/g)**
d_p<45 µm (BFS powder)	Cd^{2+}	100	104	99	1.19	1.71	8.2	1.437
	Co^{2+}	100	105	84	17.1	1.47	8.2	0.086
	Cu^{2+}	100	104	100	0.03	1.73	8.2	57.77
	Fe^{2+}	100	98	100	BDL	1.63	8.2	∞
	Mn^{2+}	100	104	62	40	1.07	8.2	0.027
+0.18-0.36 mm (BFS granules)	Cd^{2+}	100	102	18	84	0.300	6.4	0.004
	Co^{2+}	100	102	8	96	0.100	6.4	0.001
	Cu^{2+}	100	102	96	4.2	1.630	6.4	0.388
	Fe^{2+}	100	100	100	0.01	1.667	6.4	166.7
	Mn^{2+}	100	106	1.4	104.2	0.030	6.4	0.0003
(b) Metal ions at different initial concentration (with BF granules)								
Particle diameter (d_p)	**Metal Ion**	**Theoretical Conc, (mg/L)**	**Actual Conc, (mg/L)**	**Max Adsorbed (%)**	**Equil. Conc, (mg/L)**	**Q_e max mg/g**	**Equil pH**	**Distrib. Coeff., K_d (L/g)**
+45-53 µm	Cd^{2+}	40	43	100	0.12	0.85	7.9	7.083
	Co^{2+}	30	31	91	2.70	0.56	7.9	0.207
	Cu^{2+}	60	64	100	0.19	1.26	7.9	6.632
	Fe^{2+}	100	100	100	BDL	1.98	7.9	∞
	Mn^{2+}	20	21	72	5.7	0.29	7.9	0.051
+90-106 µm	Cd^{2+}	40	45	98	0.96	0.87	7.6	0.906
	Co^{2+}	30	32	62	12.0	0.39	7.6	0.033
	Cu^{2+}	60	62	100	0.16	1.22	7.6	7.625
	Fe^{2+}	100	107	100	BDL	2.12	7.6	∞
	Mn^{2+}	20	21	44	11.9	0.18	7.6	0.015
+180-212 µm	Cd^{2+}	40	44	82	7.9	0.71	7.1	0.090
	Co^{2+}	30	31	46	16.8	0.29	7.1	0.017
	Cu^{2+}	60	64	100	BDL	1.27	7.1	∞
	Fe^{2+}	100	103	100	BDL	2.05	7.1	∞
	Mn^{2+}	20	21	15	17.8	0.06	7.1	0.003
+355-425 µm	Cd^{2+}	40	44	56	19.1	0.49	6.6	0.026
	Co^{2+}	30	32	21	25.3	0.13	6.6	0.005
	Cu^{2+}	60	64	100	BDL	1.27	6.6	∞
	Fe^{2+}	100	102	100	BDL	2.03	6.6	∞
	Mn^{2+}	20	21	1.4	20.6	0.006	6.6	0.0003

6.2.2.4 Temperature

The effect of temperature on adsorption kinetics and efficiency was investigated at 30, 45, 60 and 75 ^{o}C in STR connected to a water bath for temperature control. The adsorption system consisted of metal ions at initial concentration of 100 mg/L Cd^{2+}, 60 mg/L Co^{2+}, 500 mg/L Cu^{2+}, 800 mg/L Fe^{2+} and 40 mg/L Mn^{2+}. Other solution conditions included pH 3.50, solid/liquid phase ratio of 50 g/L BFS and a size fraction of $d_p < 45$ µm.

Adsorption efficiency improved significantly with increase in temperature within the 30-75 ^{o}C range studied, especially for Mn^{2+} ions. The loading profiles of metal ions are illustrated in Figure 6.13, where complete adsorption for all ions was achieved at the highest temperature. Mn^{2+} ion loaded slowly with increase in temperature compared to other ions in the system. Any diffusional resistances, depressive and competitive effects were probably overcome with increase in temperature. Table 6.9 gives a summary of adsorption performance represented by η (%), Q_e (mg/g) and K_d (L/g). It is possible that the adsorption process is probably an endothermic process. Dimitrova (1996) found an increase in temperature to increase both hydrolysis of slag and adsorption capacity for Cu^{2+}, Ni^{2+} and Zn^{2+} ions with BF slag. Curkovic et al (2001) found Langmuir's adsorption maxima (Q_{max}) and adsorption constant (K_L) values for Pb^{2+} and Cu^{2+} ions adsorption on electric furnace slags to increase with temperature and concluded that the process of adsorption is endothermic, with up to 30.6 mg/g Pb^{2+} and 31.8 mg/g Cu^{2+} at 40 ^{o}C. The cost implication of heating requirement for any adsorption process of this nature may render this innovative process uneconomic.

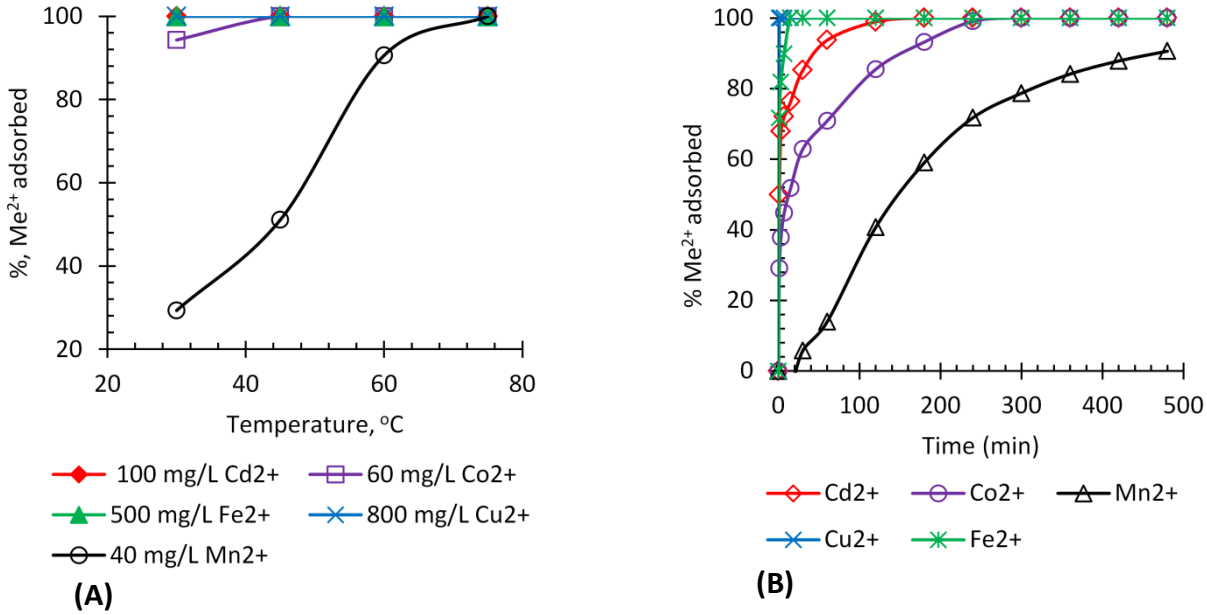

Figure 6.13: Effect of temperature on adsorption efficiency of metal ions in multicomponent systems, 30 g/L BFS powder, (A) η vs temperature; (B) η vs time at 60 °C

Table 6.9: Summary of kinetic parameters as a function of temperature in multicomponent system, 50 g/L BFS granules, STR

Temp., T, °C	Metal Ion	Theoretical Conc, (mg/L)	Actual Conc, (mg/L)	Max Adsorbed (%)	Equil. Conc, (mg/L)	Q_e max mg/g	Equil pH	Distrib. Coeff., K_d (L/g)
30 °C	Cd^{2+}	100	107	100	BDL	2.13	7.5	∞
	Co^{2+}	60	57	94	3.26	1.07	7.5	0.328
	Cu^{2+}	500	528	100	BDL	10.46	7.5	∞
	Fe^{2+}	800	786	100	BDL	15.46	7.5	∞
	Mn^{2+}	40	42	29	30	0.245	7.5	0.008
45 °C	Cd^{2+}	100	106	100	BDL	2.09	7.8	∞
	Co^{2+}	60	61	100	BDL	1.21	7.8	∞
	Cu^{2+}	500	484	100	BDL	9.57	7.8	∞
	Fe^{2+}	800	800	100	BDL	15.84	7.8	∞
	Mn^{2+}	40	43	51	21	0.434	7.8	0.021
60 °C	Cd^{2+}	100	99	100	0.105	1.95	7.8	18.57
	Co^{2+}	60	59	100	0.326	1.17	7.8	3.59
	Cu^{2+}	500	494	100	BDL	9.78	7.8	∞
	Fe^{2+}	800	719	100	BDL	14.24	7.8	∞
	Mn^{2+}	40	37	91	3.49	0.67	7.8	0.19
75 °C	Cd^{2+}	100	111	100	BDL	2.21	7.8	∞
	Co^{2+}	60	62	100	BDL	1.23	7.8	∞
	Cu^{2+}	500	518	100	BDL	10.25	7.8	∞
	Fe^{2+}	800	600	100	BDL	11.88	7.8	∞
	Mn^{2+}	40	45	98	0.876	0.87	7.8	0.99

6.2.2.5 Effect of Solid/Liquid Phase Ratio

The solid/liquid phase ratios employed were 2 g/L, 10 g/L, 30 g/L, 50 g/L and 100 g/L to investigate the effect on adsorption kinetics and efficiency in agitated bottles using powdered BFS in multicomponent solutions with initial concentration at 100 mg/L for each of Cd^{2+}, Co^{2+}, Cu^{2+}, Fe^{2+} and Mn^{2+} ions.

The level of adsorption increased with increase in mass of powdered BFS for all metal ions within 2-100 g/L phase ratios as shown in Figure 6.14(A & B)). A similar trend was obtained using coarse BFS granules (Figure 6.14(C & D)) but overall efficiencies were poor. In general, efficiency and distribution coefficients increased with increase in solids loading (phase ratios), however, adsorption capacity decreased as shown in Table 6.10. Probably total surface area and/or adsorption sites increased with increase in the mass of BFS. However, a limit is expected beyond which mass is under-utilised. There is high affinity and selectivity of BFS towards Fe^{2+} and Cu^{2+} ions as shown previously. The results confirmed the observation that the capacity of BFS to remove metal ions from acidic effluents appears to be selective, limited to certain metal ions and for others only at low concentrations.

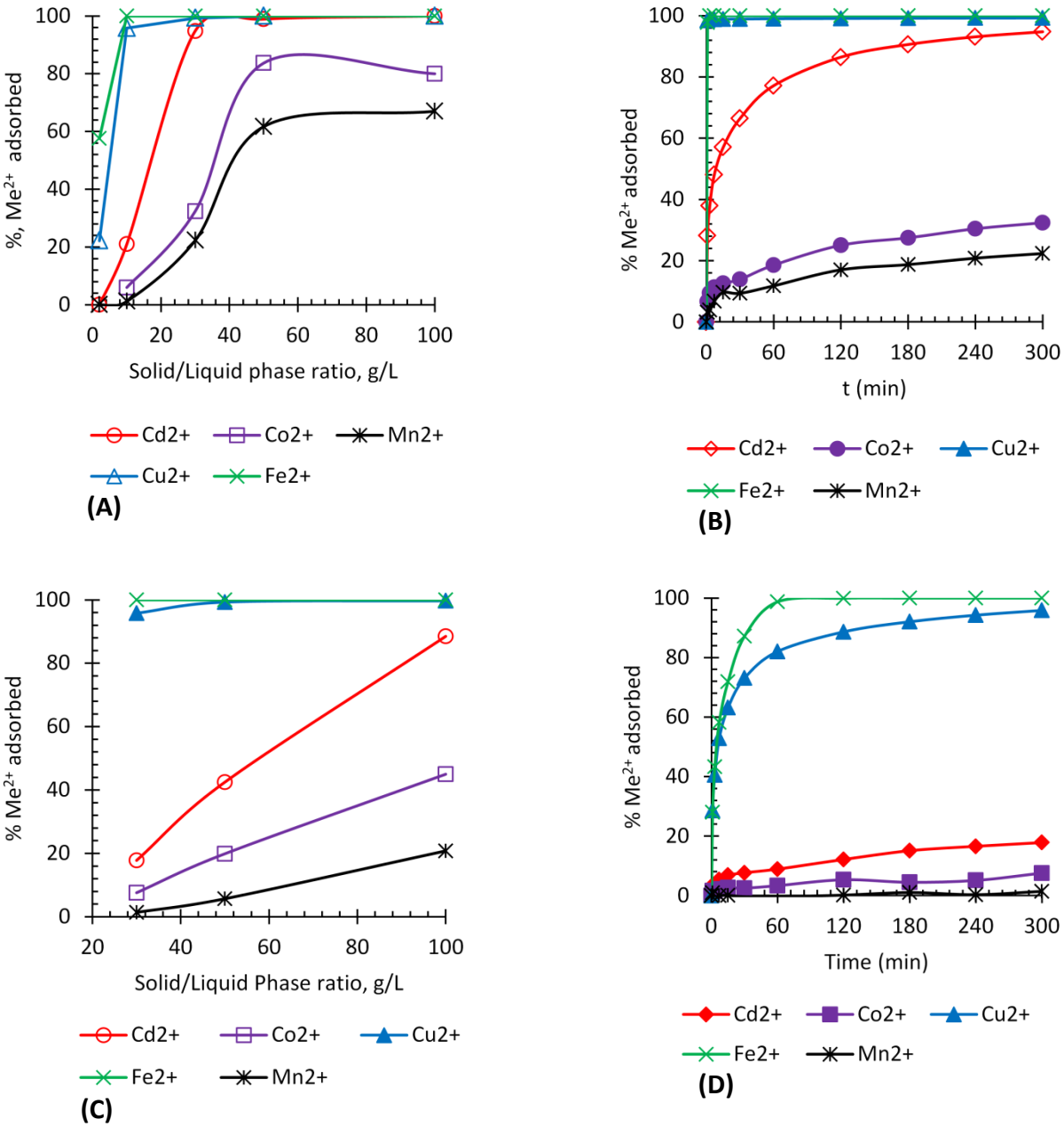

Figure 6.14: Effect of solid/phase ratios on adsorption efficiency of metal ions in multicomponent systems, (A) & (B) BFS powder; (C) & (D) Efficiency vs time at 30 g/L BFS granules

Table 6.10: Summary of kinetic parameters as a function of solid/liquid phase ratio (mass) of BFS in multicomponent solutions using STR

Solid/Liquid Phase ratio g/L BFS	d_p	Metal Ion	Theoretical Conc, (mg/L)	Actual Conc, (mg/L)	Max Adsorbed (%)	Equil. Conc, C_e (mg/L)	Q_e max mg/g	Equil pH	Distrib. Coeff., K_d (L/g)
2 g/L BFS	d_p<45 µm	Cd^{2+}	100	102	0	102	0	5.1	0
		Co^{2+}	100	97	-	-	-	5.1	-
		Cu^{2+}	100	105	22	82	5.62	5.1	0.069
		Fe^{2+}	100	111	58	46.9	15.28	5.1	0.329
		Mn^{2+}	100	106	0	106	0	5.1	0
10 g/L BFS	d_p<45 µm	Cd^{2+}	100	102	21	80.3	1.03	6.3	0.013
		Co^{2+}	100	103	6	96.7	0.30	6.3	0.003
		Cu^{2+}	100	104	96	4.33	4.77	6.3	1.102
		Fe^{2+}	100	111	100	BDL	5.35	6.3	∞
		Mn^{2+}	100	108	1	106.9	0.06	6.3	0.001
30 g/L BFS	d_p<45 µm	Cd^{2+}	100	106	95	5.6	1.61	7.3	0.288
		Co^{2+}	100	105	32	71	0.54	7.3	0.008
		Cu^{2+}	100	105	99	0.78	1.67	7.3	2.141
		Fe^{2+}	100	111	100	BDL	1.77	7.3	∞
		Mn^{2+}	100	107	22	83.4	0.38	7.3	0.005
	+0.18-0.36 mm	Cd^{2+}	100	102	18	83.7	0.30	6.4	0.004
		Co^{2+}	100	102	8	94.6	0.13	6.4	0.001
		Cu^{2+}	100	102	96	4.23	1.63	6.4	0.385
		Fe^{2+}	100	100	100	0.01	1.67	6.4	167
		Mn^{2+}	100	106	1	104	0.03	6.4	0.0002
50 g/L BFS	dp<45 µm	Cd^{2+}	100	104	99	1.19	0.98	8.2	0.824
		Co^{2+}	100	105	84	17.1	0.84	8.2	0.049
		Cu^{2+}	100	104	100	0.03	1.00	8.2	33.3
		Fe^{2+}	100	98	100	BDL	0.94	8.2	∞
		Mn^{2+}	100	104	62	39.8	0.62	8.2	0.016
	+0.18-0.36 mm	Cd^{2+}	100	103	42	59.1	0.43	6.8	0.007
		Co^{2+}	100	101	20	81	0.20	6.8	0.002
		Cu^{2+}	100	101	99	0.70	1.01	6.8	1.443
		Fe^{2+}	100	100	100	0.03	1.00	6.8	33.3
		Mn^{2+}	100	104	5.7	98.0	0.06	6.8	0.0006
100 g/L BFS	d_p<45 µm	Cd^{2+}	100	112	100	0.31	0.54	7.8	1.742
		Co^{2+}	100	109	80	21.7	0.42	7.8	0.019
		Cu^{2+}	100	107	100	0.30	0.51	7.8	1.700
		Fe^{2+}	100	111	100	BDL	0.53	7.8	∞
		Mn^{2+}	100	108	67	35.6	0.35	7.8	0.010
	+0.18-0.36 mm	Cd^{2+}	100	103	89	11.9	0.46	7.3	0.039
		Co^{2+}	100	107	45	59.1	0.24	7.3	0.004
		Cu^{2+}	100	105	100	0.36	0.52	7.3	1.444
		Fe^{2+}	100	101	100	BDL	0.51	7.3	∞
		Mn^{2+}	100	105	21	83.5	0.11	7.3	0.001

6.2.2.6 Rate of Agitation

The agitation rates employed were 400, 600 and 1000 rpm to investigate the effect on adsorption kinetics and efficiency in STR using powdered BFS (d_p < 45 µm) in multicomponent solutions with initial concentration at 100 mg/L Cd^{2+}, 60 mg/L Co^{2+}, 500 mg/L Cu^{2+}, 800 mg/L Fe^{2+} and 40 mg/L Mn^{2+} ions. The lower rates of agitation (< 400 rpm) were not studied because solids had settled out at the bottom of the adsorption vessel.

Figure 15 illustrates the fact that an increase in the rate of agitation had no significant effect on the extent of adsorption under the experimental conditions employed. The application of a fine size fraction of adsorbent (d_p < 45 µm) might have eliminated the resistive effects of film diffusion. Lui et al (2010) studied the kinetics of Pb^{2+} ion adsorption by coarse particle size fraction of steel slag. The efficiency of Pb^{2+} ion adsorption increased with increase in agitation rate up to a certain limit, beyond which efficiency was constant. This increased the diffusion coefficient of Pb^{2+} ions, thereby increasing the mass transfer flux. External diffusion was identified as rate controlling step that limited the rate of adsorption. At higher rates of agitation, resistance to bulk liquid diffusion was eliminated.

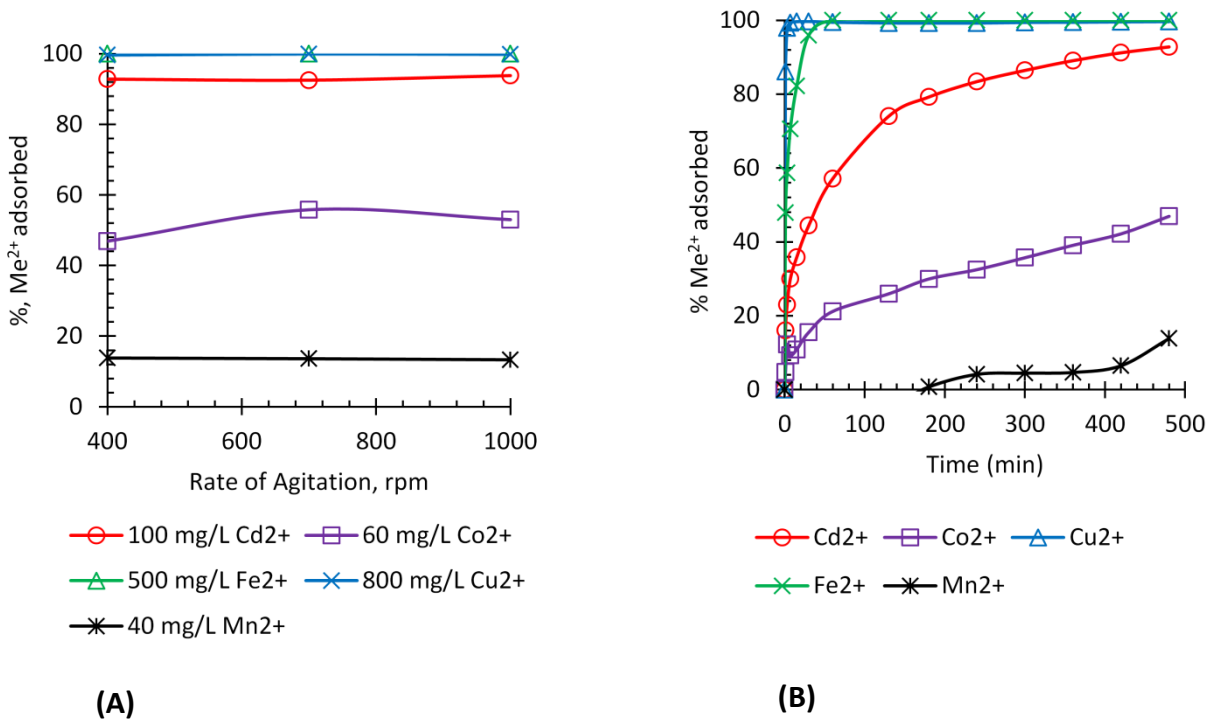

(A) **(B)**

Figure 6.15: Effect of agitation rate on adsorption efficiency of metal ions in multicomponent systems with BFS powder, 50 g/L, (A) η vs rate of agitation; (B) η vs time at 400 rpm

6.3.3 Pretreatment of Adsorbent Materials

The effect of both leaching and heating of BFS material on adsorption kinetics and efficiency of metal ions is presented and discussed in this section. The changes in adsorptive properties were analysed in Chapter 4.

6.3.3.1 Chemical Process

The effect of chemical activation of BFS by leaching with HCl on its adsorptive performance was conducted in a STR with a particle size of +180-360 µm. McCauley (2001) leached BFS and found specific surface area to increase. However, this study extended McCauley (2001)'s work by giving an analysis of the changes in the pore structure and pore size distribution in addition to specific surface area. The leach residue material was employed as

an adsorbent at 30 g/L solid/liquid phase ratio in agitated bottles in a multicomponent solutions of Cd^{2+}, Co^{2+}, Cu^{2+}, Fe^{2+} and Mn^{2+} ions at 100 mg/L for each ion.

The extent of adsorption before and after leaching of BFS adsorbent material is shown in Figure 6.16 and a summary of key figures are given in Table 6.11. Despite the fact that complete adsorption was not achieved, there was a significant increase of several magnitudes in adsorbed amounts after leaching for Cd^{2+}, Co^{2+} and Mn^{2+} ions. This is expected because values of BET surface area, total pore area and pore volume of BFS more than doubled after leaching and thus supported larger amounts of ions to be adsorbed (Chapter 4). There is potential for the leaching process to be optimised to improve both adsorptive properties and performance. The challenge of H_2S emissions from BFS leaching must be addressed.

However, the quantities of Cu^{2+} and Fe^{2+} ions adsorbed as well as equilibrium pH decreased after leaching. XRF data showed that part of lime (CaO) in BFS, which controls solution pH, was leached out. Subsequently, the adsorption system attained low equilibrium pH (4.9), below values for complete precipitation of Cu^{2+} and Fe^{2+} ions, when compared to pH attained by unleached BFS which had higher pH and adsorption efficiency (100 %) for these ions. This suggests that precipitation process may be significant for the removal of these ions. The adsorption preference of Cu^{2+}>Fe^{2+}>Cd^{2+}>Co^{2+}>Mn^{2+} obtained using leached BFS sets Cu^{2+} as first ion rather than Fe^{2+} observed in many cases.

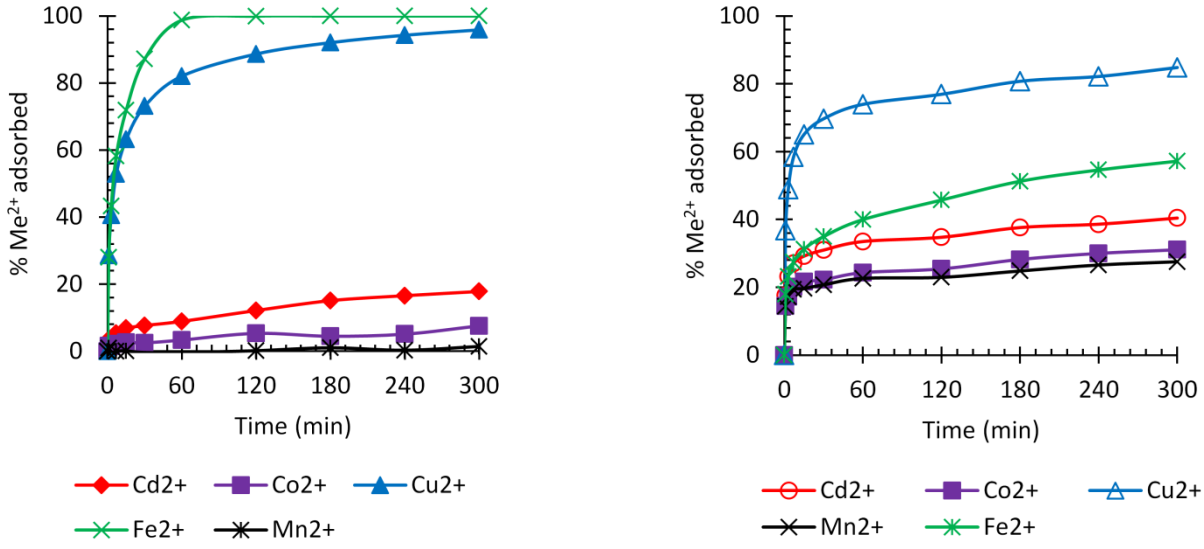

Figure 6.16: Effect of leaching of BFS on adsorption efficiency of metal ions in multicomponent systems with leached BFS granules at 30 g/L , (A) Before leaching; (B) After leaching

Table 6.11: Summary of kinetic parameters in multicomponent solutions with leached BFS

Effect of leaching	d_p	Metal Ion	Theoretical Conc, (mg/L)	Actual Conc, (mg/L)	Max Adsorbed (%)	Equil. Conc, C_e (mg/L)	Q_e max mg/g	Equil pH	Distrib. Coeff., K_d (L/g)
Before leaching BFS	0.18-0.36 mm	Cd^{2+}	100	102	18	83.7	0.30	6.4	0.004
		Co^{2+}	100	102	8	94.6	0.13	6.4	0.001
		Cu^{2+}	100	102	96	4.23	1.63	6.4	0.385
		Fe^{2+}	100	100	100	0.01	1.67	6.4	167
		Mn^{2+}	100	106	1	104	0.03	6.4	0.0002
After Leaching BFS	0.18-0.36 mm	Cd^{2+}	100	103	40	61.6	0.70	4.9	0.011
		Co^{2+}	100	103	31	71.1	0.53	4.9	0.007
		Cu^{2+}	100	102	85	15.4	1.44	4.9	0.094
		Fe^{2+}	100	105	57	44.9	1.00	4.9	0.022
		Mn^{2+}	100	102	28	74.2	0.47	4.9	0.006

6.3.3.2 Thermal Process

Thermal activation of BFS by a heating process at 200, 400, 600 and 800 ^{o}C values was conducted with a particle size of +180-360 µm. The heat pretreated materials were

employed as adsorbents at 30 g/L solid/liquid phase ratio in STR in multicomponents systems at 40 mg/L Cd^{2+}, 30 mg/L Co^{2+}, 250 mg/L Cu^{2+}, 400 mg/L Fe^{2+} and 20 mg/L Mn^{2+} ions. The heat treatment of BFS has been investigated by Dimitrova et al (2001) and Mihailova et al (2013) who reported that amorphous BFS transformed into crystalline structure and increased adsorption of metal ions. The aim here is to examine the changes in a wide range of BFS characteristics and its subsequent performance in adsorption systems.

It was hypothesised that a preheating process increases the adsorption capacity and efficiency of BFS by transforming it into a crystalline structure and increasing its surface area. The adsorption results obtained before and after preheating BFS adsorbent material between 200-800 ^{o}C are given in Figure 6.17 and summarised in Table 6.12. Although efficiency of adsorption for all metal ions is generally low, the quantities of Cd^{2+}, Cu^{2+} and Fe^{2+} ions decreased with increase in preheating temperature of BFS. There is negligible or no adsorption of Co^{2+} and Mn^{2+} ions under these conditions. In BET analysis of Chapter 4 in this study, it was established that there is a significant decrease in BET surface area and total pore area as preheating temperature was increased, which is presented again in Figure 6.17(C) below. The SEM image (Fig. 6.17(D)) also revealed that pretreatment by thermal process destroyed the structure of BFS material, as grain boundaries were distorted and surface pores reduced possibly by a sintering process of the material as temperature was increased.

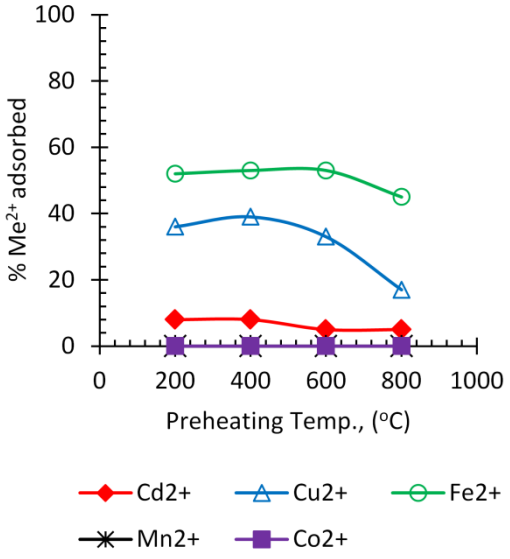

(A)

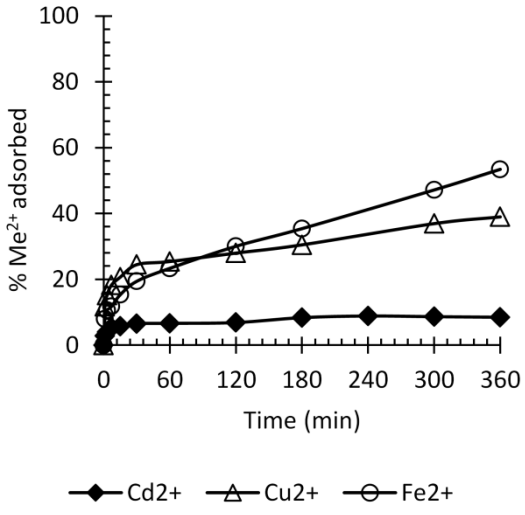

(B)

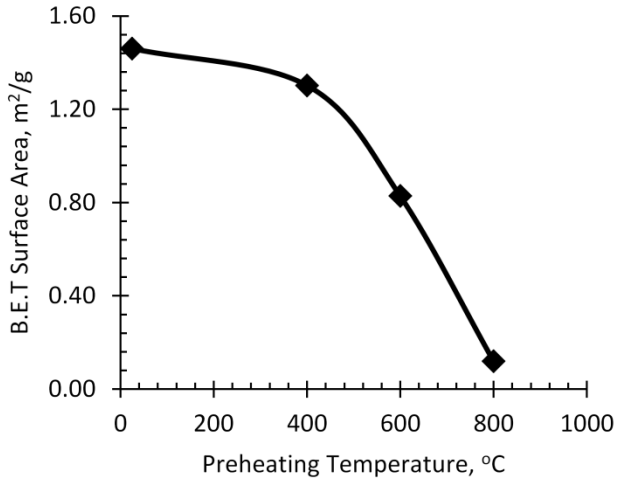

(C)

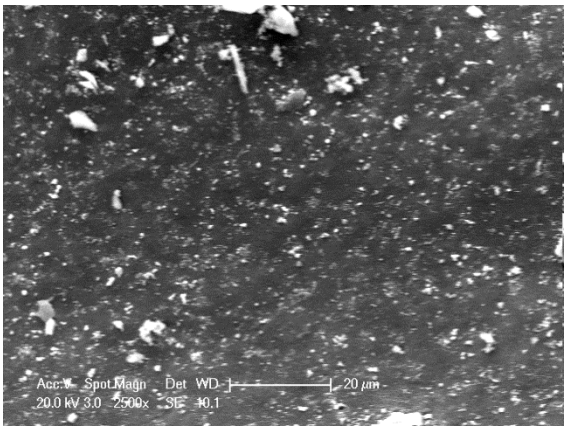

(D)

Figure 6.17: Effect of preheating of BFS on adsorption efficiency of metal ions in multicomponent systems with BFS granules at 30 g/L, (A) η vs preheating temp.; (B) η vs time at 400 °C, (C) BET surface area vs preheating temp., & (D) SEM image of BFS preheated at 800 °C

Table 6.12: Summary of kinetic parameters in multicomponent adsorption systems as a function of preheating temperature for BFS adsorbent material

Temp., T, ^{o}C	Metal Ion	Theoretical Conc, (mg/L)	Actual Conc, (mg/L)	Max Adsorbed (%)	Equil. Conc, (mg/L)	Q_e max mg/g	Equil pH	Distrib. Coeff., K_d (L/g)
200 ^{o}C	Cd^{2+}	40	39.6	8	36.3	0.11	4.9	0.003
	Co^{2+}	30	29.1	0	31.7	0	4.9	0
	Cu^{2+}	250	274.6	36	174.4	3.27	4.9	0.019
	Fe^{2+}	400	420.8	52	203.5	7.10	4.9	0.035
	Mn^{2+}	20	19.7	0	21.2	0	4.9	0
400 ^{o}C	Cd^{2+}	40	41.4	8	37.9	0.11	4.9	0.003
	Co^{2+}	30	32.1	0	32.2	0	4.9	0
	Cu^{2+}	250	262.9	39	160.5	3.35	4.9	0.021
	Fe^{2+}	400	394.3	53	183.8	6.88	4.9	0.037
	Mn^{2+}	20	20.9	0	20.9	0	4.9	0
600 ^{o}C	Cd^{2+}	40	40.8	5	38.9	0.06	4.8	0.002
	Co^{2+}	30	30.9	0	30.7	0	4.8	0
	Cu^{2+}	250	267.6	33	178.6	2.91	4.8	0.016
	Fe^{2+}	400	424.1	53	199.3	7.34	4.8	0.037
	Mn^{2+}	20	20.7	0	20.7	0	4.8	0
800 ^{o}C	Cd^{2+}	40	40.6	5	38.6	0.06	4.7	0.002
	Co^{2+}	30	29.8	0	29.5	0	4.7	0
	Cu^{2+}	250	257	17	212.1	1.47	4.7	0.007
	Fe^{2+}	400	410.2	45	226.4	6.01	4.7	0.027
	Mn^{2+}	20	20.9	0	20.4	0	4.7	0

6.3.4 Kinetic Modeling of Adsorption Systems

The rate of solute adsorption may be controlled by any of the following subprocess steps; (1) external (or film) diffusion across liquid film surrounding adsorbent particles, (2) intra particle (or internal or pore) diffusion in the internal pore sites or walls of adsorbent particles and (3) actual adsorption step which may involve one or several mechanisms, e.g., physisorption, chemisorption, ion exchange, precipitation, complexation etc. (Qiu et al., 2009). The overall rate of kinetic process is then determined by the rate of the slowest sub-process step (Dabrowski, 2001; Inglezakis & Poulopoulos, 2006b; Qiu et al., 2009).

Several kinetic models are frequently used to analyse the kinetics of an adsorption process. According to El-Khaiary et al (2010) mechanistic models give detailed analysis of adsorption dynamics but require extensive computations to solve and may be difficult to apply in practice. Lumped kinetic models are also widely used to analyse mechanisms of adsorption (Boyd et al., 1947; Weber Jr and Morris, 1963). El-Khaiary et al (2010) argues that these models are simple and preferable in industrial simulations and to analyse research data but have their own limitations. Pseudo kinetic models are useful to simulate overall rates of adsorption (Ho, 1995; Ho, 2006; Ho and McKay, 1999). However, Qui et al (2009) argues that they may not be useful in understanding adsorption mechanisms or in design of fixed bed systems compared to diffusion models. The choice of models thus must strike a balance between accuracy and simplicity. Ortiz et al (2001), Kim et al (2008), Liu et al (2010) and others have successfully applied linear forms of pseudo first order, pseudo second order and intraparticle diffusion models to analyse kinetics of adsorption of metal ions by slag materials. It was shown that pseudo second order model was more satisfactory to describe kinetic aspects of adsorption data. According to Ho (2006) this model is frequently and widely used due to its simplicity and good linear fits of data observed in modeling of numerous adsorption systems. However, El-Khaiary (2010) found that a non-linear regression approach provides the most accurate estimates of the kinetic parameters.

In this Section, the adsorption rates and mechanisms of Cd^{2+}, Co^{2+}, Cu^{2+}, Fe^{2+} and Mn^{2+} ions in multiadsorbate systems were analysed by fitting experimental adsorption data to the relevant kinetic models as a function of adsorbent particle size and mass using BFS as adsorbent. However, the common linear regression analysis technique in which nonlinear

data is transformed into linear forms is considered not accurate and outdated (Brown, 2001; El-Khaiary et al., 2010; El-Khaiary and Malash, 2011). Thus, iterative nonlinear least squares fitting approach was used in this study to obtain more accurate estimates of model parameters. The study applied models based on chemical adsorption or chemisorption theory of adsorption (Pseudo first order (PFO), Pseudo second order (PSO) & Elovich models) and those based on diffusion theory, that is, double exponential model (DEM), Boyd's diffusion and Weber-Morris Intraparticle diffusion models (Inglezakis & Poulopoulos, 2006a) to establish the fundamental adsorption theory most applicable to describe the experimental data. The chemical adsorption models were fitted to data by a nonlinear least squares fitting approach using Microsoft Excel Solver (2010) in order to analyse the rate limiting steps, estimate kinetic parameters and infer the mechanisms of metal adsorption. The "goodness" of fit were assessed by comparing values of regression coefficient (R^2), residual plots, standard errors (SE) and sum of squared errors (SSE) given by equations (6.4) to (6.6) (Brown, 2001; Motulsky and Ransnas, 1987). However, the commonly used linear regression analysis was applied in the Weber-Morris intraparticle and Boyd's diffusion models.

$$S.E. = \sqrt{\frac{\sum \left(q - q_{fit}\right)^2}{df}} \quad ---(6.4)$$

$$R^2 = 1 - \frac{\sum \left(q - q_{fit}\right)^2}{\sum \left(q - q_{mean}\right)^2} \quad ---(6.5)$$

$$S.S.E = \sum \left(q - q_{fit}\right)^2 \quad ---(6.6)$$

Where q and q_{fit} are the measured and calculated (predicted) amounts of adsorbed metal ions on the adsorbent respectively, q_{mean} is the average of the q values, df is the degrees of freedom.

A brief description of the kinetic models is given below and the fitted graphs, and estimated parameters and statistical values for each metal ion are shown in Figure 6.18 and Table 6.13 respectively.

6.3.4.1 Chemical Adsorption Models

The kinetic models based on adsorption capacity were fitted to experimental data to determine rates of adsorption for metal ions and whether chemical adsorption or chemisorption was the rate determining step. The pseudo kinetic models employed in this study are based on adsorption capacity of solid adsorbent and this differentiates them from conventional chemical kinetics based on concentration. The application of these models has been presented in many articles in the literature. Chemisorption involves electronic bonding between surface sites of adsorbents and adsorbates to form strong, stable chemical bonds than in physisorption where no chemical bonding occurs and nature of adsorption is often reversible. Also, chemisorption is limited to one monolayer surface coverage compared to physisorption where a fast, multilayer solute adsorption is achievable (Inglezakis & Poulopoulos, 2006b).

6.3.4.1.1 Pseudo First Order Model

The pseudo first order (PFO) rate equation by Lagergren (1898) as cited by Ho and McKay (1998) is among the earliest kinetic models which is widely used in solid/liquid adsorption systems. PFO model is defined as

$$\frac{dq_t}{dt} = k_1\left(q_e - q_t\right) \qquad \text{---} \qquad (6.7a)$$

Equation (6.7a) is integrated from t = 0 to t = 0 and q_t = 0 to q_t = q_t and expressed as;

$$q_t = q_e\left(1 - e^{-kt}\right) \qquad \text{---} \qquad (6.7b)$$

Where q_t and q_e are the amounts of metal ions adsorbed per unit weight of adsorbent (mg/g) at time t (min) and at equilibrium respectively, k_1 = first order adsorption constant (mg/g min). A nonlinear plot involves q_t vs time (t) of the integrated equation (6.7b).

6.3.4.1.2 Pseudo Second Order Model

The modified second order rate equation which Ho (2005) called pseudo second order (PSO) has been found to be extremely useful and applicable in analysis of kinetics in many adsorption systems. Metal ions are believed to chemically bond with various functional groups on peat surface through ion-exchange process (Ho, 2006; Ho and Mckay, 1998; Ho and Mckay, 1999; Qiu et al., 2009). This study applied pseudo second order kinetic model to analyse the experimental data and establish underlying adsorption mechanisms. It is given by the differential equation as;

$$\frac{dq_t}{dt} = k_2\left(q_e - q_t\right)^2 \qquad \text{---} \qquad (6.8a)$$

Where q_t and q_e are the amounts of metal ions adsorbed per unit weight of adsorbent (mg/g) at any time t (min) and at equilibrium respectively, k_2 is second order adsorption constant (mg/g min). Integrating equation (6.8a) between t = 0 to t = t and q_t = 0 to q_t = q_t gives;

$$q_t = \frac{q_e^2 kt}{1 + q_e kt} \qquad \text{---} \qquad (6.8b)$$

A nonlinear plot involves q_t vs time (t) of the integrated equation 6.8b, thus parameters (q_e), (k) and (h) can be estimated. $h = kq^2_e$ = initial adsorption rate (mg/g min) as t goes to zero.

6.3.4.1.3 Elovich's Model

This is another kinetic equation based on the theory of chemisorption that relates adsorption capacity, rather than concentration, with time. It has long been applied to analyse adsorption kinetics in gas/solid systems. More recently, the applications have been extended to solid/liquid systems for pollution control mostly with organic adsorbents (Ho, 2006). The differential form of the model is given by Equation (6.9a). The integrated (t = 0 to t = 0 and q_t = 0 to q_t = q_t) and linearized form is shown by Equation (6.9b).

$$\frac{dq_t}{dt} = a\, e^{-\alpha q_t} \qquad \text{---} \qquad (6.9a)$$

$$q_t = \left(\frac{2.3}{\alpha}\right)\log\left(t + t_o\right) - \left(\frac{2.3}{\alpha}\right)\log t_o \qquad \text{---} \qquad (6.9b)$$

The simplifications of Equation (6.9b) as discussed by Ho and McKay (1998) assume that the term ($a\alpha t$) >> 1 to give equation (6.9c);

$$q_t = \alpha\ln(a\alpha) + \alpha\ln(t) \qquad \text{---} \qquad (6.9c)$$

Where (a) = desorption constant (g/mg), α = initial adsorption rate (mg/g min), $t_o = 1/(\alpha a)$, q_t is the amount of metal ions adsorbed per unit weight of adsorbent (mg/g) at any time t (min). A nonlinear plot of q_t vs (t) gives a curve from which the parameters are obtained.

6.3.4.2 Film and Pore Diffusion Models

It is known that rate of solute adsorption in solid/liquid systems may be controlled by film (external) diffusion and/or intraparticle (pore/internal) diffusion steps. Thus, several diffusion models have been proposed to identify these rate controlling steps (Qiu et al., 2009). The diffusion models applied in this work are presented below.

6.3.4.2.1 Weber-Morris Intraparticle Diffusion Model

The rate expression for adsorption process that may be limited by intraparticle (internal) diffusion was presented by Weber and Morris (1963) and given in Equation 6.10 (Qiu et al., 2009). A plot of q_t vs. $t^{1/2}$ should be linear if intra particle diffusion is the rate determining step (RDS) of the process. Where the line intercept is not zero, the process could be accompanied by film diffusion.

$$q_t = k_i \sqrt{t} \qquad \text{---} \qquad (6.10)$$

Where q_t is the amount of metal ions adsorbed per unit weight of adsorbent (mg/g) at any time t (min), k_i = intra particle diffusion rate constant (mg/g $min^{-1/2}$), t = time.

6.3.4.2.2 Boyd's Diffusion Model

The diffusion model by Boyd et al (1947) was originally based on intraparticle diffusion and its now termed Boyd's film diffusion model (Eq. 6.11). The authors proposed rate of solute adsorption could be limited by diffusion through a film or boundary layer that surrounds adsorbent particles.

$$F(t) = 1 - \left(\frac{6}{\pi^2}\right)\sum_{n=1}^{\infty}\left(\frac{1}{n^2}\right)e^{-n^2Bt} \quad \text{----} \quad \text{(6.11a)} \qquad F(t) = \left(\frac{q_t}{q_e}\right) \quad \text{----} \quad \text{(6.11b)}$$

Where q_t and q_e are the amounts of metal ions adsorbed per unit weight of adsorbent (mg/g) at any time t (min) and at equilibrium respectively. As discussed by Malash et al (2010), the solution to Equation (6.11a) was approximated by integration using Fourier transforms to obtain the following sets of equations;

$$F(t) > 0.85; \quad Bt = 0.477 - ln(1 - F(t)) \quad \text{---} \quad \text{(6.11c)}$$

$$F(t) < 0.85; \quad Bt = \left(\sqrt{\pi} - \sqrt{\pi - \left(\frac{\pi^2 F(t)}{3}\right)}\right)^2 \quad \text{---} \quad \text{(6.11d)}$$

$$B = \frac{\pi^2 D_i}{r^2} \quad \text{---} \quad \text{(6.11e)}$$

Where D_i = effective diffusion coefficient, cm^2/s, r = radius of (spherical) adsorbent particles, B = rate coefficient and Bt is a function of F(t), fractional approach to equilibrium.

Thus, if the plot of Bt vs time is linear through the origin, intraparticle diffusion may be rate limiting. However, if the graph is either not linear or linear but does not pass through the origin, film diffusion or chemisorption are probably rate limiting steps.

6.3.4.2.3 Double Exponential Diffusion Model

Wilczak and Keinath (1993) proposed the double exponential model (DEM) that described adsorption kinetics of metal ions by active carbon through a two-step mechanism. The sub processes involve an initially rapid adsorption phase that involves both film and intraparticle diffusion followed by a slower phase that becomes limited by intraparticle diffusion (Eq. 6.12).

$$q_t = q_e - \frac{D_1}{m} e^{-k_1 t} - \frac{D_2}{m} e^{-k_2 t} \qquad \text{---} \quad (6.12a)$$

Where D_1 and D_2 are adsorption rate constants (mg/L) of the rapid and the slow steps respectively, K_1 and K_2 are diffusion constant (min^{-1}).

If $K_1 >> K_2$, the initial rapid adsorption step can be neglected, and simplified equation (6.12) becomes;

$$q_t = q_e - \frac{D_2}{m} e^{-K_2 t} \quad or \quad ln(q_e - q_t) = ln\left(\frac{D_2}{m}\right) - K_2 t \qquad \text{---} \quad (6.12b)$$

A plot of $\ln(q_e - q_t)$ against time can be done where D_2 and K_2 are deduced. K_1 and D_1 are then obtained by appropriate substitutions. According to Qiu et al (2009) K_1 and K_2 are insufficient to conclusively interpret the influence of film and intraparticle diffusion but can rather be used to compare individual adsorption rates between metal ions. DEM model applies where the adsorbent has one set of adsorption sites that support rapid adsorption and another set supports a slow approach to equilibrium.

6.3.4.3 Application of Kinetic Models to Single Solutes

The kinetic models were fitted to the experimental data of single adsorption systems by nonlinear regression approach using MS Excel Solver in order to analyse the rate limiting steps, estimate kinetic parameters and infer the mechanisms of metal adsorption as a function of particle size of adsorbent. The results of model fitting are shown in Figure 6.18 and Table 6.13 at specific experimental conditions of 0.18-0.36 mm adsorbent size fraction. Specific observations for each metal ion are discussed below.

Cd^{2+} Ions

For adsorbent size of 0.18-0.36 mm, R^2 values for PFO and PSO (0.96-0.99) given in Table 6.13 are indicative of satisfactory data fits, however, it cannot be concluded with certainty which model is better. The Elovich model may be inappropriate to describe the data on account of lowest R^2 value. Compared to PFO model, both PSO and DEM have the lowest SSE and SE values to suggest that these models give best fits. Further PSO gave better (closest) approximation of adsorption capacity at equilibrium relative to the experimental value. It must be noted that PSO and DEM are based on different theories and physical significance and do not have same number of parameters for any direct comparison to be made. Also, the residual errors in PSO and DEM are much lower in magnitude and more randomly distributed compared to those of PFO and Elovich models that seem to show a systematic (parabolic) pattern. This is further piece of evidence that PFO and Elovich models do not adequately describe the data.

The Cd^{2+} ion adsorption data depicted a gently rising kinetic trend with coarser size fractions of adsorbent. PFO model also fitted poorly with coarser fractions based on relatively large

SSE and systematic error pattern. However, R^2 and SSE in Elovich model were satisfactory but residual errors again appear to be systematic. At coarse size fractions, however, DEM and PSO were again superior. Because $K_1 >> K_2$ from DEM, external diffusion limitation attributed to initial stage can be neglected. Further, initial adsorption rate (h) based on PSO increased 1.5 to 2.5 times as size fraction of adsorbent was decreased by roughly half. Thus, within certain assumptions it is possible that mainly pore diffusion and partly chemisorption step may limit Cd^{2+} overall adsorption kinetics.

Co^{2+} and Mn^{2+} Ions

With reference to Figure 6.18 and Table 6.13, PFO and Elovich models do not satisfactorily support chemical adsorption step to be rate limiting for both Co^{2+} and Mn^{2+} data which have similar adsorption profiles. It must be noted that a very slow approach to equilibrium means that practically true equilibrium might not have been achieved. The overall adsorption process may be mainly diffusion limited as shown by DEM parameters, which then slows down chemisorption, another possible rate limiting step supported to some extent by PSO especially for Mn^{2+} data.

Similar adsorption kinetic profiles were observed when coarser size fractions of adsorbent were employed. The initial adsorption rates (h) based on PSO increased by factors of up to 3.0 for Mn^{2+} and 1.8 for Co^{2+} as size fractions were decreased by about half. Mn^{2+} and Co^{2+} exhibited lowest adsorption loading efficiencies which may be attributed in part to highly limited diffusivities for these ions.

Fe^{2+} and Cu^{2+} Ions

Here Fe^{2+} adsorption was rapid and completed within about 15 minutes. With the exception of the Elovich model that fitted poorly (Fig. 6.18 and Table 6.13), PFO, PSO and DEM models support chemisorption and diffusion steps to be involved within that short period of time for all three adsorbent size fractions. A distinction cannot be made to ascertain the dominant step. Also, PSO gave a close prediction of maximum adsorption capacity at equilibrium to the experimental value. Overall adsorption kinetics of Cu^{2+} appears to be limited by diffusion as supported by DEM parameters in Figure 6.18. From PSO parameters, there is likelihood of chemisorption also contributing to the limitation of Cu^{2+} loading onto BFS surfaces. With coarser sizes, however, rate of Cu^{2+} adsorption is mainly limited by pore diffusion based on DEM model, and not chemically limited on the basis of poor fits of PSO and other chemisorption models to data.

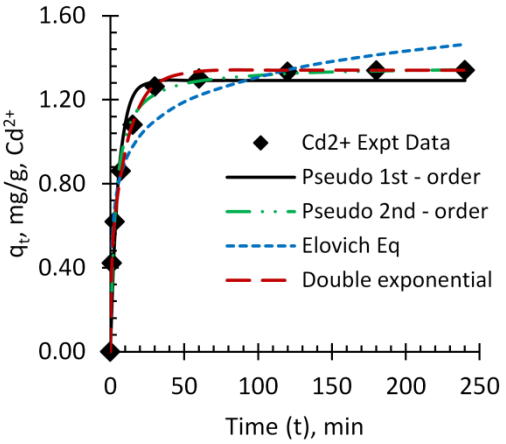

(A) Cd^{2+}

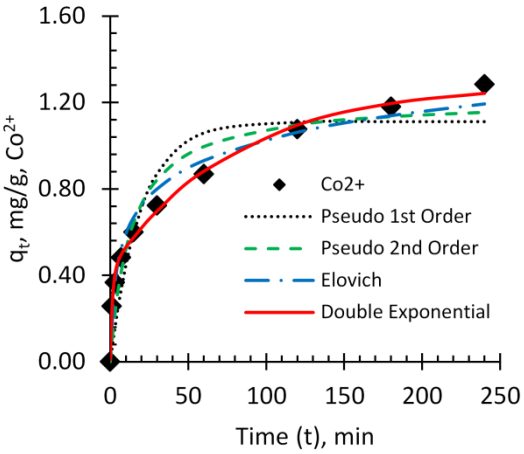

(B) Co^{2+}

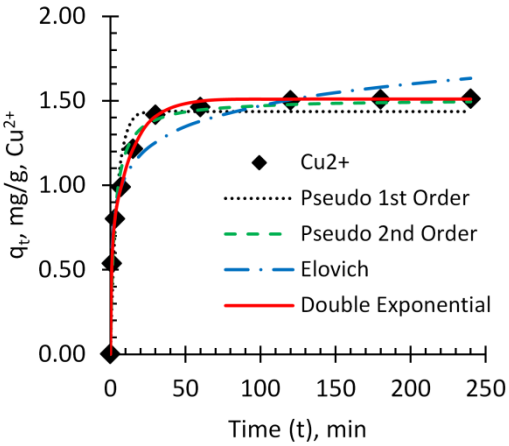

(C) Cu^{2+}

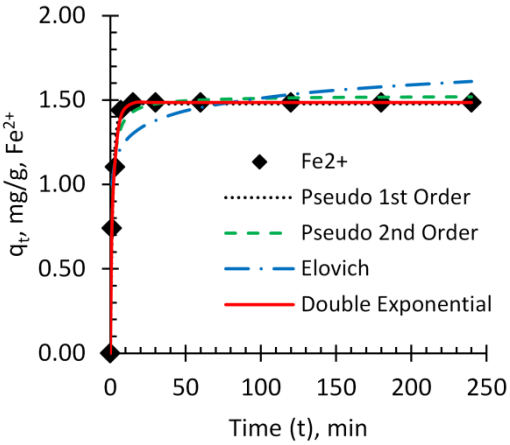

(D) Fe^{2+}

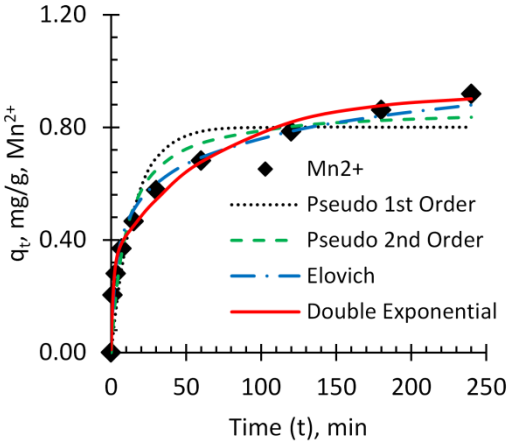

(E) Mn^{2+}

Figure 6.18: Figure 6.16: Nonlinear model fits to single component adsorption data of metal ions [(A)-(E)] with BFS granules at 30 g/L

Table 6.13: Table 6.13: Estimated kinetic model parameters in single adsorbates, 30 g/L BFS granules

Metal ion	Variable	Kinetic Models				
	Particle size	Experimental	Pseudo 1st Order	Pseudo 2nd Order	Elovich	Double Exponential
Cd^{2+}	0.18<dp<0.36 (mm) C_i =83.83 mg/L pH_{eq} = 8.9	$Q_{e,\ max}$ (mg/g) = 1.341 C_e (mg/L) = 0.04 %η = 100	K_1 = 0.187 Q_e = 1.291 R^2 = 0.962 SE = 0.097 SSE = 0.076	K_2 = 0.218 Q_e = 1.362 h = 0.405 R^2 = 0.991 SE = 0.048 SSE = 0.019	α = 5.693 a = 3.049 R^2 = 0.920 SE = 0.105 SSE = 0.077	D_1 = 12.955 K_1 = 1.609 D_2 = 27.255 K_2 = 0.085 R^2 = 0.999 SE = 0.018 SSE = 0.002
Co^{2+}	0.18<dp<0.36 (mm) C_i = 92.70 mg/L pH_{eq} = 8.2	$Q_{e,\ max}$ (mg/g) = 1.284 C_e (mg/L) = 12.45 %η = 87	K_1 = 0.051 Q_e = 1.111 R^2 = 0.874 SE = 0.158 SSE = 0.201	K_2 = 0.061 Q_e = 1.219 h = 0.091 R^2 = 0.933 SE = 0.115 SSE = 0.106	α = 5.284 a = 0.432 R^2 = 0.966 SE = 0.072 SSE = 0.037	D_1 = 12.500 K_1 = 0.677 D_2 = 25.708 K_2 = 0.013 R^2 = 0.961 SE = 0.102 SSE = 0.006
Cu^{2+}	0.18<dp<0.36 (mm) C_i =94.68 mg/L pH_{eq} = 8.1	$Q_{e,\ max}$ (mg/g) = 1.510 C_e (mg/L) = 0.29 %η = 100	K_1 = 0.231 Q_e = 1.436 R^2 = 0.942 SE = 0.131 SSE = 0.138	K_2 = 0.246 Q_e = 1.511 h = 0.562 R^2 = 0.986 SE = 0.065 SSE = 0.033	α = 5.473 a = 5.801 R^2 = 0.931 SE = 0.101 SSE = 0.071	D_1 = 19.463 K_1 = 1.325 D_2 = 25.840 K_2 = 0.071 R^2 = 0.999 SE = 0.016 SSE = 0.002
Fe^{2+}	0.18<dp<0.36 (mm) C_i =92.85 mg/L pH_{eq} = 7.9	$Q_{e,\ max}$ (mg/g) = 1.486 C_e (mg/L) = BDL %η = 100	K_1 = 0.567 Q_e = 1.477 R^2 = 0.990 SE = 0.052 SSE = 0.022	K_2 = 0.660 Q_e = 1.526 h = 1.537 R^2 = 0.991 SE = 0.049 SSE = 0.019	α = 8.981 a = 886.556 R^2 = 0.655 SE = 0.165 SSE = 0.190	D_1 = 11.845 K_1 = 16.000 D_2 = 32.723 K_2 = 0.372 R^2 = 0.999 SE = 0.018 SSE = 0.002
Mn^{2+}	0.18<dp<0.36 (mm) C_i =100.60 mg/L pH_{eq} = 8.6	$Q_{e,\ max}$ (mg/g) = 0.918 C_e (mg/L) = 43.20 %η = 57	K_1 = 0.066 Q_e = 0.800 R^2 = 0.890 SE = 0.106 SSE = 0.091	K_2 = 0.111 Q_e = 0.872 h = 0.084 R^2 = 0.947 SE = 0.074 SSE = 0.044	α = 7.444 a = 0.390 R^2 = 0.982 SE = 0.037 SSE = 0.009	D_1 = 9.716 K_1 = 0.658 D_2 = 17.521 K_2 = 0.015 R^2 = 0.993 SE = 0.030 SSE = 0.006

In summary, a comparison of SSE, SE, R^2 values and model parameter estimates, given in Table 6.13 and residual plots for all Me^{2+} ions indicate that double exponential model (DEM)

gives the best fit and thus a better diffusion theory to describe data. DEM predicts a two-step diffusion mechanism involving a rapid first phase comprising film and intraparticle diffusion followed by a slow second phase controlled by intraparticle diffusion (Wilczak and Keinath, 1993). Because $K_1 >> K_2$ for all metal ions the rapid stage may not limit the overall rate of adsorption. Therefore, intraparticle diffusion during the second stage is probably the rate limiting step. However, the pseudo second order (PSO) model fit appeared more superior for all metal ions over chemisorption based models. Based on this model, initial adsorption rates (h) and PSO adsorption constant (k_2) increased with decrease in particle diameter of adsorbent. Highest values of initial adsorption rates were obtained with the finest adsorbent particle size (0.18-0.36 mm) as follows 1.537 mg/g min Fe^{2+}, 0.562 mg/g min Cu^{2+}, 0.404 mg/g min Cd^{2+}, 0.091 mg/g min Co^{2+} and 0.084 mg/g min Mn^{2+} (Table 6.13). Thus, both intraparticle diffusion and chemisorption processes appear to control overall kinetics.

Furthermore, adsorption data for all metal ions were fitted to Boyd's and Weber-Morris diffusion models by linear regression. As shown below, Boyd's diffusion model is plotted in Figure 6.19 (A) in which graphs are linear for all metal ions until equilibrium when gradient changed for ions that adsorbed to completion, however, the graphs are offset from the origin. Similar trends were observed at different particle sizes of adsorbent (0.36-0.50 & 0.50-1.00 mm). The diffusion theory by Boyd et al (1947) proposes that either film diffusion or chemical adsorption steps to be rate controlling, and not intraparticle diffusion.

The plots for Weber-Morris intraparticle diffusion model are given in Figure 6.19 (B). There is a linear relationship between q_t and $time^{1/2}$ with a non-zero intercept for Co^{2+} and Mn^{2+}

adsorption data. However, there are two linear segments for Cd^{2+}, Cu^{2+} and Fe^{2+} ions with the second segment corresponding to complete adsorption phase of ions. It has been suggested that multi-linearity of fitted curves in general is indicative of diffusion into progressively fine pores in the adsorbent. The fact that straight lines do not pass through the origin suggest that both film and intraparticle diffusion may be limiting.

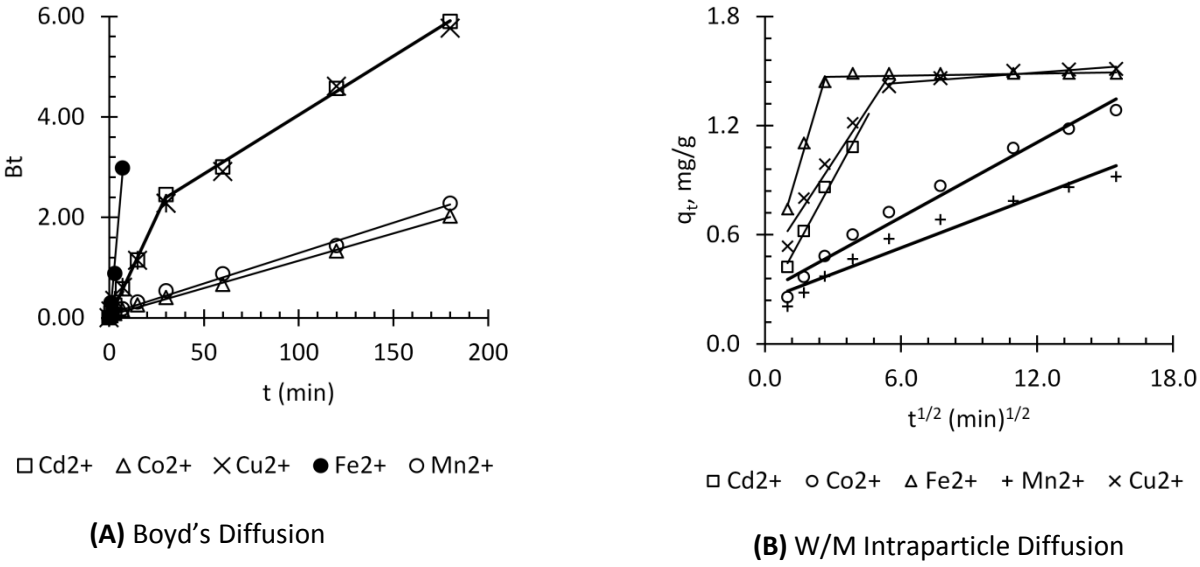

(A) Boyd's Diffusion

(B) W/M Intraparticle Diffusion

Figure 6.19:: Linear model fits to single component adsorption data of metal ions with BFS granules at 30 g/L, (A) Boyd's diffusion, (B) Weber/Morris Intraparticle diffusion model

Table 6.14: Estimated diffusion model parameters, BFS granules at 30 g/L BFS

Metal Ion	Boyd's Diffusion Model		Intra Particle Diffusion Model	
	R^2	D_i (cm^2/min)	R^2	K_i (mg/g $min^{1/2}$)
Cd^{2+}	0.999	1.492 x 10^{-6}	0.990	0.2301
Co^{2+}	0.998	2.013 x 10^{-7}	0.976	0.0684
Mn^{2+}	0.992	2.234 x 10^{-7}	0.952	0.0475

6.3.4.4 Application of Kinetic Models to Multicomponent Data

The results of curve fitting to adsorption data of multicomponent systems of metal ions at same experimental conditions as in single systems (0.18-36 mm adsorbent particle sizes, pH

3.50, 30 mg/L BFS phase ratios, all Me^{2+} ions at 100 mg/L each) are given in Figure 6.20. Because adsorption of Co^{2+} and Mn^{2+} was negligible under these conditions, only data for Cd^{2+}, Cu^{2+} and Fe^{2+} were analysed. From the model parameter estimates and statistical figures given in Table 6.15, low adsorption of Cd^{2+} ions could have been due to diffusion limitation based on a satisfactory DEM model fit. There is no suggestion of chemical adsorption limitation under these conditions. Adsorption profiles of both Cu^{2+} and Fe^{2+} ions are best described by PSO and DEM models (Fig. 6.20 & Table 6.15). Because $K_1 >> K_2$ and on the basis of random distribution nature of errors between predicted and actual q_t values as well as high R^2 values, DEM supports intraparticle diffusion limitation in the second phase of adsorption for both Cu^{2+} and Fe^{2+} ions. However, both PSO and Elovich models predicted chemisorption to be rate limiting for these ions (high R^2, low SSE & SE). However, because of the systematic distribution of errors, PSO and Elovich's models may not be suitable to describe data.

A comparative kinetic analysis of the effect of particle size in multicomponent adsorption system relative to single solutes at two other coarse sizes of 0.36-0.50 and 0.50-1.00 mm is not shown because of low solute adsorption as particle size was increased. Kinetic analysis of the effect of phase ratio showed no change in adsorption dynamics. Although adsorption efficiency generally increased with increase in phase ratio, the rate of adsorption was possibly diffusion limited for Cd^{2+}, Co^{2+} and Mn^{2+} ions based on DEM model. PSO and DEM parameters suggest both diffusion and chemisorption might be rate controlling for Cu^{2+} and Fe^{2+} ions.

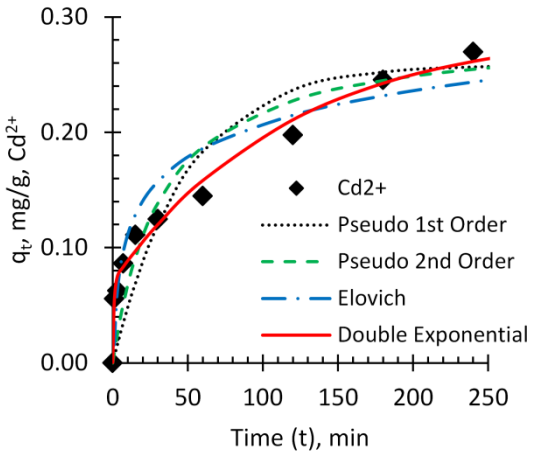

(A) Cd^{2+}

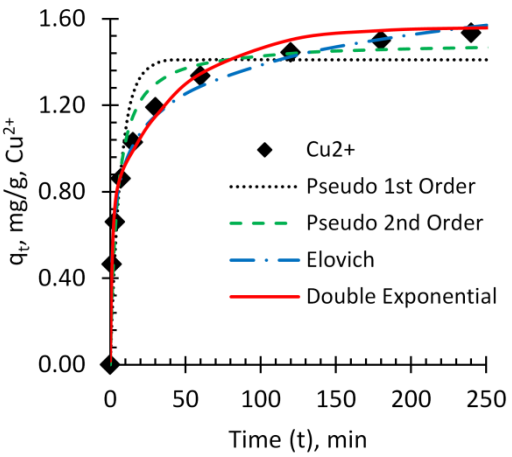

(B) Cu^{2+}

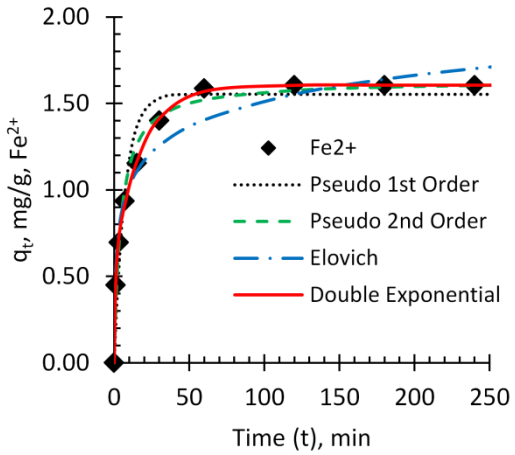

(C) Fe^{2+}

Figure 6.20: Nonlinear model fits to multicomponent adsorption data of metal ions [(A)-(C)] with BFS granules at 30 g/L

Table 6.15: Estimated kinetic model parameters in multicomponent adsorbates, 30 g/L BFS granules

Metal ion	Variable		Kinetic Models			
	Particle size	Experimental	Pseudo 1st Order	Pseudo 2nd Order	Elovich	Double Exponential
Cd^{2+}	0.18<dp<0.36 (mm) C_i = 102 mg/L	Q_e (mg/g) = 0.290 C_e (mg/L) = 84 %η = 18	K_1 = 0.021 Q_e = 0.259 R^2 = 0.850 SE = 0.039 SSE = 0.014	K_2 = 0.106 Q_e = 0.289 h = 0.0089 R^2 = 0.897 SE = 0.032 SSE = 0.009	α = 24.049 a = 0.061 R^2 = 0.892 SE = 0.030 SSE = 0.007	D_1 = 2.105 K_1 = 1.268 D_2 = 6.580 K_2 = 0.009 R^2 = 0.988 SE = 0.013 SSE = 0.001
Cu^{2+}	0.18<dp<0.36 (mm) C_i = 102 mg/L	Q_e (mg/g) = 1.561 C_e (mg/L) = 4.23 %η = 96	K_1 = 0.145 Q_e = 1.410 R^2 = 0.905 SE = 0.166 SSE = 0.247	K_2 = 0.148 Q_e = 1.494 h = 0.330 R^2 = 0.966 SE = 0.099 SSE = 0.088	α = 5.051 a = 2.201 R^2 = 0.994 SE = 0.033 SSE = 0.009	D_1 = 22.539 K_1 = 0.707 D_2 = 23.792 K_2 = 0.022 R^2 = 0.993 SE = 0.050 SSE = 0.017
Fe^{2+}	0.18<dp<0.36 (mm) C_i =100 mg/L	Q_e (mg/g) = 1.606 C_e (mg/L) = 0.01 %η = 100	K_1 = 0.140 Q_e = 1.553 R^2 = 0.949 SE = 0.134 SSE = 0.161	K_2 = 0.138 Q_e = 1.633 h = 0.368 R^2 = 0.986 SE = 0.070 SSE = 0.045	α = 4.663 a = 2.495 R^2 = 0.941 SE = 0.112 SSE = 0.100	D_1 = 17.359 K_1 = 1.098 D_2 = 30.773 K_2 = 0.056 R^2 = 0.999 SE = 0.015 SSE = 0.002

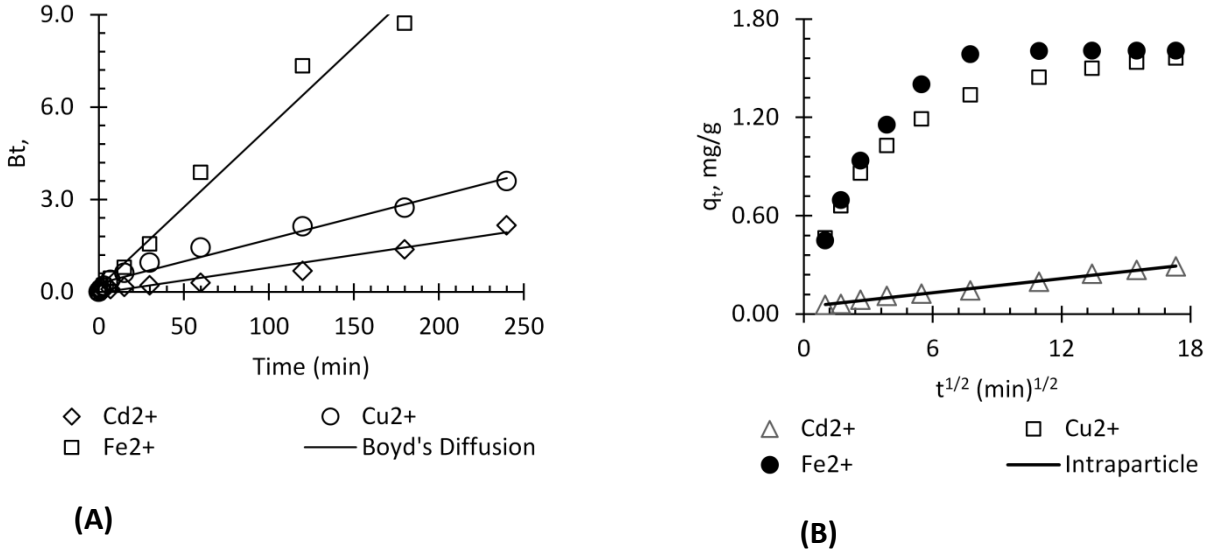

Figure 6.21: Linear model fits to multicomponent adsorption data of metal ions with BFS granules at 30 g/L, (A) Boyd's diffusion, (B) Weber/Morris Intraparticle diffusion

The good linear fits of Boyd's diffusion model to experimental data in Figure 6.21(A) above support the possibility of liquid film resistance to solute adsorption around adsorbent particles. For ions (Cd^{2+}) that exhibited low adsorption and thus did not reach complete adsorption, intraparticle diffusion resistance might be rate limiting as shown in Figure 6.21 (B). For Cu^{2+} and Fe^{2+} ions that were completely adsorbed, more than one linear segment of the intraparticle diffusion model fit was observed as shown in Figure 6.21(B). This is believed to be intraparticle diffusion resistance through progressively finely sized pores.

Table 6.16: Estimated diffusion model parameters in multicomponent adsorption system, 30 g/L BFS granules.

Metal Ion	Boyd's Diffusion Model		Intra Particle Diffusion Model	
	R^2	D_i (cm^2/min)	R^2	K_i (mg/g $min^{1/2}$)
Cd^{2+}	0.963	1.514 x 10^{-7}	0.994	0.0144
Cu^{2+}	0.975	2.622 x 10^{-7}	-	-
Fe^{2+}	0.978	9.584 x 10^{-7}	-	-

6.3.5 Mechanistic Model of Adsorption Process

For silicate based (inorganic) materials such as slags, many authors believe metal adsorption process occurs through ion exchange and metal hydroxide/silicate precipitation (Dushina & Aleskovski, 1976), physical adsorption based on ion exchange (Lopez et al., 1995), predominantly adsorption through ion exchange and some form of metal silicate precipitation (Dimitrova and Mehanjiev, 1998). Thus, depending on solution pH and metal ion concentration, hydroxide and/or silicate precipitation and complexation may be involved (Dimitrova et al., 2001; Dimitrova & Mehandgiev, 2000). The pH range for complete hydroxide precipitation of each metal ion is given in Table 6.17 below.

Table 6.17: Relationship between pH and precipitation of metal hydroxides
(Zhuang, 2009)

Metal Hydroxide species	pH for complete Precipitation
$Fe(OH)_3$	4.5-5.0
$Cu(OH)_2$	7.5-8.0
$Co(OH)_2$	9.2
$Fe(OH)_2$	9.2-9.5
$Cd(OH)_2$	9.4-9.7
$Mn(OH)_2$	9.8-10.2
$Ca(OH)_2$	12.4

This study found adsorption of Fe^{2+} and Cu^{2+} to be much stronger than other ions. One possible explanation is that if sufficient dissolved oxygen is present, it is possible that Fe^{2+} oxidized fairly quickly to the Fe^{3+} form at pH ≥ 3.5 which subsequently precipitated out at this pH or higher as insoluble ferric hydroxide (Eq. 6.13) whilst other ions requires high alkaline pH (Zhuang, 2009). The surface of ferric hydroxide precipitates have adsorptive properties and may act as adsorbents for other metal ions present depending on solution conditions (Zhuang, 2009). The experimental setup used in this study was airtight except intermittent air infiltration during solution sampling. It was assumed some iron was still present in ferrous form which precipitated out completely around pH 9.2. Mn also has variable precipitation regimes due to its many oxidation states. The pH/precipitation relationship for metal ions is given in Table 6.17 above. The minimum pH necessary for onset of precipitation may vary for these metal ions, depending on concentration, however, a highly alkaline solution is necessary for complete precipitation. Therefore, based on observed equilibrium pH (5.0-8.5) and precipitation pH regimes given in Table 6.13,

chemical precipitation mechanism for Fe^{2+} and Cu^{2+} extraction from solution is a significant process. Interactive effects among metal ions may also influence the extent of precipitation. For instance, iron can coprecipitate with manganese at about pH 8 if iron concentration is roughly four times greater than that of manganese (Skousen et al., 2000).

$$4Fe^{2+} + O_2 + 4H^+ = 4Fe^{3+} + 2H_2O \quad \text{---} \quad (6.13a)$$

$$2Fe^{3+} + 4H_2O = Fe_2O_3.\,H_2O + 6H^+ \quad \text{---} \quad (6.13b)$$

The adsorption mechanisms and pH relationships to adsorption of metal ions were also analysed from point of view of dissolution of BFS and its subsequent effect on metal extraction from solution. As discussed in Section 4.3.1.3 of Chapter 4, this study analysed fresh BFS and EAF surfaces before adsorption by SEM and EDX techniques revealing predominantly Ca^{2+}, Si^{4+}, Al^{3+}, Mg^{2+}, K^+ and Na^+ ions. After adsorption experimentation at different experimental conditions, additional metal ions were detected on the adsorbent surface which supports the fact that they were adsorbed from solution. This is graphically presented in Figure 6.20 below in a multicomponent context when all metal ion adsorbates were initially at 100 mg/L each. Further, total elemental analysis by XRF on adsorbed BFS detected adsorbed metal ions in the matrix relative to fresh unadsorbed BFS material.

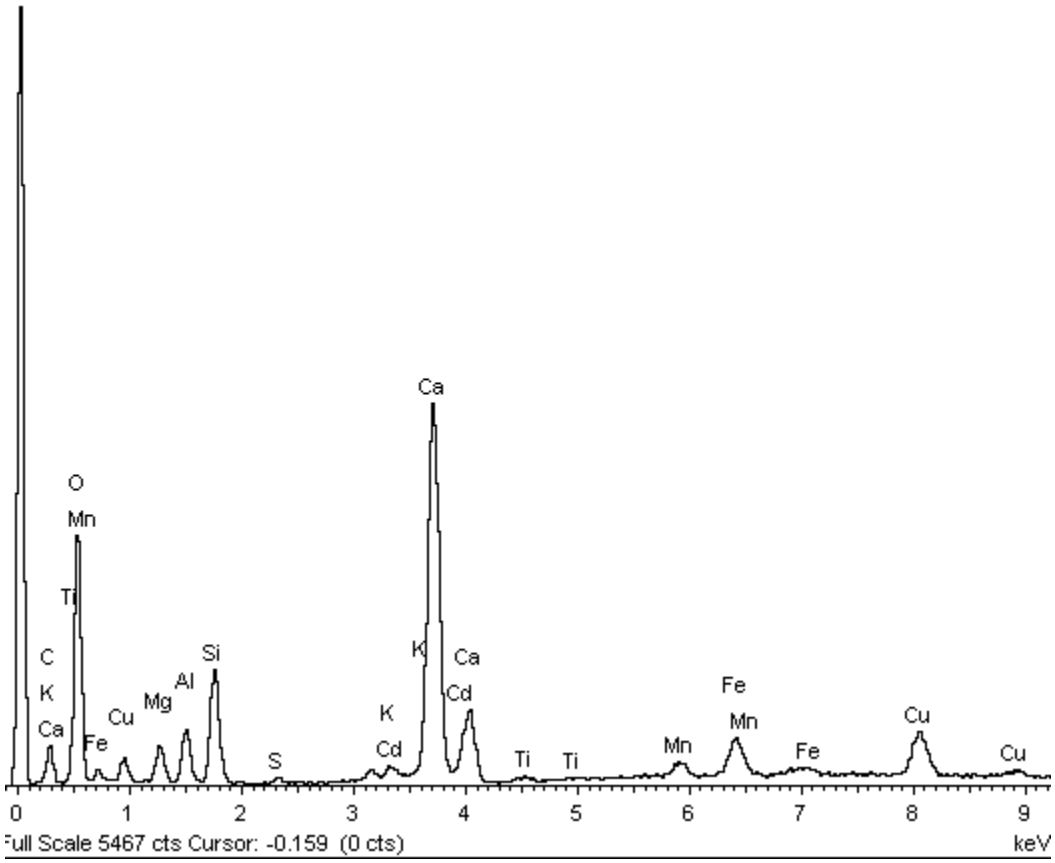

Figure 6.22: Surface composition of loaded BFS granules at 30 g/L in multicomponent system, 100 mg/L Me^{2+} ions

Various studies propose an initial slag hydrolysis step followed by adsorptive processes that involve ion exchange between alkali ions (Ca^{2+}, Mg^{2+}, Na^{+}, etc.) attached to adsorbent surface sites (Al, SiO^{-}) with metal ions (Me^{2+}). Thus, Ca^{2+}, Mg^{2+}, K^{+} & Na^{+} are potentially exchangeable cations and heavy metal ions can be removed from solution by ion-exchange process. Dimitrova (1996) believes adsorption is facilitated by chemical interaction of dissolved slag components with metal ions and subsequent deposition of such products on slag surfaces. The slag chemistry and dissolution of its constituent chemical phases and theories of adsorption mechanisms as elucidated further by Dimitrova and Mehandgiev (2000) and Dimitrova (2001) are shown in Equations (6.14) to (6.16). Commonly, the mineral

phases gehlenite ($Ca_2Al_2SiO_7$) and larnite ($2CaO.SiO_2$ or Ca_2SiO_4), given in Equations (6.14) and (6.15), hydrolyse to release ions such as Ca^{2+} and Mg^{2+} which replaces metal ion adsorbates such as Cu^{2+} in solution by a non-equivalent ion exchange process (Eq. 6.16).

Slag (silicate) Hydrolysis:

$$\overline{Ca_2Al_2SiO_7} + 5H_2O = 2Ca^{2+} + 2Al(OH)_3 + 4OH^- + \overline{SiO_2} \quad \text{---} \quad (6.14)$$

$$2\overline{CaO.SiO_2} + 2H_2O = 2Ca^{2+} + H_4SiO_4 + 4OH^- \quad \text{---} \quad (6.15)$$

Ion Exchange:

$$\overline{(Al,SiO)_2^-}Ca^{2+} + 2H^+ \Leftrightarrow 2\overline{(Al,SiO)^-}H^+ + Ca^{2+} \quad \text{---} \quad (6.16a)$$

$$\overline{(Al,SiO)_2^-}Ca^{2+} + Me^{2+} \Leftrightarrow 2\overline{(Al,SiO)_2^-}Me^{2+} + Ca^{2+} \quad \text{---} \quad (6.16b)$$

$$\overline{(Al,SiO)_2^-}Ca^{2+} + Me^{2+} + H^+ \Leftrightarrow 2\overline{(Al,SiO)_2^-}H^+ + Me^{2+} + Ca^{2+} \quad \text{---} \quad (6.16c)$$

Where bar = solid phase, (Al, SiO^-) = surface site; Me^{2+} = Metal ion (Cd^{2+}, Co^{2+}, etc.)

Yamashita et al (1983) assumed adsorption of metal ions by steel slag occurred by ion substitution with CaO and MgO species, hydroxide precipitation at high pH, sulphide precipitation and coprecipitation by sulphur and iron oxides respectively, and adsorptive effects by $2CaO.SiO_2$ phase. The BFS adsorbent used in this study consists of high amount of lime (44 % w/w CaO) for which any free lime hydrolysed to produce a solution of high pH (alkalinity) with capacity to neutralise acidic effluents such as acid mine drainage and precipitate metal ions. The lime hydrolysis and metal hydroxide reactions are given in Equations (6.17) and (6.18).

$CaO + H_2O = Ca(OH)_2$; $MgO + H_2O = Mg(OH)_2$ --- (6.17)

Metal hydroxide and silicate precipitation:

$$\overline{SiO_2} + Me^{2+} + 2OH^- = MeSiO_3 \downarrow + H_2O \quad \text{---} \quad (6.18a)$$

$$Me^{2+} + OH^- = Me(OH)^+ + OH^- = Me(OH)_2 \downarrow \quad \text{---} \quad (6.18b)$$

Where bar = solid phase, (Al, SiO^-) = surface site; Me^{2+} = Metal ion (Cd^{2+}, Co^{2+}, etc.)

Further analysis of SEM images of BFS surfaces contacted with metal ions showed precipitate-like flocs of possibly metal silicates or hydroxides. On the basis of highly alkaline pH observed in several systems studied, it is evident that precipitation and/or complexation reactions also contribute to metal ion removal especially for Fe^{2+} and Cu^{2+} ions via OH^- ions or other products of slag hydrolysis. An SEM image of BFS surface in Figure 6.23 below shows precipitate-like flocs which were confirmed to be composed of Cu^{2+} and Fe^{2+} ions by EDS. However, a definitive identification of respective metal compounds by XPS was not conclusive.

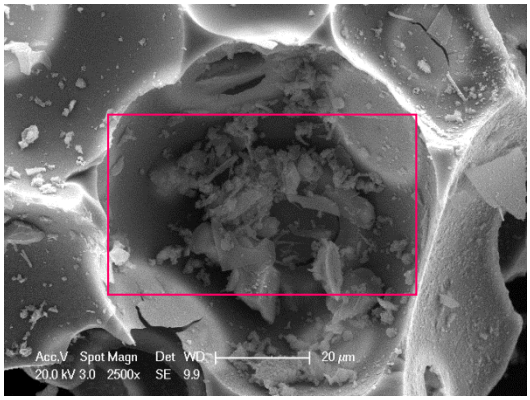

(A)

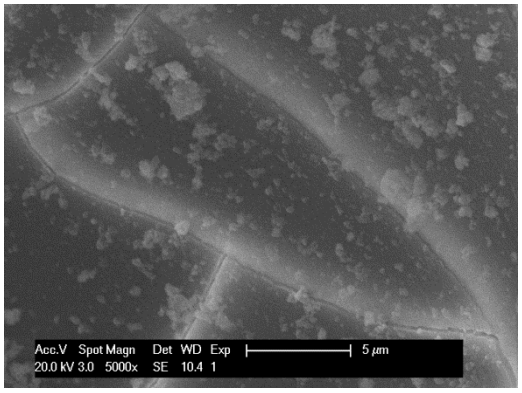

(B)

Figure 6.23: Probable flocs of loose metal precipitates on BFS granules surfaces in SEM-EDS microstructure, both (A) & (B) from multicomponent systems.

6.4. Conclusions

This Chapter has reported on investigations that were conducted to establish adsorption efficiency, kinetics and mechanisms of multiple metal ions by BFS and EAF, and explored the effects of BFS pretreatments on adsorption performance. The work has clearly shown the importance of studying solutions with multiple metal ions as a model to determine adsorption characteristics and fully understand adsorption phenomena of multicomponent adsorption systems that reflect actual industrial effluent compositions.

Single component adsorption systems

The purification of acidic waste solutions consisting of single solutes of Cd^{2+}, Cu^{2+}, Co^{2+}, Fe^{2+} and Mn^{2+} (at representative concentration of 100 mg/L each) in order to attain permissible discharge limits (< 5 mg/L) is achievable using phase ratios of up to 50 g/L BFS powder. Variation of BFS particle sizes within the coarse size range (granules) also resulted in complete adsorption of Cu^{2+}, Cd^{2+} and Fe^{2+} to permissible discharge limits except Mn^{2+} and Co^{2+} ions whose adsorption was unsatisfactory. Also, complete adsorption of Cd^{2+}, Cu^{2+} and Fe^{2+} ions by BFS granules is only achievable at pH ≥ 3.50. However, adsorption of Co^{2+} and Mn^{2+} to completion is difficult within pH 1.50 to 5.50. Furthermore, adsorption of all metal ions from strongly acidic solution is negligible.

In general, an increase in initial pH or decrease in particle size increases efficiency. Some of the highest adsorption capacities obtained in single solutes were 1.60 mg/L Cd^{2+}, 1.28 mg/g Co^{2+}, 1.85 mg/g Cu^{2+}, 1.63 mg/g Fe^{2+} and 0.92 mg/g Mn^{2+} which compares favourably with literature values. The adsorption order is proposed as $Fe^{2+}>Cu^{2+}>Cd^{2+}>Co^{2+}>Mn^{2+}$. This

sequence highlights the differences in adsorption characteristics of the metal ions. Because adsorption efficiency is greatly improved by decreasing particle sizes, subsequent adsorption studies were studied using powdered BFS in multicomponent systems under wide concentration of metal ions. At same conditions, level of adsorption for Cd^{2+}, Co^{2+} and Mn^{2+} in multicomponent adsorption system is unsatisfactory relative to single solutes, while that of Cu^{2+} and Fe^{2+} is high and unaffected. This may be due to competitive adsorptive effect among ions and limitation in the material's adsorptive properties. BET surface area and pore surface area of BFS is low and this probably limits adsorption capacity.

Multicomponent adsorption systems

Adsorption efficiency increased with an increase in initial pH within 1.50 to 7.5 but negligible in strongly acidic solutions. The system favoured selective adsorption of Cu^{2+} and Fe^{2+} ions to acceptable discharge limits (< 5 mg/L) at pH ≥ 3.50. This is partly attributed to the early onset of pH range for hydroxide precipitation as solution pH evolved freely upwards with time. Although adsorption of Cd^{2+}, Co^{2+} and Mn^{2+} is high at intermediate pH, complete separation to attain discharge limits is a challenge. However, complete adsorption of all ions to permissible discharge limits is achievable in alkaline pH. Thus, an increase in initial pH promotes adsorption and chemical precipitation of metal ions to varying degrees. The pH/adsorption relationships vary from one metal ion to another.

The efficiency of adsorption decreased with increase in initial concentration for metal ions fixed at same initial values within the range 20-1000 mg/L studied. More crucially, simultaneous adsorption of all metal ions by slags to attain permissible discharge limits appears to be effective only in relatively dilute concentrations. For metal ions at same

concentration, highest adsorption capacities were 10.17 mg/g Fe^{2+} at 1014 mg/L, 3.19 mg/g Cu^{2+} at 334 mg/L, 1.94 mg/g Cd^{2+} at 206 mg/L, 0.53 mg/g Co^{2+} at 56 mg/L and 0.48 mg/g Mn^{2+} at 54 mg/L. These are the satisfactory performance values for a discharge limit of C_e < 5 mg/L. The BFS adsorbent appeared to be selective towards Cu^{2+} and Fe^{2+} ions, moderate towards Cd^{2+} ions but had low affinity for Co^{2+} and Mn^{2+} ions. The adsorption capacities and distribution coefficients of Cu^{2+} and Fe^{2+} are greater than those of Cd^{2+}, Co^{2+} and Mn^{2+} ions, reflecting high affinity and preferential adsorption towards Cu^{2+} and Fe^{2+} ions.

Thus, adsorption of metal ions in multicomponents to acceptable discharge limits is difficult to attain at relatively high concentrations of ions. The extent of adsorption varies for different metal ions at the same level of initial concentration. Thus, adsorption may depend on the type of metal ion and interactive effects among ions. This limits the slag to adsorb specific metal ions or only those ions at low concentration. For ions at different initial concentration, highest adsorption capacities were 12.66 mg/g Fe^{2+} at 791 mg/L, 3.83 mg/g Cu^{2+} at 243 mg/L, 1.35 mg/g Cd^{2+} at 86 mg/L, 0.22 mg/g Co^{2+} at 16 mg/L and 0.13 mg/g Mn^{2+} at 11 mg/L for a discharge limit of C_e < 5 mg/L. The extent of adsorption of ions at low concentration (Cd^{2+}, Co^{2+}, Mn^{2+}) appeared to be suppressed by quickly and strongly adsorbing ions (Cu^{2+}, Fe^{2+}) at higher initial concentration by possibly competitive adsorption.

Comparatively, EAF has higher adsorption capacity and efficiency for Cu^{2+} and Fe^{2+} than BFS at moderate to higher concentration with maximum values of 55.1 mg/g Fe^{2+} at 1686 mg/L and 17.86 mg/g Cu^{2+} at 551 mg/L. However, BFS has higher affinity and faster kinetics of the initial adsorption phase than EAF towards Cd^{2+} and Co^{2+}. Only powdered BFS relative to its granulated form produced effluents with acceptable discharge limits in dilute solutions of

multiple metal ions. Consequently, it may be necessary to carry out particle size reduction to increase surface area and improve efficiency but the process has huge cost implications. Also, efficiency was improved with increase in mass (2-100 g/L) and temperature (22-75 ^{o}C). Thus, an optimum particle size and mass relative to initial concentration of metal ions is expected to work effectively in dilute solutions. A discharge limit to below 5 mg/L for all ions was achieved in the entire temperature range except Mn^{2+} that needed ≥ 60 ^{o}C.

In summary, the results means that the extent of adsorption of various metal ions depends on the type of metal ions, initial concentration and specific metal ion/adsorbent interactions involved. Adsorption of multiple different metal ions is generally feasible at low concentration under these conditions. The adsorption sequence is $Fe^{2+} > Cu^{2+} > Cd^{2+} > Co^{2+} > Mn^{2+}$. The marginally higher surface area of EAF provides higher adsorption sites for metal ions, giving it higher capacity than BFS at moderate to higher concentration. BFS has a higher affinity and faster initial adsorption kinetics than EAF, towards Cd^{2+} and Co^{2+} ions.

Effect of Adsorbent Pretreatment

This study has established that pretreatment of BFS by acid leaching process significantly increases quantities of adsorbed Cd^{2+}, Co^{2+} and Mn^{2+} ions from a multicomponent system by several magnitudes. BET surface area, total pore area and pore volume of BFS more than doubled after leaching which subsequently supported larger amounts of ions to be adsorbed. Ironically loading of Cu^{2+} and Fe^{2+}, that had showed strong adsorption in several other systems investigated, decreased. Free Lime that was leached out is thought to be responsible for good separation of Cu^{2+} and Fe^{2+} in other cases mostly through hydroxide

precipitation. Preheating of BFS as a function of temperature did not improve adsorption of metal ions. This is because key adsorption properties decreased especially surface area.

Kinetic Modeling

The rate of adsorption of metal ions and rate limiting steps depended on experimental conditions. In single solutes that adsorbed to completion (Cd^{2+}, Cu^{2+} and Fe^{2+}) pseudo second order (PSO) model predicted chemisorption theory to be the mechanism of adsorption and consequently limits overall rates of adsorption as a function of particle size. The initial rates of adsorption (h) based on PSO increased by 1.5-3 with decrease in particle size. Highest h values were 1.537 mg/g min Fe^{2+}, 0.562 mg/g min Cu^{2+}, 0.404 mg/g min Cd^{2+}, 0.091 mg/g min Co^{2+} and 0.084 mg/g min. The overall adsorption rates for Co^{2+} and Mn^{2+}, whose adsorption was poor, as a function of both pH and particle size were limited by intraparticle diffusion in the second adsorption phase based on double exponential model (DEM). This prediction was supported by Weber-Morris Intraparticle diffusion model. The multi linear fit of this model to data for ions that were completely adsorbed (Cu^{2+}, Fe^{2+}) suggested intraparticle diffusion resistance through progressively finely sized pores. Also, from the DEM model, rates of adsorption of metal ions in multiadsorbates at same conditions as in single solutes were limited by intraparticle diffusion. DEM gave the best fit and thus a better diffusion theory to describe adsorption data of all metal ions. DEM predicts a 2-step diffusion mechanism involving rapid first adsorption phase that comprises film and intraparticle diffusion followed by slow second phase that is controlled by intraparticle diffusion. Thus, both intraparticle diffusion and chemisorption steps control overall adsorption kinetics depending on solution conditions.

Adsorption Mechanisms

The adsorption mechanisms and pH relationships to adsorption have been analysed on the basis of the dissolution of slag materials, their surface chemistry and subsequent effects on separation of metal ions from solution. The mechanisms of extraction of metal ions involve adsorption, precipitation and ion exchange phenomena. SEM images and analysis of the slag surfaces by EDX supports ion exchange theory to be the mechanism of adsorption for Mn^{2+}, Co^{2+} and Cd^{2+}. The dissolution of slags releases mostly alkali ions (Ca^{2+}, etc.) that replace metal ions in solution via ion exchange. Another key pH relationship to the mechanism of separation of metal ions involves the dissolution of lime in slags to produce high pH. SEM images showed the presence of precipitate-like flocs on adsorbent surfaces contacted with metal ions, which were confirmed to be Cu^{2+} and Fe^{2+} ions. Thus, chemical precipitation is another separation mechanism for Cu^{2+} and Fe^{2+} ions. Furthermore, another possible mechanism of adsorption of metal ions from solution as predicted by pseudo kinetic model is chemisorption.

Recommendations

Solution pH is a key controller of extent of metal ion adsorption and extraction mechanisms. Thus, a detailed study of the effect of constant pH on extent of adsorption and extraction mechanisms that can propose correct mechanisms and enhance understanding of adsorption phenomenon is recommended. The efficiency of slag materials should also be investigated using real/actual acid mine drainage from variable sources that contain multiple metal ions with a wide concentration range and acidity.

It is recommended that the leaching process be optimised to improve adsorptive properties. Subsequently adsorption performance of slag materials leached with different chemicals at different conditions of pH, particle size, etc., should be investigated. Additional studies to understand the adsorption mechanisms are required. Furthermore, characterisation of BFS surfaces contacted with metal ions is necessary in order to identify surface compounds that form with metal ions and propose accurate adsorption mechanisms. The effect of anions on the adsorption capacity of slag materials as adsorbents for metals ions, especially in sulphate (SO^{2-}_4) and nitrate (NO^{2-}_3) systems must be investigated and compared.

CHAPTER 7
FIXED BED ADSORPTION KINETICS

7.1 Introduction

Investigations were conducted to evaluate the performance of blast furnace slag (BFS) material as novel adsorbent in continuous flow adsorption experiments by treating synthetic waste solutions containing multiple metal ions that simulated acid mine drainage. Experimental results from batch adsorption studies, discussed in Chapters 5 and 6, have provided fundamental information such as adsorbent efficiency, equilibria and kinetics as well as optimum experimental conditions under which adsorption of several metal ions is effective.

However, adsorption data from continuous flow adsorption experiments in fixed bed adsorption columns is required as a more realistic approach to assess the feasibility, scale up and design of adsorption systems for practical applications. Depending on process objectives, fixed bed columns may offer high productivity whereby a large volume of solution can be treated continuously, allowing a more efficient use of adsorbent capacity. Fixed bed columns are potentially more effective in that a fresh solution, with relatively constant metal concentration, is in continuous contact with adsorbent particles. This further allows a high degree of purification to be achieved in a single step process resulting in better effluent quality. Such processes are easy and relatively simple to operate in relation to adsorption/desorption cycles (Aksu, 2005; Oguz and Ersoy, 2010).

The adsorption performance of a fixed bed column is analysed by initially determining the effluent concentration/time graph or breakthrough curve (ratio of effluent to influent conc. (C_e/C_i) vs. time or volume) from which column adsorption capacity, depth of adsorption zone, shape of breakthrough curve itself, time and volume of solution treated before the breakthrough point and degree of column saturation at breakthrough point can all be determined (Armenante, 1999b). The adsorption stages in the column and breakthrough curve are depicted in Figure 7.1 below. The shape of the breakthrough curve is dictated by an adsorption isotherm and mass transfer kinetics (liquid film and pore diffusion, and adsorption steps) of the solute in the column (Inglezakis & Poulopoulos, 2006a).

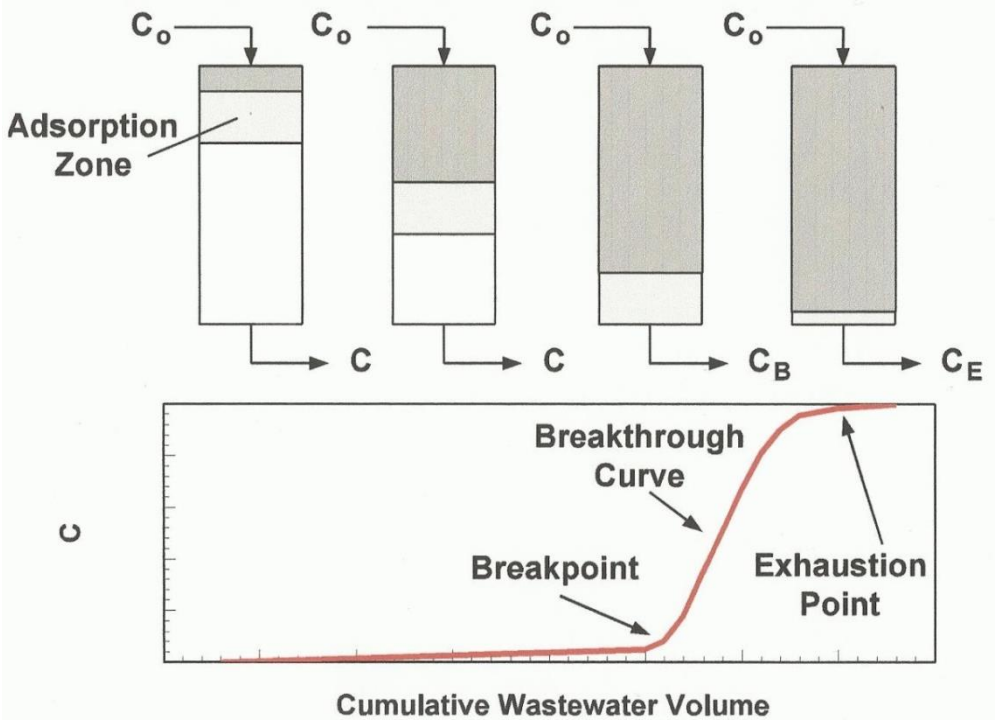

Figure 7.1: Schematic diagram of a breakthrough curve showing relative positions of the adsorption zone (Armenante, 1999b)

As the solution enters the fixed bed during the adsorption process, a solute passes through a saturated zone, adsorption zone and a downstream zone with little adsorbed solute (Fig.

7.1). The size and position of these zones in the bed vary with time whereby adsorption zone continuously moves downstream forming an adsorption wave until the entire bed is saturated. A breakthrough point (C_b) is reached when the bed begins to release solution with solute concentration higher than the desired discharge limit (roughly 5-10 % of influent value, C_o). Beyond the breakthrough point, solute concentration in the effluent rises rapidly (steep breakthrough curve) until exhaustion point (defined arbitrarily at about 90-100 % of influent value) whereby the column is nearly completely saturated and effluent concentration (C_e) leaving the bed is practically the same as the influent value (Armenante, 1999b; Seader et al., 2011). A brief summary of the literature on column studies involving mostly slag materials as adsorbents in multicomponent systems of metal ions is discussed in the next section of this chapter.

Gao et al (1995) conducted metal adsorption and desorption experiments in continuous flow fixed bed columns with iron-rich slag granules. Multi adsorbate feed stream of Na^+ = 250 mg/L; Cd^{2+}, Ni^{2+}, Pb^{2+} = 2.0 mg/L and Cu^{2+} = 0.1 mg/L at pH 4 were almost completely adsorbed. The sequence for the magnitude of % adsorption was $Pb^{2+} > Cu^{2+} >> Ni^{2+} > Cd^{2+}$ with up to 5000 bed volumes (BV) treated. As cited by Gao et al (1995), Benjamin and Leckie (1981) obtained similar results using iron oxyhydroxides as an adsorbent. Based on high distribution coefficients, slag had high affinity for metals despite the likely competitive effect of the presence of high Na^+ ion concentration. Cd^{2+} ion adsorption compared well with that of commercial chelating ion exchangers. Dimitrova (2002) investigated the adsorption of multiple metal ions from a very dilute acidic (pH 4.0) solution of 5 mg/L Pb^{2+}, 1.5 mg/L Cu^{2+}, 2.7 mg/L Cd^{2+}, 1.5 mg/L Ni^{2+} and 70 mg/L Na^+ ions by BFS granules in a fixed bed column with an empty bed contact time (EBCT) of 1.1 minutes. The author were able to

treat large bed volumes (BV) before the breakthrough point (C_e/C_o = 0.03), which depended on individual metal ions. These results demonstrated the efficacy of BFS as alternative adsorbents although it was noted that levels of concentration of metal ions treated already fell within acceptable discharge limits.

Motsi (2010) treated a much more concentrated synthetic acid mine drainage (AMD) at pH 3.5 consisting of 400 mg/L Fe^{3+}, 120 mg/L Zn^{2+}, 20 mg/L Cu^{2+} and 20 mg/L Mn^{2+} ions with natural zeolite granules in an adsorption column with bed height of 50 cm at a flow rate of 20 ml/min. A large volume of AMD was successfully treated during the first adsorption cycle before the breakthrough point (C_e/C_o set at 0.4) that depended on individual metal ions. Efficiency of adsorption, however, reduced by 28 %, 60 %, 68 % and 72 % for Mn, Cu, Zn and Fe respectively in the second cycle of adsorption after zeolite was regenerated with dilute sulphuric acid stripping solution. This was attributed to the effect of H^+ adsorption during stripping and electrostatic repulsion of metal ions by protonated zeolite surface. Motsi (2010) conducted further column tests on actual AMD solutions from Wheal Jane disused mine and treated large volumes in the first adsorption cycle. Subsequent adsorption cycles were ineffective to extract Fe, Mn and Zn except Cu that was low in concentration. The results suggests that the use of natural zeolite may be limited to single stage adsorption/desorption cycle of dilute solutions.

A more recent study involved reconstituted mining leachate containing phosphate, fluoride and metal ions that was contacted with electric furnace slag (EAF) in column tests over an extended retention time. High extraction efficiencies of 99.9 % PO_4, 85.3 % F, 98 % Mn and

99.3 % Zn were obtained from low feed concentrations of 11-107 mg/L PO_4, 9-37 mg/L F, 0.24-0.83 mg/L Mn and 0.2-3.3 mg/L Zn respectively (Claveau-Mallet et al., 2013).

Apart from the work of Dimitrova (2002) and Gao et al (1995), there are limited continuous flow adsorption studies in fixed bed columns for adsorption of metal ions by BFS materials. Therefore, this study conducted continuous flow adsorption experiments in fixed bed columns to assess the feasibility and scale up of adsorption process, extent of desorption (stripping) of metal ions from surfaces of blast furnace slag (BFS) material after adsorption stages and capability to regenerate the BFS material. Another goal was to demonstrate how wastewater purification process plant using BFS material as an adsorbent may be operated from a practical point of view. Furthermore, the results of this study may also address the question of how to dispose slag materials to meet environmental standards where dissolution of metal ions is limited to acceptable levels.

7.2 Materials and Methods

The experimental approach and column design employed in this study are based on the methods devised by Motsi (2010). About 30 litres of synthetic waste solutions with initial metal ion concentrations of 40 mg/L Cd^{2+}, 30 mg/L Co^{2+}, 250 mg/L Cu^{2+}, 400 mg/L Fe^{2+} and 20 mg/L Mn^{2+} ions were prepared from stock solutions according to the procedure described in Section 3.3.1 of Chapter 3 and added to the feed tank of the fixed bed adsorption column. Continuous flow adsorption experiments were carried out in a fixed bed column to study the effects of flow rates and bed heights on cycle time, breakthrough and exhaustion points in order to establish adsorption equilibria and kinetics. A measured

quantity of BFS (+500-1400 µm particle sizes) was packed into the column until the desired height of the bed was obtained. Then, acidic feed solutions at pH 3.50 with known concentration of metal ions were pumped at the desired volumetric flow rate into the column bed in an upward flow motion.

Some of the key design variables in fixed bed adsorption systems include internal diameter of the column, pressure drop, height of adsorption bed, adsorbent particle size, flow rate of solution to be treated, time to achieve breakthrough, adsorbent exhaustion time and solute concentration (Armenante, 1999b; Inglezakis and Poulopoulos, 2006c). This study investigated the effects of flow rates and bed height on adsorption performance of the BFS packed column shown in Figure 3.3. The effect of volumetric flow rate was carried out at 20, 40 and 60 mL/min through a bed height of 52 cm packed with BFS, and the effect of bed height was carried out at a fixed flow rate of 20 mL/min through bed heights of 27, 52 and 82 cm. Aliquots of about 20 mL were periodically taken from the column discharge point, filtered and analysed by AAS from which various parameters were calculated. The experimental setup of the adsorption column is reproduced in Figure 3.3 below. Reference is made to Section 3.3.3 of Chapter 3 for detailed description of the experimental procedure.

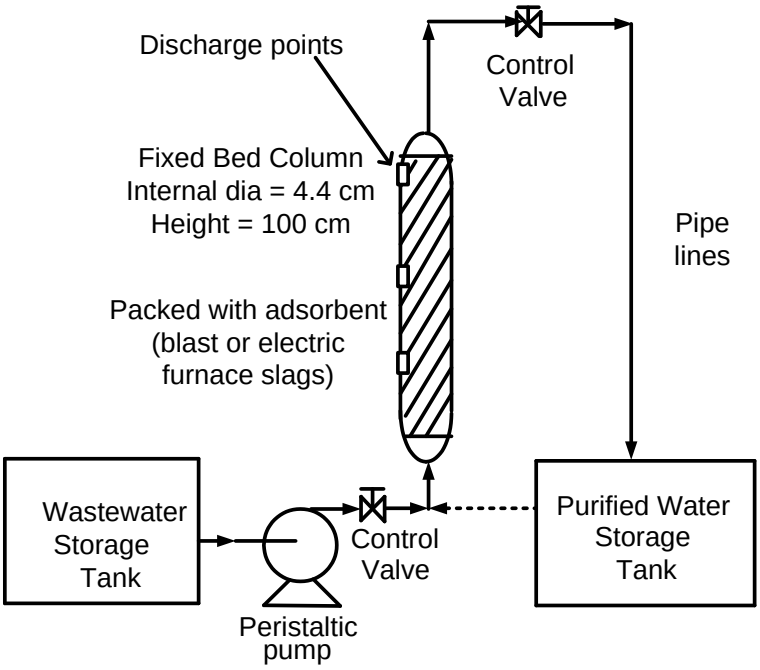

Figure 3.3 Fixed Bed Column Setup (Reproduced from Chapter 3)

The experimental design consisted of two (2) cycles of adsorption and one (1) desorption cycle with a wash cycle in between adsorption-desorption cycles. The first adsorption cycle was conducted in multicomponent adsorption systems with initial metal ion concentration of 40 mg/L Cd^{2+}, 30 mg/L Co^{2+}, 250 mg/L Cu^{2+}, 400 mg/L Fe^{2+} and 20 mg/L Mn^{2+} in solutions at initial pH 3.50, 20 mL/min, bed height of 52 cm to investigate the effect of regeneration ability of slags on cycle time and breakthrough capacity. The first adsorption cycle was followed by desorption cycle whereby metal ions were stripped from loaded slag surfaces of BFS. Dilute sulphuric acid solution at strengths of 0.40 and 2.0 % w/w H_2SO_4 at room temperature was used as a regenerating or stripping reagent, pumped at 20 ml/min through the column bed. After the first stripping or desorption cycle, the column was subjected to an intermediate wash cycle using distilled water, then followed by second adsorption cycle at same conditions as the first cycle. However, the second stripping cycle could not be done because bed had compacted, preventing the solution from flowing through it. The

compaction of the fixed bed was probably due to the breakdown of the slag structure due to exposure to acid stripping caused by the hydrolysis of calcium/magnesium silicate phases in the slag matrix leading to the formation of gelatinous precipitates that possibly blocked bed porosity (Dimitrova and Mehandgiev, 2000; Dimitrova, 2001). It is also possible that bed compaction could have been due to structural failure of the adsorbent particle surfaces (chemical instability) caused by a surface reaction with sulphuric acid, causing the particles to agglomerate and block solution flow after a total of two adsorption cycles and one desorption cycle. As will be shown later in this chapter, this limited the ability of the adsorbent material to be regenerated.

7.3 Results and Discussion

The adsorption performance of a fixed bed column was analysed by determination of breakthrough curves under various experimental conditions from which column adsorption capacity, contact (residence) time and volumes of solution treated were calculated at both breakthrough and exhaustion points using the equations 7.1 to 7.4 below. It is also necessary to establish the empty bed contact time (EBCT) which is the residence time of a water molecule in an empty bed with the same bed volume (BV). The time at breakthrough (t_b) and exhaustion (t_e) points for each adsorption cycle were extrapolated from the Mn^{2+} breakthrough curve by approximation. The t_b and t_e points were defined as 5 % (C_e/C_o = 0.05) and 90 % (C_e/C_o = 0.90) of influent concentration respectively using Mn^{2+} values in order to achieve acceptable discharge limit of ≤ 1 mg/L Mn^{2+} ions. This is in accordance with the Zambian Environmental Protection and Pollution Control Act (EPPA) of 1990 which limits the discharge concentration of metal ions studied here to 0.5 mg/L Cd^{2+}, 1.0 mg/L Co^{2+}, 1.5

mg/L Cu^{2+}, 2.0 mg/L Fe^{2+} and 1.0 mg/L Mn^{2+} ions (EPPCA, 1990). The Mn^{2+} was taken as the reference solute for all other ions in the feed solution because it is the least adsorbed ion as evidenced from batch adsorption results (Chapters 5 and 6). Therefore, Mn^{2+} is expected to be the first solute to be released (breakthrough) in the effluent from the fixed bed.

$$Empty\ Bed\ Contact\ Time\ (EBCT, min)$$

$$= \frac{Bed\ Volume}{Volumetric\ flow\ rate}$$

$$= \frac{X - sectional\ Area\ of\ Column\ (A, cm^2)\ \times Bed\ Height\ (H, cm)}{Volumetric\ flow\ rate\ (Q_v, mL/min)}$$

$$= \frac{A\ (cm^2) \times H\ (cm)}{Q\ (mL/min)}$$

--- (7.1)

Cumulative volumes of solution treated (V_b, L) at breakthrough and exhaustion (V_e, L) points is are given by;

$$V_b = Qt_b \quad \text{---} \quad \text{(7.2a)}$$

$$V_e = Qt_e \quad \text{---} \quad \text{(7.2b)}$$

Cumulative mass of solute adsorbed (m_b, mg) at breakthrough and exhaustion (m_e, mg) points is are given by;

$$m_b = Qt_bC_o \quad \text{---} \quad \text{(7.3a)}$$

$$m_e = Qt_eC_o \quad \text{---} \quad \text{(7.3b)}$$

Column adsorption capacity (q_b, mg/g) at breakthrough and exhaustion (q_e, mg/g) points is are given by;

$$q_b = \frac{Q t_b C_o}{1000 m_c} \quad \text{---} \quad (7.4a)$$

$$q_e = \frac{Q t_e C_o}{1000\, m_c} \quad \text{---} \quad (7.4b)$$

Where m_c = mass of adsorbent in the column (g), Q = volumetric flow rate (mL/min), all other variables are defined above.

Another useful variable in the analysis of fixed bed adsorption performance is what is termed as length of unused bed (LUB) in reference to fraction of unused bed at breakthrough point, here the bed is not fully utilised (McCabe et al., 1993).

$$LUB = Z\left(1 - \frac{t_b}{t_e}\right) \quad \text{---} \quad (7.5)$$

Where Z = bed height (cm); t_b, t_e = breakthrough and exhaustion (saturation) time respectively (min).

7.3.1 Effect of Flow Rate

The effect of flow rate on adsorption performance of the column packed with blast furnace slag (BFS) was carried out at 20, 40 and 60 mL/min to treat an acidic waste solution (pH 3.50) with multiple metal ions of 40 mg/L Cd^{2+}, 30 mg/L Co^{2+}, 250 mg/L Cu^{2+}, 400 mg/L Fe^{2+} and 20 mg/L Mn^{2+}. The breakthrough curves for the individual metals as a function of flow rate are shown in Figure 7.2 and a summary of adsorption performance is presented in Table 7.1.

The shapes of breakthrough curves given in Figure 7.2 below do not depict a typical 'S' shape observed in many practical fixed bed adsorption systems (McCabe et al., 1993). This is possibly due to an ineffective use of the adsorbent or that metal/slag adsorption interaction is weak and not very favourable. Furthermore, the effluent concentration of Cd^{2+}, Co^{2+} and Mn^{2+} ions became greater than their respective influent concentration with time. This suggests periods of elution of adsorbed metal ions during the course of adsorption cycle. Chen et al (2003) got similar trends during adsorption of Cu^{2+} by active carbon and attributed it to desorption of Cu^{2+} ions from surface-metal complexes. Dimitrova (2002) observed the same trends for adsorption of Ni^{2+} and Cd^{2+} by blast furnace slag (BFS) adsorbent material and suggested that the phenomenon may be associated with ion exchange or adsorption mechanisms, and ruled out precipitation.

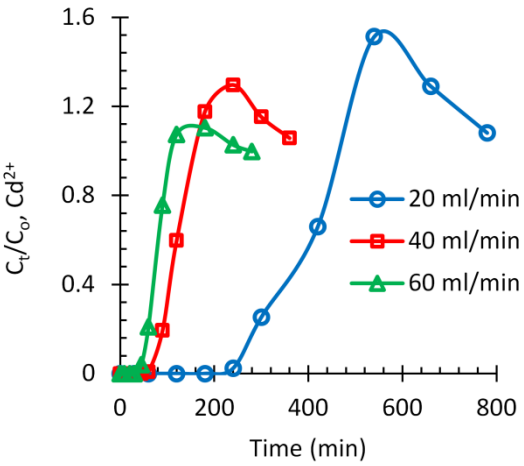

(A) Cd^{2+}

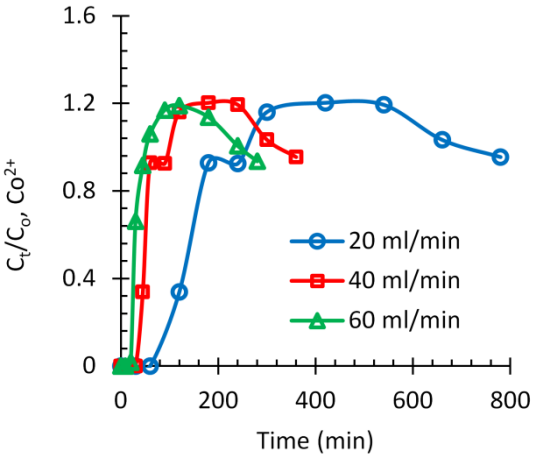

(B) Co^{2+}

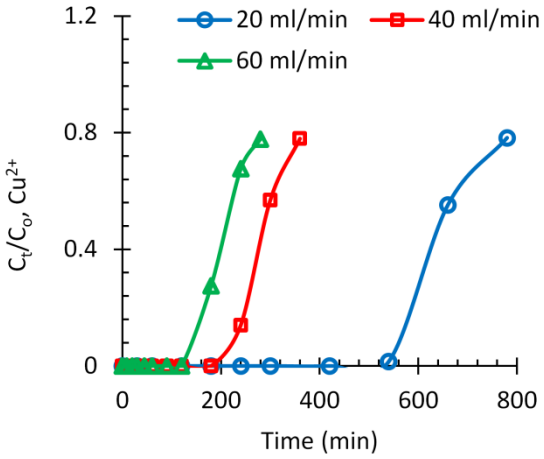

(C) Cu^{2+}

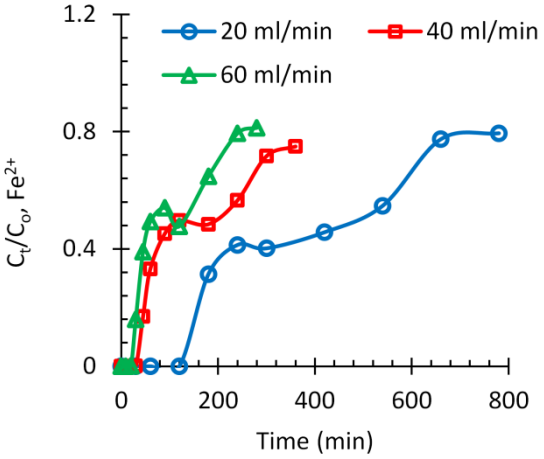

(D) Fe^{2+}

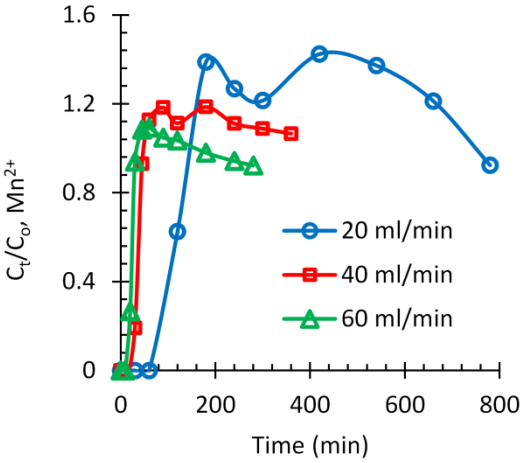

(E) Mn^{2+}

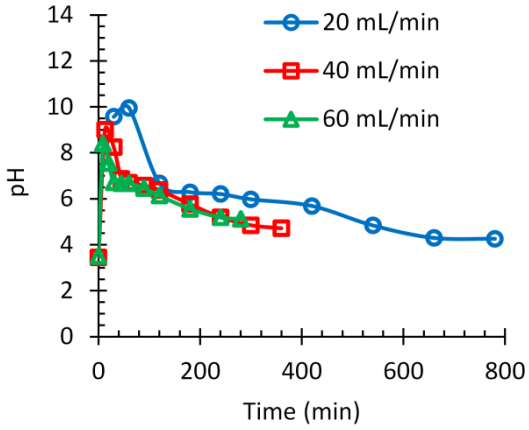

(F)

Figure 7.2: Breakthrough curves for solid phase extraction of metal ions as a function of flow rate on adsorption bed performance (A-E) & effluent pH variation (F), bed height = 52.5 cm.

In Figure 7.2, there was an initially non selective adsorption of all metal ions within the first 60 minutes at the lowest feed rate (20 mL/min) to produce a column discharge that was free of metal ions, which meets the primary objective of waste water purification plant. However, as more waste solution was treated, Mn^{2+} was the earliest ion to leak out of the column followed by Co^{2+}, Fe^{2+}, Cd^{2+} and Cu^{2+} ions, whose concentration levels increased

steeply with time in the effluent after the breakthrough point. The preferential sequence of adsorption was proposed as $Cu^{2+} > Cd^{2+} > Fe^{2+} > Co^{2+} > Mn^{2+}$. This series differs from that of batch adsorption results that were obtained. The shift in selectivity may be due to re-solubilisation and elution of precipitates of mostly Fe^{2+} ions followed by that of Cu^{2+} ions around adsorbent particle surfaces as adsorption progressed, possibly due to dynamic changes in flow regimes in the fixed beds relative to the agitated vessels. Selective adsorption of Cu^{2+} was noted with about 11.0 Litres of solution treated at breakthrough point, which suggests that adsorptive separations of metal ions of interest may be feasible. The results of this study are in agreement with results obtained by Mohan and Chander (2001) who conducted column tests to treat synthetic acid mine drainage with active carbon under similar conditions.

An increase in the flow rate of influent solution to the column shifts the relative position of breakthrough curves for individual metal ions to the left. Thus, the flow rate affects the contact time between the solution and adsorbent particles in the bed. Therefore, the effect of higher flow rates is that of a reduction in empty bed contact time (EBCT) or residence time leading to shorter breakthrough times (Table 7.1). This has an effect on the efficiency of adsorption of metal ions as noted in a study by Motsi (2010) for adsorption of metal ions by zeolites. A quantitative analysis of the performance of the column is summarised in Table 7.1 below. The lowest flow rate at 20 mL/min resulted in longest EBCT and breakthrough times for metal ions relative to higher flow rates. Consequently, a large volume of waste solution was treated to give a higher column adsorption capacity. Therefore, these values mean that the use of much lower flow rates increase the effectiveness of BFS adsorbent by increasing the volume of waste solution treated and quantities of metal ions extracted. This also increases the utilisation rate and efficiency of the adsorbent. A longer residence time

therefore provides an opportunity for intraparticle diffusion of metal ions to access more adsorption sites throughout the adsorbent structure.

Column capacity at 20 mL/min feed rate was about 24-40 % greater than that at 40 mL/min for the different metal ions. Dimitrova (2002) studied effect of flow velocity on Pb^{2+} ion adsorption by BFS in fixed bed column and obtained similar results. This is because a low flow rate increases contact time for solution/adsorbent interfaces to give an opportunity for the adsorption system to approach equilibrium and increase adsorption efficiency of metal ions. However, there was no significant difference in performance between the other two higher flow rate values of 40 and 60 mL/min flow rates. A breakthrough point of $C_e/C_o = 0.05$ sets about 1.0 mg/L for Mn^{2+} ions in the treated effluent, which is the acceptable upper discharge limit for the Zambian environmental standards (EPPCA, 1990). At this reference breakthrough point, final concentrations of other metal ions were below detection limits, with up to 1.3 Litres of solution treated. As shown in Table 7.1 below, a much larger volume can be treated before BFS is exhausted. The regeneration ability of spent BFS was studied and results are discussed in subsequent sections.

Figure 7.2 (F) above shows the evolution of pH with time, also as a function of flow rate. The lower the flow rate the higher the hydrolysis of slag and pH, whereby more OH^- ions are released to drive pH into the alkaline range (Section 6.3.5, Chapter 6). As shown in Table 7.1 below, a low flow rate and an alkaline pH supports a large volume of solution to be purified and thus a high degree of adsorption of metal ions which confirms the results of batch adsorption studies presented in Chapters 5 and 6 of this thesis. Near the end of the adsorption cycle, the bed is saturated and therefore adsorption and acid neutralisation

capacity of slag adsorbent material is exhausted and effluent pH decreases and approaches influent value.

The lengths of unused bed (LUB) generally increased with increase in flow rate (Table 7.1) possibly due to insufficient adsorbent/solution contact time leading to premature (early) breakthrough and reduced adsorption efficiency. Therefore, optimisation of the flow rate is necessary.

Table 7.1: Effect of flow rate on column performance at breakthrough (C_t/C_o = 0.05) and exhaustion points (C_t/C_o = 0.90), bed height = 52.5 cm, Adsorbent mass = 856 ± 6 g

Experimental conditions				**Breakthrough point**			**Exhaustion point**			
Metal ions	**Influent Conc., (mg/L)**	**Flow rate, Q (mL/min)**	**EBCT, (min)**	**t_b, (min)**	**Vol. Treated, V_b, (L)**	**q_b, (mg/g)**	**t_e, (min)**	**Vol. Treated, V_e (L)**	**q_e, (mg/g)**	**LUB (cm)**
Cd^{2+}	40.7	20	40.0	250	5.0	0.236	450	9.0	0.424	23.3
	40.9	40	20.0	70	2.8	0.134	150	6.0	0.287	28.0
	40.2	60	13.3	45	2.7	0.128	100	6.0	0.284	28.9
Co^{2+}	31.0	20	40.0	70	1.4	0.050	175	3.5	0.126	31.5
	27.2	40	20.0	30	1.2	0.038	45	1.8	0.057	17.5
	26.7	60	13.3	20	1.2	0.038	45	2.7	0.085	29.2
Cu^{2+}	289.0	20	40.0	550	11.0	3.684	> 780	> 15.6	> 5.22	15.5
	260.1	40	20.0	215	8.6	2.619	> 360	> 14.4	> 4.39	21.1
	261.1	60	13.3	135	8.1	2.488	> 280	> 16.8	> 5.16	27.2
Fe^{2+}	446.6	20	40.0	130	2.6	1.345	> 780	> 15.6	> 8.07	43.8
	427.9	40	20.0	35	1.4	0.701	> 360	> 14.4	> 7.22	47.4
	426.6	60	13.3	25	1.5	0.753	> 280	> 16.8	> 8.43	47.8
Mn^{2+}	18.1	20	40.0	65	1.3	0.027	140	2.8	0.059	28.1
	20.3	40	20.0	20	0.8	0.019	45	1.8	0.043	29.2
	20.7	60	13.3	10	0.6	0.015	30	1.8	0.044	35.0

7.3.2 Effect of Bed Height

The effect of bed height on adsorption performance of the column packed with BFS was carried out at 27.5, 52.5 and 80.0 cm to treat an acidic waste solution (pH 3.50) containing multiple metal ions of 40 mg/L Cd^{2+}, 30 mg/L Co^{2+}, 250 mg/L Cu^{2+}, 400 mg/L Fe^{2+} and 20 mg/L Mn^{2+}. The breakthrough curves for the individual metal ions as a function of bed height are shown in Figure 7.2 and a summary of adsorption results is given in Table 7.3.

Bed height had a similar effect to that of volumetric flow rate on the extent of adsorption of metal ions. All metal ions were extracted without selectivity up to the breakthrough point as defined by C_e/C_o = 0.05 for Mn^{2+} ion. This gave a column effluent either without metal ions (below detection) or within consent discharge limits. With continued adsorption beyond the breakthrough point, metal ions began to leak and appear in the effluent sequentially whereby Mn^{2+} was always the earliest ion to leak out of the column followed by Co^{2+}, Fe^{2+}, Cd^{2+} and Cu^{2+} ions. As shown in Figure 7.3 below, the breakthrough curves are shifted to the right as the height of the bed is increased. The larger the bed height, the longer the breakthrough, EBCT, contact times and hence more waste solution is treated. This is because an increase in bed height by the addition of more adsorbent mass is expected to increase surface area and adsorption sites that support large amounts of metal ions to be extracted. Motsi (2010) found similar results for the adsorption of Fe^{2+} and Zn^{2+} by natural zeolite. Furthermore, higher EBCT improved Cu^{2+} adsorption by activated carbon as result of longer residence time between solution/carbon contacts (Chen et al., 2003). As shown in Table 7.2, the volume of purified solution for Cd^{2+}, Cu^{2+} and Fe^{2+} nearly increased by 50 % as the bed height was changed by 27.5 cm upward increments. However, there were marginal increases in values of adsorption capacity at the breakthrough point.

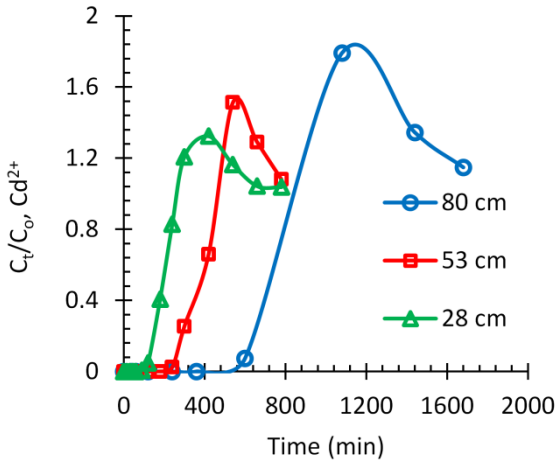

(A) Cd^{2+}

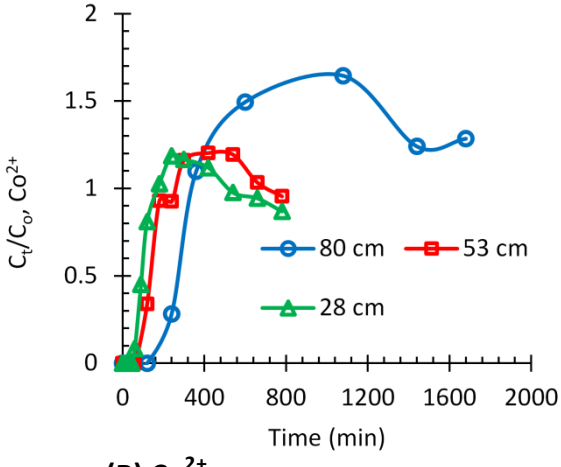

(B) Co^{2+}

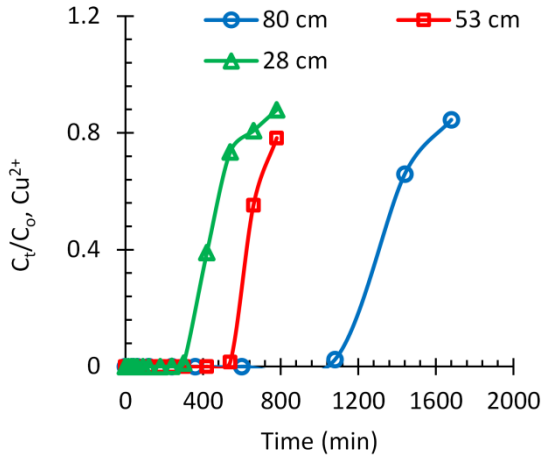

(C) Cu^{2+}

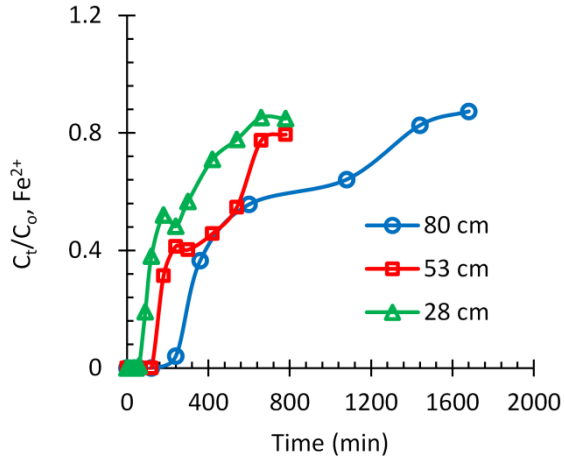

(d) Fe^{2+}

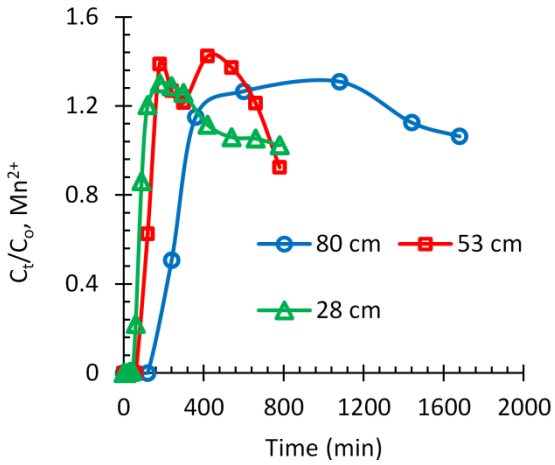

(E) Mn^{2+}

Figure 7.3: Breakthrough curves for solid phase extraction of metal ions as a function of bed height on adsorption column performance, flow rate = 20 mL/min (A-E).

The effect of bed height on column performance is also summarised in Table 7.2 below. At the highest bed height (80.0 cm), EBCT, breakthrough and adsorbent exhaustion times are longest that facilitated a large volume of waste solution to be treated. Since concentration of metal ions in this study are two or three times higher than reported figures in acid mine drainages of Zambian Copperbelt, a large volume of solution is expected to be purified if the concentration levels of metal ions are relatively low. This is because characterisation results in Chapter 4 of this thesis, i.e., surface area, pore size distribution and other key adsorbent properties of BFS material were found to be low. It can also be seen in Table 7.2 that longer beds result in greater fraction of the bed to be utilised and therefore increases the effectiveness of BFS.

Table 7.2: Estimated fixed bed adsorption performance for the effect of bed height at breakthrough (C_t/C_o = 0.05) and exhaustion points (C_t/C_o = 0.90), flow rate = 20 mL/min

Experimental conditions				**Breakthrough point**			**Exhaustion point**			
Metal ions	**Influent Conc., (mg/L)**	**Bed Height, (cm)**	**EBCT, (min)**	**t_b, (min)**	**Vol. Treated, V_b, (L)**	**q_b, (mg/g)**	**t_e, (min)**	**Vol. Treated, V_e (L)**	**q_e, (mg/g)**	**LUB (cm)**
Cd^{2+}	42.3	27.5	20.9	120	2.4	0.208	250	5.0	0.433	14.3
	40.7	52.5	40.0	250	5.0	0.236	450	9.0	0.424	23.3
	39.3	80.0	60.8	590	11.8	0.351	820	16.4	0.488	22.4
Co^{2+}	30.2	27.5	20.9	55	1.1	0.068	140	2.8	0.173	16.7
	31.0	52.5	40.0	70	1.4	0.050	175	3.5	0.126	31.5
	28.2	80.0	60.8	150	3.0	0.064	320	6.4	0.137	42.5
Cu^{2+}	283.0	27.5	20.9	315	6.3	3.653	>780	>15.6	>9.047	16.4
	289.0	52.5	40.0	550	11.0	3.684	>780	>15.6	>5.224	15.5
	272.2	80.0	60.8	1110	22.2	4.578	>1680	>33.6	>6.929	27.1
Fe^{2+}	440.0	27.5	20.9	70	1.4	1.262	>780	>15.6	14.066	25.0
	446.6	52.5	40.0	130	2.6	1.345	>780	>15.6	8.073	43.8
	423.1	80.0	60.8	250	5.0	1.603	>1680	>33.6	10.770	68.1
Mn^{2+}	21.4	27.5	20.9	50	1.0	0.044	95	1.9	0.083	13.0
	18.1	52.5	40.0	65	1.3	0.027	140	2.8	0.059	28.1
	19.6	80.0	60.8	140	2.8	0.042	300	6.0	0.089	42.7

7.3.3 Adsorbent Regeneration

Two (2) cycles of adsorption and desorption with a wash cycle were carried out in a system of multiple metal ions of 40 mg/L Cd^{2+}, 30 mg/L Co^{2+}, 250 mg/L Cu^{2+}, 400 mg/L Fe^{2+} and 20 mg/L Mn^{2+} ions at pH 3.50, flow rate of 20 ml/min, bed height of 52 cm to investigate the regeneration ability of BFS. The first adsorption cycle was followed by stripping of metal ions from BFS surfaces by dilute sulphuric acid in an attempt to regenerate the spent adsorbent (slag material) for the next adsorption cycle. The effect of acid strength at 0.4 and 2.0 % w/w on the extent of desorption was also investigated. The column was then subjected to a wash cycle using distilled water after desorption. This was followed by second adsorption cycle under same conditions. However, the second stripping cycle was not successful because the solid bed had compacted, preventing the flow of stripping solution through it.

7.3.3.1 Adsorption Cycles

The quantity of metal ions adsorbed (m_{ads}) was calculated by using Equation (7.6) below. The integral was computed as the area above the breakthrough curve (Concentration (C_t) versus time (t) graph) by trapezoidal rule approximation (Aksu and Gonen, 2004).

$$m_{ads} = Q \int_0^t C_t \, dt \qquad \text{---} \qquad (7.6)$$

The total amount of metal ions fed to the column (m_{total}) was calculated as

$$m_{total} = \frac{QtC_o}{1000} \qquad \text{---} \qquad (7.7)$$

Therefore, quantity of metal ions extracted by adsorption is;

$$Adsorption, \% = \frac{m_{ads}}{m_{total}} \times 100 \quad \text{---} \quad (7.8)$$

Where C_o = initial solution concentration (mg/L), Q = volumetric flow rate (mL/min), and t = total adsorption time (min), C_t = solute concentration (mg/L) as a function of time.

Figure 7.4 below gives the breakthrough curves of solid phase extraction of metal ions from solution depicting two cycles of adsorption by fresh BFS (Cycle 1) and chemically regenerated BFS (Cycle 2). The estimated breakthrough response variables for the fixed bed adsorption performance are presented in Table 7.3a below. There is a significant loss of adsorption capacity at breakthrough of approximately 90 % Cd^{2+}, 76 % Co^{2+}, 90 % Cu^{2+}, 77 % Fe^{2+} and 77 % Mn^{2+} between the two cycles as shown in Table 7.3. The breakthrough time is shortened leading to low volume of solution to be purified during cycle 2. Comparatively, a 5-9 % decrease in the second adsorption cycle of several metal ions at 5 mg/L in the feed solutions by zeolites in fixed bed column study with empty bed contact time (EBCT) of 11.5 min has been reported (Nguyen et al., 2015). The zeolite results are expected since most studies involving zeolites as adsorbents have reported larger specific surface area than slag materials and thus they perform relatively better.

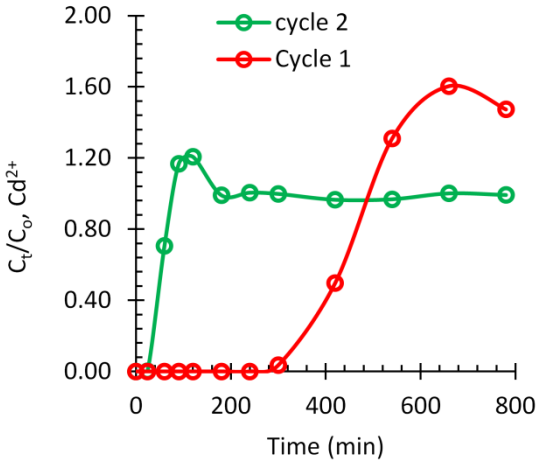

(A) Cd^{2+}

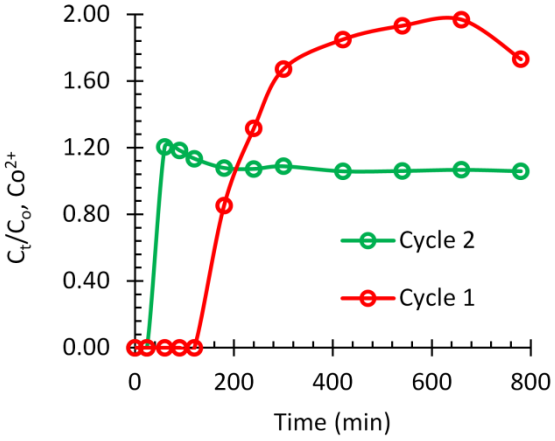

(B) Co^{2+}

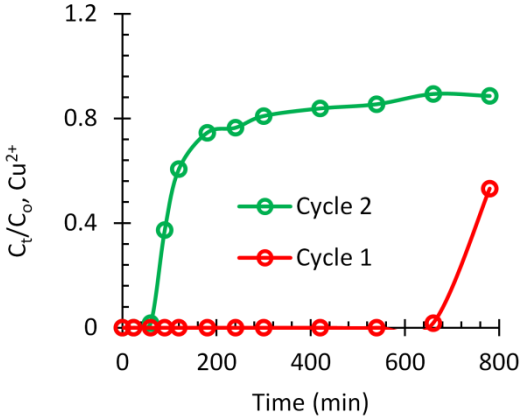

(C) Cu^{2+}

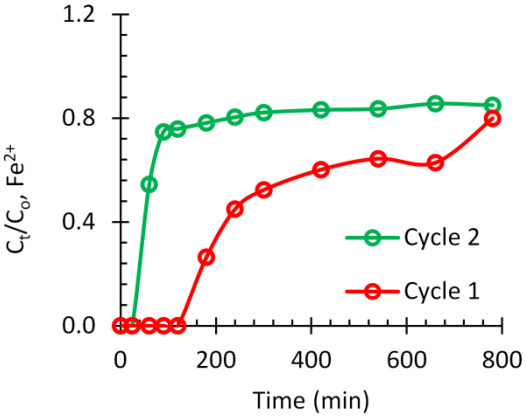

(D) Fe^{2+}

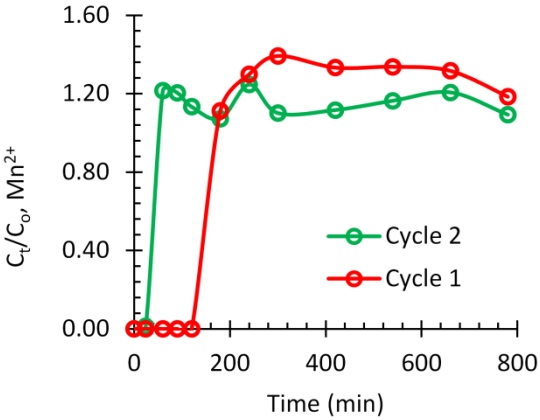

(E) Mn^{2+}

Figure 7.4: Breakthrough curves of solid phase extraction of metal ions depicting two cycles of adsorption by fresh (Cycle 1) & chemically regenerated BFS (Cycle 2), flow rate = 20 mL/min

As shown in Table 7.3 (a) and (b) below, adsorption capacity, adsorption efficiency and acid neutralisation capacity decreased significantly in the second cycle. Such a huge loss in adsorption efficiency may be due to the loss of some lime from the adsorbent matrix responsible for control of pH towards alkaline range that favours high adsorption of metal ions. It is also possible that adsorption of H^+ ions from sulphuric acid that was used as a regenerating solution may have rendered adsorption sites to be unavailable to metal ions (Gao et al., 1995b). As discussed further in the next section, the results of this study suggest a limited ability for BFS to be regenerated by H_2SO_4 solution although more extensive studies are needed that involve other reagents at different strengths.

Table 7.3 (a): Fixed bed adsorption performance by fresh BFS adsorbent (Cycle 1) & chemically regenerated BFS (Cycle 2) at the breakthrough point (C_t/C_o = 0.05), flow rate = 20 mL/min, Adsorbent mass = 864 g

Experimental conditions				**Breakthrough point**			
Metal ions	**Influent Conc., C_i, (mg/L)**	**No. of Adsorption Cycles**	**EBCT, (min)**	**t_b, (min)**	**Vol. Treated, V_b, (L)**	**q_b, (mg/g)**	**Loss in adsorption capacity between Cycles 1 & 2, (%)**
Cd^{2+}	37.7	Cycle 1	40	305	6.1	0.266	90 %
	38.6	Cycle 2	40	30	0.6	0.027	
Co^{2+}	27.1	Cycle 1	40	125	2.5	0.078	76 %
	32.6	Cycle 2	40	30	0.6	0.023	
Cu^{2+}	249.8	Cycle 1	40	670	13.4	3.874	90 %
	254.2	Cycle 2	40	65	1.3	0.382	
Fe^{2+}	405.1	Cycle 1	40	130	2.6	1.219	77 %
	395.8	Cycle 2	40	30	0.6	0.275	
Mn^{2+}	19.4	Cycle 1	40	125	2.5	0.056	77 %
	18.7	Cycle 2	40	30	0.6	0.013	

Table 7.3 (b): Efficiency of adsorption cycles by fresh BFS adsorbent (Cycle 1) & chemically regenerated BFS (Cycle 2), bed height = 52.5 cm, flow rate = 20 mL/min

Experimental conditions				Efficiency of adsorption cycles	
Metal ions	**Influent conc., C_o, (mg/L)**	**No. of adsorption cycle**	**Mass Adsorbed (mg)**	**Mass fed to the column (mg)**	**Adsorption efficiency (%)**
Cd^{2+}	37.70	Cycle 1	550.4	588.1	93.6
	38.61	Cycle 2	51.2	602.2	8.5
Co^{2+}	27.14	Cycle 1	240.0	422.8	56.8
	32.63	Cycle 2	32.0	508.6	6.3
Cu^{2+}	249.81	Cycle 1	3750.4	3896.9	96.2
	254.21	Cycle 2	627.2	3965.5	15.8
Fe^{2+}	405.06	Cycle 1	3360.0	6319.6	53.0
	395.79	Cycle 2	537.6	6174.5	25.3
Mn^{2+}	19.43	Cycle 1	86.4	302.6	28.5
	18.73	Cycle 2	19.2	291.7	6.6

Another interesting aspect of these results is that BFS material can selectively extract large quantities of Cu^{2+}, Cd^{2+} and Fe^{2+} ions relative to Co^{2+} and Mn^{2+} in the first adsorption cycle. It is proposed that the use of several adsorption columns in a parallel configuration and fed at different flow rates to attain differential or selective adsorption by increasing contact time for metal ion(s) of interest in any of the columns is likely to significantly increase the volume of waste solution treated per unit time. The use of columns in series that provide a longer residence time might also achieve the similar results.

The adsorption characteristics of BFS material is comparable to results for adsorption of metal ions from synthetic as well as Wheal Jane's actual acid mine drainage by natural zeolites (Motsi, 2009) and basic oxygen sludge (Jafaripour, 2013). Motsi (2010) found

adsorption of Cu^{2+} and Fe^{2+} in fixed beds by natural zeolite to be selective and higher than that of Mn^{2+} and other ions. Jafaripour (2013) employed a modified adsorption column set up that was packed with powdered basic oxygen furnace sludge (BOS) to simulate a passive treatment process for acid mine drainage and reported high adsorption of Cu^{2+} and Fe^{2+} whose final concentration levels fell within discharge limits except Mn^{2+} ions. The challenge lies in how to improve Mn^{2+} ions adsorption to satisfactory levels.

7.3.3.2 Desorption Cycles

Among the characteristic requirements of any adsorbent is the capability to be regenerated. A variety of chemical and thermal regeneration techniques for carbon adsorbents are available (Deng, 2006; McCabe et al., 1993; Seader et al., 2011). Understanding the process conditions under which multiple or selective desorption of metal ions from the adsorbent surface is achievable is important in order to use the adsorbent multiple times before it becomes a spent material. Also, an effective desorption or metal stripping step can provide an opportunity to recover metals by such processes as solvent extraction, cementation, gaseous sulphide precipitation by H_2S and electrolytic reduction in order to give a saleable or recycled metal product.

The quantity of metal ions desorbed (m_{des}) was approximated by calculating the area under the elution curve (conc., vs. time) using Equation (7.9). The mass of ions adsorbed was calculated by Equation (7.6), given in Section 7.3.3.1. Thus, elution efficiency (E, %) was subsequently calculated by using Equation (7.9).

$$m_{des} = Q \int_0^t C_t dt$$

--- (7.9)

$$Elution\ efficiency\ (E), \% = \frac{m_{des}}{m_{ads}} \times 100$$

--- (7.10)

Desorption step attempts to transfer adsorbates from adsorbent surfaces back into solution (reverse of adsorption) suitable for recycle, confinement or reductive recovery of metals. The effectiveness of sulphuric acid as a stripping agent was assessed and the effect of its concentration on the extent of desorption of metal ions are given in elution curves in Figure 7.5. There was a rapid increase in concentration of metal ions in the eluant with the time to some maximum values relative to their respective influent values. The rate of desorption of ions later decreased owing to the decrease in adsorbed species within the adsorbent matrix. The use of a more concentrated sulphuric acid solution produced faster desorption kinetics and gave a smaller volume of concentrated solution of metal ions. At relatively high acid strength, more Cd^{2+}, Cu^{2+} and Co^{2+} ions were stripped off adsorbent surfaces within a short time while Fe^{2+} and Mn^{2+} appeared to require much longer time. Also, an even much longer time was required, especially for Mn^{2+} when low concentration of acid was used. The results from batch adsorption studies in this thesis suggested one of the adsorption mechanisms of ion attachment to the adsorbent sites is chemisorption whose strong chemical bonds may be difficult to reverse during desorption step.

Dimitrova (2002) used 0.01 M HNO_3 and $NaNO_3$ to strip Pb^{2+} ions from BFS surface in a fixed bed column to get 68 % desorption efficiency. The findings that the limited ability of BFS adsorbent material to be regenerated in this study support earlier views by Dimitrova (2002)

who suggested that loaded slag should not be regenerated on account of dissolution of some slag chemical phases when more concentrated strip solutions were used.

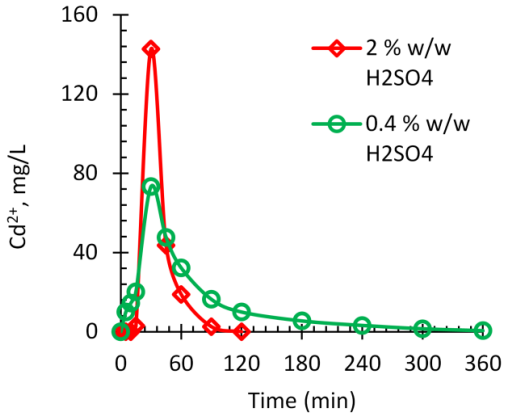

(A) Cd^{2+}

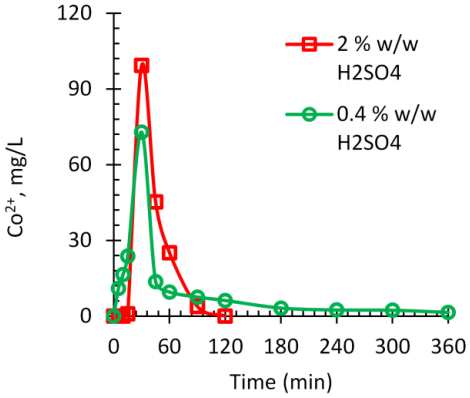

(B) Co^{2+}

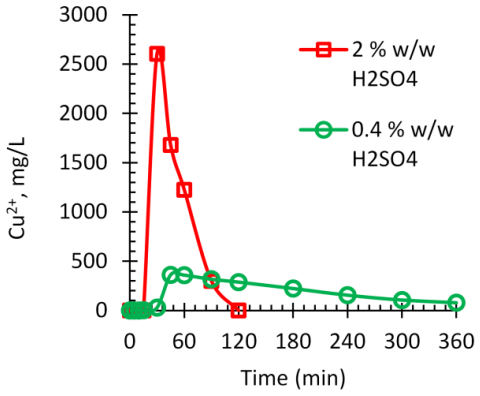

(C) Cu^{2+}

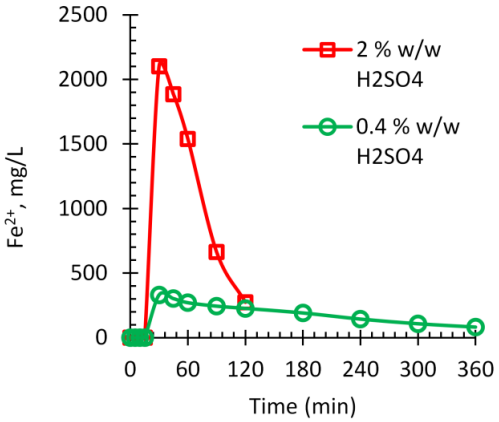

(D) Fe^{2+}

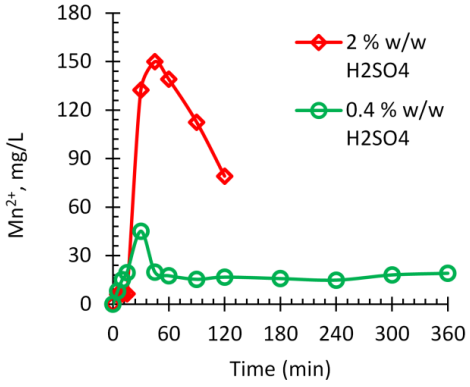

(E) Mn^{2+}

Figure 7.5: Effect of sulphuric acid strength on the extent of desorption of metal ions from BFS surface, acid flow rate = 20 mL/min, fixed bed height = 52.5 cm.

The use of sulphuric acid at high concentration produced higher efficiency of desorption and faster kinetics than acid solution at low concentration as shown in Table 7.4. The large decrease in desorption efficiency may be partly due to the formation of chemical adsorption bonds that are difficult to reverse by contact with acid solution at low strength. This means that in order to successfully strip metal ions from BFS surfaces, a regenerating acid solution at relatively high concentration is required. However, the dissolution of certain BFS components such as Mn^{2+} ions and emission of H_2S gas during desorption pauses some challenges and limits acid concentration that can be employed. In Table 7.4, the concentration of Mn^{2+} ions in solution increased by approximately 1.5-3.0 times when compared to the quantities that could have been desorbed from BFS surface. This is evidence that in addition to Mn^{2+} ions being successfully desorbed from surfaces, additional Mn^{2+} ions are solubilised from BFS material. Therefore, further adsorption/desorption studies are needed that involve different reagents at different strengths (e.g., EDTA) in order to improve desorption and BFS regeneration efficiency and limit Mn^{2+} dissolution.

Table 7.4: Efficiency of desorption cycles as a function of concentration of stripping solution; bed height = 52.5 cm, flow rate = 20 mL/min

Experimental conditions				Efficiency of desorption cycles		
Metal ions	**No. of desorption cycle**	**Strength of strip solution (H_2SO_4), (% w/w)**	**Influent conc., C_o, (mg/L)**	**Mass Adsorbed, (m_{ad}),(mg)**	**Mass desorbed, (m_d) (mg)**	**desorption efficiency (%)**
Cd^{2+}	Cycle 1	2.0	40.66	525.6	482.0	91.7
	Cycle 2	0.4	37.70	550.4	94.1	17.1
Co^{2+}	Cycle 1	2.0	30.95	80.8	56.9	70.4
	Cycle 2	0.4	27.14	240.0	59.5	24.8
Cu^{2+}	Cycle 1	2.0	289.02	3250.0	2899	89.2
	Cycle 2	0.4	249.81	3750.0	1338.0	35.7
Fe^{2+}	Cycle 1	2.0	446.64	2500.0	2400	96
	Cycle 2	0.4	405.06	3360.0	1266.0	37.7
$^{\#}Mn^{2+}$	Cycle 1	2.0	18.09	62.4	$185.76^{\#}$	-
	Cycle 2	0.4	19.43	86.4	$130.56^{\#}$	-

#Higher Mn^{2+} ion concentration in solution than initially adsorbed is attributed to both desorption and dissolution from BFS adsorbent matrix.

The results in general have provided evidence that desorption of metal ions from the slag surfaces is feasible and satisfactory. However, because of the limited ability of the slag material to be regenerated, the objective of any desorption step may be for metal recovery by such processes as electrolysis, cementation, etc., rather than adsorbent regeneration. In this way, the spent adsorbent (slag materials) can be disposed of in designated landfills without the risk of dissolution of metal ions.

7.3.4 BDST Model Analysis

There are several mathematical models that are used to analyse data and predict solute adsorption for scale up of fixed bed adsorption systems (Inglezakis & Poulopoulos, 2006a). This study employed well known bed depth service time (BDST) theory to analyse

experimental data in order to fundamentally understand the adsorption process under the employed conditions. BDST is among most widely used models to predict the relationship between column bed height and service time due to its relative simplicity. The BDST expression and its simplified form are given in Equations (7.11) and (7.12) below (Bohart and Adams, 1920; Hutchins, 1974). BDST proposes that the rate of solute adsorption is limited by the surface reaction between the adsorbate and unused adsorbent capacity, and ignores mass transfer resistive effects (Inglezakis & Poulopoulos, 2006a).

$$In\left(\frac{C_o}{C_b}-1\right)=ln\left[exp\left(\frac{K_aN_oZ}{u}\right)-1\right]-K_aC_ot$$

--- (7.11)

$$t=\frac{N_oZ}{C_ou}-\frac{1}{K_aC_o}ln\left(\frac{C_O}{C_b}-1\right) \quad \rightarrow \quad t=mZ-b$$

--- (7.12)

Where C_o, C_b = initial and breakthrough solute concentration respectively (mg/L); N_o = dynamic adsorption capacity of bed (mg/L); u = linear velocity (cm/min); K_a is the adsorption rate constant (L/(mg min)) and Z = column bed depth (cm); t = service time at breakthrough point (min).

A plot of time (t) against bed height (Z) should be linear from which the dynamic adsorption capacity (N_o) and the adsorption rate constant (K) can be calculated using the slope (*m*) and intercept (*b*) values. Therefore, the breakthrough service time (t_b) can be predicted by specifying bed depth (Z) and other adsorption process variables involved.

A plot of bed height against service time for the adsorption system under investigation is shown in Figure 7.6. The regression coefficients ($R^2 > 0.950$) for Cd^{2+}, Cu^{2+} and Fe^{2+} are low but indicative of a linear bed depth/service time relationship within experimental uncertainty. However, much lower R^2 values for Co^{2+} and Mn^{2+} ions suggest more data is necessary. Table 7.5 gives the calculated values of dynamic adsorption capacity (N_o) and adsorption rate constant (K_a) at 5 % breakthrough. The critical depth (Z_o), theoretical depth to prevent solute concentration exceeding the breakthrough value, C_b, was also determined by using Equation (7.12) at time (t) equal to zero (0). A critical bed depth of < 10 % of the total bed height indicates a column that is working efficiently and enables scale up. The values reported here fell short of this guideline but give insight into the feasibility of the process. High K_a values for Cu^{2+} and Fe^{2+} confirms a high affinity of adsorption for these ions by BFS material as reported in batch adsorption experiments. A low K_a value requires a much longer bed to prevent premature breakthrough. Thus BDST model parameters can be used to scale up the process at other flow rates without further experiments.

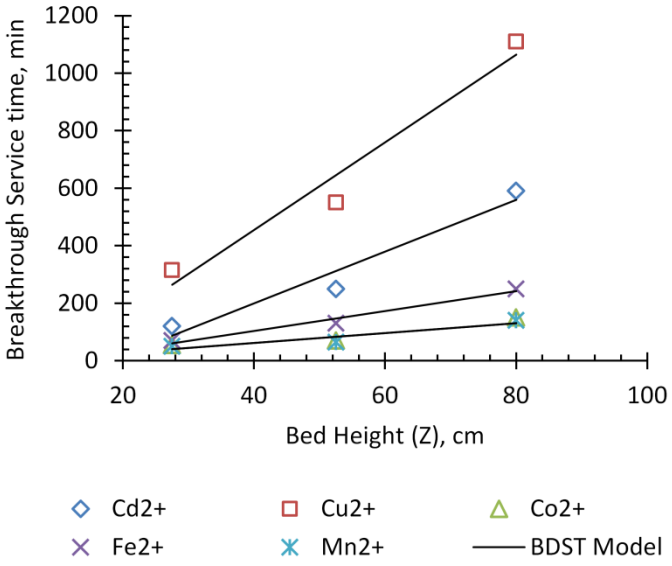

Figure 7.6: Linearised BDST model fitted to adsorption data of multiple metal ions at breakthrough (C_b/C_o) = 5 %, u = 1.315 cm/min, Internal column diameter = 4.4 cm, pH 3.50

Table 7.5: Estimated BDST model parameters for adsorption data of multiple metal ions at breakthrough (C_b/C_o) = 5 %, u = 20 mL/min, Internal column diameter = 4.4 cm, pH 3.50

Metal ions	K, x 10^{-4} (L/mg min)	N_o (mg/L)	Z_o (cm)	R^2
Cd^{2+}	4.45	483.0	17.8	0.950
Co^{2+}	0.017	71.6	3.2	0.883
Cu^{2+}	68.0	5635.7	10.1	0.959
Fe^{2+}	2.00	1977.2	9.8	0.974
Mn^{2+}	0.020	44.8	4.2	0.889

7.4 Conclusions

The application of a fixed bed adsorption column to treat waste solutions that simulated the chemical composition of acid mine drainage has been demonstrated in this study. The effects of bed height and flow rate on adsorption behaviour of multiple metal ions and the capability of the BFS adsorbent material to be regenerated were studied.

The extraction efficiencies results of up to 93.6 % Cd^{2+}, 56.8 % Co^{2+}, 96.2 % Cu^{2+}, 53.0 % Fe^{2+} and 28.5 % Mn^{2+} by fresh BFS material indicate that it can be an effective adsorbent in fixed bed adsorption systems to purify waste solutions under continuous flow operation by extracting metal ions and neutralising acidity levels to meet environmental discharge limits. However, the adsorbent was easily exhausted and thus adsorption cycle time is limited. Optimisation of process variables, such as use of low flow rates and high bed heights can increase the effectiveness of BFS material by providing longer adsorbent/solution contact time that facilitates adsorption equilibrium to be attained. This can increase adsorption

capacity and efficiency, that is, more volume of waste solution can be purified with large quantities of metal ions extracted. The results also indicate that BFS material can selectively extract relatively large quantities of Cu^{2+}, Fe^{2+} and Cd^{2+}. It was therefore assumed that any experimental design setup that involves multiple columns to incorporate differential or selective adsorption of these metal ions may improve the efficiency and capacity of the BFS material and increase the volume of waste solution that can be treated. The linear relationship for the bed depth/service time obtained using bed depth service time (BDST) model gives the validity of data for a potential scale up.

The significantly high loss of adsorptive performance during second adsorption cycle at breakthrough point (C_e/C_o = 0.05) after regeneration step with dilute sulphuric acid solution suggests a limited ability for the BFS material to be regenerated although more studies are necessary. The use of other acids as stripping solutions ($NaNO_3$ and HNO_3) were equally ineffective in other reported studies. Interestingly, desorption of metal ions from BFS material appears highly favourable. This may provide an opportunity for metal ions in the stripping solution to be recovered as saleable/recycled products and also for the spent adsorbent to be safely disposed of in designated landfills without risk of solubilisation of metal ions.

The dissolution of Mn^{2+} ions and emission of trace H_2S gas from BFS material during desorption cycle with sulphuric acid solution pause some challenges. One proposal would be to test different reagents at different strengths such as weak organic acids (e.g., EDTA) in order to improve desorption and BFS regeneration efficiency and limit Mn^{2+} dissolution. It is also recommended that more extensive investigations that involve the effects of

concentration of metal ions, particle size, column diameter and other variables on the efficiency of BFS material be conducted under continuous flow adsorption conditions. As already suggested for batch adsorption experiments, the efficiency of BFS material should also be studied using actual acid mine drainage from different mine sites containing multiple metal ions of wide concentration range and acidity.

CHAPTER 8
CONCLUSIONS AND RECOMMENDATIONS

8.1 Conclusions

This study has investigated the potential of developing adsorbents from BFS and EAF materials as a low cost method to purify AMD. The experimental framework included a detailed characterisation, assessment and improvement of key adsorptive characteristics of BFS and EAF materials. This was followed by batch experiments to understand the adsorption behaviour of a multicomponent system of Cd^{2+}, Co^{2+}, Cu^{2+}, Fe^{2+} and Mn^{2+} ions in terms of efficiency, kinetics, adsorbent capacity and adsorption mechanisms. The feasibility of a scale up of the adsorption process was also assessed in fixed bed columns. The main findings and conclusions drawn from this investigation are presented below.

8.1.1 Characteristics of BFS and EAF Adsorbent Materials

From XRD spectra, both BFS and EAF materials are mainly amorphous with minor crystalline phases of $CaCO_3$ and Fe_2O_3 respectively. XRF analysis showed that about 90 % of BFS is composed of CaO, SiO_2, Al_2O_3 and MgO. The high CaO content at 44 % for BFS implies that it has the capacity to neutralise AMD and precipitate metal ions. Both mercury porosimetry and N_2 gas adsorption measurements revealed that the adsorbent materials were largely macroporous. The intrusion/extrusion graphs indicated that the majority of pore sizes/pore volume occurred in the range 50-3000 nm. A BET surface area of less than 3 m^2/g for the slag materials is low relative to current adsorbents that have in excess of 300 m^2/g although porosity at 55-60 % is comparatively satisfactory. Further, they have inferior pore structure,

pore size distribution and low surface area which limit their effectiveness in adsorption systems of high solute concentration. The powdered BFS showed superior characteristics to its granulated form. Thus, a particle size reduction may improve BFS properties although it requires a costly energy input.

8.1.1.1 BFS Activation

The pretreatment of BFS granules by leaching with HCl (aq) at pH 2-4 increased both pore volume and BET surface area by over three (3) times and the total pore area also doubled. This process can potentially produce a SiO_2-rich BFS product with a specific surface area of up to 400 m^2/g at about 80 % SiO_2 content. However, a heating process (at 25-800 ^oC) appeared to have destroyed the internal structure of the material whereby surface area decreased with increase in preheating temperature.

8.1.2 Batch adsorption equilibria, kinetics and efficiency

The results have provided some understanding of the effects of key variables on adsorption equilibria and kinetics of a metal/slag system as well as conditions under which complete adsorption of multiple metal ions is achievable or can be improved to meet the permissible discharge limits. By fitting several kinetic models to experimental data, adsorption capacity, overall adsorption rates and mechanisms have been evaluated.

8.1.2.1 Single Adsorbate Systems

A combination of fine size fraction BFS granules (0.18-0.36 mm, 30 g/L BFS, 100 mg/L metal ions) and high pH (≥ 3.5) resulted in 100 % adsorption for Cu^{2+}, Cd^{2+} and Fe^{2+} except Co^{2+}

and Mn^{2+} ions which were limited to 72 % and 57 % respectively. However, use of powdered BFS (d_p < 45 μm) resulted in instantaneous and complete adsorption of all metal ions. Also, complete adsorption (C_e < 5 mg/L) of Cd^{2+}, Cu^{2+} and Fe^{2+} by BFS granules is only achievable at pH ≥ 3.5 but complete adsorption of Co^{2+} and Mn^{2+} ions was difficult under most values of pH and particle sizes employed. Adsorption of all metal ions at pH 1.5 is poor due to competitive adsorptive effect of H^+ ion. This confirms the belief that solute adsorption is only effective in alkaline pH. Thus, an increase in initial pH or a decrease in particle size increased adsorption efficiency, adsorption capacity (q_e) and distribution coefficients (K_d). The highest q_e in single solutes were 1.60 mg/g Cd^{2+}, 1.28 mg/g Co^{2+}, 1.85 mg/g Cu^{2+}, 1.63 mg/g Fe^{2+} and 0.92 mg/g Mn^{2+} which compares favourably with literature values. From q_e and K_d, selectivity sequence is proposed as Fe^{2+}>Cu^{2+}>Cd^{2+}>Co^{2+}>Mn^{2+}. This adsorption behaviour highlights differences in adsorption characteristics of the five metal ions involved.

Comparatively, adsorption efficiency drastically reduced in multiadsorbates relative to single adsorbates, i.e., from 100 to 18 % Cd^{2+}, 87 to 7.6 % Co^{2+}, 100 to 96 % Cu^{2+}, 57 % to negligible value for Mn^{2+} but Fe^{2+} was unaffected at 100 % with BFS granules. This may be attributed to low surface area of BFS, competitive adsorptive effect among solutes and differences in metal ion characteristics. In conclusion, adsorption response of Cd^{2+}, Cu^{2+} and Fe^{2+} ions is high but Mn^{2+} and Co^{2+} ions are resistant to adsorption. Hence, adsorption of metal ions under a wide concentration range was investigated further in multiadsorbates systems.

8.1.2.2 Multiadsorbate systems

The pH had the greatest influence on adsorption efficiency of metal ions by slag materials. In dilute solutions of metal ions fixed at different initial concentration (< 200 mg/L), the

adsorption efficiency increased with increase in pH (1.5-7.5). A complete extraction of all metal ions is achievable at high pH, with metal hydroxide precipitation contributing up to 50-100 % for Cu^{2+} and Fe^{2+} at pH ≥ 5.5, and about 68 % Cd^{2+}, 84 % Co^{2+} and 25 % Mn^{2+} at pH 7.5 before adsorption tests. At intermediate pH, the system favours selective adsorption of Cu^{2+} and Fe^{2+} ions to completion (100 %) and significant amounts of Cd^{2+}, Co^{2+} and Mn^{2+} ions but attaining acceptable discharge limits is a challenge. Thus, an increase in initial pH promotes adsorption as well as hydroxide precipitation of metal ions to varying degrees.

The efficiency of adsorption increased with decrease in initial concentration for metal ions fixed at same initial values (20-1000 mg/L). The highest concentration of metal ions treated by powdered BFS (pH 3.5, 50 g/L phase ratio) and their respective adsorption capacities for complete adsorption (100 %) or acceptable discharge limit (< 5 mg/L) were 10.17 mg/g Fe^{2+} at 1014 mg/L, 3.19 mg/g Cu^{2+} at 334 mg/L, 1.94 mg/g Cd^{2+} at 206 mg/L, 0.53 mg/g Co^{2+} at 56 mg/L and 0.48 mg/g Mn^{2+} at 54 mg/L. BFS is selective towards Cu^{2+} and Fe^{2+} ions, moderate towards Cd^{2+} ions but has low affinity for Co^{2+} and Mn^{2+} ions. Adsorption capacity, distribution coefficient and separation factors of Cu^{2+} and Fe^{2+} are greater than those of Cd^{2+}, Co^{2+} and Mn^{2+} ions, reflecting high affinity and preferential adsorption. Thus, adsorption of multiple metal ions is only effective in relatively dilute solutions. The extent of adsorption varies for different metal ions at the same initial concentration. Thus, adsorption may depend on the type of metal ion and interactive effects among ions. This limits BFS to adsorb specific metal ions or only those ions at low concentration.

For metal ions at different initial concentration, highest adsorption capacities were 12.66 mg/g Fe^{2+} at 791 mg/L, 3.83 mg/g Cu^{2+} at 243 mg/L, 1.35 mg/g Cd^{2+} at 86 mg/L, 0.22 mg/g

Co^{2+} at 16 mg/L and 0.13 mg/g Mn^{2+} at 11 mg/L for a discharge limit of C_e < 5 mg/L. The extent of adsorption of Cd^{2+}, Co^{2+} and Mn^{2+} ions in the low concentration range appear to be suppressed by quickly and strongly adsorbing Cu^{2+} and Fe^{2+} ions at higher initial concentration by possibly competitive adsorptive effects.

By comparison, EAF has higher capacity and efficiency for Cu^{2+} and Fe^{2+} ions than BFS at moderate to higher concentration with maximum values of 55.1 mg/g Fe^{2+} at 1686 mg/L and 17.86 mg/g Cu^{2+} at 551 mg/L. However, BFS has higher affinity and faster kinetics towards Cd^{2+} and Co^{2+} in the initial reaction stages than EAF. Only powdered BFS produced effluents with acceptable discharge limits of all metal ions. Consequently, particle size reduction may be necessary to improve adsorption efficiency. Also, efficiency was improved with increase in phase ratio and temperature (22-75 ^{o}C). A discharge limit to below 5 mg/L for all ions was achieved in the entire temperature range except Mn^{2+} that needed ≥ 60 ^{o}C. Thus, the results and observations suggest that the extent of adsorption of various metal ions is dependent on the type of metal ions, initial concentration and specific metal ion/adsorbent interactions involved. Adsorption of multiple different metal ions is generally feasible at low concentration. The adsorption sequence is Fe^{2+}>Cu^{2+}>Cd^{2+}>Co^{2+}>Mn^{2+}.

8.1.2.3 Effect of Activated BFS on Adsorption Efficiency

Activation of BFS by an acid leaching process significantly increased quantities of adsorbed amounts by about two (2), four (4) and five (5) times for Cd^{2+}, Co^{2+} and Mn^{2+} ions respectively from a multicomponent system. This is attributed to significant increases in BET surface area, total pore area and pore volume of BFS after leaching. Ironically, loading of Cu^{2+} and Fe^{2+} ions decreased because free lime that was leached out is thought to be

responsible for good separation of Cu^{2+} and Fe^{2+} mostly through hydroxide precipitation. Preheating of BFS decreased adsorption efficiency possibly because the internal structure collapsed and key properties decreased especially surface area.

8.1.2.4 Kinetic Modeling

The adsorption trends depicted a two stage extraction process for metal ions with an initially fast loading kinetic profile followed by a slower phase towards equilibrium. For single solutes of Cd^{2+}, Cu^{2+} and Fe^{2+} ions that were adsorbed completely, pseudo second order (PSO) was the more satisfactory model to describe experimental data. This model predicts a chemisorption step to limit overall rate of adsorption. The initial rate of adsorption (h_2) was found to increase by 1.5-3.0 with decrease in BFS particle size. Highest h_2 values were 1.54 mg/g min Fe^{2+}, 0.56 mg/g min Cu^{2+}, 0.40 mg/g min Cd^{2+}, 0.09 mg/g min Co^{2+} and 0.08 mg/g min. However, the overall adsorption rates of Co^{2+} and Mn^{2+} ions, which exhibited poor adsorption efficiencies, were limited by intraparticle diffusion as a function of both pH and particle size based on the double exponential model (DEM). This prediction was supported by the Weber-Morris Intraparticle diffusion model. The multi linear fit of this model to data for Cu^{2+} and Fe^{2+} ions that were completely adsorbed suggested intraparticle diffusion resistance through progressively finely sized pores of BFS.

The rates of adsorption of metal ions in multicomponent systems at the same conditions as in single solute systems were mainly limited by intraparticle diffusion. The DEM model gave the best fit and thus a better diffusion theory to describe adsorption data of all metal ions. DEM predicts a 2-step diffusion mechanism involving rapid first adsorption phase that comprises both film and intraparticle diffusion followed by slow second phase that is

controlled by predominantly intraparticle diffusion. Thus, it can be concluded that both intraparticle diffusion and chemisorption steps control overall adsorption kinetics depending on solution conditions. The use of fine particle size of adsorbent tends to reduce diffusion resistance.

8.1.2.5 Adsorption Mechanisms

The mechanisms of extraction of metal ions are complex that involve adsorption, precipitation and ion exchange phenomena in both single and multiple systems. Analysis of adsorbent surfaces by SEM and EDS techniques support ion exchange theory to be the mechanism of adsorption for Mn^{2+}, Co^{2+} and Cd^{2+} ions. The dissolution of slag materials releases alkali ions of Ca^{2+}, Mg^{2+}, K^{+}, Na^{+}, etc. that replace metal ions via ion exchange. An analysis of adsorbed BFS surfaces confirmed the presence of metal ions but their definitive chemical compounds could not be identified. Using theoretical pH for metal hydroxide precipitation in relation to observed experimental pH, significant amounts of Cu^{2+} and Fe^{2+} precipitated as metal hydroxides. Also, SEM images showed precipitate-like flocs on adsorbent surfaces that were loaded with metal ions. Thus, chemical precipitation is also a major separation mechanism for Cu^{2+} and Fe^{2+} ions whereby a high pH promoted adsorption possibly by precipitation and/or ion exchange processes. Chemisorption is another mechanism of adsorption of metal ions as predicted by pseudo kinetic model.

8.1.2.6 Adsorption Equilibria

The BFS and EAF adsorbent materials have a very high adsorption affinity for metal ions, and exhibit Type (I) isotherms and the sub-type ‘L’ (Langmuir) and ‘H’ (high affinity) isotherms but easily attain saturation. The maximum adsorption capacities were 2.83 mg/g Cd^{2+}, 0.95

mg/g Co^{2+} and 0.51 mg/g Mn^{2+} using BFS and 16.38 mg/g Cu^{2+} and 26.97 mg/g Fe^{2+} using EAF. The adsorption capacities for Cu^{2+} and Fe^{2+} ions compares well with literature data than those of Cd^{2+}, Co^{2+} and Mn^{2+} ions that are relatively low. The selectivity sequence in multicomponents is also proposed as Fe^{2+}>Cu^{2+}> Cd^{2+}>Co^{2+}>Mn^{2+} for both BFS and EAF materials. Thus, adsorption of metal ions is selective whether ions are at the same initial concentration or not. However, the selectivity sequence was not consistent with several ionic properties but consistent with solubility products of metal hydroxides. This supports hydroxide precipitation to be a significant mechanism of extraction of metal ions.

The mechanism of adsorption of metal ions is probably by chemisorption as indicated by Langmuir and Freundlich models. Langmuir isotherm gave better fits of adsorption data for Cd^{2+}, Co^{2+}, Cu^{2+} and Mn^{2+} ions than Freundlich isotherm when BFS adsorbent was used. However, Freundlich isotherm was a more satisfactory adsorption theory to describe Cd^{2+} and Cu^{2+} ion adsorption than the Langmuir theory when EAF adsorbent was used. This is probably because EAF supports multilayer adsorption with possible adsorbate interactions.

8.1.3 Fixed Bed Adsorption Kinetics

The extraction efficiencies of up to 93.6 % Cd^{2+}, 56.8 % Co^{2+}, 96.2 % Cu^{2+}, 53.0 % Fe^{2+} and 28.5 % Mn^{2+} by fresh BFS material during the first adsorption cycle indicate that it can be an effective adsorbent in fixed bed columns to purify AMD but BFS was easily exhausted. Process optimisation may increase the effectiveness of BFS material. The results also indicate that BFS material can selectively extract relatively large quantities of Cu^{2+}, Fe^{2+} and Cd^{2+}. The satisfactory linear relationship for the bed depth/service time obtained using bed depth service time (BDST) model validates the data for a potential scale up.

The high loss of adsorption efficiency during second adsorption cycle at breakthrough point (C_e/C_o = 0.05) after the regeneration step suggests a limited ability for the BFS material to be regenerated. Interestingly, desorption of metal ions from BFS material with the strip solution at high strength (2 % w/w H_2SO_4 (aq)) appears highly favourable. This may provide an opportunity for metal ions in the strip solution to be recovered as recyclable products and also for the spent BFS to be safely disposed of in designated landfills without risk of re-solubilisation of metal ions. The dissolution of Mn^{2+} ions and emission of trace H_2S gas from BFS during desorption cycle with H_2SO_4 (aq) pose some challenges. One proposal would be to test different stripping reagents such as weak organic acids (e.g., EDTA) in order to improve desorption and BFS regeneration efficiency and limit Mn^{2+} dissolution.

8.2 Recommendations for Further Work

This study has demonstrated the feasibility of using slag materials as adsorbents in AMD treatment. However, there are several areas that need to be investigated further. It was shown that leaching BFS improved its properties and increased the adsorbed amounts of metal ions. Thus, it is recommended that leaching conditions are optimised and adsorption performance of leached slags is investigated. Also, more characterisation studies of the slags are needed to understand their surface chemistry. Further equilibrium studies in multicomponents are required to determine the effect of more variables on adsorption capacity. It is also suggested that extended equilibrium experiments are conducted to generate enough equilibrium data in order to apply multicomponent isotherms such as

extended Langmuir and Freundlich isotherms and other relevant competitive isotherms that take into account interactive effects of adsorbates.

This study evaluated the effect of pH that continuously varied with time. Consequently a freely changing pH may have introduced additional variables and affected adsorbent surface characteristics, adsorbent/adsorbate interactions and speciation of metal ions. Thus, a detailed study of the effect of constant pH on adsorption that can also propose correct mechanisms is recommended. Additional studies to understand the adsorption mechanisms are required. The experiments may involve determination of quantitative relationships between dissolved alkali metal ions from the slag matrix and metal ions in multicomponents as function of pH in order to determine any exchange ratios and/or confirm whether ion exchange is equivalent or non-equivalent in nature. Further characterisation of BFS surfaces adsorbed with metal ions is necessary in order to identify surface compounds that form with metal ions and propose accurate adsorption mechanisms.

The effect of anions on the adsorption efficiency of slag materials for metals ions in both sulphate and nitrate systems must be investigated. The effect of other variables on efficiency of BFS material should be conducted under continuous flow adsorption conditions using both synthetic and actual acid mine drainage from different mine sites containing multiple metal ions, wide concentration range and acidity.

REFERENCES

Ahmaruzzaman, M. (2011) Industrial wastes as low-cost potential adsorbents for the treatment of wastewater laden with heavy metals. **Advances in Colloid and Interface Science,** 166 (1-2): 36-59

Ahrens, L. H. (1951) The use of ionization potentials, Part 1. ionic radii of the elements. **Geochimica et Cosmochimica Acta,** 2 155-169

Akcil, A. and Koldas, S. (2006) Acid Mine Drainage (AMD), causes, treatment and case studies. **Journal of Cleaner Production,** 14 1139-1145

Aksu, E. (2005) Application of biosorption for removal of organic pollutants: a revew. **Process Biochemistry,** 40 997-1026

Aksu, Z. and Gonen, F. (2004) Biosorption of phenol by immobilised activated sludge in a continuous packed bed: prediction of breakthrough curves. **Process Biochemistry,** 39 599-613

Allred, A. L. (1961) Electronegativity values from thermochemical data. **Journal of Inorganic and Nuclear Chemistry,** 17 215-221

Anirudhan, T. S. and Sreekumari, S. S. (2011) Adsorptive removal of heavy metal ions from industrial effluents using activated carbon derived from waste coconut buttons. **Journal of Environmental Sciences,** 23 (11): 1989-1998

Armenante, P.M. (1999a) **Adsorption** [online]. cpe.njit.edu/dlnotes/CHE685/Cls11-1.pdf

Armenante, P.M. (1999b) **Adsorption with granular activated carbon (GAC)** [online]. http://cpe.njit.edu/dlnotes/CHE685/Cls12-1.pdf

Averill, B. A. & Eldredge, P. (2011) "Appendix B: Solubility-Product Constants (K_{sp}) for Compounds at 25 ^{o}C". In: **Principles of General Chemistry**.

Bailey, S. E., Olin, T. J., Briska, R. M. and Adrian, D. D. (1999) A Review of Potentially Low-Cost Sorbents for Heavy Metals. **Water Research,** 33 (11): 2469-2479

Banks, D., Younger, P. L., Arnesen, R. T., Iversen, E. R. and Banks, S. B. (1997) Mine-water chemistry: the good, the bad and the ugly. **Environmental Geology,** 32 (3): 157-174

Barakat, M. A. (2011) New trends in removing heavy metals from industrial wastewater. **Arabian Journal of Chemistry,** 4 361-377

Bell, F. G., Bullock, S. E. T., Halbich, T. F. J. and Lindsay, P. (2001) Environmental impacts asociated with an abandoned mine in the Witbank Coalfield, South Africa. **International Journal of Coal Geology,** 45 195-216

Blodau, C. (2006) A review of acidity generation and consumption in acidic coal mine lakes and their watersheds. **Science of the Total Environment,** 369 307-332

Bodurtha, P. and Brassard, P. (2000) Neutralization of Acid by Steel-Making Slags. **Environmental Technology,** 21 (11): 1271-1281

Bohart, G. S. and Adams, E. Q. (1920) Some aspects of the behaviour of charcoal with respect to chlorine. **Journal of the American Chemical Society,** 42 523-544

Boon, M. (1996) **Theoretical and experimental methods in modeling bio-oxidation kinetics of sulphide minerals.** PhDThesis, Technical University Delft.

Boyd, G. E., Adamson, A. W. and Myers Jr, L. S. (1947) The Exchange Adsorption of Ions from Aqueous Solutions by Organic Zeolites, II. Kinetics. **Journal of the American Chemical Society,** 69 (11): 2836-2848

Breed, A. W. and Hansford, G. S. (1999) Studies on the mechanism and kinetics of bioleaching. **Minerals Engineering,** 12 (4): 383-392

Brown, A. M. (2001) A step-by-step guide to non-linear regression analysis of experimental data using a Microsoft Excel spreadsheet. **Computer Methods and Programs in Biomedicine,** 65 191-200

Brown, H., Skousen, J. and Renton, J. (1994) Stability of flocs produced by chemical neutralization of acid mine drainage . **Green Lands,** 24 (3): 34-39

Bunce, N. J., Chartrand, M. and Keech, P. (2001) Electrochemical treatment of acidic aqueous ferrous sulphate and copper sulphate as models for acid mine drainage. **Water Research,** 35 (18): 4410-4416

Burwell, R. L. (1976) Manual of symbols and terminology for physicochemical quantities and units - appendix II (IUPAC). Part II: Heterogeneous catalysis. **Pure and Applied Chemistry,** 46 71-90

Chan, B. K. C., Bouzalakos, S. and Dudeney, A. W. L. (2008) Integrated waste and water management in mining and metallurgical industries. **Transactions of nonferrous metals society of China,** 18 1497-1505

Chen, J. P., Yoon, J.-T. and Yiacoumi, J. (2003) Effects of chemical and physical properties of influent on copper sorption onto activated carbon fixed-bed columns. **Carbon,** 41 1635-1644

Claveau-Mallet, D., Wallace, S. and Comeau, Y. (2013) Removal of phosphorus, fluoride and metals from a gypsum mining leachate using steel slag filters. **Water Research,** 47 1512-1520

Cobzaru, C. & Inglezakis, V. J. (2015) "Ion Exchange". In: Tarleton S. (eds.) **Progress in Filtration and Separation**. Academic Press, Elsevier. pp. 425-496.

Curkovic, L., Cerjan-Stefanovic, S. and Rastovean-Mioe, A. (2001) Batch Pb^{2+} and Cu^{2+} Removal by Electric Furnace Slag. **Water Research,** 35 (14): 3436-3440

Dabrowski, A. (2001) Adsorption - from Theory to Practice. **Advances in Colloid and Interface Science,** 93 135-224

Darkwah, L. (2005) **Remediation of Acid Mine Drainage.** PhD Thesis, University of Birmingham, Department of Chemical Engineering, United Kingdom.

Das, B., Prakash, S., Reddy, P. S. R. and Misra, V. N. (2007) An Overview of Utilization of Slag and Sludge from Steel Industries. **Resources, Conservation and Recycling,** 50 40-57

Deng, S. (2006) "Sorbent Technology". In: Lee S. (eds.) **Encyclopedia of Chemical Processing**. Second ed. New York: Taylor and Francis Group. pp. 2825-2845.

Dimitrova, S., Nikolov, V. and Mehandgiev, D. (2001) Effect of the Heat Treatment on the Morphology and Sorption Ability to Metal ions of Metallurgical Slag. **Journal of Material Science,** 36 2639-2643

Dimitrova, S. V. (1996) Metal Sorption on Blast Furnace Slag. **Water Research,** 30 (1): 228-232

Dimitrova, S. V. and Mehandgiev, D. R. (1998) Lead Removal from Aqueous Solutions by Granulated Blast Furnace Slag. **Water Research,** 32 (11): 3289-3292

Dimitrova, S. V. and Mehandgiev, D. R. (2000) Interaction of Blast furnace Slag with Heavy Metal Ions in Water Solutions. **Water Research,** 34 (6): 1957-1961

Dimitrova, S. V. and Mehanjiev, D. R. (1998) Lead Removal from Aqueous Solutions by Granulated Blast Furnace Slag. **Water Research,** 32 (11): 3289-3292

Du, Q., Liu, S., Cao, Z. and Wang, Y. (2005) Ammonia removal from aqueous solution using natural chinese clinoptilolite. **Separation and Purification Technololgy,** 44 229-234

Dushina, A. and Aleskovski, V. (1976) Ion Exchange as First Stage of the Solid Substance Transformation into Electrolytic Solutions. **Journal of Applied Chemistry,** 49 41-49

El-Haggar, S. M. (2007) "Sustainability of industrial waste management". In: **Sustainable industrial design and waste management**. USA: Elsevier Academic Press. pp. 307-369.

El-Khaiary, M. I. and Malash, G. F. (2011) Common data analysis errors in batch adsorption studies. **Hydrometallurgy,** 105 314-320

El-Khaiary, M. I., Malash, G. F. and Ho, Y.-S. (2010) On the Use of Linearized Pseudo-Second Order Kinetic Equations for Modeling Adsorption Systems. **Desalination,** 257 93-101

EPPCA (1990) The Water Pollution Control (Effluent and Waste Water) Regulations: Statutory Instrument No 72 of 1993. The Zambia Environmental Protection and Pollution Control Act (EPPA) No 12 of the Laws of Zambia. **Republic of Zambia Government,** 257-273

Erdem, E., Karapinar, N. and Donat, R. (2004) The removal of heavy metal cations by natural zeolites. **Journal of Colloid and Interface Science,** 280 309-314

Everett, D. H. (1986) Reporting Data on Adsorption from Solution at the Solid/Solution Interface (Recommendations 1986). **Pure and Applied Chemistry,** 58 (7): 967-984

Farley, K. J., Dzombak, D. A. and Morel, F. M. M. (1985) A surface precipitation model for the sorption of cations on metal oxides. **Journal of Colloid and Interface Science,** 106 226-242

Feng, D., Aldrich, C. and Tan, H. (2000) Treatment of acid mine water by use of heavy metal precipitation and ion exchange. **Minerals Engineering,** 13 (6): 623-642

Feng, D., van Deventer, J. S. J. and Aldrich, C. (2004) Removal of Pollutants from Acid Mine Wastewater Using Metallurgical By-Product Slags. **Separation and Purification Technololgy,** 40 61-67

Fenglian, F. and Wang, Q. (2011) Removal of Heavy Metal Ions from Wastewaters: A Review. **Journal of Environmental Management,** 92 407-418

Ferguson, K. D. & Erickson, P. M. (1988) "Approaching the AMD problem- from prediction and early detection". In: **Internation conference on control of environmental problems from metal mines**. Roros, Norway.

Foo, K. Y. and Hameed, B. H. (2010) Insights into Modeling of Adsorption Isotherm Systems. **Chemical Engineering Journal,** 156 2-10

Gao, Y., Sengupta, K. A. and Simpson, D. (1995) A New Hybrid Inorganic Sorbent for Heavy Metals Removal. **Water Research,** 29 (9): 2195-2205

Giesche, H. (2006) Mercury Porosimetry: a General (Practical) Overview. **Particle and Particle Systems Characterisation,** 23 1-11

Giles, C. H., Smith, D. and Huitson, A. (1974) A general Treatment and classification of the solute adsorption isotherm. I. Theoretical. **Journal of Colloid and Interface Science,** 47 755-765

Goetz, R. E. and Riefler, R. G. (2014) Performance of steel slag leach beds in acid mine drainage treatment. **Chemical Engineering Journal,** 240 579-588

Gordon, A. R. (1994) Environmental Consequences of Coal Mine Closure. **The Geographical Journal,** 160 (1): 33-40

Gorgievski, M., Stankovic, D. B. and Bogdanovic, G. (2009) Copper electrowinning from acid mine drainage: A case study from the closed mine "Cerovo". **Journal of Hazardous Materials,** 170 716-721

Gray, N. F. (1997) Environmental Impact and Remediation of Acid Mine Drainage: A Management Problem. **Environmental Geology,** 30 (1/2): 62-71

Grontmij (2012) **Tier 1 Water environment screening criteria (England and Wales)** [online].[Accessed 12 July 2015]

Gupta, V. K. (1998) Equilibrium uptake, sorption dynamics, process development, and column operations for the removal of copper and nickel from aqueous solution and wastewater using activated slag, a low cost adsorbent. **Industrial and Engineering Chemistry Research,** 37 192-202

Hamilton, R. M., Bowen, G. G., Postlethwaite, N. A., & Dussek, C. J. (1994a) "The abandonment of Wheal Jane, a tin mine in South West England". In: **5th International Mine Water Congress**. Nottingham, United Kingdom:pp. 543-551.

Hamilton, R. M., Taberham, J., Waite, R. R. J., Cambridge, M., Coulton, R. H., & Hallewell, M. P. (1994b) "The development of a temporary treatment solution for acid mine water discharge at Wheal Jane". In: **5th International Mine Water Congress**. Nottingham, United Kingdom:pp. 643-656.

Ho, Y.-S. (1995) **Adsorption of Heavy Metals from Waste Streams by Peat.** Ph.D Thesis, University of Birmingham, United Kingdom.

Ho, Y.-S. (2006) Review of Second-Order Models for Adsorption Systems. **Journal of Hazardous Materials,** 136 (3): 681-689

Ho, Y. S. & Mckay, G. (1998) "A Comparison of Chemisorption Kinetic Models Applied to Pollutant Removal on Various Sorbents". In: **Transactions for Institution of Chemical Engineers (Trans IChemE)**.

Ho, Y. S. and McKay, G. (1999) Pseudo Second Order Model for Sorption Processes. **Process Biochemistry,** 34 451-465

Holdich, R. G. (2002) "Particle Characterisation". In: **Fundamentals of Particle Technology**. Leicestershire: Midlands Information Technology and Publishing.

Huang, C. P. and Rhoads, E. A. (1989) Adsorption of Zn(II) onto Hydrous Aluminosilicates. **Journal of Colloid and Interface Science,** 131 (2): 289-306

Hui, K. S., Chao, C. Y. H. and Kot, S. C. (2005) Removal of mixed heavy metal ions in wastewater by zeolite 4A and residual products from recycled coal fly ash. **Journal of Hazardous Materials,** B127 89-101

Huifen, Y., Wen, M., Weina, Z., & Zhiyong, W. (2011) "Steel Slag as Multi-Functional Material for Removal of Heavy Metal Ions in Wastewater". In: Z. Liu & F. Huilin, eds. **2011 International Conference on Computer Distributed Control and Intelligent Environmental Monitoring CDCIEM 2011**. Hunan, China: IEEE Computer Society. pp. 1287-1290.

Huisman, J. L., Schouten, G. and Schultz, C. (2006) Biologically produced sulphide for purification of process streams, effluent treatment and recovery of metals in the metal and mining industry. **Hydrometallurgy,** 83 (1): 106-113

Hutchins, R. A. (1974) New method simplifies design of activated carbon systems. **Chemical Engineering,** 80 133-138

Hutchins, S. R., Davidson, M. S., Brierley, J. A. and Brierley, C. L. (1986) Microorganisms in reclamation of metals. **Annual Review of Microbiology,** 40 311-336

Inglezakis, V. J., Loizidou, M. D. and Grigoropoulou, H. P. (2002) Equilibrium and kinetic ion exchange studies of Pb^{2+}, Cr^{3+}, Fe^{3+} and Cu^{2+} on natural clinoptilolite. **Water Research,** 36 2784-2792

Inglezakis, V. J. & Poulopoulos, S. G. (2006a) "Adsorption and Ion Exchange". In: **Adsorption, Ion Exchange and Catalysis: Design of Operations and Environmental Applications**. First ed. Amsterdam, The Netherlands: Elsevier Science. pp. 243-353.

Inglezakis, V. J. & Poulopoulos, S. G. (2006b) **Adsorption, Ion Exchange and Catalysis: Design of Operations and Environmental Applications.** First edn. Amsterdam, The Netherlands: Elsevier Science.

Inglezakis, V. J. & Poulopoulos, S. G. (2006c) "Reactors Scale-up". In: **Adsorption, Ion Exchange and Catalysis: Design of Operations and Environmental Applications**. First ed. Amsterdam, The Netherlands: Elsevier Science. pp. 523-550.

Jafaripour, A. (2013) **Utilisation of waste gas sludge for waste water treatment.** PhD Thesis, University of Birmingham.

Johnson, D. B. and Hallberg, K. B. (2005) Acid mine drainage remediation options: a review. **Science of the Total Environment,** 338 3-14

Kim, D.-H., Shin, M.-C., Choi, H.-D., Seo, C.-I. and Baek, K. (2008) Removal Mechanisms of Copper Using Steel-Making Slag: Adsorption and Precipitation. **Desalination,** 223 283-289

Knaebel, K.S. (2012) **Adsorbent Selection** [online]. http://adsorption.com/publications/AdsorbentSel1B.pdf

Komarneni, S., Breval, E., Roy, D. M. and Roy, R. (1988) Reactions of some calcium silicates with metal ions. **Cement and concrete research,** 18 204-220

Kuyucak, N. (2002) Role of Microorganisms in Mining: Generation of Acid Rock Drainage and Mitigation and Treatment. **The European Journal of Mineral Processing and Environmental Protection,** 2 (3): 179-196

Kuyucak, N. (2006) **Selecting Suitable Methods for Treating Mining Effluents** [online]. http://www.minem.gob.pe/minem/archivos/file/dgaam/publicaciones/curso_cierreminas/02_T%C3%A9cnico/10_Tratamiento%20de%20Aguas/TecTratAgu-L1_AMD%20treatment%20options.pdf [Accessed 20 February 2012a]

Kuyucak, N. (2001) **Implementation of a High Density Sludge "HDS" Treatment Process at the Kristineberg Mine Site** [online]. http://partner.boliden.com/www/bolidense.nsf/(LookupWebAttachment)/Library%20Lectures/$file/HDS_Treatment_Kristineberg.pdf [Accessed 22 February 2012]

Limousin, G., Gaudet, J.-P., Charlet, L., Szenknect, S., Barthes, V. and Krimissa, M. (2007) Sorption isotherms: A review on physical bases, modeling and measurement. **Applied Geochemistry,** 22 249-275

Liu, S.-Y., Gao, J., Qu, B. and Ang, Y.-J. (2009) "Adsorption Behaviors of Heavy Metal Ions by Steel Slag-An Industrial Solidwaste". In: D. Romeo, D. Graffox, & G. MacPherson, eds. **3rd International Conference on Bioinformatics and Biomedical Engineering iCBBE 2009**. Beijing, China: IEEE eXpress Conference Publishing.

Liu, S.-Y., Gao, J., Yang, Y.-J. and Ye, Z.-H. (2010) Adsorption Intrinsic Kinetics and Isotherms of Lead Ions on Steel Slag. **Journal of Hazardous Materials,** 173 558-562

Lopez, F. A., Perez, C., Sainz, E. and Alonso, M. (1995) Adsorption of Pb^{2+} on Blast Furnace Sludge. **Journal of Chemical Technology and Biotechnology,** 62 (2): 200-206

Lopez-Delgado, A., Perez, C. and Lopez, F. A. (1998) Sorption of Heavy Metals on Blast Furnace Sludge. **Water Research,** 32 (4): 989-996

Lottermoser, B. G. (2007) **Mine wastes: characterisation, treatment, environmental impacts.** Second edn. New York, USA: Springer.

Luis, A. T., Teixeira, P., Almeida, S. F. P., Matos, J. X. and da Silva, E. F. (2011) Environmental impact of mining activities in the Lousal area (Portugal): Chemical and diatom characterization of metal-contaminated stream sediments and surface water of Corona stream. **The Science of the Total Environment,** 409 4312-4325

Malvern Instruments Limited (2015) **A basic guide to particle characterisation**. http://www.malvern.com/en/support/resource-center/Whitepapers/WP120620BasicGuidePartChar.aspx

McCabe, W. L., Smith, C. J., & Harriot, P. (1993) "Adsorption". In: **Unit Operations of Chemical Engineering**. Fifth ed. Singapore: McGraw-Hill Inc.

(2001) **Process for Producing High Surface Area Material by Controlled Leaching of Blast Furnace Slag**, (patent) US6284207 B1.

McDonald, D. M., Webb, J. A. and Taylor, J. (2006) **Chemical Stability of Acid Rock Drainage Treatment Sludge and Implications for Sludge Management**. **Environmental Science and Technology,** 40 (6): 1984-1990

McGinness, S. (1999) Treatment of acid mine drainage (research paper 99/10). **House of Commons Library, UK Parliament,**

Mielke, R. E., Pace, D. L., Porter, T. and Southam, G. (2003) A Critical Stage in the Formation of Acid Mine Drainage: Colonization of Pyrite by *Acidithiobacillus ferrooxidations* Under pH-neutral Conditions. **Geobiology,** 1 81-90

Mihailova, I., Dimitrova, S. and Mehandjiev, D. (2013) Effect of the Thermal Treatment on the Pb (II) Adsorption Ability of Blast Furnace Slag. **Journal of Chemical Technology and Metallurgy,** 48 (1): 72-79

Mohan, D. and Chander, S. (2001) Single component and multicomponent adsorption of metal ions by activated carbons. **Colloids and Surfaces A: Physicochemical and Engineering Aspects,** 177 183-196

Mohan, D. and Chander, S. (2006) Removal and recovery of metal ions from acid mine drainage using lignite - A low cost sorbent. **Journal of Hazardous Materials,** B137 1545-1553

Motsi, T. (2010) **Remediation of Acid Mine Drainage using Natural Zeolite.**PhD Thesis, University of Birmingham, United Kingdom.

Motsi, T., Rowson, N. A. and Simmons, M. J. H. (2009) Adsorption of Heavy Metals from Acid Mine Drainage by Natural Zeolite. **International Journal of Mineral Processing,** 92 42-48

Motulsky, H. J. and Ransnas, L. A. (1987) Fitting curves to data using nonlinear regression: a practical and nonmathematical review. **The FASEB Journal,** 1 (5): 365-374

Murr, L. E. (1980) Theory and practice of copper sulphide leaching in dumps and in-situ. **Minerals Science Engineering,** 12 (3): 121-189

Naiker, N., Cukrowska, E. and McCarthy, T. S. (2003) Acid Mine Drainage arising from Gold Mining Activity in Johannesburg, South Africa and Environs. **Environmental Pollution,** 122 29-40

Nguyen, T. C., Loganathan, P., Nguyen, T. V. and Vigneswaran, S. (2015) Simultaneous adsorption of Cd, Cr, Cu, Pb, and Zn by an iron-coated Australian zeolite in batch and fixed-bed column studies. **Chemical Engineering Journal,** 270 393-404

Nieto, J. M., Sarmiento, A. M., Olias, M., Canovas, C. R., Riba, I., Kalman, J. and Delvalls, T. A. (2007) Acid mine drainage pollution in the Tinto and Odiel rivers (Iberian pyrite belt, S. W. Spain) and bioavailability of the transported metals to the Huelva Estuary. **Environmental International,** 33 445-455

Nightingale, E. R. (1959) Phenomenological theory of ion solvation. Effective radii of hydrated ions. **Journal of Physical Chemistry,** 63 (9): 1381-1387

Oguz, E. and Ersoy, M. (2010) Removal of Cu^{2+} from aqueous solution by adsorption in a fixed bed column and neural network modeling. **Chemical Engineering Journal,** 164 56-62

Oh, C., Rhee, S., Oh, M. and Park, J. (2012) Removal Characteristics of As(III) and As(V) from Acidic Aqueous Solution by Steel Making Slag. **Journal of Hazardous Materials,** 213-214 147-155

OSMRE (2009) **Acid Drainage Technology Initiative (ADTI) - Acid Mine Drainage** [online]. http://www.techtransfer.osmre.gov/NTTMainSite/Initiatives/ADTI/adtiOSMinfo.shtm [Accessed 6 October 2011]

Park, D., Lim, S.-R., Lee, H. W. and Park, J. M. (2008) Mechanism and kinetics of Cr(IV) reduction by waste slag generated from iron making industry. **Hydrometallurgy,** 93 72-75

Peter, R. W., Ku, Y. and Bhattacharyya, D. (1985) Evaluation of recent treatment techniques for removal of heavy metals from industrial wastewaters. **AICHE Symposium series,** 81 (243): 165-203

Qiu, H., Lv, L., Pan, B.-C., Zhang, Q.-J., Zhang, W.-M. and Zhang, Q.-X. (2009) Critical Review in Adsorption Kinetic Models. **Journal of Zhejiang University Science A,** 10 (5): 716-724

Rao, S. R. (2006) "Metallurgical Slags, Dust and Fumes". In: **Resource Recovery and Recycling from Metallurgical Wastes**. Elsevier Science B. V. pp. 269-327.

Richardson, J. F., Harker, J. H., & Backhurst, J. R. (2002) "Adsorption". In: **Coulson and Richardson's Chemical Engineering**. 5th ed. Great Britain, Bath: Butterworth-heinemann, Elsevier Science.

Robb, G. A. and Robinson, J. D. F. (1995) Acid Drainage from Mines. **The Geographical Journal,** 161 (1): 47-54

Rodda, D. P., Johnson, B. B. and Wells, J. D. (1993) The Effect of Temperature and pH on the Adsorption of Copper(II), Lead(II), and Zinc(II) onto Geothite. **Journal of Colloid and Interface Science,** 161 57-62

Rossi, G. (1990) **Biohydrometallurgy.** Hamburg, Germany: McGraw-Hill.

Rouquerol, F., Rouquerol, J., Sing, K. S. W. and Llewellyn, P. (2014) **Adsorption by Powders and Porous Solids: Principles, Methodology and Applications.** Second edn. Poland: Academic Press Elsevier.

Ruthven, D. M. (1984) **Principles of adsorption and adsorption processes.** United States of America: John Wiley and Sons.

Schippers, A. and Sand, W. (1999) Bacterial leaching of metal sulphides proceeds by two indirect mechanisms via thiosulphate or via polysulfides and sulphur. **Applied Environmental Microbiology,** 65 319-321

Seader, J. D., Henley, E. J., & Roper, D. K. (2011) "Adsorption, Ion Exchange, Chromatography, and Electrophoresis". In: **Separation Process Principles**. Third ed.

Sing, K. S. W. (1982) Reporting physisorption data for gas/solid systems. Pure and applied chemistry, 54(11): 2201-2218

Skousen, J. et al (1998) **Handbook of Technologies for Avoidance and Remediation of Acid Mine Drainage** [online].The National Mine Land Reclamation Centre, West Virginia University,

Morgantown, West Virginia http://www.techtransfer.osmre.gov/NTTMainSite/Library/hbmanual.shtm [Accessed 22 February 2012]

Skousen, J. G., Sextone, A., & Ziemkiewicz, P. F. (2000) "Acid Mine Drainage Control and Treatment". In: **Reclamation of Drastically Disturbed Lands**. Agronomy No. 41 ed. American Society of Agronomy and American Society for Surface Mining and Reclamation. pp. 1-42.

Smith, D. W. (1977) Ionic hydration enthalpies. **Journal of Chemical Education,** 54 (9): 540-542

Talling, B. & Krivenko, P. (1997) "Blast furnace slag - The ultimate binder". In: Chandra S. (eds.) **Waste Materials used in Concrete Manufacturing**. New Jersey, USA: Noyes Publications. pp. 235-266.

U.S.EPA (1994) **Technical Document: Acid Mine Drainage Prediction** [online].U. S. Environmental Protection Agency, Office of Solid Waste, Special Waste Branch, 401 M Street, SW, Washington DC 20460 http://water.epa.gov/polwaste/nps/upload/amd.pdf [Accessed 25 February 2012]

UK Environmental Agency (2008) **Abandoned Mines and the Water Environment** [online]. http://publications.environment-agency.gov.uk/PDF/SCHO0508BNZS-E-E.pdf

US EPA (2000) **Abandoned Mine Site Characterisation and Cleanup Handbook** [online]. http://www.epa.gov/superfund/policy/remedy/pdfs/amscch.pdf [Accessed 25 February 2012]

Watzlaf, G. R. & Casson, L. W. (1990) "**Chemical Stability of Manganese and Iron in Mine Drainage Treatment Sludge: Effects of Neutralization Chemical, Iron Concentration, and Sludge Age** ". In: **990 Mining and Reclamation Conference and Exhibition, West Virginia University, Morgantown, WV**. pp. 3-9.

Webb, P.A. (1993) **Data Collection, Reduction and Presentation** [online].Micromeritics Instrument Corporation
http://depts.washington.edu/mseuser/Equipment/RefNotes/Hg%20Porosimetery%20paper.pdf

Webb, P.A. (2001) **An Introduction To The Physical Characterization of Materials by Mercury Intrusion Porosimetry with Emphasis On Reduction And Presentation of Experimental Data** [online]. http://www.micromeritics.com/pdf/app_articles/mercury_paper.pdf

Webb, P.A. (2010) **Mercury Intrusion Porosimetry** [online].

Weber Jr, W. J. and Morris, J. C. (1963) Kinetics of Adsorption on Carbon from Solution. **Journal of the Sanitary Engineering Division ASCE,** 89 (2): 31-60

Wilczak, A. and Keinath, T. M. (1993) Kinetics of Sorption and Desorption of Copper (II) and Lead (II) on Activated Carbon. **Water Environment Research,** 65 238-244

Xue, Y., Hou, H. and Zhu, S. (2009) Competitive Adsorption of Copper(II), Cadmium(II), Lead(II) and Zinc(II) onto Basic Oxygen Furnace Slag. **Journal of Hazardous Materials,** 162 391-401

Xue, Y., Wu, S. and Zhou, M. (2013) Adsorption Characterization of Cu(II) from Aqueous Solution onto Basic Oxygen Furnace Slag. **Chemical Engineering Journal,** 231 355-364

Yan, J., Moreno, L. and Neretnieks, I. (2000) The Long-Term Acid Neutralizing Capacity of Steel Slag. **Waste Management,** 20 217-223

Yi, H., Xu, G., Cheng, H., Wang, J., Wan, Y. and Chen, H. (2012) An Overview of Utilisation of Steel Slag. **Procedia Environmental Sciences,** 16 791-801

Yildirim, I. Z. and Prezzi, M. (2011) Chemical, Mineralogical and Morphological Properties of Steel Slag. **Advances in Civil Engineering,** 2011 1-13

Younger, P. L. (2001) Mine Water Pollution in Scotland: Nature, Extent and Preventative Strategies. **The Science of the Total Environment,** 265 309-326

ZCCM-IH (2005) **Consolidated environmental management plan, Phase II (CEMP II), Copperbelt environmental project (CEP), Zambia.**

Zhuang, J.-M. (2009) Acidic Rock Drainage Treatment: A Review. **Recent Patents on Chemical Engineering,** 2 238-252

Ziemkiewicz, P. F. & Skousen, J. (1998) "The use of steel slag in acid mine drainage treatment and control". In: **19th Annual West Virginia Surface Mine Drainage Task Force Symposium**. West Virginia, USA.

Zinck, J. (2005) **Review of Disposal, Reprocessing and Reuse Options for Acidic Drainage Treatment Sludge** [online].Mine Environment Neutral Drainage (MEND) Program http://www.mend-nedem.org/reports/files/3.42.3.pdf [Accessed 20 February 2012]

APPENDICES

Appendix A: Examples of adsorption data spreadsheets

Appendix B: Experimental rig

Appendix C: Chemical precipitation

Appendix D: Publications

Appendix A: Examples of experimental adsorption data spreadsheets

(a) Multiadsorbate system

Exp 6: Bottle-Roller; Initial pH_o = 3.50; Adsorbent/sorbate Ratio = 5% w/v (25g/500 ml); Me^{2+} = 100 ppm; Particle Size = 0.18 < d_p < 0.36 mm; Temp. = room; Initial Vol = 500 mL.

Solution conditions				Cd2+			Co2+			Cu2+			Fe2+			Mn2+		
ID	T (m)	**pH**	Temp (^oC)	AAS (ppm)	C_e (ppm)	**Adsor %**	AAS (ppm)	C_e (ppm)	**Adsor %**	AAS (ppm)	C_e (ppm)	**Adsor %**	AAS (ppm)	C_e (ppm)	**Adso %**	AAS (ppm)	Ce (ppm)	**Adsor %**
t0	0	**3.5**	23.8	4.106	102.7	**0**	4.039	101.0	**0**	4.059	101.5	**0**	3.995	99.88	**0**	4.155	103.9	**0**
t1	1	**5.5**	23.9	3.871	96.78	**5.7**	3.809	95.23	**5.7**	2.177	54.43	**46**	2.038	50.95	**49**	4.082	102.1	**2**
t2	3	**5.6**	23.9	3.846	96.15	**6.3**	3.813	95.33	**5.6**	1.502	37.55	**63**	1.29	32.25	**67.7**	4.121	103.0	**1**
t3	7	**5.7**	23.9	3.75	93.75	**8.7**	3.776	94.4	**6.5**	1.008	25.20	**75**	0.676	16.9	**83.1**	4.132	103.3	**1**
t4	15	**5.8**	23.9	3.617	90.43	**11.9**	3.734	93.35	**7.6**	0.622	15.55	**85**	0.163	4.08	**95.9**	4.11	102.8	**1**
t5	30	**6.0**	23.9	3.465	86.63	**15.6**	3.633	90.83	**10.1**	0.384	9.60	**91**	BDL	0.18	**99.8**	4.079	102.0	**2**
t6	60	**6.2**	24.2	3.247	81.18	**20.9**	3.547	88.68	**12.2**	0.219	5.48	**95**	BDL	0.05	**99.9**	4.055	101.4	**2**
t7	120	**6.4**	24.6	2.936	73.4	**28.5**	3.461	86.53	**14.3**	0.108	2.70	**97**	BDL	0.02	**100**	4.004	100.1	**4**
t8	180	**6.6**	24.7	2.686	67.15	**34.6**	3.422	85.55	**15.3**	0.065	1.63	**98**	BDL	0.02	**100**	3.979	99.48	**4**
t9	240	**6.7**	24.6	2.506	62.65	**39.0**	3.356	83.9	**16.9**	0.042	1.05	**99**	BDL	0.03	**100**	3.947	98.68	**5**
t10	300	**6.8**	24.8	2.363	59.08	**42.5**	3.236	80.9	**19.9**	0.028	0.70	**99**	BDL	0.03	**100**	3.918	97.95	**6**

BDL = below detection limit of AAS instrument (~ < 0.1 mg/L)
C_e = equilibrium concentration at time t
% Adsor = Percentage of adsorption; S/L = Solid/Liquid
Samples were diluted accordingly during AAS measurements (≤ 5 mg/L Max)

(a) Single adsorbate system

Exp 63: Bottle-Roller; initial pH_o = 3.50; Adsorbent/adsorbate Ratio = 3% w/v (15g/500 ml); Initial conc (C_o) = 100 ppm Cd^{2+}; Particle Size = 0.18 < d_p < 0.36 mm; Temp. = room; Initial Vol = 500 mL

Sample ID	Time (min)	pH	Temp (^oC)	C_e (ppm)	C_e (x25) (ppm)	Adsor (%)
t0	0	3.5	20.6	3.353	84	**0**
t1	1	6.8	21.2	2.300	58	**31**
t2	3	7.1	21.4	1.806	45	**46**
t3	7	7.3	21.6	1.203	30	**64**
t4	15	7.6	21.6	0.652	16	**81**
t5	30	7.9	21.7	0.196	5	**94**
t6	60	8.4	21.7	0.000	3	**97**
t7	120	8.8	22.0	0.000	1	**99**
t8	180	9.0	22.2	0.000	0	**100**
t9	240	9.1	22.0	0.000	0	**100**

C_e = equilibrium concentration at time t
% Adsor = Percentage of adsorption; S/L = Solid/Liquid

Appendix B: Images of experimental rigs

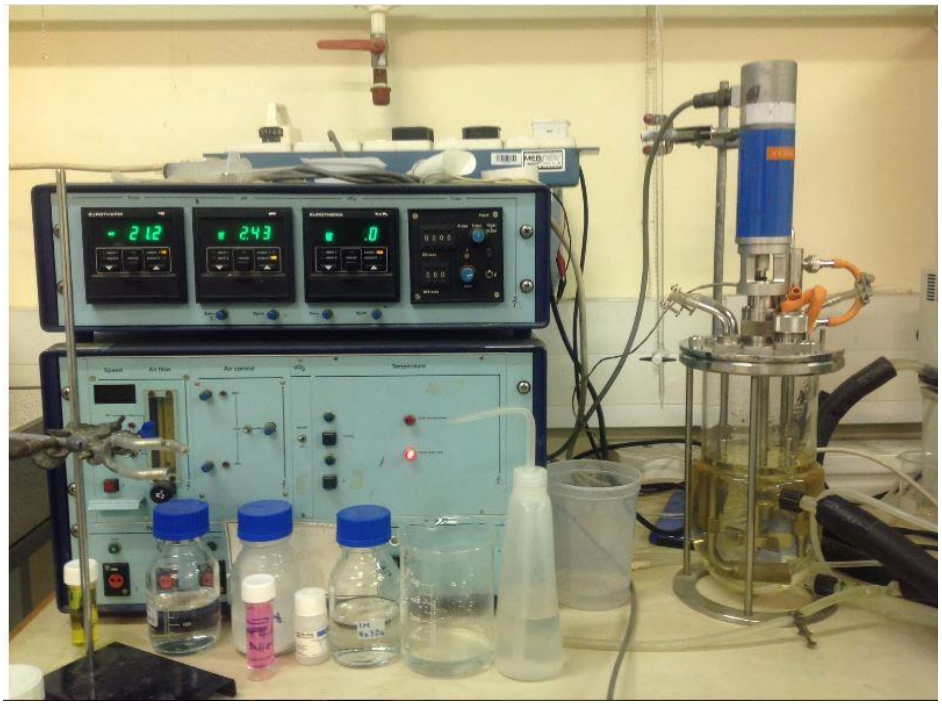

(a) Thermostated stirred tank reactor (STR)

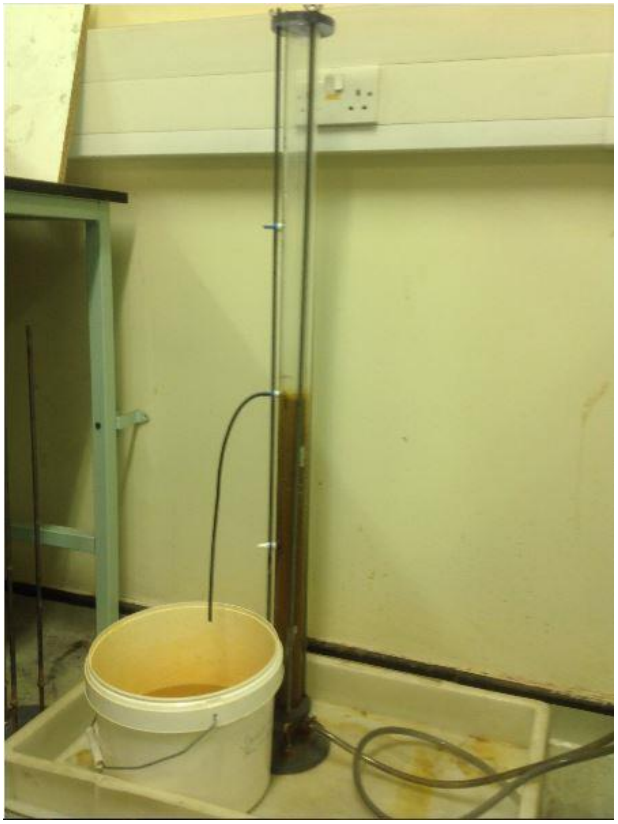

(b) Fixed bed column

Appendix C: Chemical precipitation

Hydroxide Precipitation --- with 1 molar CaO (making 1 molar $Ca(OH)_2$ -- (in Stirred Tank Reactor (STR))

Initial pHo = 3.50; Temp = room (22 ^oC); STR @ 400 rpm;
1 Molar solid CaO (56.08 g/L dissolved in 1L H_2O); ------- $CaO + H_2O = Ca(OH)_2$

Wastewater composition = 60 mg/L Cu2+; 1mole CaO = I mole $Ca(OH)_2$
Initial pH 3.50 100 mg/LFe2+;
20 mg/L Mn2+

					Cu2+			Fe2+			Mn2+		
					Dilut	x15		Dilut	x25		Dilut	x 5	
ID	T (m)	**pH**	t(^oC)	**Vol., (ml) $Ca(OH)_2$**	AAS, mg/L	Ce, mg/L	**% pptn**	AAS, mg/L	Ce, mg/L	**% pptn**	AAS, mg/L	Ce, mg/L	**% pptn**
t0	0	**3.5**	21.6	**0.0**	4.23	63.41	**0.0**	4.05	101.4	**0.0**	4.12	20.61	**0.0**
t1	1	**-**	22.2	**6.5**	4.16	62.37	**1.6**	3.91	97.86	**3.4**	4.02	20.12	**2**
t2	3	**5.1**	22.2	**10.0**	4.00	60.07	**5.3**	3.62	90.62	**10.6**	3.88	19.39	**5**
t3	7	**5.4**	22.2	**20.0**	3.64	54.60	**13.9**	2.79	69.66	**31.3**	3.90	19.51	**5**
t4	15	**5.5**	22.2	**50.0**	1.17	17.59	**72.3**	0.51	12.87	**87.3**	3.15	15.77	**24**
t5	30	**10**	22.2	**68.7**	BDL	0.00	**100**	BDL	0.00	**100**	BDL	0.00	**100**
t6	60	**10**	22.5	**69.5**	BDL	0.00	**100**	BDL	0.00	**100**	BDL	0.00	**100**
t7	120	**9.8**	22.9	**72.8**	BDL	0.00	**100**	BDL	0.00	**100**	BDL	0.00	**100**
t8	180	**9.8**	23.0	**80.6**	BDL	0.00	**100**	BDL	0.00	**100**	BDL	0.00	**100**

C_e = equilibrium concentration at time t ; BDL =below detection limit; % pptn = % of precipitation;

Approximate amount of $CaO/Ca(OH)_2$ used: -Vol $Ca(OH)_2$ = 68.7 ml; Conc = 1M = 56.08 g/L

Thus, amount of $CaO/Ca(OH)_2$ = 56.08 g/L X (68.7/1000) L ≤ 3.85 g $CaO/Ca(OH)_2$ in 1L of wastewater ------ for complete precipitation of metal ions.

Notes: - Low solubility of CaO in water
- Slow precipitation kinetics

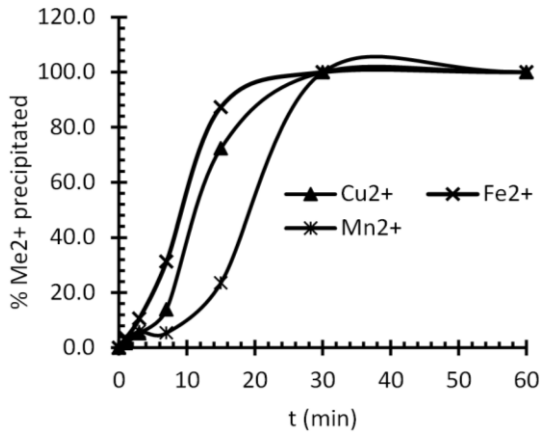

Appendix D: Publications

Conference proceedings & presentations:

- Manchisi, J., N. A. Rowson, and M. J. H. Simmons (2013), **Kinetics of Heavy Metal Adsorption in Acid Mine Drainage Treatment with Blast Furnace Slag**, Proceedings of 23rd International Mining Congress and Exhibition of Turkey,16-19 April, Antalya, Turkey

- Manchisi, J., N. A. Rowson, and M. J. H. Simmons (2013) **Competitive Metal Adsorption Phenomena in Acid Mine Drainage Treatment Using Blast Furnace Slag as Functional Adsorbent**, Proceedings of 23rd World Mining Congress, 11-15 Aug., Montreal, Canada

Poster presentations:

- Manchisi, J., N. A. Rowson, and M. J. H. Simmons (2012), **Use of Sustainable Adsorbents to Treat Acid Mine Drainage**, University of Birmingham Graduate School Research Poster Conference, 19th June, Birmingham, United Kingdom

- Manchisi, J., N. A. Rowson, and M. J. H. Simmons (2014) **Use of Slag Materials as Sustainable Adsorbents to Treat Waste Streams**, Particulate System Analysis, 15-17 Sept, Manchester Conference Centre, Manchester, United Kingdom

Papers for journal publications

- Assessment and improvement of adsorptive characteristics of sustainable adsorbents
- Multicomponent adsorption of metal ions from waste solutions by sustainable adsorbents